

DEVELOPMENT OF A WIRELESS FORCE SENSOR

SARAVANAN S/O VELAYUTHAM
(B.ENG, NUS)

**A THESIS SUBMITTED FOR THE DEGREE OF
MASTER OF ENGINEERING
DEPARTMENT OF MECHANICAL ENGINEERING
NATIONAL UNIVERSITY OF SINGAPORE**

2006

ACKNOWLEDGEMENTS

First and foremost, I would like to express my deepest gratitude to my supervisors, Prof. Andrew A. O. Tay and A/Prof Lian Yong for their invaluable guidance, supervision, advice and encouragement throughout my postgraduate studies. I am extremely grateful towards them for giving me the opportunity to work in this field and for their patient guidance.

Special thanks go to A/Prof Adrian Yap U Jin formerly from the National University hospital for his kind issues on the medical aspect of this project.

Finally, I would like to thank my parents, laboratory colleagues and friends for their constant support and help.

TABLE OF CONTENTS

ACKNOWLEDGEMENTS	i
TABLE OF CONTENTS	ii
SUMMARY	vii
LIST OF FIGURES	ix
LIST OF TABLES	xii
CHAPTER 1 INTRODUCTION	1
1.1 Jaw Muscles and Movements	1
1.2 Temporomandibular Disorders (TMD)	2
CHAPTER 2 LITERATURE REVIEW	5
2.1 Electromyography	5
2.2 Piezoelectric transducers	9
2.2.1 Piezoelectric sensors	10
2.2.2 Piezoelectric actuators	13
2.2.3 Working Principle of a piezoelectric film (Sensors)	15
2.3 Strain gage sensors	20
2.3.1 Types of strain gages	21
2.3.2 Working principle of strain gage sensor	23
2.4 Piezoresistive sensors	32
2.4.1 Working principle of a piezoresistive sensor	34
2.5 Capacitive sensor	40
2.5.1 Working principle of a capacitive sensor	41

2.6 Other pressure sensors	46
2.6.1 T-scan	46
2.6.1 Pressure Sensitive Film	46
2.6.3 Pressure measurement by resistance change	48
2.6.4 Force sensing resistors	49
2.7 Photodiodes and its working principles	56
CHAPTER 3 EXPERIMENTAL METHOD and PROCEDURE	59
3.1 Piezoelectric sensor experimental setup	59
3.1.1 Sample preparation	60
3.1.2 Experimental procedures and results	64
3.2 Piezoresistive sensor (Honeywell FSL05N2C) experimental setup	66
3.3 Thin film flexi-force sensor experimental setup	70
3.4 Photo-sensitive force sensor experimental setup	75
3.5 Strain gage force sensor experimental setup	77
3.6 Piezoresistive force sensor experimental setup	80
CHAPTER 4 RESULTS and DISCUSSIONS	81
4.1 Piezoelectric sensor	81
4.2 Piezoresistive sensor	83
4.3 Thin film flexi-force sensor	90
4.4 Photo-resist sensor	98
4.5 Strain gage sensor (with diaphragms)	99
4.6 Piezoresistive strain gage sensor	114

CHAPTER 5 WIRED PRESSURE SENSOR INTERFACED TO A SD CARD 123

5.1 S8051 signal processing chip	123
5.1.1 SD card boot loader	125
5.1.2 SD card	126
5.1.3 Serial peripheral Interface	127
5.1.4: Data exchange protocol	128
5.2: SPI bus protocol	129
5.3 FAT16	139
5.3.1 Overview of FAT16 file system	140
5.3.2 Master boot record	141
5.3.3 FAT16 boot record	143
5.3.4 FAT tables	145
5.3.5 Directory table	147
5.3.6 Data area	148
5.4 Analogue portion of chip	149
5.5 Circuit Design	150
5.6 PCB fabrication	151
5.7 Testing	154

CHAPTER 6 Wireless Sensor 154

6.1 Introduction to Zigbee	155
6.2 Zigbee solution	155
6.2.1 Microcontroller	155

6.2.2 Transceiver unit	156
6.2.2 Antenna	157
6.3 Full wireless module	158
6.4 Implementation	159
6.4.1 Development tools	159
6.4.1.1 Codewarrior development suite	159
6.5 Application	162
6.6 Results and discussion	163
6.6 Validation of sensor module as bruxism force detector	167
6.8 Final prototype	172
CHAPTER 7 SUMMARY AND CONCLUSION	174
REFERENCES	177
APPENDIX	184

Summary

Although there have been many studies on bruxism forces and bruxism activities, no real medical device has been developed to measure the forces that arise due to bruxism activities. In this thesis, different types of sensors were investigated to develop a suitable bruxism force detector. This sensor was also interfaced to a wireless transceiver to form a wireless pressure sensor.

The sensors that were investigated included piezoelectric sensors, piezoresistive sensors (Honeywell FSL05N2C), the Thin Film Flexi-force Sensor, constantan strain gage sensor and piezoresistive strain gage sensor. The sensors were subjected to different load cycle patterns at different rates to a maximum force of up to 200 N. The sensors were tested for their repeatability, linearity, hysteresis and drift. Experimental results show that piezoresistive strain gage sensors are best suited sensors for bruxism force detection. These types of sensors are small in size; they do give consistent results and have high voltage output that is very important for the wireless transmission

The piezoresistive based bruxism force detector was interfaced to a wireless module (Zigbee) to form a complete wireless pressure sensor that could be used to measure bruxism forces.

List of Figures

	Page
Fig. 1.1: Facial muscles	1
Fig. 1.2: One type of temporomandibular disorder	9
Fig. 2.2(a): Before polling	10
Fig. 2.2(b): After polling.	10
Fig. 2.3: Strain gage Sensor	20
Fig 2.3.1: Unbonded metal-wire strain gage	21
Fig. 2.3.1.1: Different pattern of strain gage foils etched on a substrate	25
Fig. 2.3.2: Wheatstone bridge.	27
Fig. 2.3.2.1: Bite force sensor	32
Fig. 2.3.2.2: Elimination of inconsistency due to position of bite	33
Fig. 2.3.3.2: LMSG sensor	29
Fig. 2.3.3.3: Circuit used to measure voltage output	30
Fig. 2.3.3.4: Sensor developed by Platt.et.al	31
Fig. 2.4.1: Cubic element	34
Fig. 2.2.1: Capacitive sensor	41
Fig. 2.5.1.1(a): Sensor schematic	44
Fig. 2.5.1.1(b): Diagram of sensor and readout circuitry	44
Fig. 2.6.4.1: Conductive polymer sensor	52
Fig. 2.6.4.2: Matrix structure of the FSR	50
Fig. 2.6.4.3: Inner Sensor of bite force instrument and its basic components	55
Fig. 2.6.4.4: Schematic views and dimensions of the constructed bite force sensor	55

Fig. 2.7.1: Pressure sensor photo-diode and light emitting diode	57
Fig. 3.1.1: Piezoelectric sensor	60
Fig. 3.1.2: Sample preparation of the PVDF Sensor	61
Fig. 3.1.3: A typical low pass filter with an Operating Amplifier	62
Fig. 3.1.4: Calibration of the piezoelectric sensor	62
Fig. 3.1.5: Actual setup to calibrate the piezoelectric sensor	63
Fig. 3.1.6: Typical results obtained from the oscilloscope while calibrating the piezoelectric sensor	64
Fig. 3.1.7: Piezoelectric sensor used in this experiment	65
Fig. 3.1.9: Setup to calibrate the piezoelectric sensor	66
Fig. 3.2: (Honeywell FSL05N2C) piezoresistive sensor	66
Fig. 3.2.1(a): Piezoresistive sensor	68
Fig. 3.2.1(b): Piezoresistive sensor	68
Fig. 3.3: Flexi force sensor	70
Fig. 3.3.1: Circuitry for the flexi force sensor	71
Fig. 3.3.2: Cross sectional view of the experimental setup	72
Fig. 3.3.2(b): Actual experimental setup	73
Fig. 3.4: Cross-sectional view of a photo-resist sensor	75
Fig. 3.4.1: Interface circuitry for photo-resist sensor	76
Fig. 3.4.2(a): Experimental setup	77
Fig. 3.4.2(b): Experimental setup	77
Fig. 3.5: Dimensions of the stainless/Aluminum diaphragm.	78
Fig. 3.5.1: Strain gage in comparison with a Singapore 5-cents coin	78
Fig. 3.5.2: Experimental setup for the strain gage sensor	79

Fig. 3.5.3: Circuitry for the strain gage sensor	79
Fig. 4.1: Experimental results obtained from the piezoelectric sensor	81
Fig. 4.1.2: Equivalent circuit for a piezoelectric sensor	82
Fig. 4.2.1: A Load of 200N was applied for a time span of 20 seconds. The 200N force was applied for another 60 seconds and the force was gradually reduced to zero force within another 20 seconds.	84
Fig 4.2.2 : A load of 200N was applied continuously for a time span of 10 seconds and that load was gradually removed to zero force within a time span of another 10 seconds	85
Fig 4.2.3: A Load of 200N was applied for a time span of 10 seconds. The 200N force was applied for another 60 seconds and the force was gradually reduced to zero force within another 10 seconds.	86
Fig 4.2.4: A load of 200N was applied continuously for a time span of 5 seconds and that load was gradually removed to zero force within a time span of another 5 seconds	87
Fig 4.2.5: A Load of 200N was applied for a time span of 5 seconds. The 200N force was applied for another 10 seconds and the force was gradually reduced to zero force within another 5 seconds.	88
Fig 4.2.6: Loading Unloading Graph of the Sensor	89
Fig. 4.3.1: A Load of 200N was applied continuously for a time span of 20 seconds and that load was gradually reduced to zero force within another 20 seconds.	91
Fig 4.3.2 : A Load of 200N was applied for a time span of 60 seconds. The 200N force was applied for another 10 seconds and the force was gradually reduced to zero force within another 60 seconds.	92
Fig 4.3.3: A Load of 200N was applied continuously for a time span of 10 seconds and that load was gradually reduced to zero force within another 10 seconds.	93
Fig 4.3.4: A Load of 200N was applied for a time span of 10 seconds. The 200N force was applied for another 60 seconds and the force was gradually reduced to zero force within another 10 seconds	94

Fig 4.3.5: A Load of 200N was applied continuously for a time span of 5 seconds and that load was gradually reduced to zero force within another 5 seconds.	95
Fig 4.3.6: A Load of 200N was applied for a time span of 2 seconds. The 200N force was applied for another 3 seconds and the force was gradually reduced to zero force within another 2 seconds.	96
Fig 4.3.7: Loading and Unloading graph for the flexi force sensor	97
Fig 4.4.1: Calibration curve for the photo-resist sensor	98
Fig. 4.5.1: A Load of 200N was applied for a time span of 30 seconds. The 200N force was applied for another 60 seconds and the force was gradually reduced to zero force within another 30 seconds.	100
Fig 4.5.2 : A load of 200N was applied continuously for a time span of 20 seconds and that load was gradually removed to zero force within a time span of another 20 seconds	100
Fig 4.5.3: A Load of 200N was applied for a time span of 20 seconds. The 200N force was applied for another 60 seconds and the force was gradually reduced to zero force within another 20 seconds.	102
Fig 4.5.4: A load of 200N was applied continuously for a time span of 10 seconds and that load was gradually removed to zero force within a time span of another 10 seconds	103
Fig 4.5.5: A Load of 200N was applied for a time span of 10 seconds. The 200N force was applied for another 60 seconds and the force was gradually reduced to zero force within another 10 seconds.	104
Fig 4.5.6: A load of 200N was applied continuously for a time span of 5 seconds and that load was gradually removed to zero force within a time span of another 5 seconds	105
Fig 4.5.7: A Load of 200N was applied for a time span of 2 seconds. The 200N force was applied for another 3 seconds and the force was gradually reduced to zero force within another 2 seconds.	106
Fig 4.5.8 : The direction of measurement of the voltage output	107
Fig. 4.5.9: A Load of 200N was applied for a time span of 30 seconds. The 200N force was applied for another 60 seconds and the force was gradually reduced to zero force within another 30 seconds.	108

Fig 4.5.10 : A load of 200N was applied continuously for a time span of 30 seconds and that load was gradually removed to zero force within a time span of another 30 seconds	109
Fig 4.5.11: A Load of 200N was applied for a time span of 10 seconds. The 200N force was applied for another 60 seconds and the force was gradually reduced to zero force within another 10 seconds.	110
Fig 4.5.12: A load of 200N was applied continuously for a time span of 10 seconds and that load was gradually removed to zero force within a time span of another 10 seconds	111
Fig 4.5.13: A load of 200N was applied continuously for a time span of 5 seconds and that load was gradually removed to zero force within a time span of another 5 seconds	112
Fig 4.5.14: A Load of 200N was applied for a time span of 2 seconds. The 200N force was applied for another 3 seconds and the force was gradually reduced to zero force within another 2 seconds.	113
Fig 4.6.1 : A load of 200N was applied continuously for a time span of 30 seconds and that load was gradually removed to zero force within a time span of another 30 seconds	115
Fig 4.6.2: A Load of 200N was applied for a time span of 30 seconds. The 200N force was applied for another 60 seconds and the force was gradually reduced to zero force within another 30 seconds.	116
Fig 4.6.3: A load of 200N was applied continuously for a time span of 20 seconds and that load was gradually removed to zero force within a time span of another 20 seconds	117
Fig 4.6.4: A load of 200N was applied continuously for a time span of 10 seconds and that load was gradually removed to zero force within a time span of another 10 seconds	118
Fig 4.6.5: A Load of 200N was applied for a time span of 10 seconds. The 200N force was applied for another 60 seconds and the force was gradually reduced to zero force within another 10 seconds.	119
Fig 4.6.6: A load of 200N was applied continuously for a time span of 5 seconds and that load was gradually removed to zero force within a time span of another 5 seconds	120

Fig 4.6.7: A Load of 200N was applied for a time span of 2 seconds. The 200N force was applied for another 3 seconds and the force was gradually reduced to zero force within another 2 seconds.	121
Fig 4.6.8: Loading and Unloading graph of a piezoresistive sensor	122
Fig 5.1.1: S8051 chip	123
Fig 5.1.2: The functions of the S8051 chip	124
Fig 5.1.3: Block diagram of the 8051 chip	126
Fig 5.1.4: Single slave and master	128
Fig 5.1.5: Cascading several SPI devices	128
Fig 5.1.6: Typical SPI communication	129
Fig 5.3.2: FAT16 partition	141
Fig 5.3.7: Entries of FAT	146
Fig 5.3.9: Data entry diagram	148
Fig 5.4.1: Analogue portion of the s8051	150
Fig 5.6.1: Metcal AR500 rework station	152
Fig 5.6.2: Surface mounting of components using the Metcal AR500	152
Fig 5.6.3: The interface circuitry	153
Fig 6.3.1: Transceiver module	158
Fig 6.3.2: Sensor module	158
Fig 6.4.1: Editor and compiler	160
Fig 6.4.2: BDM multi-link cable	161
Fig 6.5.1: Full setup for the test procedure	163
Fig 6.6.1: Experimental setup for calibration of the sensor	165
Fig 6.6.2: The full setup for the calibration of the wireless pressure sensor	165

Fig 6.6.3: Sensor and fixture to simulate teeth	166
Fig 6.6.4: The sensor,transmitter,wheatstone bridge and amplifier	166
Fig 6.6.5: Receiver	166
Fig 6.6.6: Voltage output and force display	167
Fig 6.6.7: Calibration curve	167
Fig 6.7.1: Experimental setup for simulating an actual bruxism event	169
Fig 6.7.2: Simulated bruxism event	169
Fig 6.7.3: Voltage output Vs Time graph	170
Fig 6.7.4: Load Vs Time graph	170
Fig 6.7.5: Actual simulated bruxism event	171
Fig 6.7.6: Reference graph	171
Fig 6.8.1: Backview of the final prototype	173
Fig 6.8.2: Frontview of the final prototype	173
Fig A.1: Top Layer for the PCB design for interfacing the sensor to the SD card	184
Fig A.2: Bottom Layer for the PCB design for interfacing the sensor to the SD card	185
Fig A.3 Schematic circuit diagram for interfacing the sensor to the SD card	186

List of Tables

Page

Table: 2.2.1: Behavior of piezoelectric films subjected to force.	12
Table: 2.2.2: Behavior of piezoelectric film as an actuator	14
Table: 2.2.3: Typical values of the different constants for different types of piezoelectric material	16
Table: 3.1: Piezoelectric film properties used in this experiment	59
Table: 3.3: Sensor property of the flexi force sensor	74
Table: 5.2.1: SPI messages	129
Table: 5.3.1: Layout of a FAT16 file system	140
Table: 5.3.3: Breakdown of the MBR and its hexadecimal offsets	142
Table: 5.3.4: One partition entry	142
Table: 5.3.5: Information to one single partition	143
Table: 5.3.6: FAT16 boot record with the appropriate offsets	144
Table: 5.3.6: Valid FAT16 values	146
Table 6.6: Voltage output table	164

CHAPTER 1: Introduction

1.1 Jaw Muscles and Movements

Temporomandibular disorders (TMD) are a commonly used term to describe various problems that are related to the jaw muscles and the temporomandibular joints. The temporomandibular joints, also known as TMJs, are the joints that are located on both sides of the face in front of our ears. As can be seen from figure 1.1, they connect the jaw bone (mandible) to a part of the skull (temporal bone). They could be considered as one of the most complicated joints in the human body since besides providing rotating movements like any other joints, they do also provide sliding movement or also more commonly known as translation motion. Between the top ends of the jaw (condyle) and the socket in the skull is a disc of cartilage. These discs serve as shock absorbers protecting the bones from hitting each other, like any other discs in our neck or in our back. One of the unique features of the TMJ discs is its ability to permit both the sliding as well as the rotating motion while performing normal mouth function.

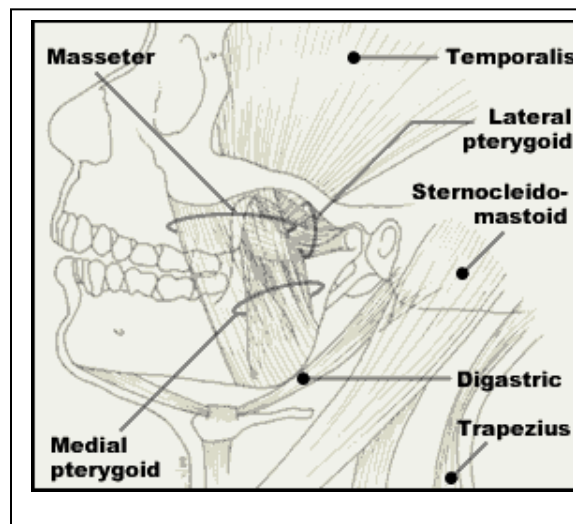


Fig 1.1: Facial muscles

The Jaw movement is orchestrated by a very complex set of muscles which are in turn controlled by the body's local as well as the central system. These systems are collectively known as the neuromuscular system. The whole joint system is held together by ligaments that limits the movement range. The TMJ joint system works in a very unique way, where the opening, lateral and the forward motion of the jaws are controlled by the shape of the bones, the muscles and the ligaments, the closing end point of the jaw movement is controlled together by the teeth (the bite or occlusion).

In order for the TMJ system to function properly, all the components mentioned earlier in the paragraph, inclusive of the muscles, nervous system, ligaments, joints (bones, discs and connecting tissues) and the dental occlusion (teeth) must perform normally.

1.2 TEMPOROMANDIBULAR DISORDERS (TMD)

Temporomandibular disorders or commonly known as TMD are often mistaken as "TMJ". "TMJ" actually only refers to the jaw joint themselves as described in the previous section [1]. TMD is actually a description of a group of disease that involves the jaw joints, the muscles that control the jaw movement and the dental occlusion. TMDs are physical disorders that arise due to imbalance in the working condition of the jaw and the skull with the muscles that attach to and move the jaw as well as with the nervous systems that are associated with these systems. Figure 1.2 [1] clearly depicts one type of physical disorder that arises.

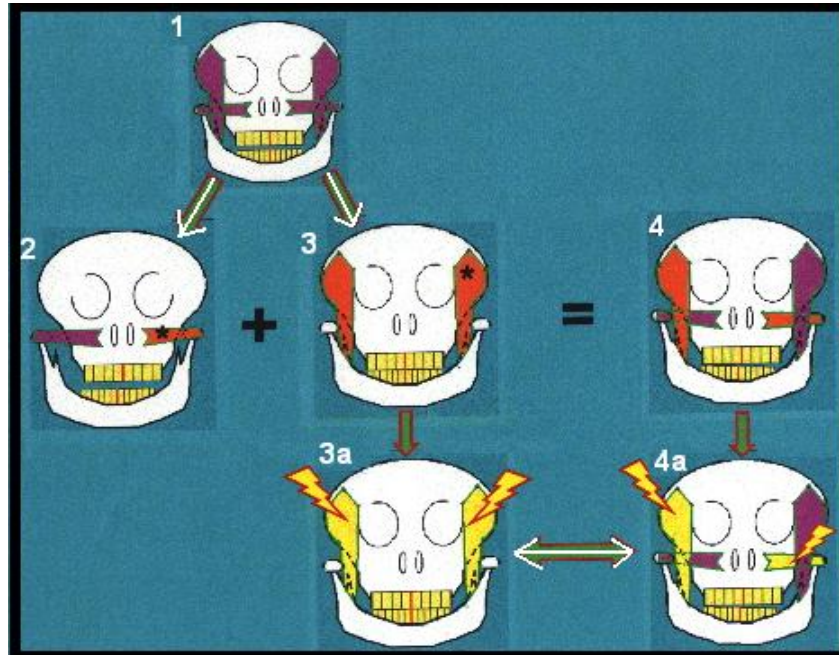


Fig 1.2: One type of Temporomandibular Disorders (TMD)

In normal rest position as can be seen from picture 1 of Figure 1.2, the temporalis would be sufficiently relaxed in order to provide a “free space” between the teeth. If one of the lateral pterygoid were to contract (as can be seen from Figure 1.2) without the contraction of a temporalis, it would cause the mandible to move sideways, without any resistance to the lateral pterygoids attempts. If the temporalis were to contract without the contraction of the lateral pterygoids, it would cause the mandible to elevate till the teeth occlude, as can be seen from Figure 1.2(3). When one temporalis contracts in conjunction with an opposite lateral pterygoid, as can be seen from Figure 1.2(4) it results in a functional movement that is necessary for mastication. Once the teeth are in contact, the whole movement is complete and hence the contraction would end. Clenching is defined as the continued contraction of the temporalis following the occlusion of the teeth, as can be seen from Figure 1.2(3a). The degree of symptoms that arise from this process is a

function of the intensity, duration and frequency of the activity. Following a functional movement (figure 1.2(4)), the musculature is actually intended to relax, before another functional masticatory movement begins. Vigorous alternating contractions of the lateral pterygoids during the occluding of the teeth (by the temporalis) results in the grinding of the teeth.

This oral habit consisting of involuntary rhythmic or spasmodic nonfunctional gnashing, grinding or clenching of teeth is defined as Bruxism [2]. When this process is repeated frequently, it would result in various types of pain and dysfunction in the orofacial region [3, 4]. This process might occur without any signs or symptoms or without any harmful effects to the masticatory system, but it proves to be a problem in the increased tooth wear and pain [4]. Bruxism may occur anytime and people are usually unaware of its occurrence. Therefore, an instrument that is able to continuously monitor and measure the Bruxism forces would help the patients to detect Bruxism events. The following chapter describes some methods that are currently used to detect Bruxism events.

CHAPTER 2: LITERATURE REVIEW

2.1 Electromyography

Electromyography or commonly known as EMG involves the monitoring or recording of the electrical activities of muscles. In short it can be defined as the summated electrical potentials produced by the muscular activation [5]. When a muscle fiber undergoes contraction, it generates a single electrical potential and this potential could be detected by placing the electrodes either within the muscle or on the skin's surface, directly above the muscle that is being monitored.

The magnitudes of the spike potentials are roughly proportional to the muscular tension and hence a resting or an inactive muscle would not result in any electrical activity. The EMG signals obtained reflect the average electrical spikes resulting from the muscle fibers. The EMG signals obtained are very important in the studying patterns of muscle activity that might be related to the nervous or the muscular activity diseases and the signals could also prove to be very vital in diagnostic aid.

Generally two types of electrodes, needle and surface, are used in the EMG monitoring. The needle electrodes are more commonly used in research work, as they allow smaller regions to be monitored which results in the monitoring of fewer muscle fibers which results in a more accurate measurement.

Surface electrodes are more commonly used in active subjects to detect large-muscle activity. Sufficient care should be taken when applying these electrodes onto the skin as any slight movement would result in the detection of the redundant movement

force. Electrode pastes are used between the metal electrode and the skin to overcome any disturbance due to the metal electrode and skin movement.

The frequency content of the EMG signals varies from 0 to 1000 Hz, and the amplitude could vary from 20 to 5000 μ V depending on the electrode location as well as the preparation of the skin [6]. The Electromyogram is used clinically to diagnose problems with neuromuscular transmission and other pathological conditions, such as muscular dystrophy and myotonia. In recent years it has also been used frequently in dental studies to determine various physiology activities relating to dental purposes.

Ahlgren and Owall [7] had developed a polygraphic method to study the relationship between EMG activity, mandibular movements and chewing force. This method involved the direct and integrated EMG recording from the temporal and the masseter muscles. Some of the chosen subjects were told to chew peanuts and the rest were told to chew gum while their EMG activity and mandibular movements were recorded simultaneously on a Mingograph. The opening and the closing phases of the chewing action were simultaneously recorded with the aid of the EMG by a photoelectric arrangement. The photoelectric aided in the mandible movement detection by means of light-intensity variations. It was concluded that the maximal chewing force was developed during the occlusal phase. Although a direct relationship between integrated EMG from the temporal and masseter muscle was recorded during the biting motion, it was stated that during chewing the relationship between the occlusal loads and the EMG readings were not very clear and the actual chewing force was not measured. The recordings of masticatory load was used as an index of the chewing force. It was also

stated that the mean delay time between peak EMG and peak chewing force was about 45msec.

Carlsson and Gale [8] had used an EMG to aid in the Biofeedback treatment for muscle pain. EMG was also used to record the muscular activities of the masseter muscle. Electrodes were fixed to the masseter muscle of the test subject and the resulting voltage was captured on a digital voltmeter. The patient was asked to bite down with varying degree of pressure and was told to note the voltmeter readings corresponding to the bite. The patient was also trained to learn the type of activities and the type of jaw postures that would result in a lower muscle tension. This process was undertaken, so that when the biting pressure exceeds a minimum threshold, (higher voltage) the patient would be able to relax the muscles. All the measurements were based on the digital voltmeter reading. No calibration was done to determine the actual force that the person exerted.

Feehan and Marsh [9] had used EMG biofeedback to reduce bruxism. The subject was supplied with and trained in the use of a portable biofeedback device. The subject was required to affix the electrode unit over the masseter with a tape before sleeping. When the preset EMG threshold was exceeded, it produced an audible tone which acted like an indicator. There was no clear indication of the exact force that the masseter muscle exerts; the results were based on a threshold.

Miyawaki et al. [11] had used electromyography to study the relationship among nocturnal muscle activities, decreased esophageal pH and sleep positions. 12 subjects, of which 4 were bruxism patients participated in the study. Disposable bipolar surface electrodes were used to record the unilateral temporal muscle activities and the data were

recorded on a portable EMG telemetry device. Only the temporal muscle activity was measured by means of the EMG bursts and the actual forces were not measured.

Casas et al. [12] had used contingent nocturnal EMG feedback to alter bruxism behavior. A portable contingent EMG feedback system was designed to emit audible sound when masseter muscle activity exceeded the minimum threshold that was set for each participant. One disadvantage of this method is that the surface EMG electrode would vary with skin resistance over the night even though the clenching force might be the same. Another problem that might arise from this detection method, is the loud noise produced that might wake the patient leading to sleep deprivation

Nishigawa et al. [13] had developed a contingent electrical lip stimulation device for sleep bruxism. In this research, an on-off switch was placed between the maxillary and mandibular orthotics which would be used to trigger an electrically powered lip simulator. This was based on the report by Godaux and Desmedth [14] who had stated that a single electrical stimulation to the gums and mucosa inside the mouth would be able to suppress the masseter and temporalis muscle activity in normal waking subjects. The design involved closing of the switch when the clenching force was greater than 220 g. EMG signals were used to quantify the force. The EMG signals were quantified by the percentage of MVB and there was no mention of the actual force measurement by the EMG.

Takeuchi et al. [20] had compared the signals of simulated bruxism events obtained from EMG recordings as well as from piezoelectric film based intrasplint recordings. He had placed the EMG electrodes on the masseter muscle just like the

experiments carried out by some researchers mentioned before. He had stated that masseter EMG recording would be more suitable for the recording of forceful closure of the teeth in a static jaw position and since bruxism also involves the lateral motion of the mandible, the signals recorded would not be able to produce accurate results.

2.2 Piezoelectric transducers

Piezoelectricity, discovered by Pierre and Jacques Curie, is a property that certain classes of materials possess. Some of the more common materials that possess such property include natural crystal of quartz, Rochelle Salt and Tourmaline as well as manufactured ceramics, such as Barium Titanate and Lead Zirconate Titanates (PZT) [15]. These materials possess piezoelectric because, some atomic lattice structures have as an essential unit (or "cell") a cubic or rhomboid cage made of atoms, and this cage holds a single semi-mobile ion which has several stable quantum position states inside the cell. The ion's position state can be caused to shift by either deforming the cage (applied strain) or by applying an electric field. The coupling between the central ion and the cage provides the basis for transformation of mechanical strain to internal electric field shifts and vice versa [16]. The piezoelectric effect of a material is greatly dependent on the type of piezoelectric material that is being used and the mechanical as well as the electrical axes of operation could be precisely orientated within the shape of the ceramic. These axes could be set during the process known as "poling". This process induces the piezoelectric properties in the material. The orientation of the dc poling field determines the orientation of the mechanical as well as the electrical activities. It is also important to note that piezoelectric materials are anisotropic and thus their properties differ with direction of the piezofilm.

The poling field could be applied in order for the material to exhibit piezoelectric responses in different directions or even in a combination of directions. This explains as to why piezoelectric materials are anisotropic. It is also important to know that when poling is done, it permanently changes the dimensions of the material. The dimensions between the poling electrodes would be increased and the dimensions parallel to the electrodes would decrease [15]. This is clearly depicted in the following figure 2.2.

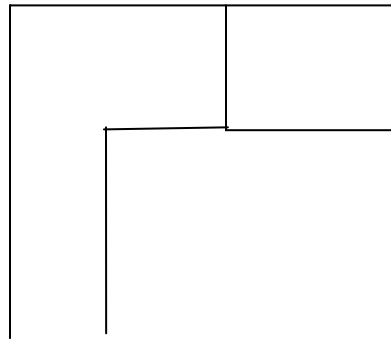


Fig 2.2 (a): Before poling

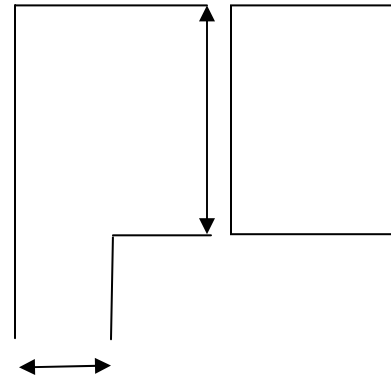


Fig 2.2 (b): After poling: It can be seen that there is an increase in the length between the electrodes and the length parallel to the electrodes is reduced

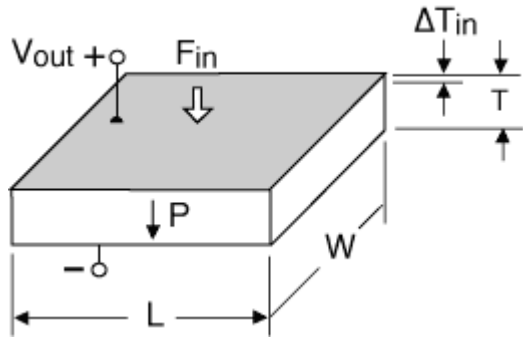
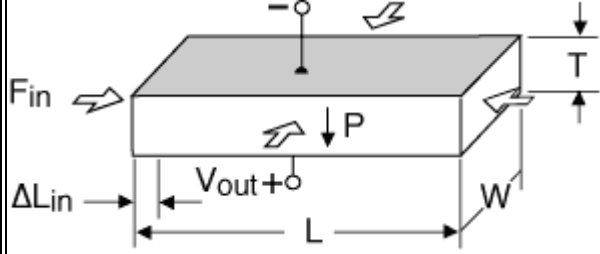
The piezoelectric film could be either used as an actuator or a sensor. The following paragraphs would describe on the two different function of a piezo-film, namely as a sensor and as an actuator.

2.2.1 Piezoelectric Sensors

Once the poling process is completed, a compressive or a tensile force applied to the film would result in a generation of electricity. Whenever there is any compressive

force applied parallel to the poling axis or any tensile force applied perpendicular to the polling axis, it would result in a voltage generation of the same polarity. A voltage of opposite polarity results from a tensile force parallel to the poling axis or a compressive force perpendicular to the poling axis. In retrospective, it could be seen that any voltage generation (either positive or negative) results from a dual action. The dual action keeps the volume of the film constant (i.e. contraction in one axis results in the expansion in the other axis) although there might be small discrepancies in some films; it is not very obvious unless there is magnification under mechanical resonance. The table 2.2.1 illustrates the behavior of the piezoelectric film when it is subjected to forces.

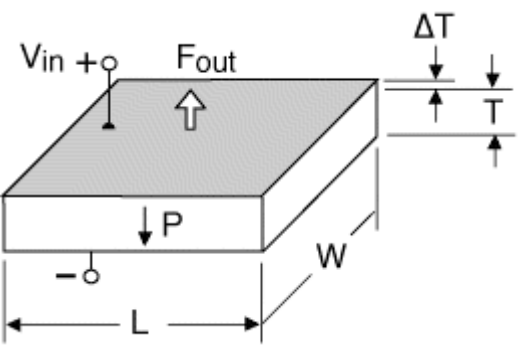
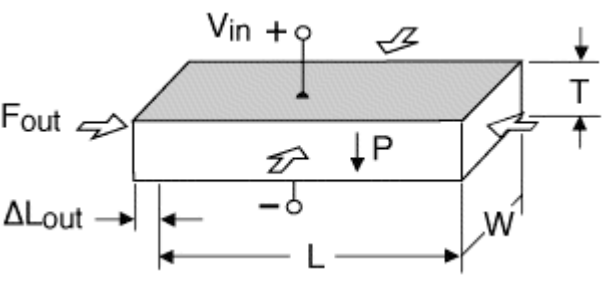
Table 2.2.1: Behavior of Piezoelectric films when subjected to force.

<p>Single Layer Generators</p> <p><i>Longitudinal and transverse generators:</i> When a mechanical stress is applied to a single sheet of piezo-film in the longitudinal direction (parallel to polarization), a voltage is generated which tries to return the piece to its original thickness.</p> <p>Similarly, when a stress is applied to a sheet in a transverse direction (perpendicular to polarization), a voltage is generated which tries to return the piece to its original length and width. A sheet bonded to a structural member that is stretched or flexed will induce electrical generation.</p> <p>By convention, the mechanical axis (n) of the applied stress (or strain) is of as follows:</p> <ul style="list-style-type: none"> 1= length (or stretch) direction 2= Width (or transverse) direction 3= thickness direction 	 <p>Longitudinal (d33) Generator</p>  <p>Transverse (d31) Generator, compressed on sides</p>
---	--

2.2.2 Piezoelectric Actuators

It be seen from the previous paragraph that a mechanical force results in the voltage generation by the piezoelectric film. Piezoelectric materials do also exhibit reverse behavior. When a voltage of the same polarity as the poling voltage is applied to the film, it would result in an additional expansion along the poling axis and contraction perpendicular to the poling axis. When a voltage of opposite polarity to that of the poling voltage is applied, it results in the contraction of the film in the poling axis and the expansion perpendicular to the poling axis. In both the cases whenever the external voltage is removed, it would cause the piezoelectric film to return to its poled dimensions. The Table 2.2.2 illustrates the behavior of a piezoelectric film as an actuator.

Table 2.2.2: Behavior of a piezoelectric film as an actuator

<p>Single Layer Motors</p> <p><i>Longitudinal and Transverse Motors:</i> When an electrical field having the same polarity and orientation as the original polarization field is placed across the thickness of a single sheet of piezoceramic, the piece expands in the thickness or "longitudinal" direction (i.e., along the axis of polarization) and contracts in the transverse direction (perpendicular to the axis of polarization).</p> <p>When the field is reversed, the motions are reversed. Sheets and plates utilize this effect. However, the motion of a sheet in the thickness direction is extremely small (on the order of tens of nanometers). On the other hand, the transverse motion along the length is generally larger (on the order of microns to tens of microns) since the length dimension is often substantially greater than the thickness. The transverse motion of a sheet laminated to the surface of a structure can induce it to stretch or bend, a feature often exploited in structural control systems.</p>	 <p>Longitudinal (d33) Motor</p>  <p>Transverse (d31) Motor, Contracting</p>
---	---

Due to the versatile function of the piezoelectric film, it is very commonly used in many sensors and actuators.

2.2.3 Working Principle of a Piezoelectric Film (Sensors)

Whenever there is any external force stressing the piezoelectric film, it results in the generation of charge Q . This charge Q that is being discharged is proportional to the force that is being applied [17]. Under conditions approaching a short circuit, the charge that has been generated could be defined as follows:

$$Q = d_{3n} \sigma_n A_c = d_{3n} F \quad (1)$$

where d_{3n} is the piezoelectric strain constant it is commonly expressed in pC/N

σ_n is the stress that is applied in the nth axis

A_c is the surface area of the film.

The potential difference V across the piezofilm can be related to the discharge of charges by the following equation.

$$V = \frac{Q}{C} \quad (2)$$

By substituting equation 1 into 2,

$$V = \frac{d_{3n} F t}{\epsilon A} \quad (3)$$

Thus in theory it can be concluded that the voltage output of the film is directly proportional to the force applied, provided that the thickness and the given strain constant do not change.

The open circuit output voltage is given by:

$$V_0 = -g_{3n}\sigma_n t \quad (4)$$

where g is defined as the appropriate piezoelectric coefficient for the axis of applied stress or strain.

σ_n is the stress that is applied in the relevant direction

The values of d_{3n} and g_{3n} differ from material to material and the values can be obtained from the data sheet of the manufacturer.

Some typical values for different type of piezoelectric materials are given in Table 2.2.3[18].

Table 2.2.3: Typical values of the different constants for different type of piezoelectric material

Property	Units	PVDF Film	PZT	BaTiO ₃
Density	10 ³ kg/m ³	1.78	7.5	5.7
Relative Permittivity	ϵ/ϵ_0	12	1200	1700
D ₃₁ Constant	(10 ⁻¹²) C/N	23	110	78
G ₃₁ Constant	(10 ⁻³)Vm/N	216	10	5
K ₃₁ Constant	% at 1 kHz	12	30	21
Acoustic Impedance	(10 ⁶)kg/m ² s ⁻¹	2.7	30	30

In recent times, piezoelectric films have also been used in the field of dentistry to detect occlusion and Bruxism behaviours. The following paragraphs would highlight some of the work that has been done in the field of dentistry using piezoelectric materials.

Sakaguchi et al. [17] used a piezoelectric film transducer for dental occlusal analysis. The transducer was designed to provide occlusal contact force information. The piezoelectric film force transducer was subjected to different varying loads, cycling frequencies, surface area of contact and the transducer surface areas. It was concluded that the voltage generated increased with a decrease in the area of the piezoelectric film, which is consistent with the properties of the piezoelectric film. Theoretically the output voltage is supposed to be independent of the contact frequency, but observations made by Sakaguchi et al. showed otherwise. It was clearly observed that there was decay in the voltage output for frequencies that were above 5Hz. Sakaguchi et al. had stated that this might be due to the deterioration of the thin film sensor due to the high load impacts which might have plastically deformed the film.

Another important observation was also made. Theoretically it is very obvious that the contact area would not contribute to any changes in the voltage output. The voltage is just dependent on the area of the piezoelectric film used and the load applied. Experiments done by Sakaguchi et al. showed that there was a significant difference in the voltage output when the film was loaded with a 3mm striker and a 6mm striker. They had stated that this unusual phenomenon could be attributed to factors such as bending and shearing of the piezoelectric film which could cause the deviations from its properties.

Based on all the observations made by Sakaguchi et al., it can be concluded that the output signals of the piezoelectric film is only consistent for smaller load applications and hence it might not be a very good transducer for detection of heavy occlusal forces.

Rottner and Richter [19] had attempted to determine the accuracy of thin film transducer (piezoelectric film) for different cuspal inclinations by measuring the effect of the occlusal morphology on the output signal that is obtained from these transducers. They had concluded that the actual tooth load is considerably smaller than that was recorded in vivo occlusal forces and the correction factor is a function of an individual's occlusal morphology.

Takeuchi et al. [20] had used piezoelectric film-based intra-splint for the detection of bruxism events in humans. He had compared the signals that were obtained using piezoelectric film to that of the signals obtained by EMG. Experimental results had shown that during grinding, the signals obtained by the piezoelectric sensor were stronger as compared to that obtained from EMG sensors. He had also stated that steady-state clenching task was best captured in the EMG sensor, but the change in occlusal force was strongly captured by the Piezoelectric sensor, which reiterates the point that piezoelectric sensors are not suitable for static force detection but are very good candidates for dynamic motions. In conclusion they had stated that no substantial differences were found between the masseter EMG and ISFD signal with regard to detecting simulated bruxism event. Another important point to take note is in the paper, there was no mention

of any absolute force detected during bruxism. The force measured was reflected as a percentage of the maximum voluntary bite more commonly known as MVB.

Watanabe et al. [21] had used a piezoelectric based sensor to monitor bruxism levels and correlate it to the daily behaviors (e.g.: stress, physical activity, anger) of patients. They had used a telemetric device to record the data. He had set a bench-mark for bruxism behaviors where he had pre-defined bruxism as a force applied to the splint at or above a level of 10% of the maximum voluntary contraction (MVC). Only voltage readings that were at least 60% of the difference between the minimum baseline value and the maximum value of the output were taken into consideration to avoid recording the noise from the background. He termed such readings as “on”. From the data that was obtained, he had defined bruxing event as any set of contiguous or consecutive “on” event. The paper just described the bruxing event of the patients based on the preset conditions and there was no mention of any absolute force measurement during bruxism.

Baba et al. [22], had attempted to detect bruxism by means of a piezoelectric Film based recording device in sleeping humans. They had clearly stated that the piezoelectric film would only be able to detect dynamic motions and would not be able to detect static forces. But he had justified his claims of using piezoelectric film as a detector by stating that bruxism events tend to be of short durations and very few of them are prolonged, steady state clenching. In this case the threshold level of bruxism detection was set at an arbitrary value of 15% of maximum voluntary contraction (MVC). The masseter EMG signals and the ISFD (intra-splint force detector) of a patient were recorded and

compared. It was concluded that there was good concordance between the EMG and ISFD signals obtained from bruxism events in a sleeping subject.

2.3 Strain Gauge Sensors

Strain gauges are one of the most widely used force transducers in research. Although it is not purely a force transducer (they do exhibit some properties of a displacement sensor), it is a simple device that produces a change in its resistance that varies linearly with the strain. This property boils down from the basic electronics, where it is understood that the resistance of a wire is directly proportional to its resistivity and its length and inversely proportional to its cross-sectional area. This is depicted in the Figure 2.3

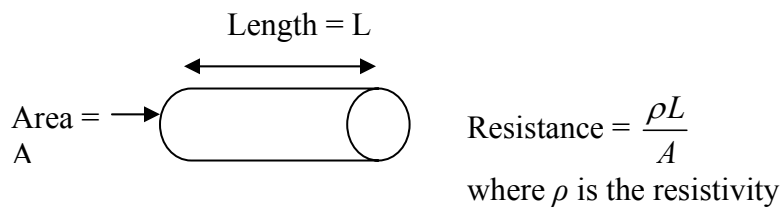


Fig 2.3: Strain gauge sensor

In order to obtain a voltage signal that is proportional to strain, the strain gauge must be used in conjunction with an additional external circuitry. The circuitry usually consists of a Wheatstone bridge (more explanation is given in the latter part of the chapter) and a differential amplifier.

2.3.1 Types of Strain Gauges

There are different types of resistance strain gauges that are commonly used as transducer elements. This includes the unbonded metallic-filament strain gauge, the bonded metallic foil gauge and the bonded piezoresistive gauge.

The unbonded strain gauge element consists of one or more filaments of resistance wire stretched between the supporting insulators. The supports are either attached directly to an elastic member that is used as a sensing element or it is fastened independently, with a rigid insulator that couples the elastic member to the taut filaments. The displacement of the sensing element would cause a change in the filament length which would result in a change in resistance [6]. Although the unbonded strain gauges have become obsolete, they do still have some applications such as an accelerometer. Figure 2.3.1 depicts the unbonded strain gauge.

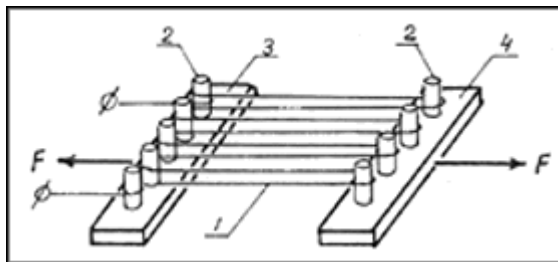


Fig 2.3.1: Unbonded metal-wire strain gauge.

F = force. 1 = strain-sensitive stretched wire, 2 = post, 3 and 4 = moving parts.

The more commonly used strain gauges are known as foil gauges. The simplest type of this kind of gauges consists of a foil of a resistance alloy, such as constantan, that is bonded to an epoxy backing film (or also known as substrate) which is an insulator. The foil is either etched or die cut to produce a grid pattern that is sensitive to the strain along one axis. When the substrate is cemented to the surface of measurement, its deformation is transferred to the foil of the resistance alloy, through the substrate, providing a change in the resistance of the alloy. Several foil gauges placed in the substrate to measure the strain in different directions are known as rosettes. The axis of the gauges along the stresses to be measured can be orientated 45° , 60° or 90° to each other which would allow the magnitudes of the principle stresses, shear stresses to be determined. Figure 2.3.1.1 shows the different pattern of foils that has been etched on a substrate [24].

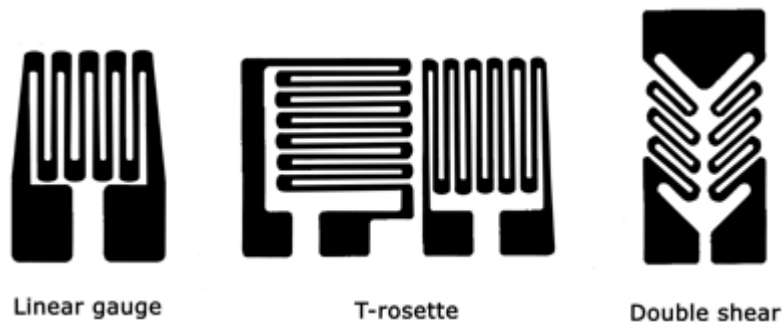


Fig 2.3.1.1: Different pattern of strain gauge foils etched on a substrate.

2.3.2 Working Principle of Strain Gauge Sensor [5]

If we consider a wire of length L , cross-sectional area A , and resistivity ρ , the unstretched resistance of the wire could be denoted as follows:

$$R_u = \frac{\rho L}{A} \quad (1)$$

Now suppose if the wire were to be stretched by a small length ΔL . Since the volume of the wire has to be constant, the increase in the length would lead to a decrease in the cross-sectional area.

$$(LA)_{unstretched} = (L + \Delta L)(A_{stretched}) \quad (2)$$

$$A_{stretched} = \frac{LA}{L + \Delta L} \quad (3)$$

Now the resistance of the stretched wire is given by:

$$R_{stretched} = \frac{\rho L_{stretched}}{A_{stretched}} = \frac{\rho(L + \Delta L)}{LA/(L + \Delta L)} \quad (4)$$

The increase in the resistance of the stretched wire is as follows:

$$\begin{aligned}\Delta R &= R_{stretched} - R_u = \frac{\rho}{A} \left(\frac{(L + \Delta L)^2}{L} - L \right) \\ &= \frac{\rho}{A} \times \frac{L^2 + 2L\Delta L + \Delta L^2 - L^2}{L}\end{aligned}\tag{5}$$

As $\Delta L \ll L$, equation 5 could be simplified to

$$\begin{aligned}\Delta R &= \frac{\rho}{A} \times 2\Delta L \\ \Delta R &= \frac{R_u}{L} \times 2\Delta L\end{aligned}\tag{6}$$

From Equation 6 it can be deduced that:

$$\frac{\Delta R / R_u}{\Delta L / L} = 2\tag{7}$$

This factor that has been just found is known as gauge factor. The gauge factor is around 2 for all metals. The gauge factor could be as high as 100 for semiconductors. As a result of the high gauge factor, when the semiconductor gauges are connected to the arms of a Wheatstone bridge, it would result in a large voltage output, which makes the subsequent amplification of the signals unnecessary. But it is important to note that, such a large resistance changes produce a large unbalance in the Wheatstone bridge with constant-voltage excitation, resulting in a very nonlinear outputs. However this problem can be solved by exciting the bridge from a constant-current supply. Even though the foil gauge

transducer needs amplification due to its low bridge output, it produces a linear output signal.

Wheatstone bridges are commonly used to convert resistance changes in a circuit into voltage output. A good example would be in the use of Wheatstone bridge in a strain gauge force transducer. A simple Wheatstone bridge is presented below in Figure 2.3.3.3

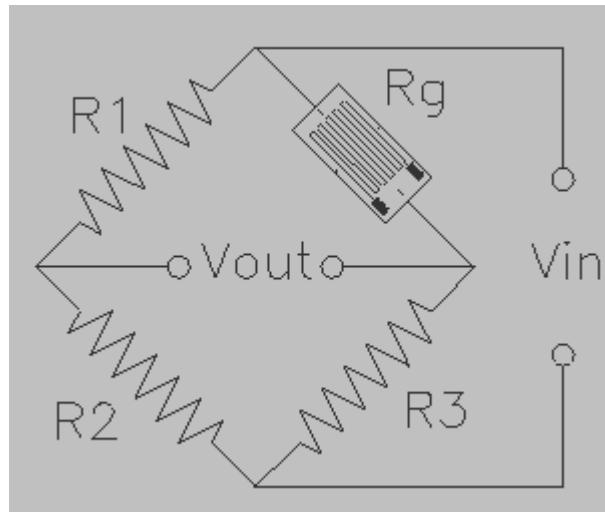


Fig 2.3.2: Wheatstone Bridge

The output V_{out} of the Wheatstone bridge presented above shown in the following equation:

$$V_{out} = \left(\frac{R_2}{R_1 + R_2} - \frac{R_3}{R_g + R_3} \right) V_{in}$$

Strain gauges have been widely used in the field of dentistry to measure bite forces.

Dechow and Carlson [28] had developed a bite force sensor that consisted of two differential strain beams with four strain gauges in a full bridge configuration to measure the bite forces in rhesus monkeys. A full bridge configuration was chosen over the more common half-bridge configuration in order to obtain a voltage output that was proportional to the differences in strain between the two gauges in one beam and the other two gauges in the other beam. Figure 2.3.2.1 shows the setup. This was done in order to eliminate the inconsistency that could arise due to the position of the biting of the monkey on the device. Figure 2.3.2.2 shows how the inconsistency could be eliminated. Calibration of the bite force sensor resulted in a linear output.

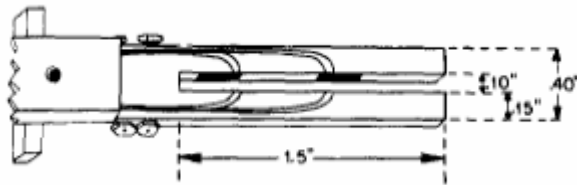


Figure 2.3.2.1: Bite Force Sensor [28]



Figure 2.3.2.2: Elimination of inconsistency due to position of bite

From Figure 2.3.3.2, it can be concluded that

$$\text{The overall axial force} = P_o \cos \phi - P_o \cos \phi = 0$$

Hence the measured load would vary according to $P_o \sin \Phi$.

It was concluded that the method that was used to measure the bite force is reliable and useful.

Lundgren and Laurell [29] had developed a method to study the occlusal forces in prosthetically restored dentitions. This was an improved version of the previous method as mentioned earlier in this chapter. In this method, the magnitude, duration and the frequency of the forces could be measured in various parts of the dentition simultaneously. The measurements were based on miniature strain gauges (the total transducer size was about 5.2 by 5.2 mm) that were placed into artificial crowns, bridge-pontics or removable dentures without causing any obstruction to occlusion. The output signals were obtained by connecting the strain gauges to a Wheatstone bridge circuit which in turn was connected to a specially designed bridge amplifier. Results show that the magnitude of the output signal from the transducers were linear with respect to the applied load. Although measuring only axially directed forces might not be sufficient when studying occlusal forces for example during eating and chewing, It was justified that Axial forces are the predominant forces during the above mentioned activities and it was also stated that when chewing or biting force reaches its maximum, there is no

mandibular movement and hence there is no horizontal force components due to the sliding of the mandible. The predominant force would than be the axial force.

Sinn et al. [30] had used custom strain gauges to measure the bite force of patients with temporomandibular joint disorders after surgery. The bite force gauge consisted of 4 strain gauges that were mounted on 2 stainless steel bars. The tapered ends of the bars were covered with polypropylene tubing and were adjusted to a 15 mm opening. When the patient bites the stainless steel bar, the load changes in the steel bar would produce a measurable voltage change across the four strain gauges forming a Wheatstone bridge.

Bergmann et al. [31] had developed multi channel strain gauge telemetry for orthopedic implants. The sensor is a small telemetry that consisted of three strain gauges. It was listed that in order to have a good orthopedic telemetry, the following conditions must be satisfied:

1. Small integration to allow an integrated implant design of sufficient strength
2. Low energy consumption and possibly an inductive power supply
3. Long-term safe encapsulation
4. Possibility of measuring several strain gauge signals

Ravary et al. [44] had listed in his review paper about a new type of strain gauge, the liquid metal strain gauge or shortly know as (LMSG). This type of strain gauge consists of 1 or 2 compliant capillaries (for example in a soft polymer as silicone), that is filled with a conducting liquid such as mercury or a mixture of gallium and

indium. The two ends of the tube are closed by means of a platinum wire and lead wires are soldered to them. The liquid metal column is contained in a slightly overpressured tube so that it would prevent any subpressure that would be created during straining as the creation of subpressure during straining might predispose the penetration of water through the slightly permeable silicone tube wall. Figure 2.3.3.2 clearly depicts the sensor. The working principle of the LMSG is the same as normal strain gauges where the output signal changes with the resistance of the “resistor” in question. In this case, when there is a strain, it would result in the elongation of the tube, causing an increase in the liquid metal column and a decrease in the cross sectional area that would result in an increase in the electrical resistance.

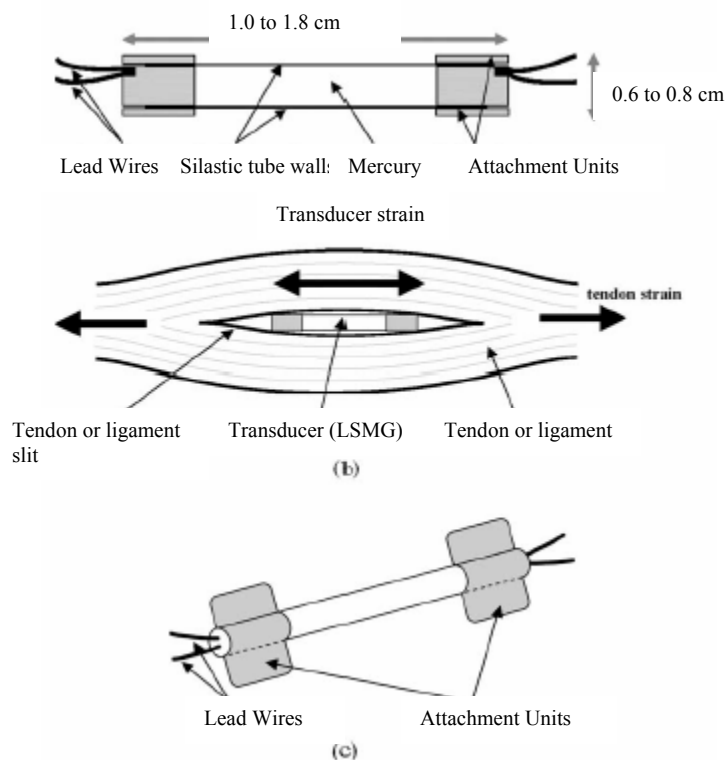


Fig 2.3.3.2: LMSG Sensor

Halachmi et al. [32] had used two linear miniature strain gauges (bonded to the cervical area of the buccal and lingual aspects of the first molar teeth) to measure the voltage output resulting from the compressive force on the teeth.

Nielsen et al. [39] had developed a novel C-shaped strain gauge force transducers (outer diameter 6.0 mm, inner diameter 5.0mm and width 2.0mm) to measure the dynamic measurements of the tension of the individual mitral valve chordae tendineae during the cardiac cycle. 2 miniature strain gauges were cemented onto the C-shaped frame and the strain gauges were connected to a Wheatstone bridge as shown in Figure 2.3.3.3 and subsequently amplified.

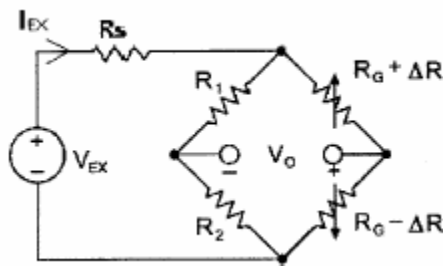


Fig 2.3.3.3: Circuit used to measure voltage output [39].

Calibration was done on the sensor for loads up to 542g. Results show that there was a linear relationship between output voltage and the load applied in the range of 0 to 542 g.

Platt et al. [51] had developed a novel force transducer for the measurement of Tendon force in Vivo. The transducer consisted of a base-plate with a central titanium deflection leaf. Two strain gauges were bonded on both the sides of the deflection leaf

and these strain gauges were then connected to a Wheatstone bridge to determine the voltage output that results from the strain on the gauges. Figure 2.3.3.4 gives a clear depiction of the sensor that was developed.

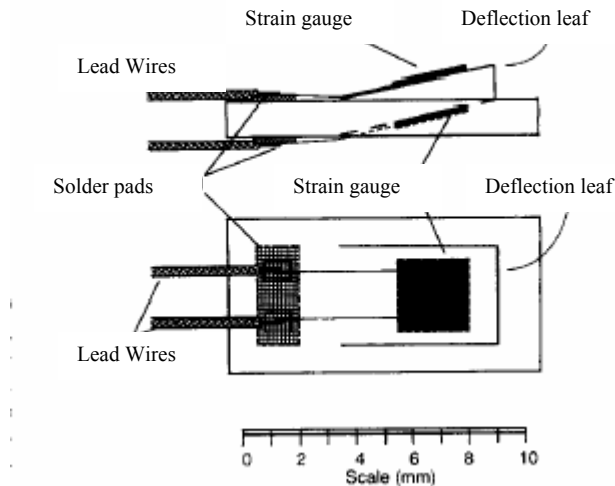


Fig 2.3.3.4: Sensor Developed by Platt et al. [51]

The working principle of the sensor is as follows. When there is any transmission of tensile force through the tendon, it would cause the deflection leaf to bend inwards, thus resulting in a strain in the gauges that would result in a voltage output. It was reported that there was a linear voltage output with the applied force on the deflection leaf and when the sensor was implanted within the tendon, the sensor exhibited an approximately linear relationship between the tendon force and the gauge output for forces above 300-500N. The non-linearity at forces lower than 500N was attributed to the lateral deformation of the fiber composite structure that would occur at low loads. It was also reported that cyclic loading did not affect the results at all.

2.4 Piezoresistive Sensors

The piezoresistance effect could be defined as the change in the electrical resistance of the material with respect to the applied stress. Generally all conducting materials do exhibit this property but the effect is larger in some semiconductors and hence the change in resistivity of these type of semiconductor materials is more significant as compared to other materials. The change in resistivity is actually due to the structural changes in the volume that occur due to the application of stress on the material. When stress is applied to the semiconductor, it would cause an energy gap change between the valence band and the conduction band. This change in energy gap affects the change in the charge carriers, which would result in the change of resistance of the material [43]. The overall change in resistance of a material could be summarized by the following equation.

$$\frac{\Delta R}{R} = \frac{\Delta l}{l} - \frac{\Delta A}{A} + \frac{\Delta \rho}{\rho} \quad (1)$$

Where

R = resistance of the material

A = area of the material

ρ = resistivity of the material

In most of the piezoelectric pressure/force sensors, the resistance effect due to the change in length and area is minimized by adopting a wire like structure so that the piezoresistive effect is more prominent which would then result in a proportional change

of resistance with respect to the pressure/force load applied. The resistivity could be generalized by Matthiessens's rule which goes as follows [25, 26]:

$$\rho(p, T) = \rho_G(p, T) + \rho_s \quad (2)$$

where

ρ_G term is attributed to the resistivity due to the lattice vibrations of the atom. The intensity of the lattice vibration is largely dependent on the conductor temperature as well as the external pressure. When the temperature of the conductor increases, it leads to an increase in the movement of the solid metal ions which would also lead to a greater number of collisions between the electrons and the solid ions. This would result in an increase in the resistivity. As for the pressure, when the pressure increases (due to compression), it would lead to an attenuation of the lattice vibration, hence the number of collision between the electrons and the solid ions would decrease and thus the resistivity also would decrease.

ρ_s term of the resistivity describes the electron movement in a conductor due to the structural defects for example: vacancies, interstitials and dislocations as well as the boundary layers. This term is very important in thin film sensors as these sensors have a film thickness $d_s < 1\mu\text{m}$. As the film thickness decreases, it would lead to an increase in the resistivity. This phenomenon could be attributed to the "path length" effect. If the film thickness is small, the mean free path of the electron is limited by the spacing of the interfaces of the layer. If the film thickness falls below the order of magnitude of the mean free path λ of the conduction electrons in a metal lattice, there would be a

significant increase in the resistivity due to the increase in the collision between the electrons and the boundary layers.

2.4.1 Working Principle of a Piezoresistive Sensor

Consider a cubic element as shown in figure 2.4.1 below which is subjected to a uniaxial state of stress (in the **x**-direction) [27]:

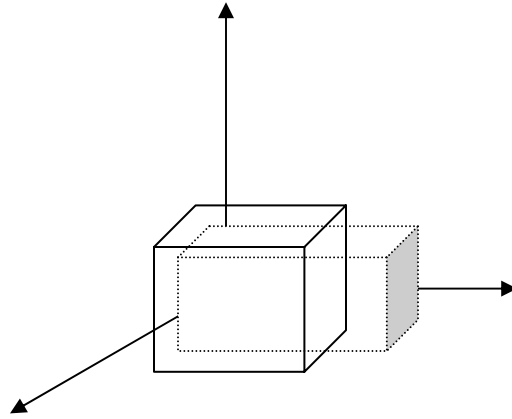


Fig 2.4.1: Cubic Element

From the diagram it could be seen that

$$\varepsilon_y = \varepsilon_z = -\nu \frac{\sigma_x}{E}$$

Where ν is defined Poisson's ratio:

$$\nu = -\frac{\text{Lateral Strain}}{\text{Axial Strain}}$$

Resistance of a conductor could be related to its resistivity, its length and its cross-sectional area by the following equation:

$$R = \rho \frac{l_x}{A}$$

$$A = l_z \times l_y$$

Hence R can be expressed as

$$R = \rho \frac{l_x}{l_y \times l_z}$$

For the cubical conductor:

$$\frac{\Delta R}{R} = \frac{\Delta l_x}{l_x} - \frac{\Delta A}{A} + \frac{\Delta \rho}{\rho}$$

$$\frac{\Delta R}{R} = \frac{\Delta l_x}{l_x} - \frac{\Delta l_y}{l_y} - \frac{\Delta l_z}{l_z} + \frac{\Delta \rho}{\rho}$$

$$\frac{\Delta l_x}{l_x} = \frac{\sigma_x}{E} = \epsilon_x, \quad \frac{\Delta l_y}{l_y} = -\nu \frac{\sigma_x}{E} = -\nu \epsilon_x \quad \text{and} \quad \frac{\Delta l_z}{l_z} = -\nu \frac{\sigma_x}{E} = -\nu \epsilon_x$$

Hence,

$$\frac{\Delta R}{R} = \epsilon_x + 2\nu \epsilon_x + \frac{\Delta \rho}{\rho}$$

At constant temperature, the pressure dependence of the resistivity could be expressed by the following equation [26].

$$\alpha_p = \frac{1}{\rho} \left(\frac{\partial \rho}{\partial p} \right)_T$$

When the applied pressure or stress is constant,

$$\frac{\Delta \rho}{\rho} = \alpha_p p$$

By combining all the equations,

$$\frac{\Delta R}{R} = \varepsilon_x + 2\nu\varepsilon_x + \frac{\Delta \rho}{\rho}$$

$$\frac{\Delta R}{R} = \varepsilon_x + 2\nu\varepsilon_x + \alpha_p P$$

$$\frac{\Delta R}{R} = \varepsilon_x + 2\nu\varepsilon_x + \alpha_p E \varepsilon_x$$

$$\frac{\Delta R}{R} = \varepsilon_x (1 + 2\nu + \alpha_p E)$$

$$\frac{\frac{\Delta R}{R}}{\varepsilon_x} = (1 + 2\nu + \alpha_p E) = \text{Gauge factor}$$

where α_p is defined as the piezoresistive constant in the x-axis [6]

It is also important to note that Plastic deformation also raises the resistivity due the increased numbers of electron-scattering dislocations. Generally silicon has been used to develop piezoresistive sensors, due to their excellent properties. Silicon has strength comparable to that of steel with a tensile strength that can exceed 689 MPa. Silicon is

also theoretically a perfect elastic material as it has no grain boundaries thus eliminating the creep and hysteresis effects. High gauge factors could also be achieved [48].

Piezoresistive sensor has been widely studied for pressure sensing. Tun et al. [40] had developed and tested the pressure sensitiveness of silicon based $\text{Al}_x\text{Ga}_{1-x}$ pressure sensors. It was reported that these types of pressure sensors are suitable for both dynamic and static pressure measurements with a wide range of applied pressure. The pressure sensors were fabricated with two different types of substrates (Silicon and GaAs) and they were then tested under different loading tests to determine, the contact pressure sensitivity, linearity, hydrostatic pressure sensitivity, hysteresis, temperature sensitivity and long time stability. Results show that silicon-based pressure sensors have more than 1.5 times higher sensitivity than that of GaAs-based sensors. This phenomenon was attributed to the nature of bonding interface and surface integrity of pressure sensing film on silicon substrate. It was stated that the bonding between the GaAs and the film (Covalent bonds) was stronger than bonding between the Silicon and the film (weak Van-der-waals forces), which contributes to the ease of slippage between the film and the substrate for the latter case, thus resulting in a certain shear stress beneath the film that explains the higher sensitivity of a silicon-based pressure sensor in comparison with GaAs-based ones. Hysteresis behavior did occur in both of these sensors. It was also reported that the silicon-based pressure sensors were more sensitive to temperature changes as compared to that of GaAs-based sensors.

Pressure sensors using p-type polycrystalline diamond piezoresistors were developed by Yamamoto et al. [41], hot filament CVD (chemical vapor deposition) method was undertaken to deposit boron-doped polycrystalline diamonds on Si substrate. Boron-doped diamonds were deposited on an isolation layer of the undoped diamond film. The diaphragm thickness and the boron doping depth were varied to determine the sensitivity of the sensor and the sensors were also subjected to temperature changes and pressure changes to determine their property. It was reported that the sample with thin boron-doped layer showed the highest gauge factor of 22 and the maximum sensitivity of the pressure sensors was 0.19% of resistance change at the differential pressure of 0.07 MPa at room temperature. It was also reported that there was a decrease in sensitivity with an increase in temperature.

Druzhinin et al. [42] had developed piezoresistive pressure sensors on the basis of semiconductor microcrystals and laser recrystallized SOI layers. It was reported that the strain gauges that were developed on the basis of Si microcrystals were able to operate to more than 10^7 load cycles of alternating strain with amplitude of $\varepsilon = \pm 1 \times 10^{-3}$ and a frequency of 50 Hz to 1 kHz. It was also stated that the sensor could also be used for impact and impulse loading without loss of sensitivity. One of the stated applications of the sensor was its use for the diagnostics of cerebral traumas in neurosurgery. The total height of the sensor developed was about 2.5 mm and its weight was less than 3 g. The sensor was capable of measuring pressure ranging from $(0-4) \times 10^4$ Pa. It was also stated that the output signal of the sensor was 40-60 mV

for an input excitation current of 10mA. There was no mention of the sensitivity of this sensor.

Blechsmidt et al. [46] had developed a pressure sensor probe that consists of 10 piezoresistive sensors and of overall dimension (4.5 x 5.5 x 1.4 mm) to assess the dynamic rectal pressure profile

Ferrarin et al. [47] had used piezoresistive sensor matrix to quantify parameters referred to pressure distribution in his study of comparative biomechanical evaluation of different wheelchair seat cushions. It was reported that by using these sensors, it was possible to analyze the pressure peaks, contact surfaces and the sitting modalities of different type of patients.

Wang and Beebe [47] had developed a silicon sensor that was able to measure both compressive (0-30N) and shear forces (5-40N) at the skin. The sensor design was based on the piezoresistive effect and was fabricated using an integrated circuit and MEMS technology. The sensor consisted of a silicon diaphragm structure that was instrumented with four piezoresistors. Each of the four piezoresistors works as an independent gauge. As force is applied to the sensor, the diaphragm is deformed resulting in the change of the resistance for each of the four resistors and from these resistor changes, one is able to resolve both the compressive and normal components of the force applied. It was reported that the sensors produced good repeatability and good accuracy measurements.

Beebe et al. [48] had attempted to convert a silicon based piezoresistive sensor from a pressure transducer to a force transducer. It was done by adding a force transmission structure (solid dome) to distribute an applied force load over the diaphragm surface. Two types of solid domes were fabricated. One was made of epoxy and the other was made of Torlon. Results show that the Solid dome made of Torlon produced low hysteresis and good repeatability. Load calibration results show that the sensor output (voltage output) was linear at low forces (up to 10 N) and they became non-linear for forces above 10 N. This might not be a good sensor for high force measurements such as for occlusion.

2.5 Capacitive Sensor

Capacitors are actually electrical energy storage devices that consist of two conductive plates that are separated by a dielectric material. The capacitor size or commonly known as capacitance is dependent on the plate area, the distance between the plates and the dielectric constant (permittivity) of the material that is separating the two plates. (The following figure clearly depicts a capacitor).

The relationship could be expressed mathematically by the following equation and the figure 2.5.1 depicts a capacitive sensor.

$$C_0 = \epsilon \left(\frac{A}{d} \right) \quad (1)$$

Where C= capacitance

ϵ = Dielectric Constant (permittivity) of the material

A = Plate area

d= Distance between the two plates

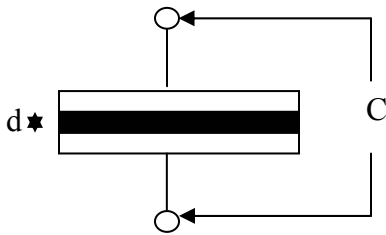


Fig2.5.1: Capacitive sensor

Capacitive type sensors, like piezoresistive sensor generates an electrical signal as a result of elastic deformation of a membrane. In this case, it is not the built-up stress in the membrane that leads to the signal generation; rather it is the displacement change in the membrane that results in the generation of the signal.

2.5.1 Working Principle of a Capacitive Sensor

If the dielectric layer is subjected to a uniform stress over the entire surface of the capacitive plates, such that there is a slight change in displacement Δd between the plates which are still parallel and the area remains constant, the resultant capacitance would be of as follows:

$$C = \epsilon \left(\frac{A}{d + \Delta d} \right) \quad (2)$$

From equation (1) and (2),

$$\begin{aligned} \frac{C}{C_o} &= \frac{\epsilon \left(\frac{A}{d + \Delta d} \right)}{\epsilon \left(\frac{A}{d} \right)} \\ &= \frac{d}{d + \Delta d} = d(d + \Delta d)^{-1} \\ &= d \times \frac{1}{d} \left(1 + \frac{\Delta d}{d} \right) \end{aligned}$$

using binomial expansion and since $\Delta d \ll d$,

$$\frac{C}{C_o} \approx 1 - \frac{\Delta d}{d} \quad (3)$$

The derived expression shows a linear relationship.

From equation 1, it can also be shown that

$$\frac{dC}{dd} = -\epsilon \frac{A}{d^2} \quad (4)$$

This equation shows that the sensitivity of the capacitor (the capacitance effect) increases proportionally with the square of distance d between the electrodes. Hence it could be concluded that for a small gap, a high sensitivity could be expected.

It should be noted that the above mentioned derivations were made on the assumption that the capacitors remain parallel while being subjected to stress. This is highly unlikely to happen in real situations. In most of the cases, the capacitance would be changed by

the deformation of one of the electrodes itself. As a result of this phenomenon, equations 2 and 3 would no longer be valid. Equation 2 could be written as

$$C = \iint_{x,y} \frac{\epsilon}{(d-w)} dx dy$$

where w is a function of the local deflection (x as well as y direction), due to the stress exertion on the sensor.

From equation 4, it could be deduced that, there is a non-linear relationship between the capacitance and the pressure/stress that is applied.

Pures [32] had stated some advantages of capacitive sensors, especially in the field of Bioinstrumentation. It was stated that capacitive sensors are temperature insensitive unlike other sensors, such as piezoresistive sensors which are very temperature dependent. It was also stated that the more commonly used sensors such as strain gauge are not very reliable for very low pressure changes as these sensors drift about 100 Pa per day. It was also stated in the paper that capacitive sensors have superiority against fluid-filled catheters. Although fluid-filled catheters do give accurate pressure readings, the external circuit is too cumbersome and it would also strain the patients' movement. It also hinders the use in telemetry devices. The lesser power consumption of capacitive sensors against the more commonly used sensors such as piezoresistive sensors makes the capacitive sensors very suitable for bio-medical use.

Clark and Wise [33] had stated some advantages of capacitive sensors against piezoresistive sensors. It was stated that capacitive sensors need less extensive processing as compared to the piezoresistive mail, as the former just requires just an electrode and also it is less susceptible to misalignment error. But even though it was stated that it is less susceptible to misalignment error, it is also important to note that the interelectrode distance is a very important parameter to be considered.

Sun et al. [61] had fabricated a MEMS micro force sensor to determine the flight force measurements of *Drosophila* (a type of fruit fly). Capacitive sensors were used as they had the advantage of low power, low noise, high sensitivity and they were insensitive to temperature variations. The Schematic diagram of the sensor design is depicted in the figures 2.5.1.1(a) and 2.5.1.1(b):

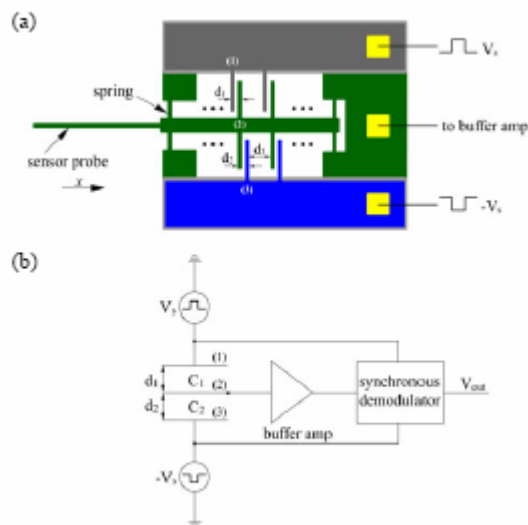


Fig2.5.1.1 (a): Sensor Schematic

Fig2.5.1.1 (b): Diagram of Sensor and Readout Circuitry

When a force is applied the sensor probe transmits the force causing the spring to deflect. This deflection would displace plate 2 away from plate 1 and displaces it closer to plate

When an AC signal is applied to the outer stationary capacitor, a voltage divider as would be formed. The resulting signal V_{out} would be:

$$V_{out} = V_s \left(\frac{C_1 - C_2}{C_1 + C_2} \right) \quad (3)$$

Where

$$C_1 = K\varepsilon \frac{A_1}{d_1} + K\varepsilon \frac{A_1}{d_3}, \quad C_2 = K\varepsilon \frac{A_2}{d_2} + K\varepsilon \frac{A_2}{d_3}$$

K is defined as the dielectric constant of the air and ε is defined as the permittivity of free space. The Areas A_1 and A_2 were same. The spacing d_o between the plates were such that:

$$d_o = \frac{d_1 + d_2}{2} \quad (4)$$

The plate distances were than defined as:

$$\begin{aligned} d_1 &= d_o + \Delta d \\ d_2 &= d_o - \Delta d \end{aligned} \quad (5)$$

In order to minimize the undesired additional parallel capacitance effect, the design was such that:

$$d_1 = d_2 \ll d_3 \quad (6)$$

From equation 2 and from the condition such that $d_1 = d_2 \ll d_3$, it can be deduced that

$$V_{out} = V_s \left(\frac{\Delta d}{d_o} \right) \quad (7)$$

The Stiffness of the spring was determined by the spring constant and the springs were modeled as two fixed beams with a point load applied in the middle such that:

$$\Delta d = \frac{Fl^3}{4Ew^3t} \quad (8)$$

Where F is the total applied force

E=Young's modulus

l=length of the spring

w = width of the spring

t= thickness of the spring

It was reported that the force sensor calibration resulted in a linear relationship between the voltage output and the force applied. The sensitivity of the sensor was reported as 1.35μN/mV.

2.6 Other Pressure Sensors

In recent times, pressure sensitive devices have been widely used in the field of dentistry to detect bruxism forces and occlusion forces. Some of the pressure sensitive devices would be discussed briefly in the following paragraphs

2.6.1 T-Scan

Over the years, dental occlusion had been a mystery for dentist. Dentists were using very remote methods of articulation paper, waxes and pressure indicator paste to assess and balance the forces of occlusion. These methods did not yield good results as they were not sensitive enough to detect the distribution of tooth contacts and the relative timing of them. Tekscan had developed the T-Scan system that was possible to detect the distribution of tooth contacts and the relative timing of them [34].

Studies have shown that the T-scan often gave misleading information. Harvy et al.[35] had investigated on the ability of the T-Scans' reproducibility by comparing 2 sets of occlusal data that was generated by an articulator that was set with 0 and 0.2 mm immediate side shift. Sensors were selected randomly and they were used in each of the 2 settings, three levels of load were applied to each sensor, and 5 repetitive tests were done. Results show that there was a substantial variability in the results that were obtained from the slide shifting of the articulator, different levels of force and also the different uses.

Studies by Hsu et al. [37] showed that the T-scan sensors did not have the same sensitivity throughout their surface and it always recorded fewer occlusal contacts than were actually present as checked by occlusal foils.

Saracoglu [38] had tested the sensitivity and reliability of articulating papers, foils, silk strips and T-scan system when used as an occlusal indicator. Special test was conducted to test the sensitivity of the T-Scan system. The evaluation was conducted with an aid of a universal testing machine. The sensors of the T-scan system were applied to the universal testing machine by means of special devices where three different sensors were placed at three different locations. Forces of 5kg, 10 kg and 20 kg were applied at the anterior region, premolar region and the molar region respectively. Results were obtained from 10 replications. Results show that the application of repeated strokes in the T-scan actually has led to a loss of sensitivity.

2.6.2 Pressure Sensitive Film (Dental Prescale, Fuji Film)

A newer but similar device has been introduced by Fuji Films Japan, to record the locations and the force of occlusal contacts with the film. The working principle of this film involves a layer of microencapsulated color-forming material and another layer of color-developing material. When there is any pressure applied, it would break the microcapsules and the color forming material would react with the color developing material forming red patches to appear on the film. The color density formed actually indicates the pressure level.

Hattori et al. (1994)[49] had evaluated the reliability of the Pressure Sensitive Film (Dental Prescale, Fuji film). It was reported that there was a linear relationship between the applied and measured loads.

Studies by Araki et al. [49] show that there was no bilateral balance of the occlusal forces in the patient.

Harris et al. (1999) [50] had used the Fuji films and K-scan sensors to measure tibiofenoral contact area. It was reported that contact area measured with the Fuji-films were 11-36% lower than that was measured with another type of sensor known as K-scan.

2.6.3 Pressure Measurement by Resistance change

Dobo-Nagy et al. [36] had developed a new pressure apparatus to provide measurements in simulated apical tissue of the pressure caused by occlusal loading. A minute resistor was used as a sensor to detect the pressure changes in the simulated occlusal loading experiment. The resistors were initially calibrated by finding the relationship between the pressure change and the resistor change in a pressure chamber prior to the actual experiment. The resistance changes to pressure changes were determined by the four resistances method based on Ohm's law. The calibration results showed a linear relationship between the pressure change and the resistance change. Favorable results were also obtained when the "device" was used in the actual experiment paving way for a new method of occlusion measurement in the field of dentistry.

2.6.4 Force Sensing Resistors

Force sensing resistors or more commonly known as FSR have gained popularity in recent times and have been widely used in the field of orthopedics and it is also widely used as tactile sensors for robotics applications. These sensors work on the principle of resistivity and their basic characteristics are piezoresistive i.e.: its resistance decreases with increasing normal pressure. These sensors can be manufactured in very small dimensions which give them an added advantage over the piezoresistive sensors mentioned in the earlier paragraphs.

Papakostas et al. [52] had developed a large area, flexible, tactile sensor that was based on the novel contact piezoresistive effect. It was reported that the contact resistance of the sensor was a function of the resistivity of the contacting surfaces, force and the roughness and elastic properties of the surface. The following equation clearly demonstrates the relationship.

$$R_c \propto \frac{\rho}{F} K \quad (9)$$

Where R_c is defined as the Contact resistance,

ρ is defined as the resistivity of the contacting surfaces

F is defined as the force

K is defined as a function of the roughness and elastic properties of the surfaces.

Novel gauge factor (GF_c) was defined to characterize the force sensitivity of contact piezoresistive sensors: The following equation defines the gauge factor

$$GF_c = \frac{d\left(\frac{1}{R_c}\right)}{dF} \propto \frac{1}{\rho K} \quad (10)$$

Where all the symbols that have been used have been defined before

From the equations defined above, it is very apparent that the sensitivity of the FSR could be altered by changing any of the parameters mentioned above.

It was reported that the sensor consisted of two 25 μ m thick polyester sheets that were laminated with adhesive in the non-sensing region. These sheets actually carried parallel,

thermoplastic, Ag-filled polymer conductive traces covered by a thermoplastic semiconductive ink of resistivity ρ . The materials were deposited by means of screen print technology. The orientation of the two sheets was such that their traces formed a grid with the semiconductive layers facing each other. This was done in such a way that each cross-section of the grid formed a contact piezoresistive force sensor. Although the paper provided detailed information on the manufacturing process of the FSR, there was no mention of the sensitivity of the FSR in the paper.

Jensen et al. [53] had developed a conductive polymer sensor for measuring external finger forces. The sensor consisted of a conductive polymer sensing element. The sensing elements were made two conducting inter-digitated patterns deposited on a thermoplastic sheet facing against another sheet containing a conductive polyetherimide film. The following figure 2.6.4.1

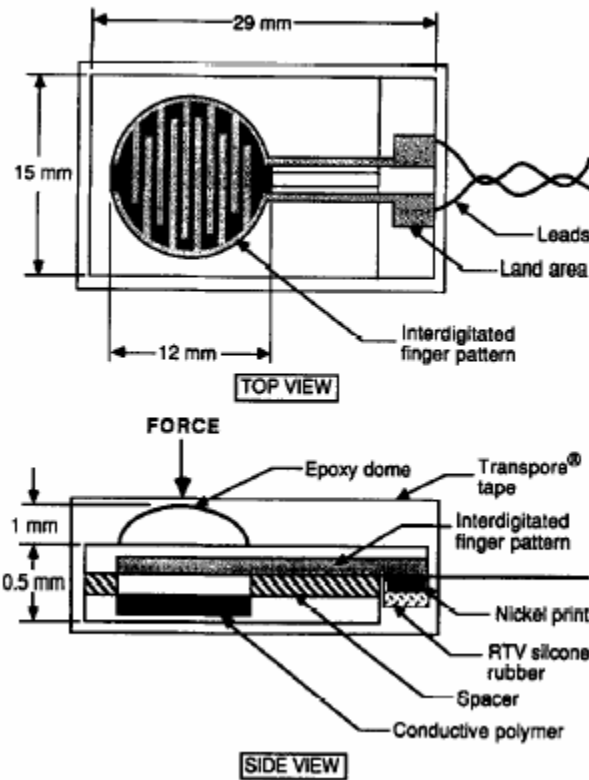


Fig2.3.6.4: Conductive Polymer Sensor

As can be seen from the diagram, there is a small cutout from the spacer that would allow the interdigitated finger pattern to come in contact with the conductive polymer when there is any application of pressure resulting in an electrical contact but otherwise it would result in the sensor having infinite impedance in an unloaded state. When pressure is applied, it causes an increase in contact area that subsequently decreases the electrical resistance and creates a shunt between the interdigitated patterns.

An epoxy dome was attached to the sensor to quantify the area, so the sensor could be used as a force sensor rather than a pressure sensor. The overall dimension of the polymer sheets were $29 \times 15 \times 0.5 \text{ mm}$

From experiments that were conducted, it was concluded that the conductive polymer sensing elements were sensitive to bending and the sensor response characteristics were

quadratic and its sensitivity decreased with applied force. It was also reported that these sensors had very low sensitivity to shear forces.

Hedman [54] had developed a new transducer comprising of a Force Sensing Resistor in series with a pressure-sensitive film to measure the time-dependent loads in human lumbar facet joints. The pressure-sensitive film was used to quantify the contact area as the FSR is sensitive to both force and the contact area. Calibration done of the FSR showed the presence of the hysteresis and this phenomenon was attributed to the visco-elastic nature of the isolated FSR. It was stated that the FSR showed good repeatability as when the FSR were set up loaded, removed and then repositioned and loaded again, the average peak load resistances of the nine cycles were identical and the initial load resistances varied by less than 10%.

It was reported that when the FSR was tested in a cyclic mode for 20 seconds, there was slight depression of the resistance in the unloaded state for subsequent cycle. This again was attributed to the visco-elastic nature of the FSR.

Experimental results also showed that unloading the FSR requires at least 4 seconds to minimize the effect of stress relaxation. It was concluded that because of its inherent visco-elastic nature, the device is deemed unfit for unloading measurements.

Nikonovas et al. [55] had developed a system to measure forces over the entire hand by means of a thin-film sensors (based on FSR technique) and associated electronics. The system developed was able to obtain force readings from up to 60 thin film sensors at a rate of up to 400 samples per sensor. Tekscan Flexiforce® was used as

the thin-film sensor. It was reported that the linearity of the sensors tended to decrease with use and this phenomenon was attributed to the plastic nature of the constituent materials.

Carpaneto et al. [56] had developed a sensor that was able to provide force measurement during grasp. The sensor consisted of a matrix structure ($24.36 \times 34.9 \text{ mm}$) with 64 sensitive sites based on FSR technology (Interlink Inc® Camarillo, CA). The matrix of the sensor is presented below in figure 2.6.4.2

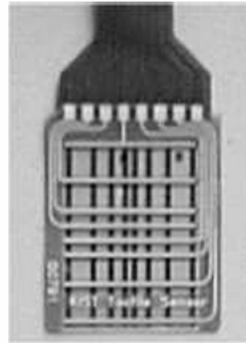


Fig 2.6.4.2: Matrix structure of the FSR

Based on the experiments carried out, it was concluded that the sensor had problems regarding the linearity (response output with respect to the load) and hysteresis and it might not be a very good sensor for processes involving precise measurements.

Fernandes et al. [57] had developed a novel force sensor to determine bite forces. The Bite sensor consisted of an inner sensor, an intermediate sensor and an outer surface. The inner sensor was made up of a circular conductive polymer pressure sensing resistor (FSR® Interlink Electronics, Luxembourg), the dimensions of the sensor is of as follows: diameter was 12mm and its thickness was about 0.25mm. The working principle

of the FSR has been described in the previous paragraphs. In order to convert the pressure sensor to a force sensor, the contact area was restricted by means by a steel plate whose thickness was 0.5mm and the diameter was 12mm. The restricted area was obtained by incorporating a central spherical depression into the steel plate. Figures 2.6.4.3 and 2.6.4.4 clearly depict the sensor.

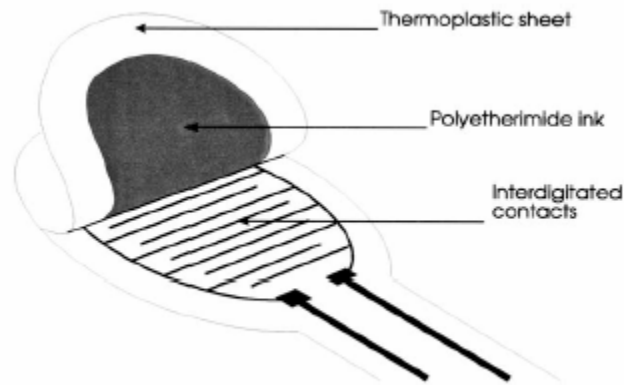


Fig2.6.4.3: Inner Sensor of Bite Force Instrument and Its Basic Components

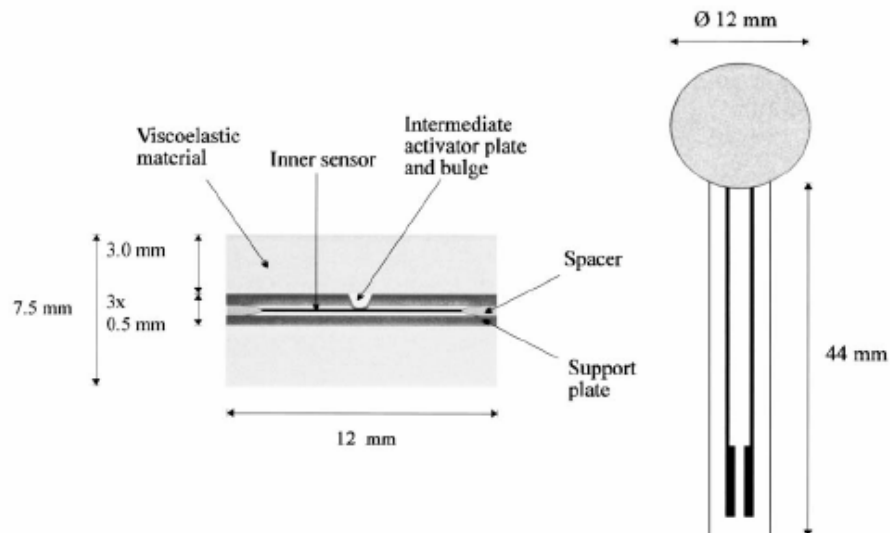


Fig2.6.4.4: Schematic Views and Dimensions of the Constructed Bite Force Sensor

Experimental studies on the sensor showed that the sensor had a non-linear relationship between the applied load and the sensor output. There was also a significant degree of hysteresis during the unloading process during calibration of the sensor. It was also reported that the loading rate also affected the linearity of the sensor. i.e.: only loading rates between 300 and 100 N/s had a linear response

2.7 Photo Diodes and its Working Principles

Photodiodes are semiconductor devices that react to high-energy particles and photons. Photodiodes operate by absorbing photons or charged particles producing a flow of current in an external circuit and this current flow in the external circuit is proportional to the incident power. It is a well known fact that the current through a reverse-biased semiconductor (for example a photodiode) arises due to the energetic creation of electron-hole pairs in the depletion region at the junction. This creation of electron-hole pairs could be done by means of thermal generation or by electromagnetic radiation of proper energy. If the rate of charge-carrier production by the electromagnetic radiation exceeds the rate of thermal radiation, the reverse bias current would be directly proportional to the photon flux or the light energy. Under limiting current conditions, the reverse bias current could be defined as follows [58]:

$$-I_p = b_\lambda Q_e P_k$$

where I_p is defined as the photo-current

P_k is the photon arrival rate or the flux

B_λ is quantum efficiency of the metal i.e. the number of photoelectrons that are emitted per incident photon

Q_e is the charge on the electron

Photo-diodes have been widely used for the measurement of pressure, temperature, flow, deflections and etc. They have many advantages, for example, they are able to operate at very high temperatures as well as very low temperatures and they offer good safety and noise immunity. Maalej and Webster [59] had developed an electrooptical force sensing transducer from a U-shaped metal spring. The working principle of the sensor is such that when a force is applied to the open end of the spring, it reduces the amount of light passing from the light emitting diode to the light-sensing photo-diode. It was claimed that the force transducer was able to measure forces up to 50N with a non-linearity of less than 7 percent and hysteresis less than 3 percent. It was also reported that the sensor cost only \$2 to build and it was used to measure forces on the side of the foot during normal human gait.

Sombatsompop et al. [60] had developed a new pressure sensor based on a photo-diode and a light emitting diode. The following figure 2.7.1 clearly depicts the sensor that was fabricated.

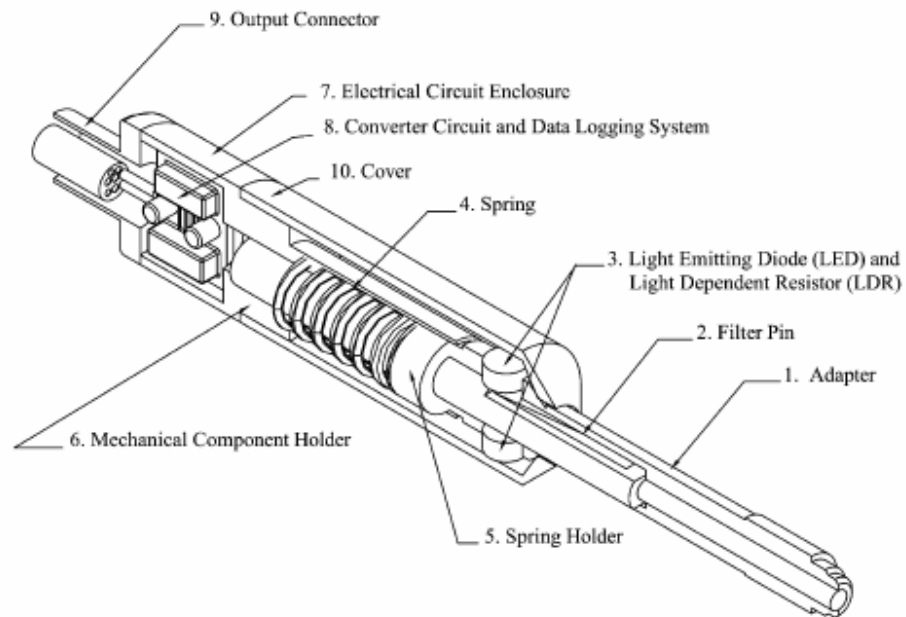


Fig 2.7.1: Pressure sensor photo-diode and a light emitting diode

The working principle of the sensor is such that when pressure is transmitted onto one end of the filter pin, it would result in the movement of the filter pin as well as the filter according to the amount of pressure applied. During the movement, it would allow different amount light to be transmitted from the light emitting diode to the light dependent resistor and hence resulting in a varying resistance of the light dependent resistor. By direct calibration, the resistance changes are converted to electrical voltage and hence the amount of pressure applied could be determined from the voltage output from the sensor. Their experiments showed that the voltage output was directly proportional to the pressure applied and the non-linearity of the sensor is less than 0.5% under full scale and the average hysteresis error was found to be $\pm 1.85\%$ full scale.

CHAPTER 3: EXPERIMENTAL METHOD and PROCEDURE

3.1 Piezoelectric Sensor Experimental Setup

The experimental setup is shown in the following Figure 3.1.4. The system consists of a load cell that had been calibrated prior to the use in this experiment, two amplifiers and an oscilloscope. One amplifier was used to amplify the charge generated from the piezoelectric sensor by 100 times and the other sensor was used to amplify the voltage produced from the load cell. The calibration of the load cell was such that 1 volt produced by the load cell due to an impact force equals to 444.8 N. A polyvinylidene fluoride (PVDF) [62] film of thickness 25 μ m coated with complete gold over platinum metallization over the two sides was used in this experiment. This type of piezoelectric film was chosen as it is completely bio-compatible material and it has been widely used in clinical settings previously [3, 17, 19, and 20].

The specification of the piezoelectric film that was used in this experiment is highlighted in table 3.1.1 [62]:

Table 3.1: Piezoelectric film properties used in this experiment

	d33 (pC/N)	d31 (pC/N)	d32 (pC/N)	Max. temp. use (°C)	Relative Epsilon
mono-oriented PVDF	20/23	-16	-3	75-80	11

where

$-d_{3j}$ refers to the piezo activity of the film. This corresponds to the delivery of electrical charges by 1 mm² of the film when it is subjected to a pressure of 1 pa along the defined “j” direction.

3.1.1 Sample Preparation

The piezoelectric sensors were cut to a dimension of 10mm (length) by 3mm (width) as shown in the following figure 3.1.1.

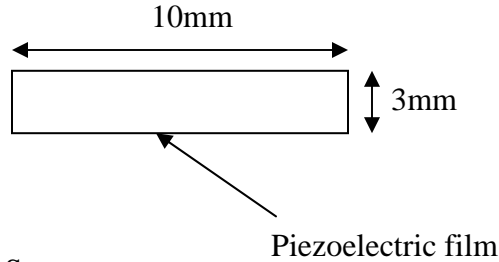


Fig 3.1.1: Piezoelectric Sensor

Tests were initially conducted by just dropping the impactor directly onto the piezoelectric film (without any protection). After numerous drops, it was observed that the piezoelectric film got permanently damaged. As the piezoelectric sensor is very easily susceptible to damage, it was embedded in a layer of orthodontic resin of about 1.5mm as a form of protection. 1.5mm was chosen based on two conditions. Firstly the layer of the orthodontic resin is thick enough to protect the piezoelectric film and secondly the thickness is thin enough so that the person who is wearing the Bruxism guard does not feel uncomfortable and this sensor (embedded into the mouth guard) does not impede the normal mandibular closure. Similar thickness was successfully used by Takeuchi et al [20]. Before the Piezoelectric sensor was embedded in orthodontic resin, a small piece of cellophane tape was used to cover the top surface of the piezoelectric film to prevent the orthodontic resin (in solution form, when it is in the process of curing) from seeping onto the film, thus damaging it. As the piezoelectric film is not able to withstand high temperature, (it can only withstand up to 80°C) [62], it was not possible to solder electrical contacts directly onto the film. Thus copper tapes (3M 1182 copper tapes) were used as the interface between the external connections and the piezoelectric film. One

side of the copper tape is attached to the piezoelectric film and the other side is used to solder to the connecting wires. The film together with the copper tape was trapped with a Teflon tape before the sensor was embedded in the orthodontic resin. This is done in order to prevent any short circuit from occurring. The following figure 3.1.2 gives a very clear depiction of the process mentioned above.

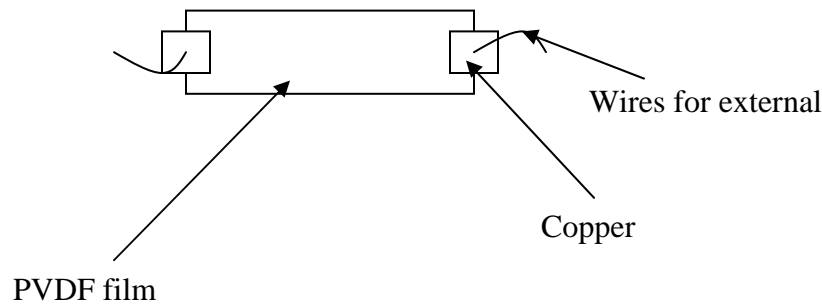


Fig 3.1.2: Sample Preparation of the PVDF Sensor

The wires were then connected to a charge amplifier. The charge amplifier had an inbuilt low pass filter. There is a need for the charge amplifier (incorporated with a low pass filter) since the charge produced by the film drains rapidly after the initial contact, an amplifier is necessary to sample and record the peak output signal at the time of load application. The low pass filter was necessary to filter out the high frequency electrical noise. The low pass filter setting was set to 30Hz (i.e. the filter cuts off or attenuates signals that are higher than 30Hz) with a time constant of 10s (i.e.: the time taken charge the capacitor to 63.2% of the input voltage). A typical first order low pass filter and a typical 1st order low pass filter with Op amp are shown in the figure 3.1.3 [63]. The sensitivity of the amplifier was tuned to 23 pC/N as specified by the manufacturer.

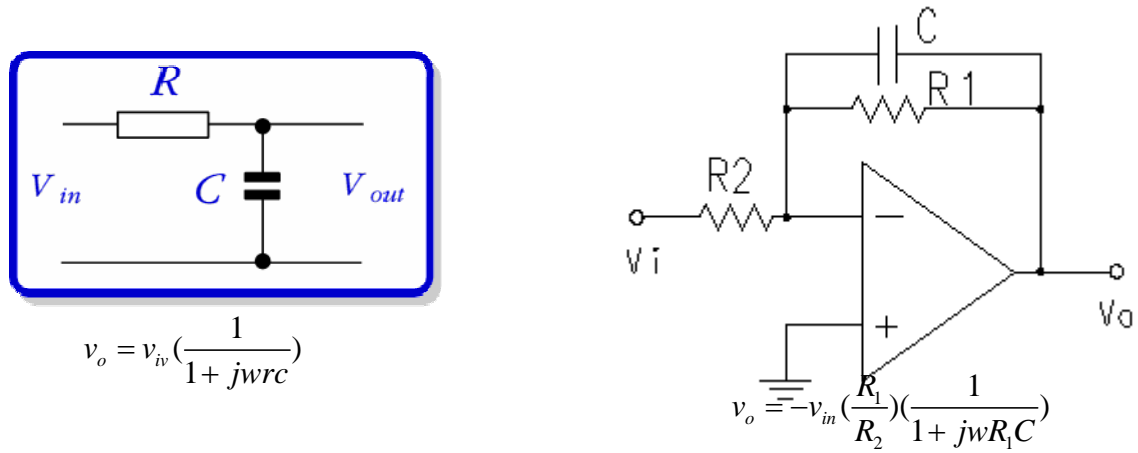


Fig 3.1.3: A Typical Low pass filter with an Operating Amplifier

As for the load cell, the amplification was set to 10 times and the amplifier also had an inbuilt low pass filter. The low pass filter was tuned to a rating of 30Hz with a time constant of 10s as well.

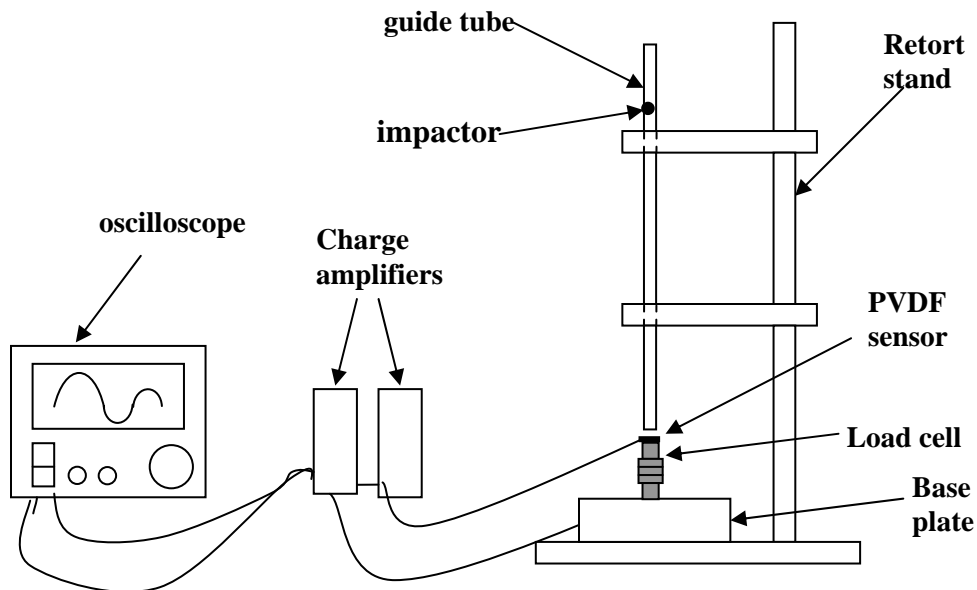


Fig3.1.4:Calibration of the Piezoelectric Sensor

The whole experimental setup to calibrate the piezoelectric sensor is shown in figure 3.1.4. The PVDF film was secured strongly to the load cell by a double sided tape. The actual setup is shown below in figure 3.1.5.

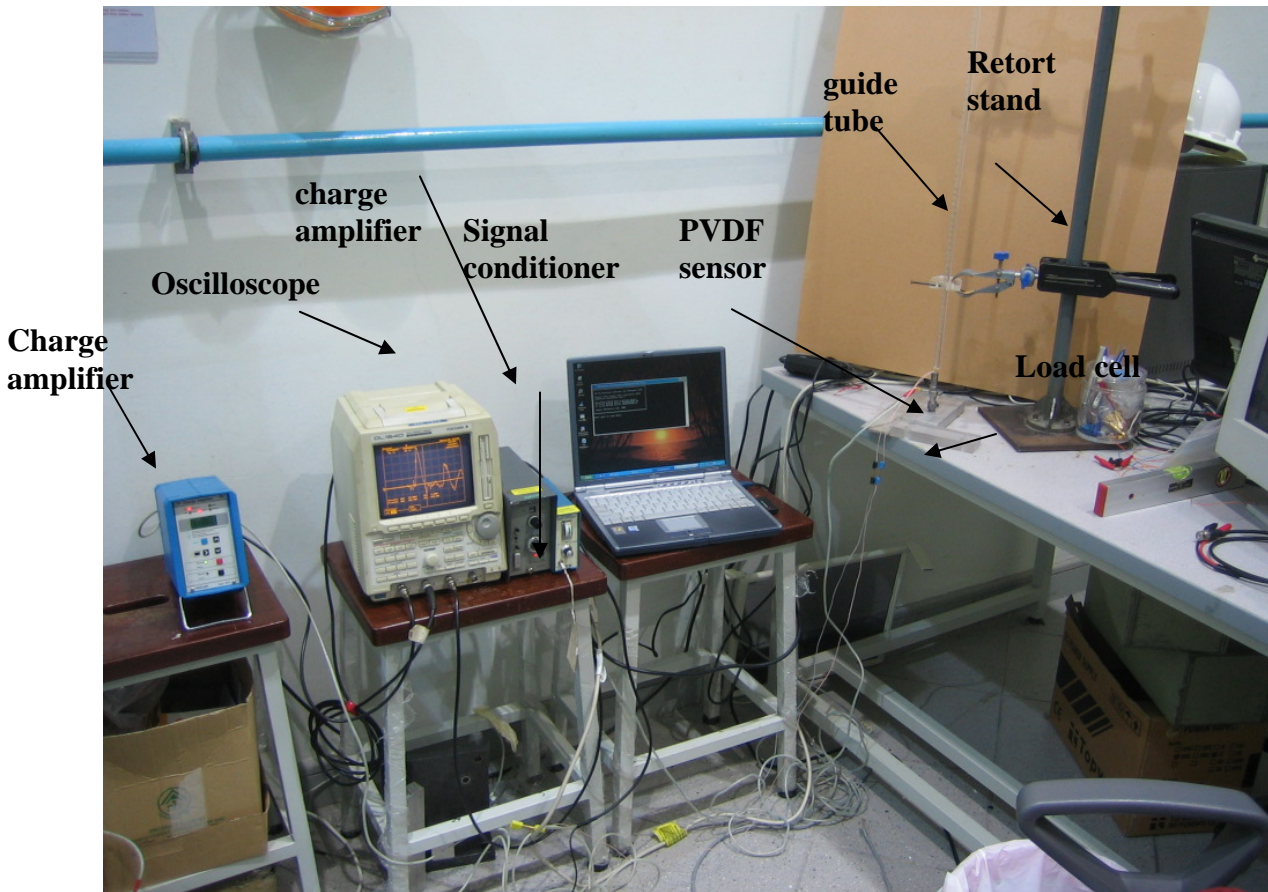


Fig 3.1.5: Actual Setup to calibrate the Piezoelectric Sensor

The impactor was released from various marked positions on the guide tube to calibrate for different forces. When the impactor hits the load cell, the impact produced by the impactor created signals in the oscilloscope and with prior calibration, the actual force exerted on the load cell as well as the PVDF film was determined from the voltage signals that were obtained. Figure 3.1.6 shows typical results obtained from the oscilloscope.

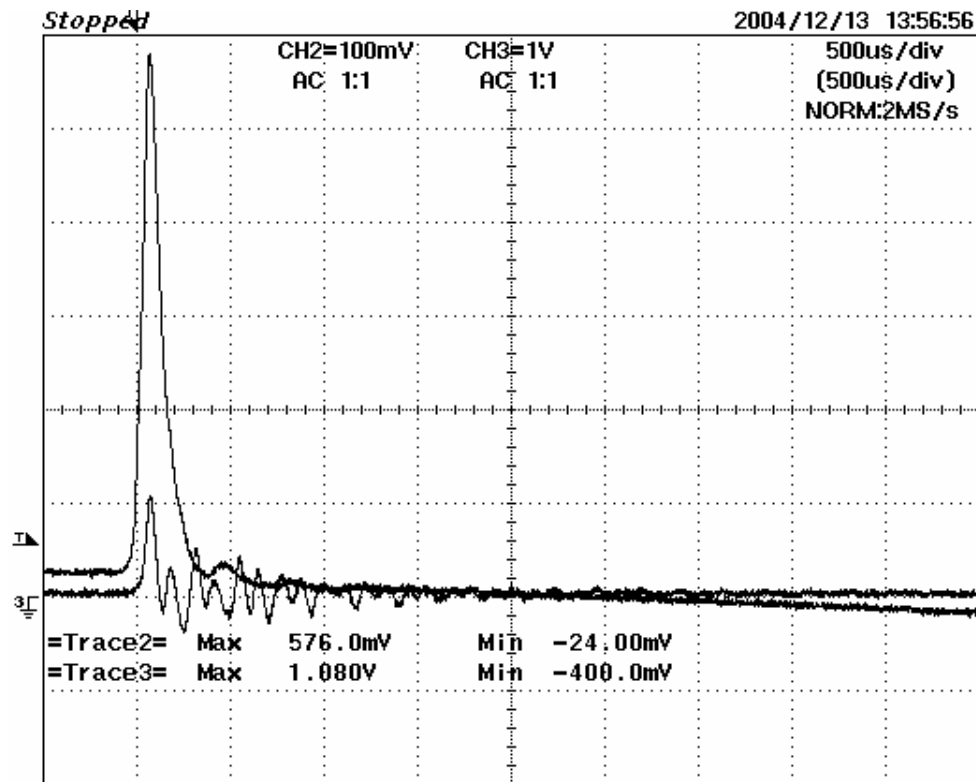


Fig 3.1.6: Typical Results obtained from the oscilloscope while calibrating the Piezoelectric Sensor

3.1.2 Experimental Procedure and Results

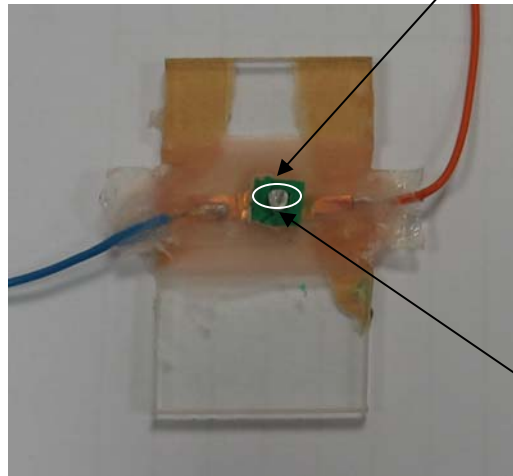
The impactor was dropped from heights ranging from 60mm to 80mm to create different impact forces. With prior calibration (1V is equivalent to 444.8N), the force exerted was determined by the peak voltage signal produced by the load cell. The peak voltage signal produced by the piezoelectric film was also noted. The experimental results would be discussed in the following paragraphs.

In the initial run of experiments, the piezoelectric film was directly embedded into the orthodontic resin of about 1.5 mm (as shown in the Figure 3.1.7). The voltage output was not very high. This could be attributed to the absorption of energy by the orthodontic

resin upon impact. The detector system was then modified to obtain a higher voltage output. An aluminum metal sheet was planted onto the orthodontic resin as shown in Fig 3.1.7. This modification was done so that there is direct contact between the teeth and the piezoelectric sensor thus exerting maximum force onto the piezoelectric sensor. Figure 3.1.7 shows the Sensor.

Orthodontic
Resin

Aluminum
metal



Silicone
Rubber

Fig 3.1.7: Piezoelectric Sensor Used for this Experiment

The sensor was tested for compressive force by means of Instron 5848 Microtester. Instron Blue-hill software was used to simulate a continuous compressive force. The output from the sensor was observed through the oscilloscope. The whole set-up is depicted below in figure 3.1.9 for reference.

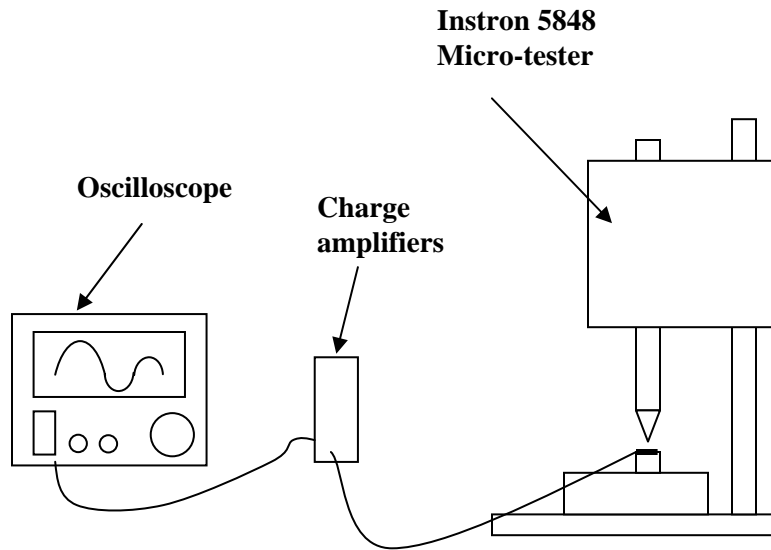


Fig: 3.1.9: Setup to calibrate the Piezoelectric Sensor

3.2 Piezoresistive Sensor (Honeywell FSL05N2C) Experimental Setup

Piezoresistive sensors have been widely used as pressure sensors for a long time. Piezoresistive force sensors (Honeywell FSL05N2C) [64] were next used to detect bruxism forces. A clear depiction of these sensors is given below in Figure 3.2.



Fig 3.2: (Honeywell FSL05N2C) Piezoresistive Sensor

This sensor features a proven sensing technology that makes of specialized piezoresistive micro-machined sensing element. This sensor works on the principle that

the resistance of the piezoresistors made of silicon increases when flexed under an applied force. The sensor concentrates force from the application through the stainless steel plunger which is directly in contact with the silicon sensing element. The amount of resistance change is proportional to the amount of force exerted. This change in resistance could be converted to a voltage output by connecting the sensor to a calibrated Wheatstone bridge. Detailed working principles of piezoresistive sensors have earlier been explained in the literature review. In accordance with the specifications given by the manufactured (Honeywell), it is widely used in the following areas:

- Medical infusion pumps
- Ambulatory non-invasive pump pressure
- **Occlusion detection**
- Kidney dialysis machines
- Load and compression sensing
- Variable tension control
- Robotic end-effectors
- Wire bonder equipment

Thus this sensor would be suitable for this application. As this sensor is only able to measure forces up to only 15N, some modification has to be done in order to use it for bruxism force detection that requires a force measurement to at least 200N. The top layer of the sensor was removed and the stainless steel plunger was subsequently removed. A layer of silicone rubber (mixture of Cavex Stabisil Washer and Cavex Stabisil activator that acts as a catalyst) and a layer of orthodontic resin (Melidont self cure denture repair

material and Heraeus Kulzer Meliodent Rapid repair) of 2mm were used to attenuate the force, so that the sensor is able to overcome forces up to 200N. The figures 3.2.1(a) and 3.2.1(b) below depicts the sensor (all dimensions given in mm):

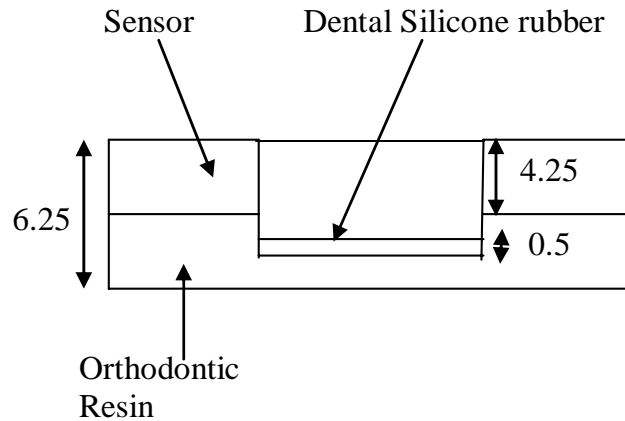


Fig 3.2.1(a): Piezoresistive Sensor

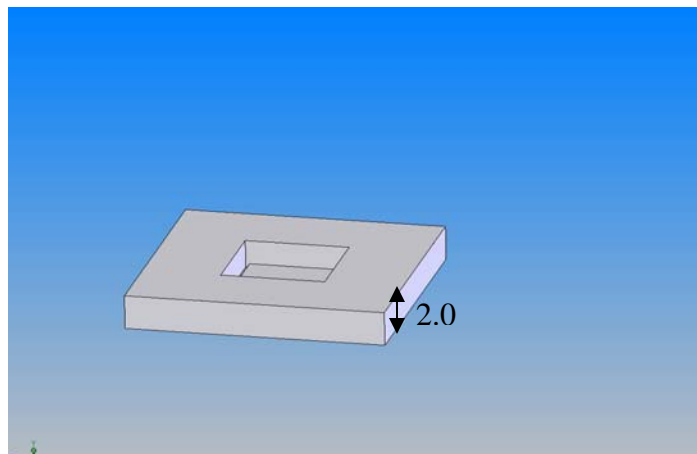


Fig 3.2.1(b): Piezoresistive Sensor

The Piezoresistive sensor would be placed inside the cavity. 2mm of orthodontic resin was used as any thinner would result in the damage of the sensitive silicon sensitive element and any thicker would not be viable in our application. The sensor was then tested with the 5848 Instron Microtester. In this case Instron Wave-maker together with Instron Blue-hill software were used as besides calibrating the sensor, it was also used to

simulate at various load conditions to test for the **Repeatability**, **Linearity**, **Hysteresis** and the **Drift** of the sensor under the various test conditions.

Repeatability:

Repeatability is the ability of the sensor to respond in the same way to a repeatedly applied force.

Linearity:

Linearity refers to the sensor's response (digital output) to the applied load, over the range of sensor. This sensor should ideally be linear; any non-linearity of the sensor is the amount that its output deviates from this line.

Hysteresis:

Hysteresis is the difference in the sensor output response during the loading and unloading, at the same force. Generally for static forces, and force application that if only increased and not decreased, the effects of hysteresis are minimal. If an application includes both load decrease and as well as load increase, there might be higher chance of error introduced by hysteresis that is not accounted for by calibration.

Drift:

Drift is the change in sensor output when a constant force is applied over a period of time.

3.3 Thin film flexi force Sensor Experimental Setup

The Flexiforce sensor uses a resistive-based technology (similar to piezoresistive technology). The application of a force on the sensing area of the sensor results in the change of the resistance of the sensing element that is inversely proportional to the force that had been applied. Figure 3.3 shows the flexi-force.



Fig 3.3: Flexi force Sensor

The flexi force sensor is an ultra-thin and flexible printed circuit that could be easily integrated into most applications that requires force measurements. The sensors are constructed of 2 layers of substrate. This substrate is composed of polyester film. On each layer, a conductive material (silver) is applied, followed by a layer of sensitive ink. The sensor is then formed by laminating the two layers by means of an adhesive. The silver circle on top of the pressure-sensitive ink defines the “active sensing area.” Silver extends from the sensing area to the connectors at the other end of the sensor, forming the conductive leads. The sensor acts as a variable resistor in an electrical circuit. When there is no load on the sensor, the resistance of the sensor is very high (it is much greater than 5 Meg-ohm). When a force is applied, its resistance decreases. In order to convert the resistance change to voltage output, a circuit shown below in Figure 3.3.1 was designed.

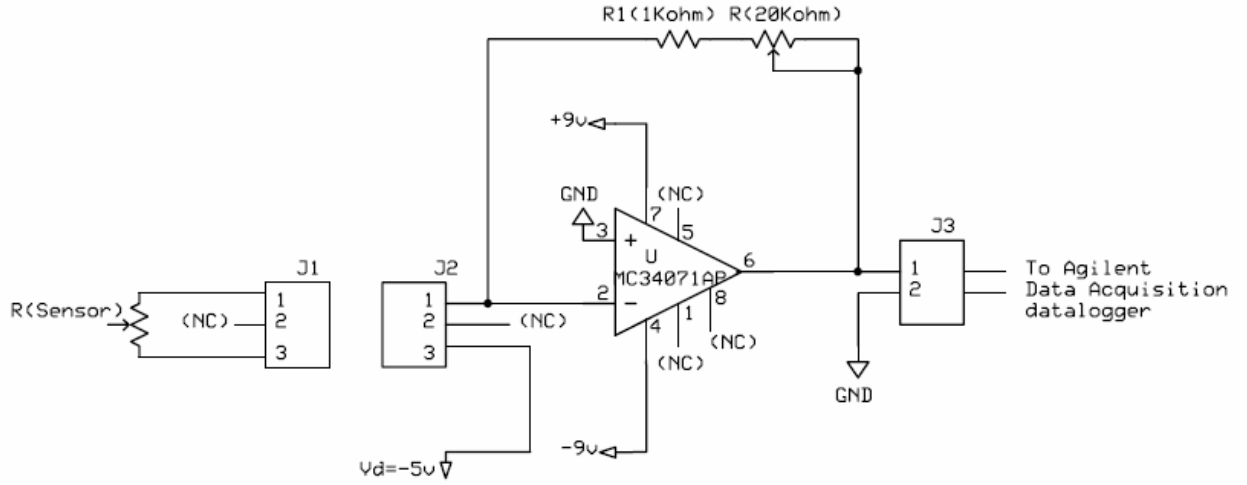


Fig 3.3.1: Circuitry for the Flexi force Sensor

The sensor was connected to connector (J1). The connector is connected to an inverting operational amplifier as shown. (MC34071AP). This type of operational amplifier was chosen due to its high bandwidth product (4.5MHz) and due to its high slew rate (13V/μs).

From op-amp analysis it can be seen:

$$\frac{V_{out} - V_-}{R_F} + \frac{V_D - V_-}{R_{S1}} = 0,$$

$$\text{Where } R_F = R_1 + R_{F1}$$

Assuming ideal Op-Amp (High input impedance)

$$V_- = V_+ = 0V$$

$$\therefore V_{out} = -V_D \times (R_F / R_{S1})$$

As the Agilent Data-logger (34901A, 20 channel multiplexer; data acquisition unit) has an inbuilt Analog to Digital converter, the output from the sensor could be directly attached to the Data-logger; there is no need for an external Analog to Digital converter chip. The Experimental setup is shown below in figure 3.3.2(a) and 3.3.2(b):

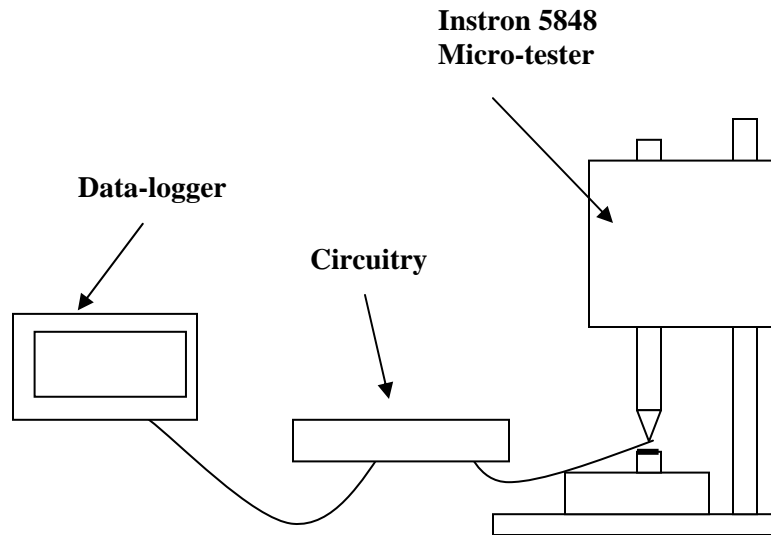


Fig 3.3.2(a): Cross-Sectional View of the Experimental Setup

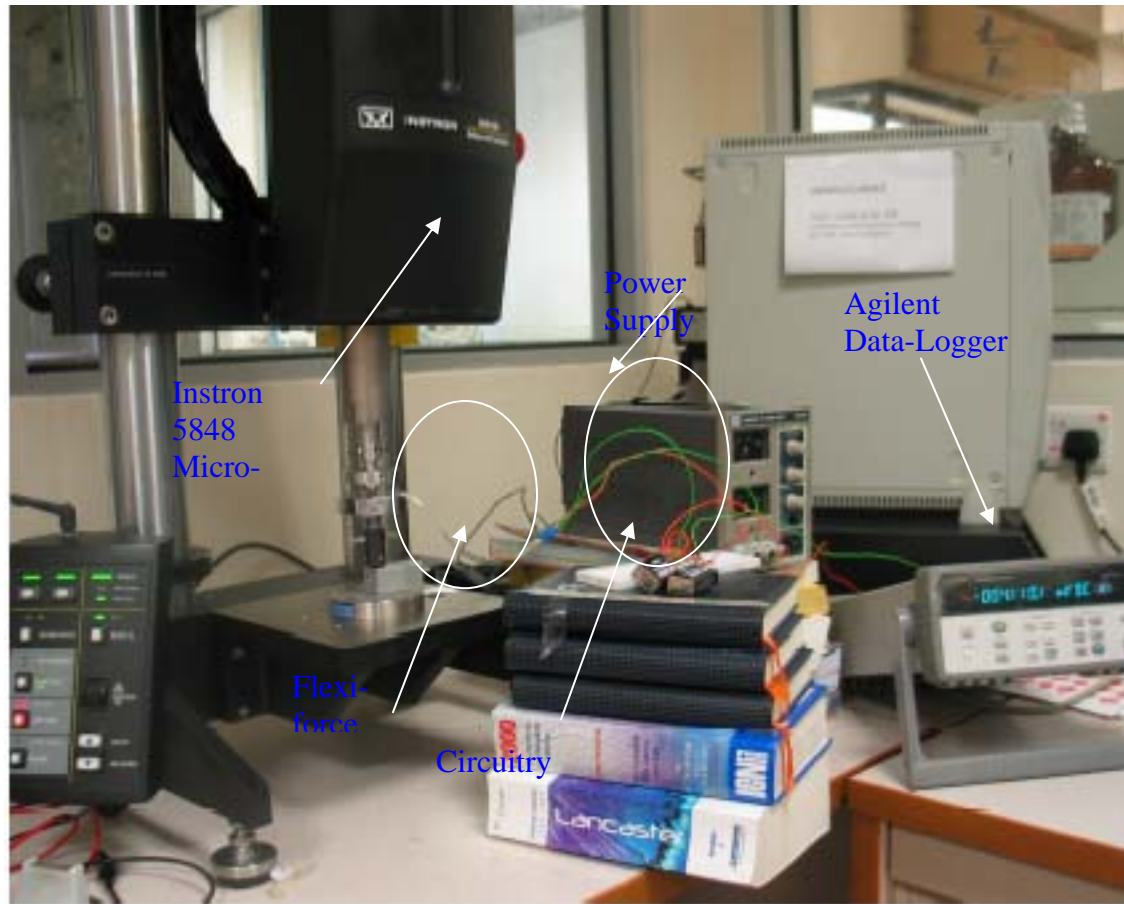


Fig 3.3.2(b): Actual Experimental setup.

A puck of 1.5 mm of orthodontic resin was placed on the sensing area of the sensor before any force was applied as direct contact of the impactor with the sensor would damage the sensor. It was also noted that that the puck just covered the sensing area and it did not touch any of the edges of the sensing area, or otherwise, these edges may support some of the load and give an erroneous reading. Before testing the sensor, it was conditioned to lessen the effects of drift and hysteresis. Conditioning is required for new sensors, and for sensors that has not been used for a length of time.

According to the specifications given by the manufacturer, the sensor was conditioned by placing 110% (220N) of the test weight on the sensor. The sensor was then allowed to stabilize, and subsequently the weight was removed. The sensor properties (as given by the manufacturer) [34] are given below in Table 3.3 for reference.

Table 3.3: Sensor Properties of the Flexiforce Sensor

Sensor Properties	Model A201
Operating Range	15°F(-9°C) to 140°F(60°C)
Linearity (Error)	<+/-5%
Repeatability	<+/-2.5% of full scale (conditioned sensor,80% force applied)
Hysteresis	<4.5% of full scale (conditioned sensor,80% force applied)
Drift	<3% per logarithmic time scale (constant load of 90% sensor rating)
Temperature Sensitivity	Output variance up to 0.2% Per degree F (approximately 0.36% per degree C). For loads>10 lbs., operating temperature can be increased to 165°F (74°C)

From the specifications given by the manufacturer it seems to be an ideal sensor for our application.

3.4 Photo-Sensitive force Sensor Experimental Setup

Next a photo-sensitive sensor was developed. As the photo-sensitive sensor could be made small, it seems to be a good choice for our application. The working principle would be discussed in the following paragraphs. Figure 3.4 shows a cross-section of the transducer

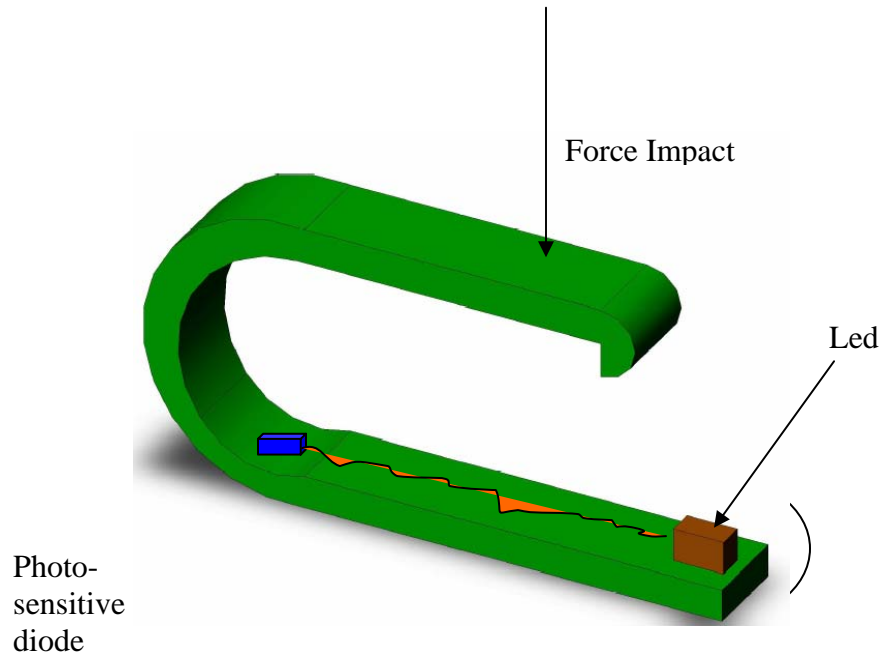


Fig3.4: Cross-sectional View of a Photo-Resist Sensor

The transducer consists of a flat U-shaped metal spring as shown. When a load is applied at the top of the metal surface, the upper beam of the spring would deflect towards the lower beam. This deflection would then be used to hinder the light beam from the Led to the light sensor that is mounted inside the metal beam. The light sensor voltage output changes linearly with the amount of incident light power. Although the relationship between the beam deflection and the light transmission would be expected to

be non-linear, with appropriate amplification and biasing circuit, the voltage output could be measured.

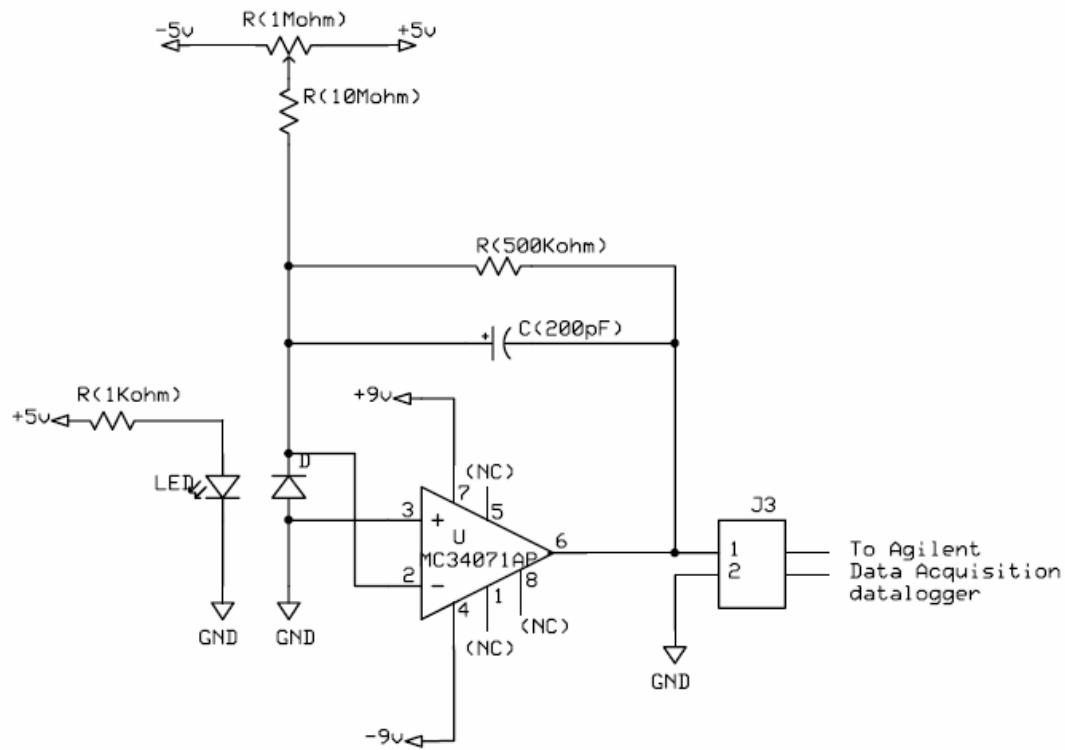


Fig3.4.1: Interface Circuitry for Photo-Resist Sensor

The output of the photodiode has signal values on the order of tens of nano-amperes to tens of microamperes, thus the signal requires amplification to provide useful readings. The amplification is provided by the inverting amplifier (MC34071AP). A low pass filter of time constant $100\mu\text{s}$ ($T=RC=500*10^3*200*10^{-12}$) was also designed to filter off the high frequency noise and light interference. Figure 3.4.1 shows the interface circuitry for the Photo-Resist Sensor

The sensor was subjected to different load by means of the Instron Micro-Tester. The voltage output with respect to the force was observed. Figures 3.4.2(a) and 3.4.2(b) clearly depicts the experimental setup.

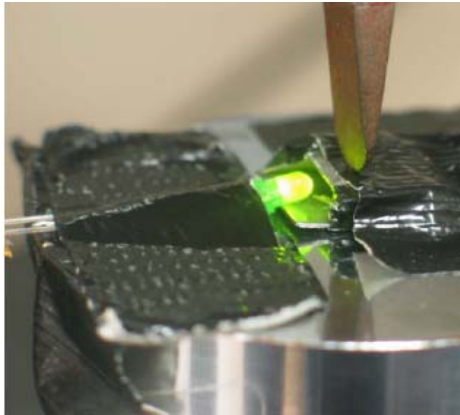


Fig 3.4.2(a): Experimental setup

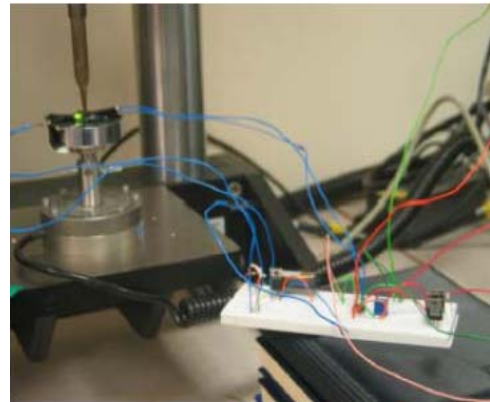


Fig3.4.2 (b) Experimental Setup

3.5 Strain Gage Force Sensor Experimental Setup

Strain gage sensors (constantan strain gages) were used. Strain gages were used mainly due to their small size, cheap cost and accurate signal outputs. A miniature button sensor as shown in the Figure 3.5 was fabricated. Small button strain gage sensors were developed with various thicknesses to determine the voltage output with respect to the applied forces. A schematic diagram of a button strain gage sensor (of diaphragm thickness 0.7mm) is depicted below in Figure 3.1.18. Diaphragms made of both stainless steel and aluminum were tested to determine their voltage output. These materials were chosen for their bio-compatibility nature

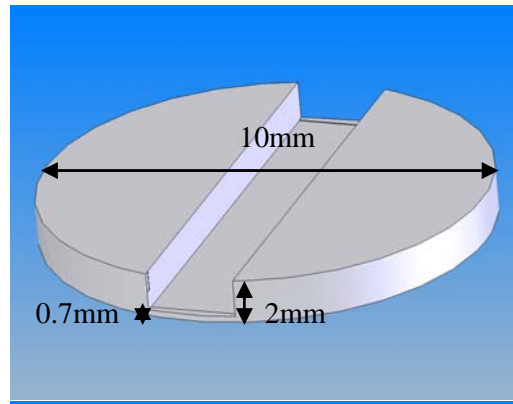


Fig3.5: Dimensions of the stainless steel/Aluminum diaphragm. The strain gage would be placed in the cavity.

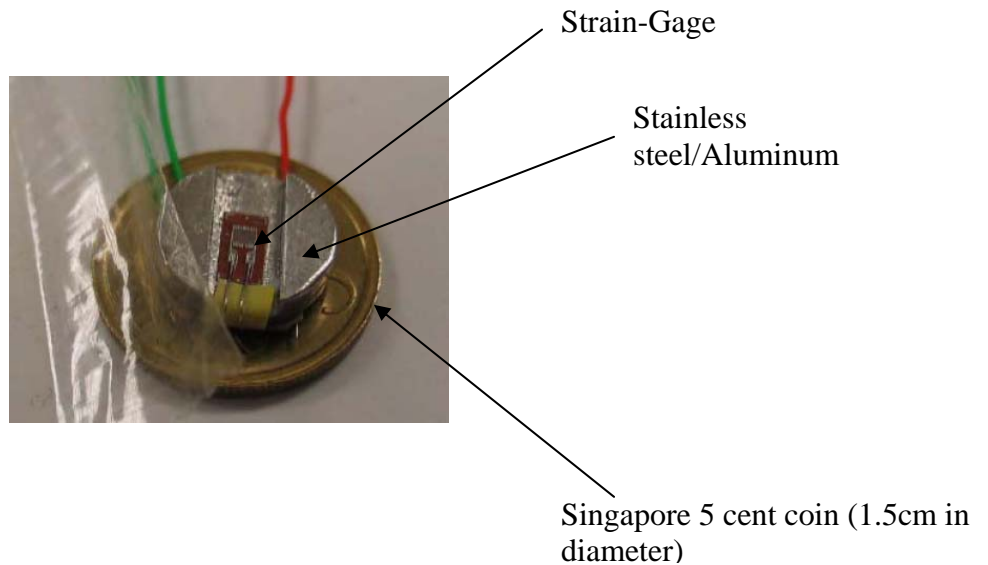


Fig3.5.1: Strain gage sensors in comparison with a Singapore 5 cents coin (1.5cm in diameter)

The experimental setup is quite similar to the previous setups and thus would not be explained in depth. The experimental setup is depicted below in Figure 3.5.2.

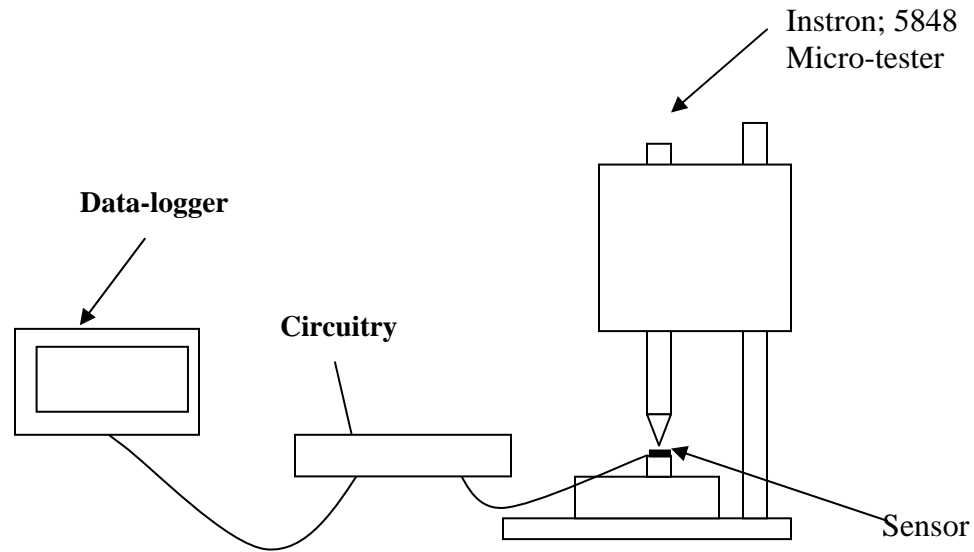


Fig 3.5.2: Experimental Setup for the strain Gage Sensor

The circuitry consists of 1 active gage and 3 wire system. The following figure 3.5.3 depicts the circuitry.

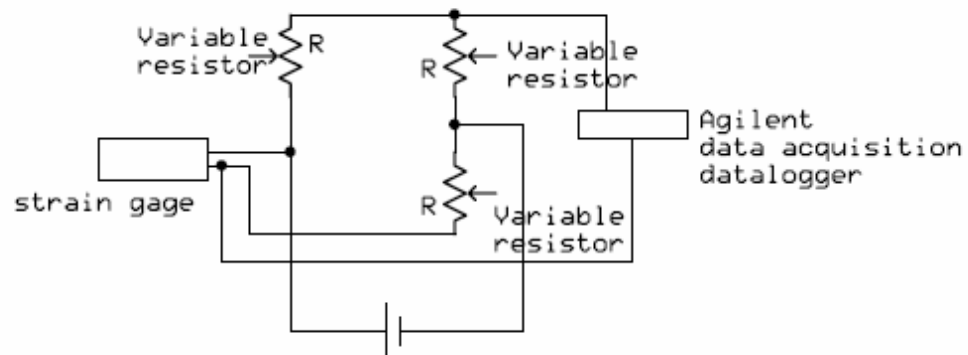


Fig3.5.3: Circuitry for the Strain Gage Sensor

The two different (stainless steel/Aluminum) diaphragms were subjected to different load profiles and their output voltage output was observed.

3.6 Piezoresistive Strain Gage force Sensor Experimental Setup

The experimental setup is exactly the same as for the constantan strain gages and thus no further explanation would be given. Only the variable resistors were adjusted to suit the piezoresistive strain gage (KSP-1-350-E4, Kyowa semiconductor strain gages). Tests were carried out with different load profiles and the results obtained would be discussed in the following Chapter:

CHAPTER 4: RESULTS AND DISSCUSSIONS

4.1 Piezoelectric Sensor

The piezoelectric sensor was first subjected to varying dynamic forces. The experimental procedure was discussed in the previous chapter. Figure 4.1 shows the experimental results that were obtained.

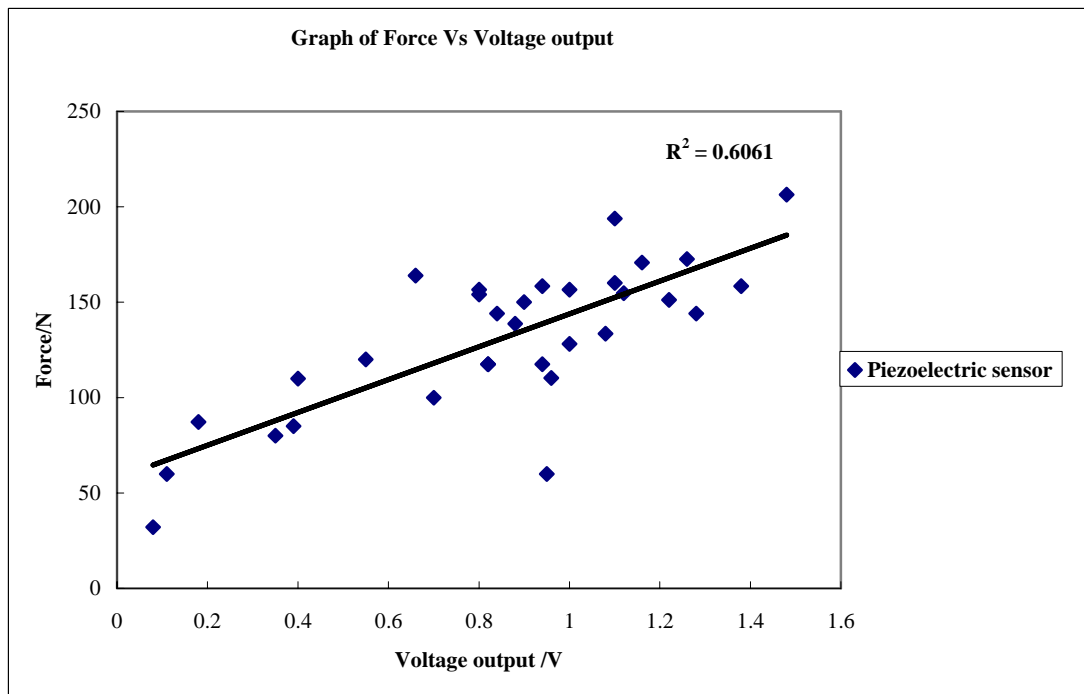


Fig 4.1: Experimental results obtained from the piezoelectric sensor

From the experimental results obtained, it can be seen that the piezoelectric sensor produces a relatively linear output. The slight variation in the outputs can be attributed to the slight movement of the sensor upon impact by the impactor on the sensor system. From this calibration curve it was proven that the piezoelectric sensor seems to be a suitable sensor for impact motion. The sensor was next tested for compressive force as bruxism consists of both dynamic and compressive motion.

The sensor was tested for compressive force by means of Instron 5848 Microtester. Instron Blue-hill software was used to simulate a continuous compressive force. The output from the sensor was observed through the oscilloscope. The actual setup was explained in the previous chapter. There were signals only during the first impact (when the impactor first touches the sensor) and subsequently when the impactor was released from the sensor (after the sensor has gone through the 200N compression and returns to its original position). These experiments clearly show that although piezoelectric sensors are ideal for our application, it is only capable of measuring dynamic forces and is not suitable for the measurement of static forces which makes it unsuitable for our application. This phenomenon of piezoelectric sensors being able to measure only dynamic forces can be attributed to the fact that the material has its own internal resistance and any charge that is produced across the film by a steady force would be dissipated away quickly. Piezoelectric transducers could be modeled as an equivalent circuit consisting of a capacitor and a resistor as shown in the following figure 4.1.2.

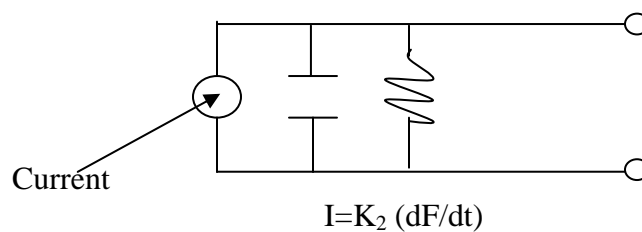


Fig 4.1.2: Equivalent Circuit of a Piezoelectric Sensor

When a steady force is applied, it does not produce any current which results in zero voltage. This is the reason why piezoelectric sensors are more suitable for dynamic

motions and not static motions. Takeuchi et.al [20] had used piezoelectric film based intra-splint for the detection of bruxism events in humans and had compared to that of measurements taken using EMG. He had concluded that steady-state clenching task was best captured in the EMG sensor although he did not mention that no signals were obtained in the case of piezoelectric sensors.

4.2 Piezoresistive Sensor (Honeywell FSL05N2C)

The piezoresistive sensors were subjected to different loading patterns to determine the output and to check its consistency under the different loading rates and patterns. Instron 5848 Microtester Instron Blue-hill software was programmed to simulate the loading profiles.

A force of 200N was applied at different loading rates and patterns to determine the repeatability of the sensor. The load profile and the sensor response (in terms of volts) are shown in Figures 4.2.1 to 4.2.5

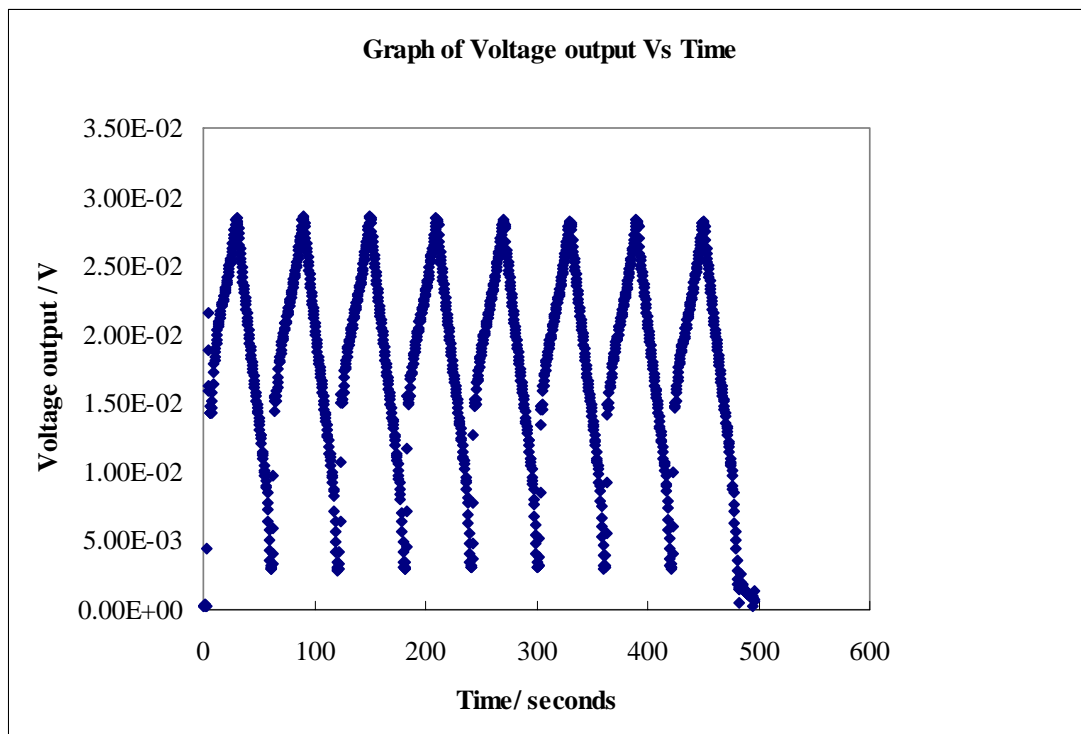
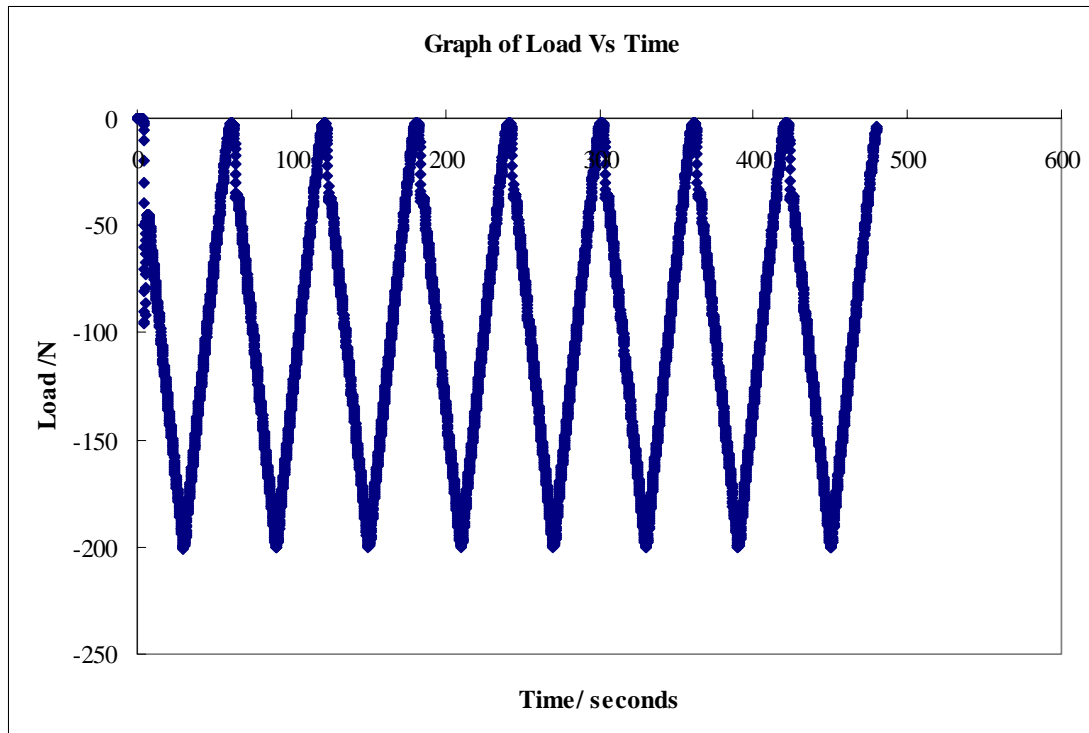


Fig4.2.1: A load of 200N was applied for a time span of 20 seconds. The 200N force was applied for another 60 seconds and the force was gradually reduced to zero force within another 20 seconds.

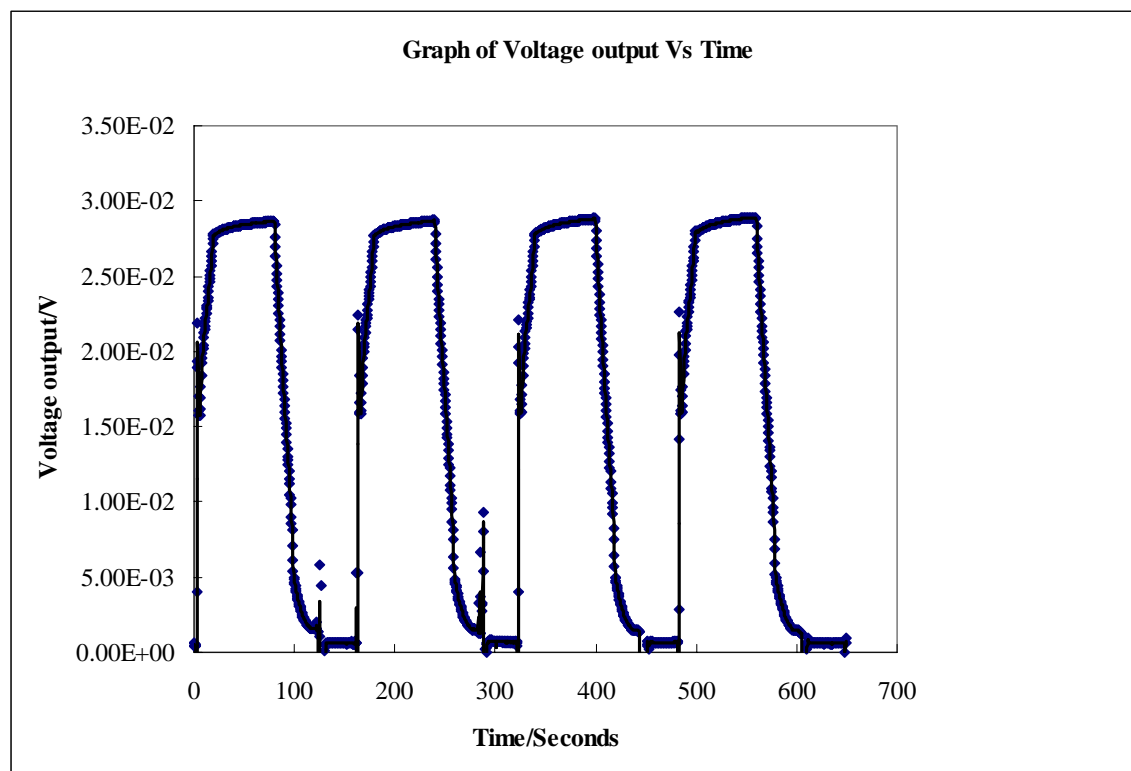
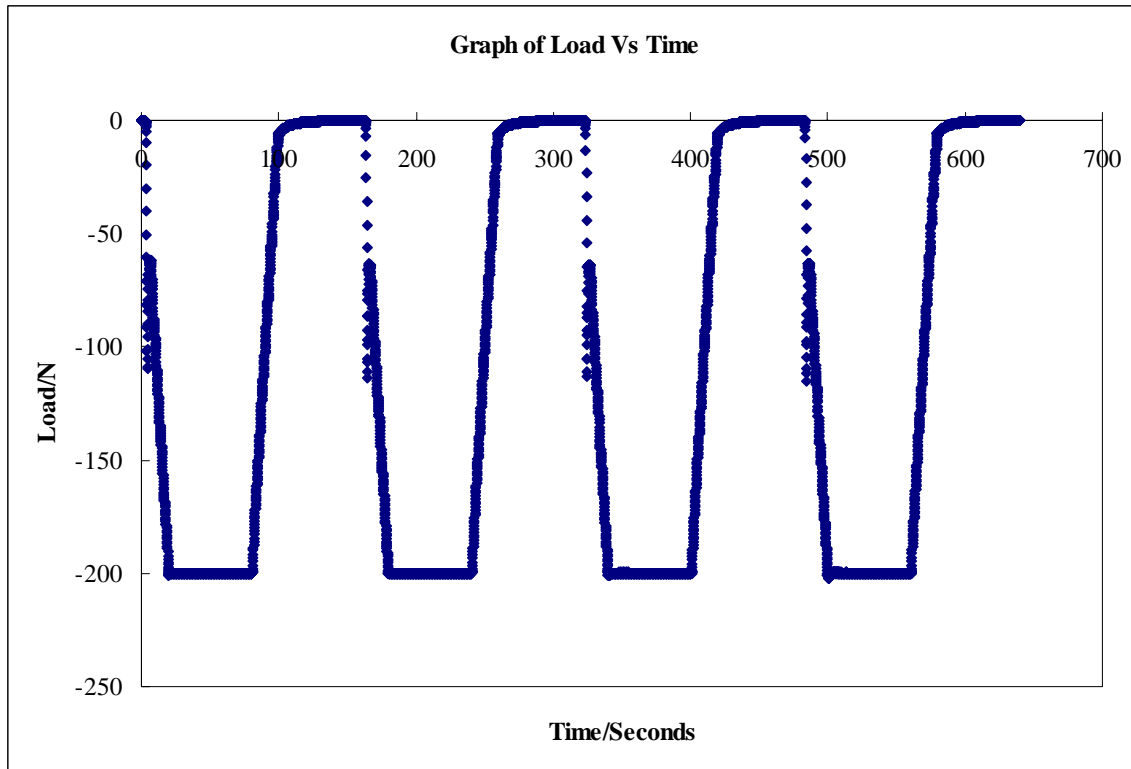


Fig4.2.2: A load of 200N was applied continuously for a time span of 10 seconds and that load was gradually removed to zero force within a time span of another 10 seconds

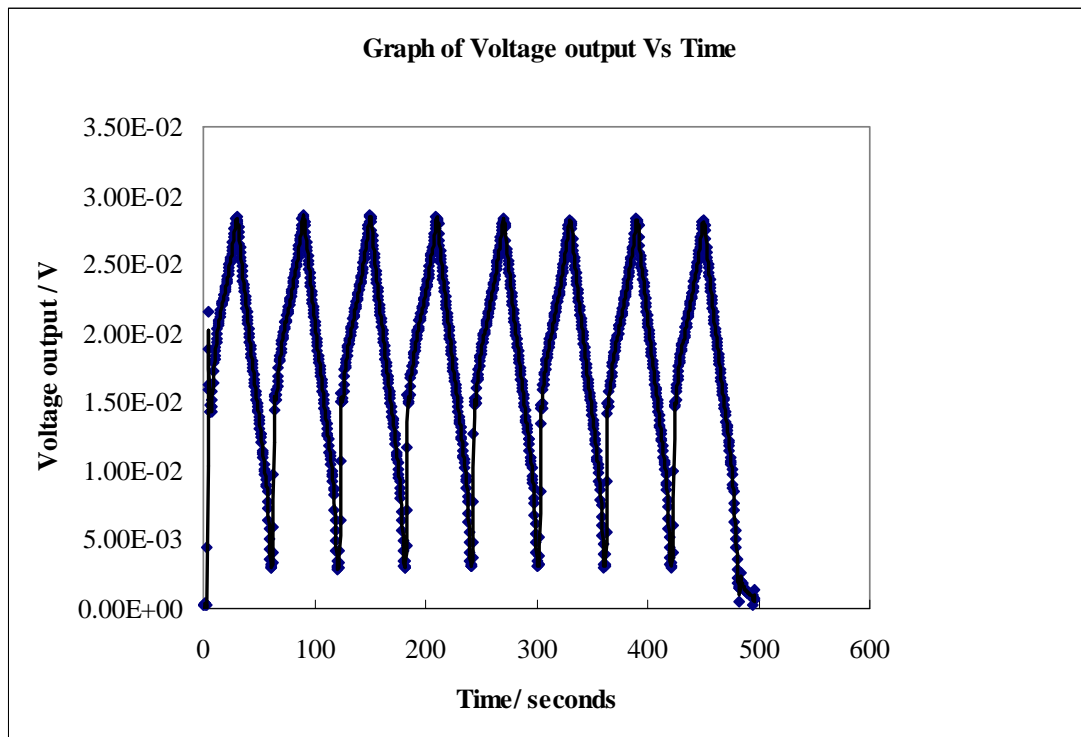
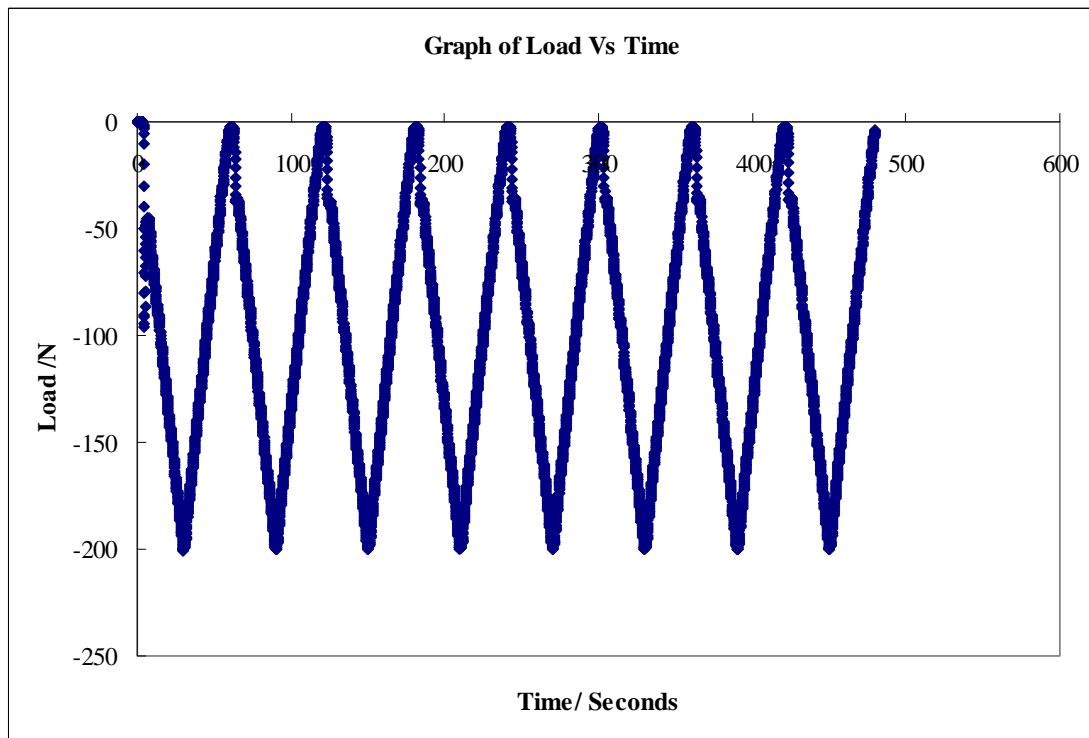


Fig4.2.3: A load of 200N was applied for a time span of 10 seconds. The 200N force was applied for another 60 seconds and the force was gradually reduced to zero force within another 10 seconds.

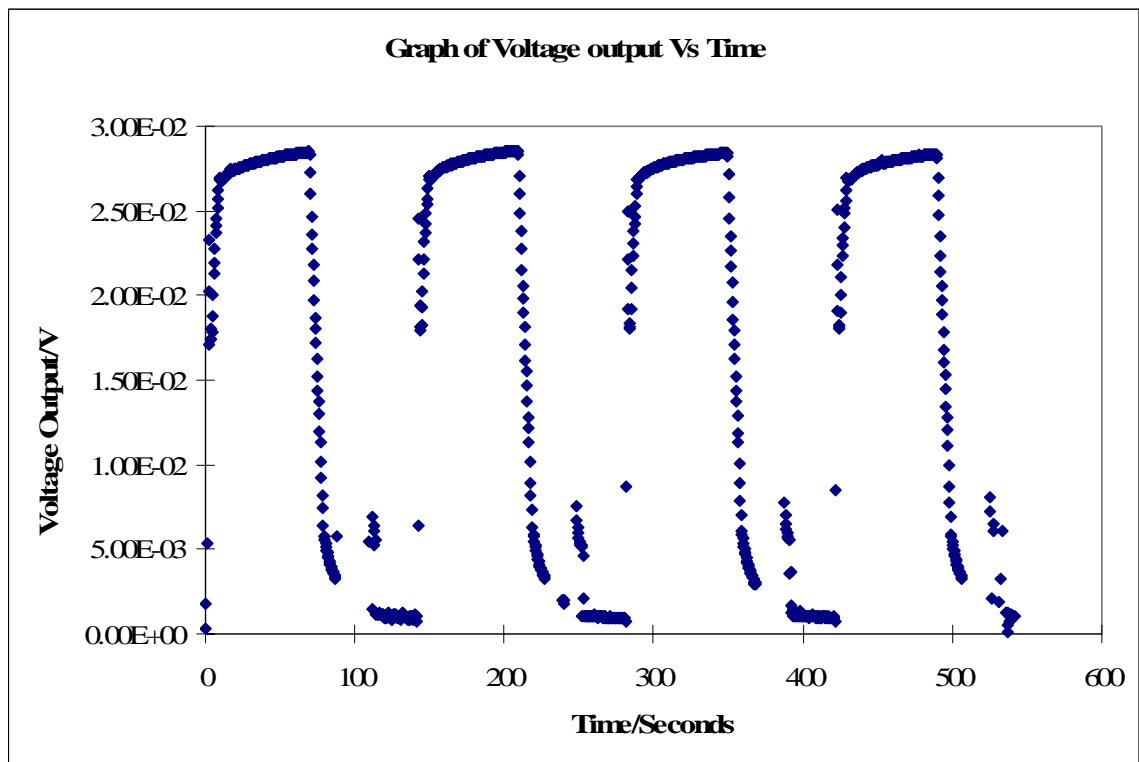
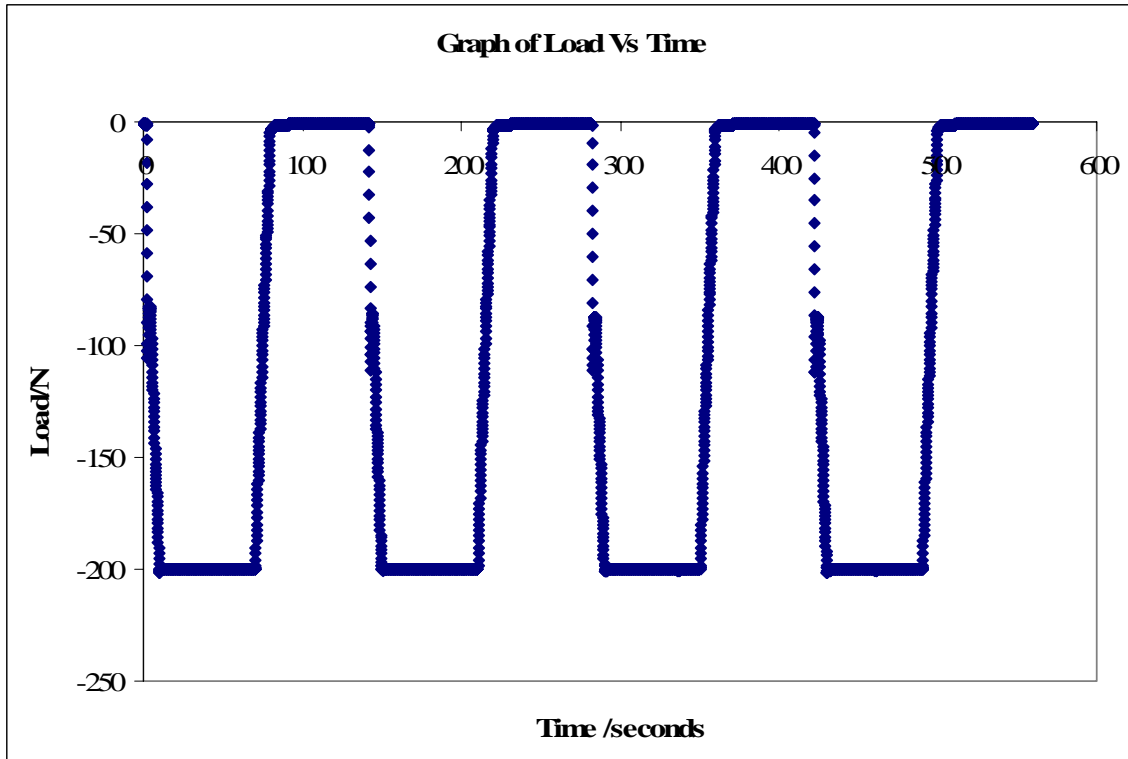


Fig4.2.4: A load of 200N was applied continuously for a time span of 5 seconds and that load was gradually removed to zero force within a time span of another 5 seconds.

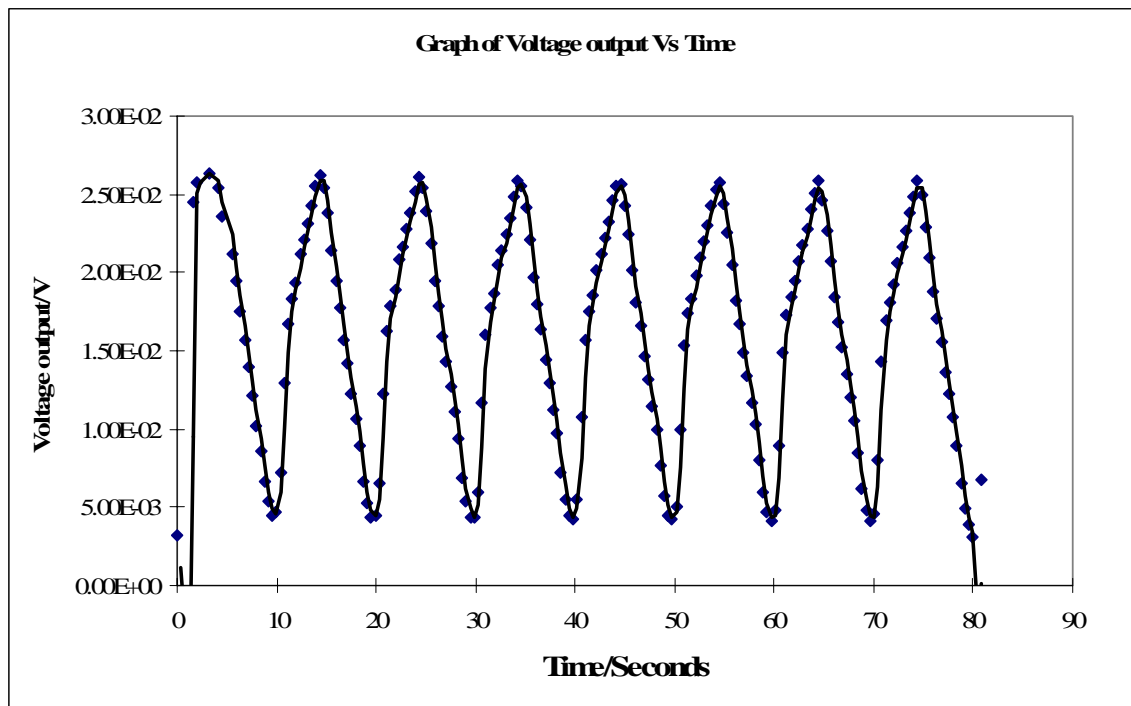
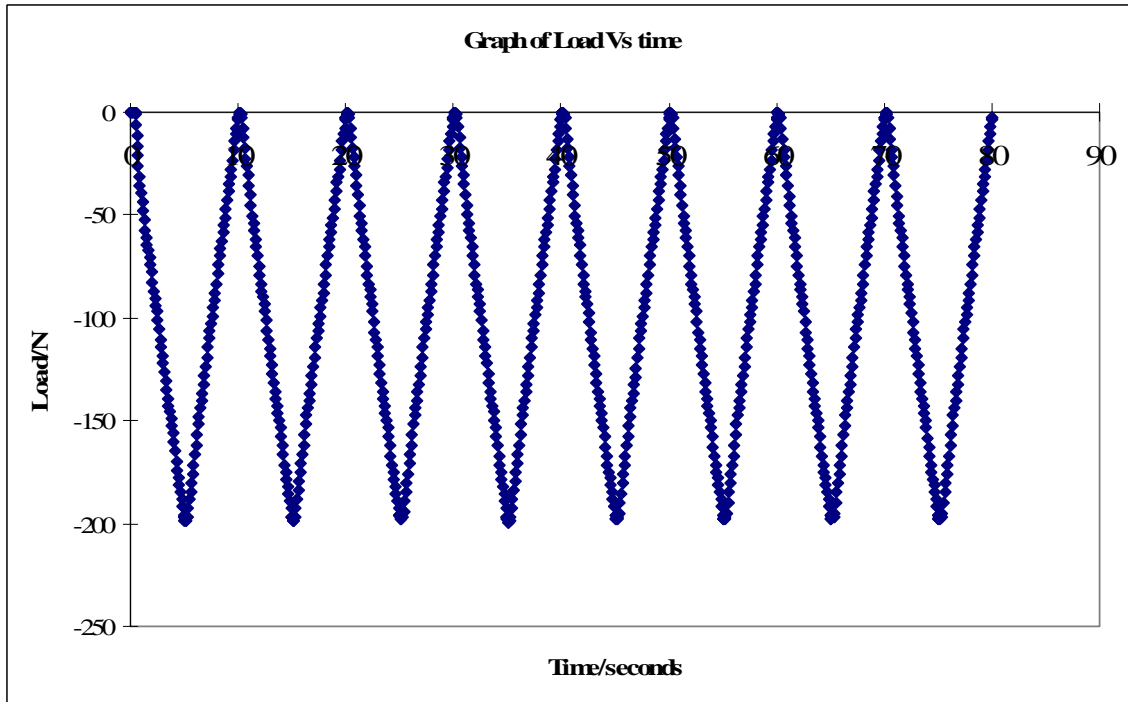


Fig4.2.5: A Load of 200N was applied for a time span of 5 seconds. The 200N force was applied for another 10 seconds and the force was gradually reduced to zero force within another 5 seconds.

The Sensor was calibrated by loading the sensor and observing the voltage output of the sensor. The results are presented in the following Figure 4.2.6.

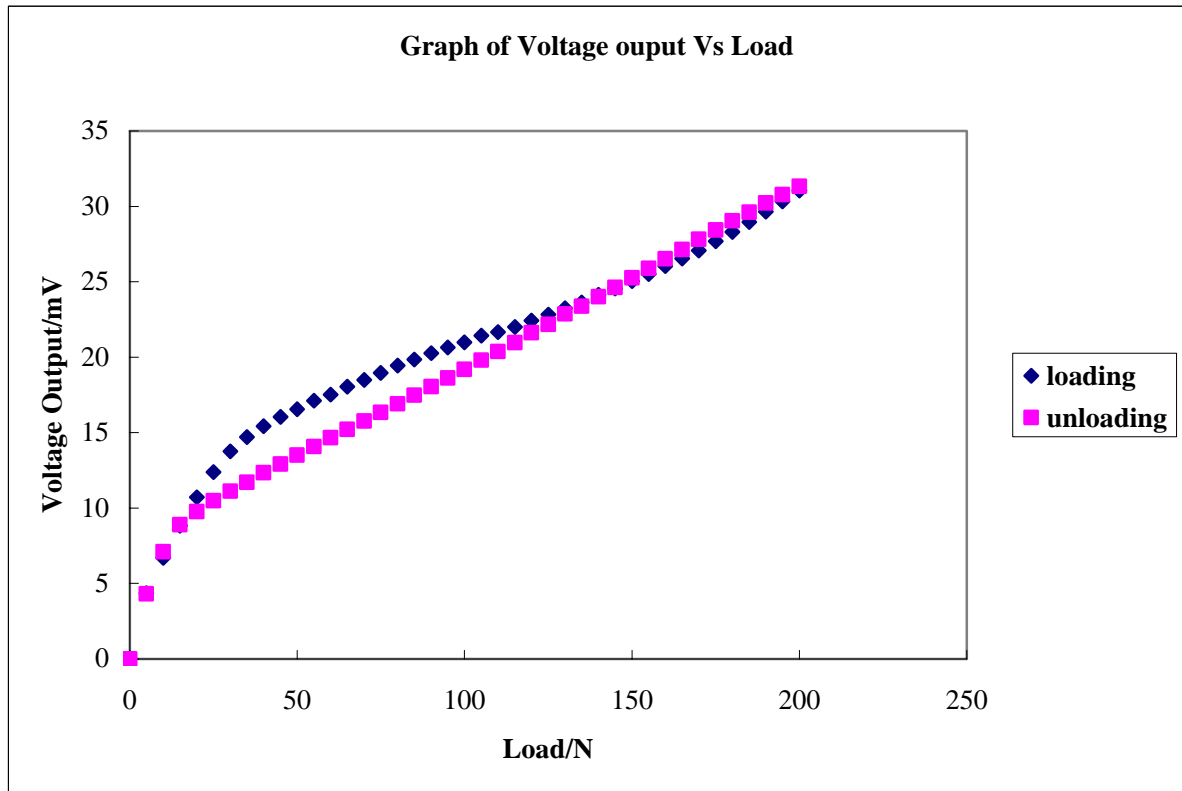


Fig4.2.6: Loading Unloading Graph of the Sensor

The piezoresistive sensor gives a more linear output as compared to the piezoelectric sensors and the output is also quite consistent as can be seen from the different loading patterns. It can be seen from the experimental graph that the voltage output is not exactly very linear as the force level changes. This phenomenon could be attributed to the visco-elastic nature of the dental silicon rubber that was used in embedding the sensor. Although the sensor gives a relatively consistent result, upon consultation with a dentist, it was realized that the sensor is too thick (6.25mm) for it to be attached to the splint and

the patient might be uncomfortable while sleeping. Thus an alternative sensor was needed.

4.3 Thin Film Flexi-Force Sensor

The Flexi-force Sensor was subjected to different loading patterns to determine the output and to check its consistency under the different loading rates and patterns. Instron 5848 Microtester Instron Blue-hill software was programmed to simulate the loading profiles. The results are given in the following Figures.

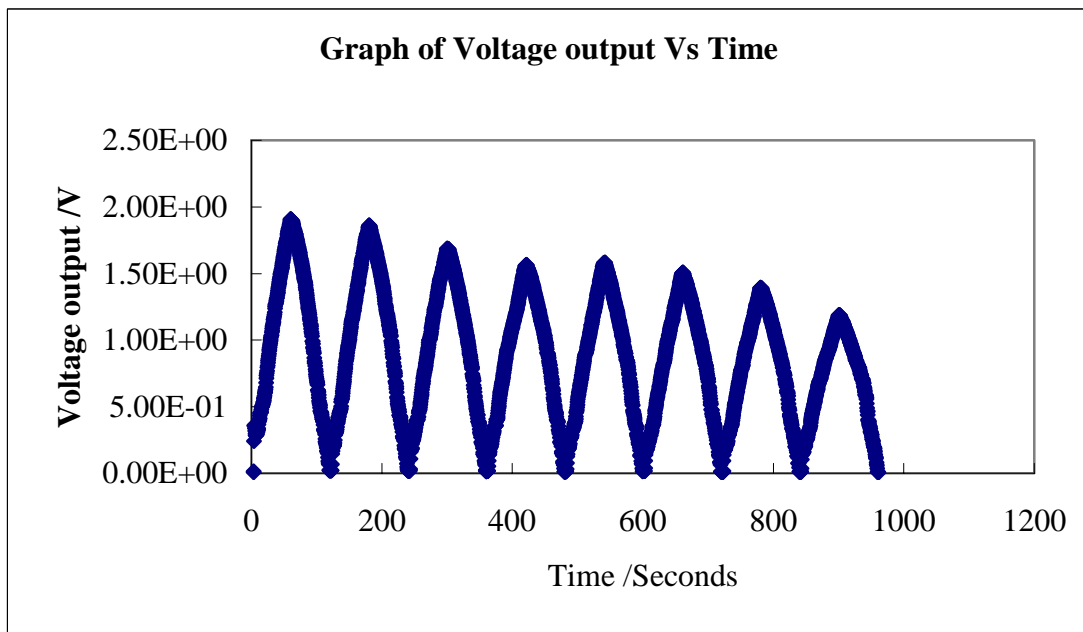
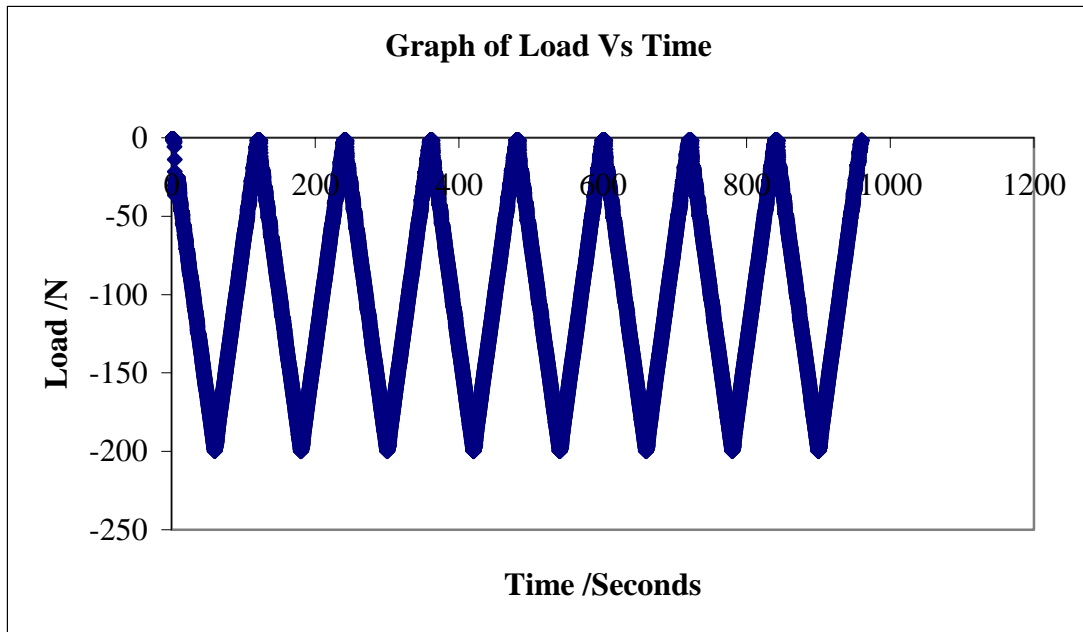


Fig4.3.1: A load of 200N was applied continuously for a time span of 60 seconds and that load was gradually removed to zero force within a time span of another 60 seconds

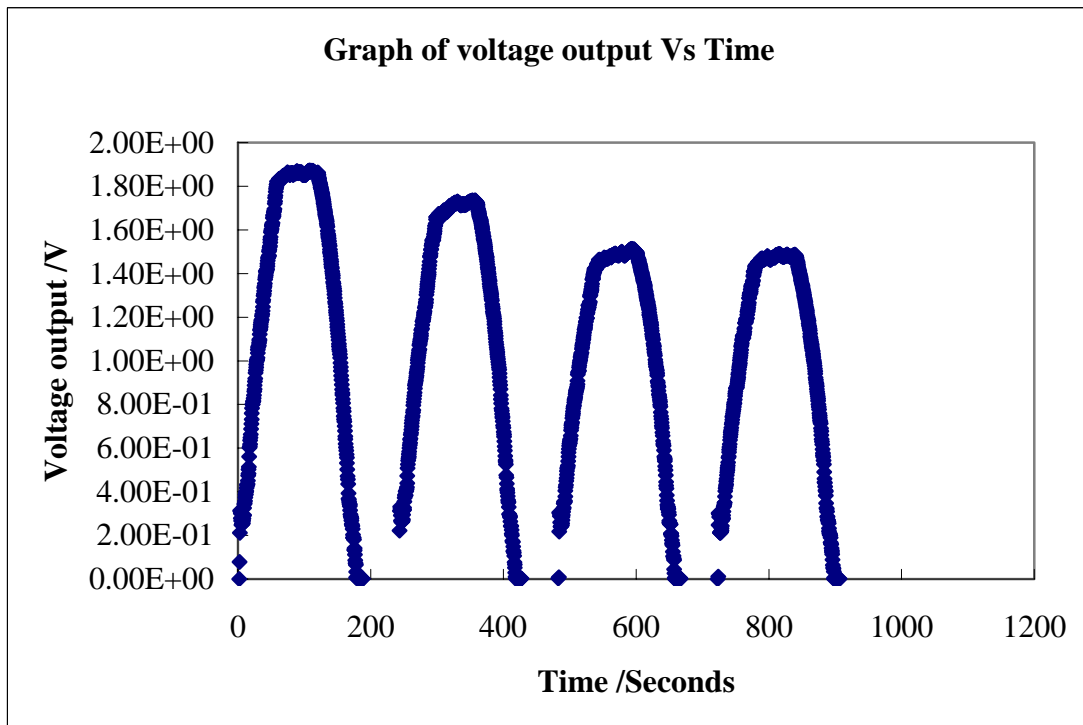
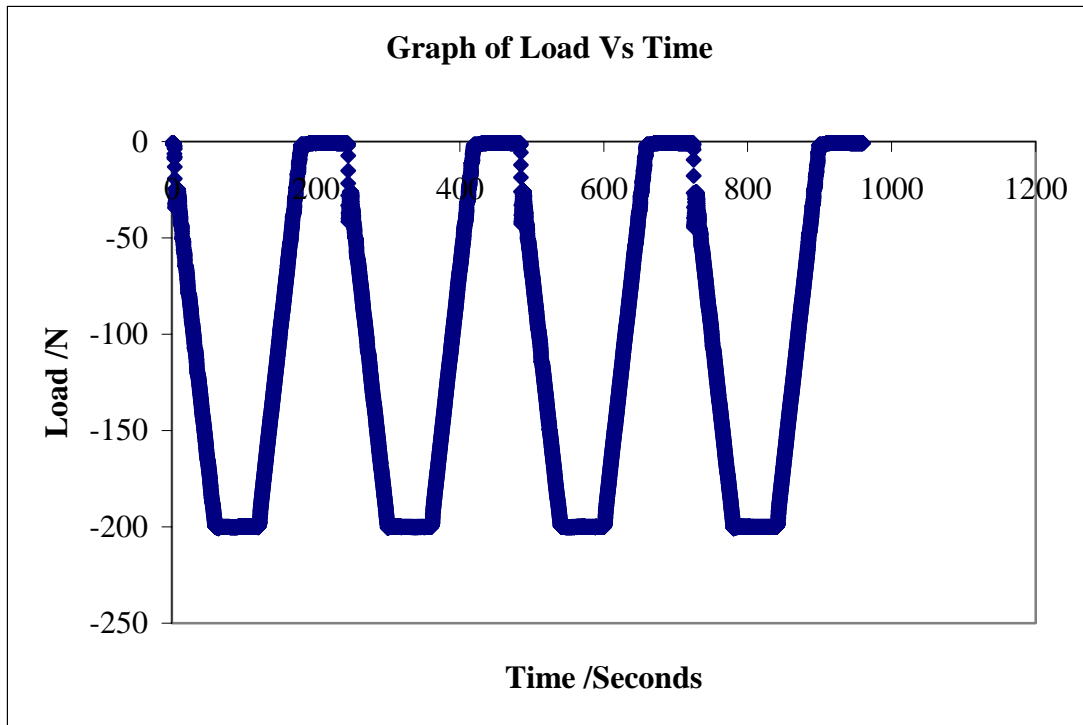


Fig4.3.2: A load of 200N was applied for a time span of 60 seconds. The 200N force was applied for another 60 seconds and the force was gradually reduced to zero force within another 60 seconds.

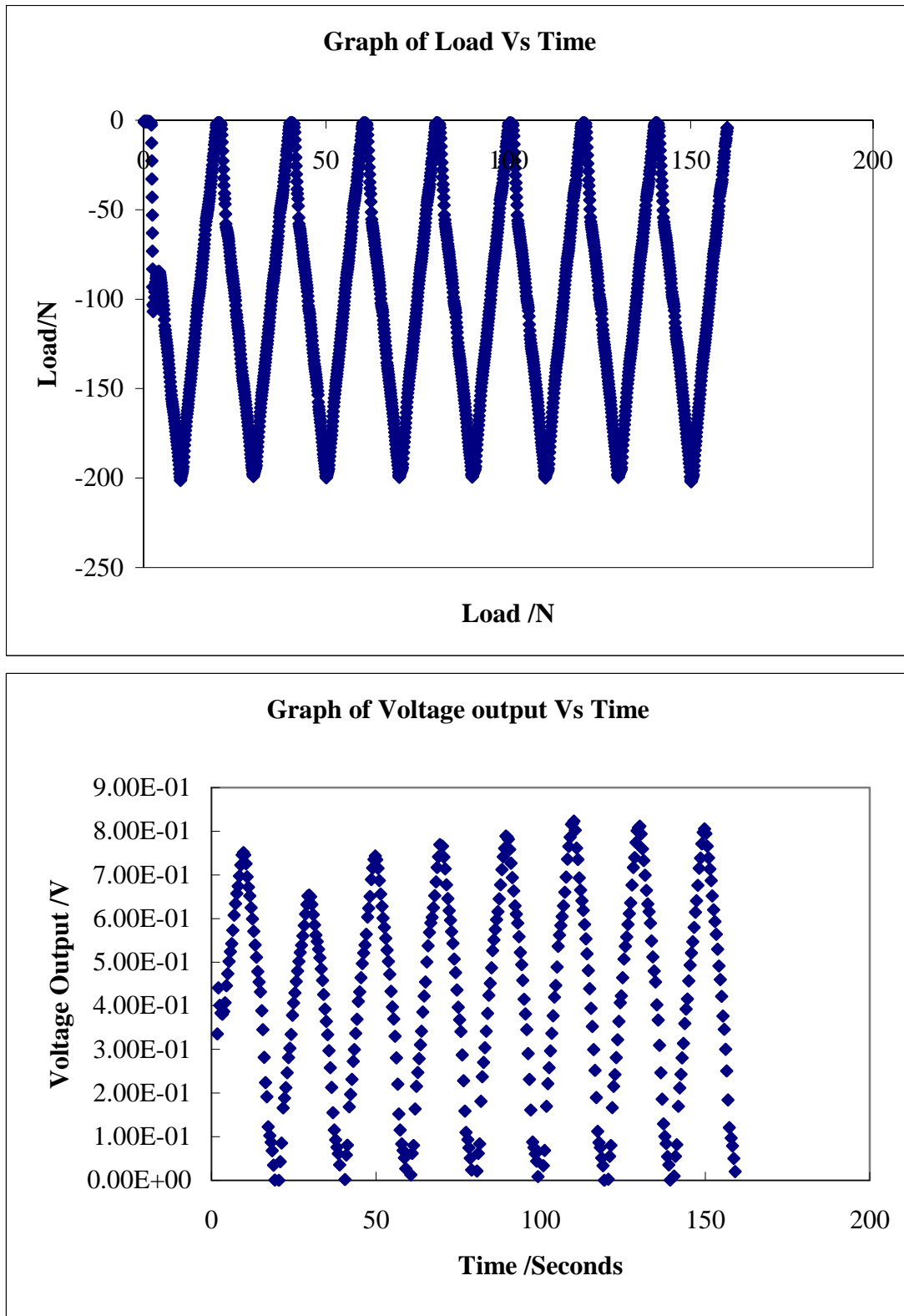


Fig4.3.3: A load of 200N was applied continuously for a time span of 10 seconds and that load was gradually removed to zero force within a time span of another 10 seconds

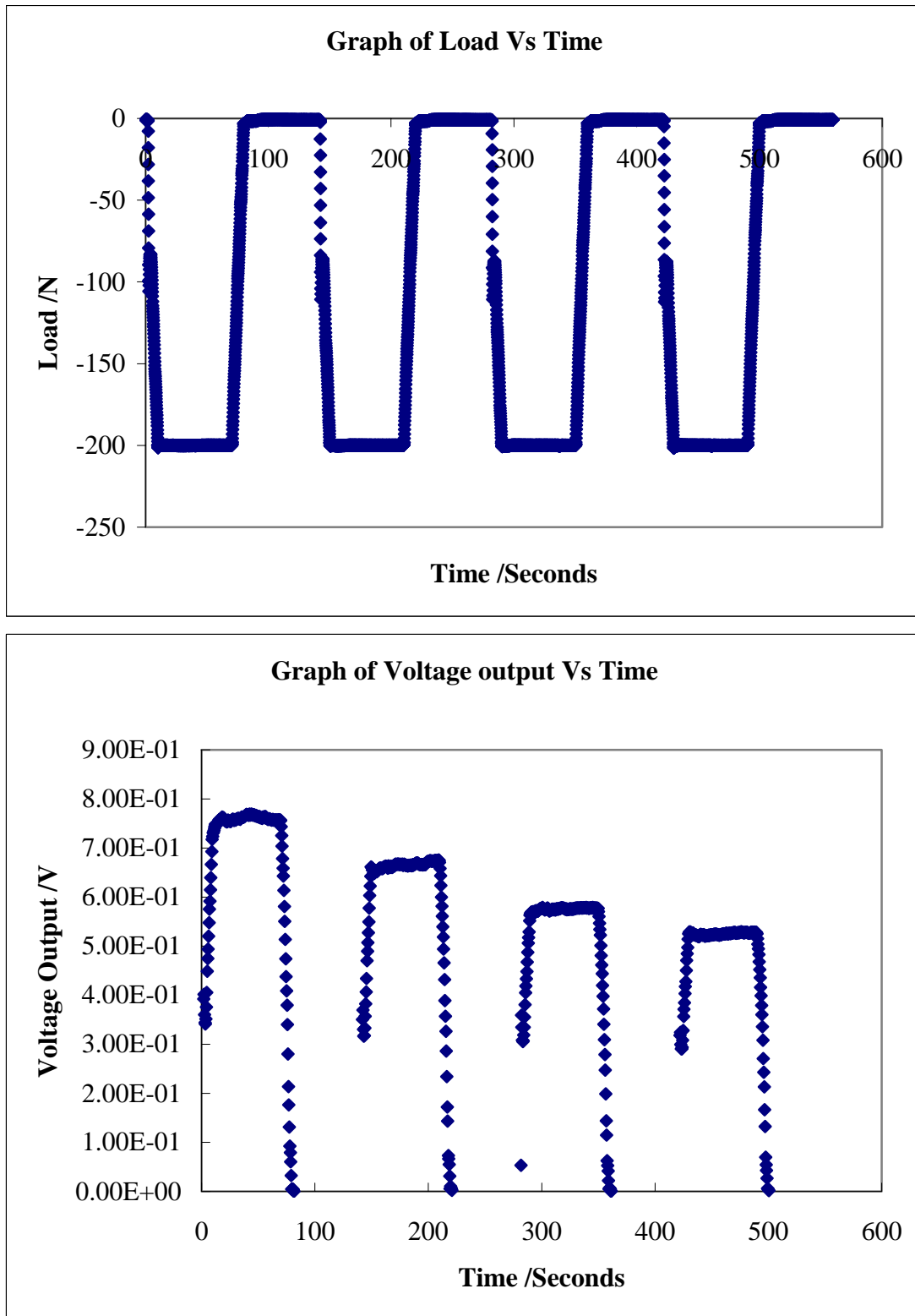


Fig4.3.4: A load of 200N was applied for a time span of 10 seconds. The 200N force was applied for another 60 seconds and the force was gradually reduced to zero force within another 10 seconds.

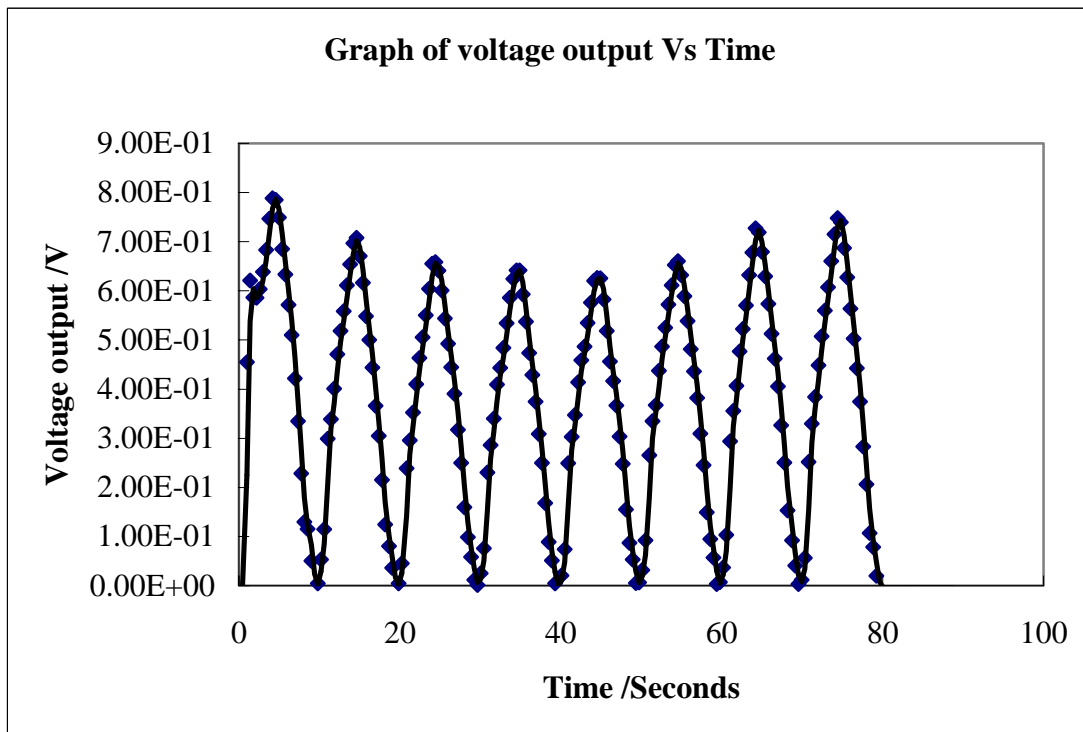
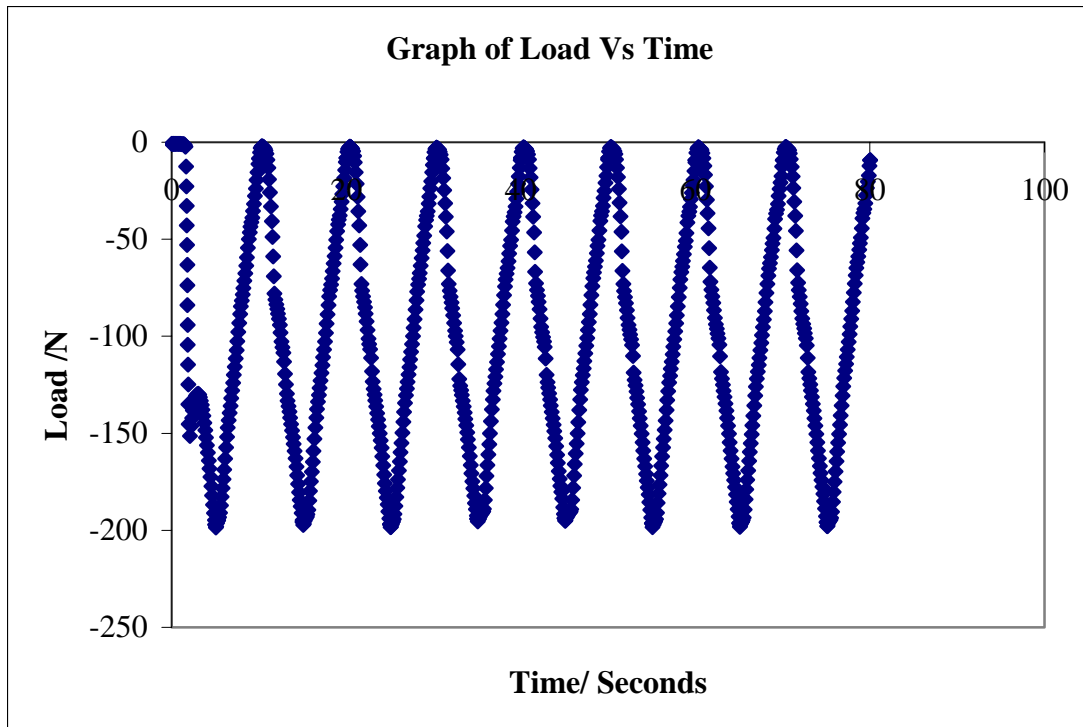


Fig4.3.5: A load of 200N was applied continuously for a time span of 5 seconds and that load was gradually removed to zero force within a time span of another 5 seconds

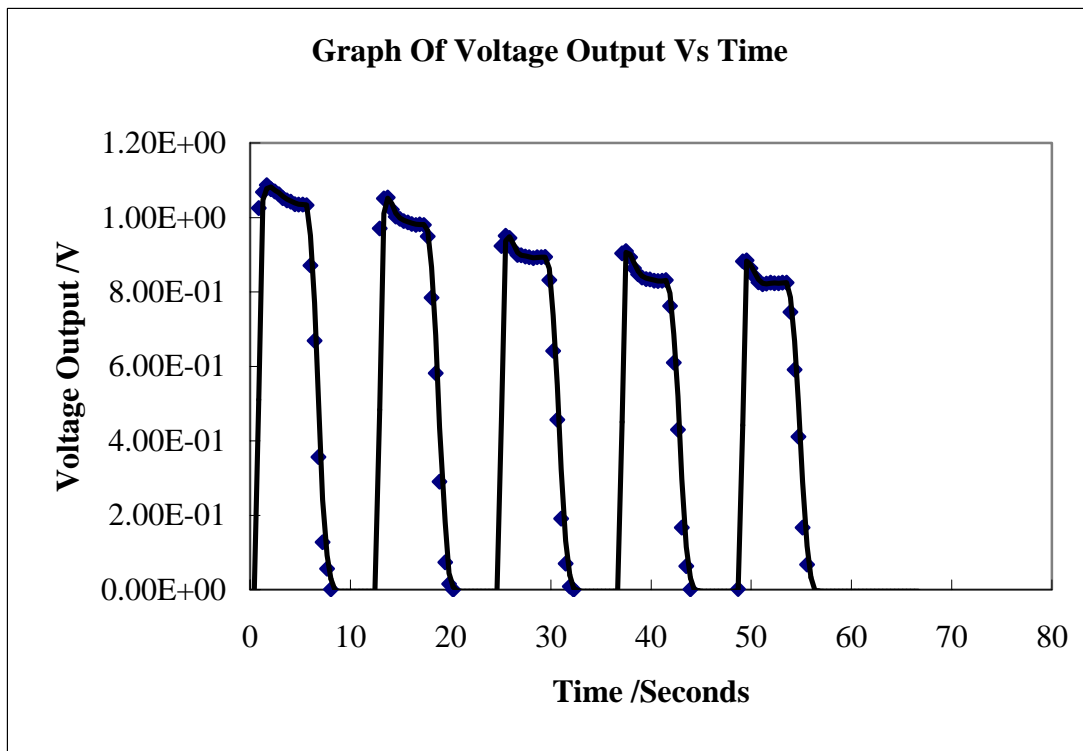
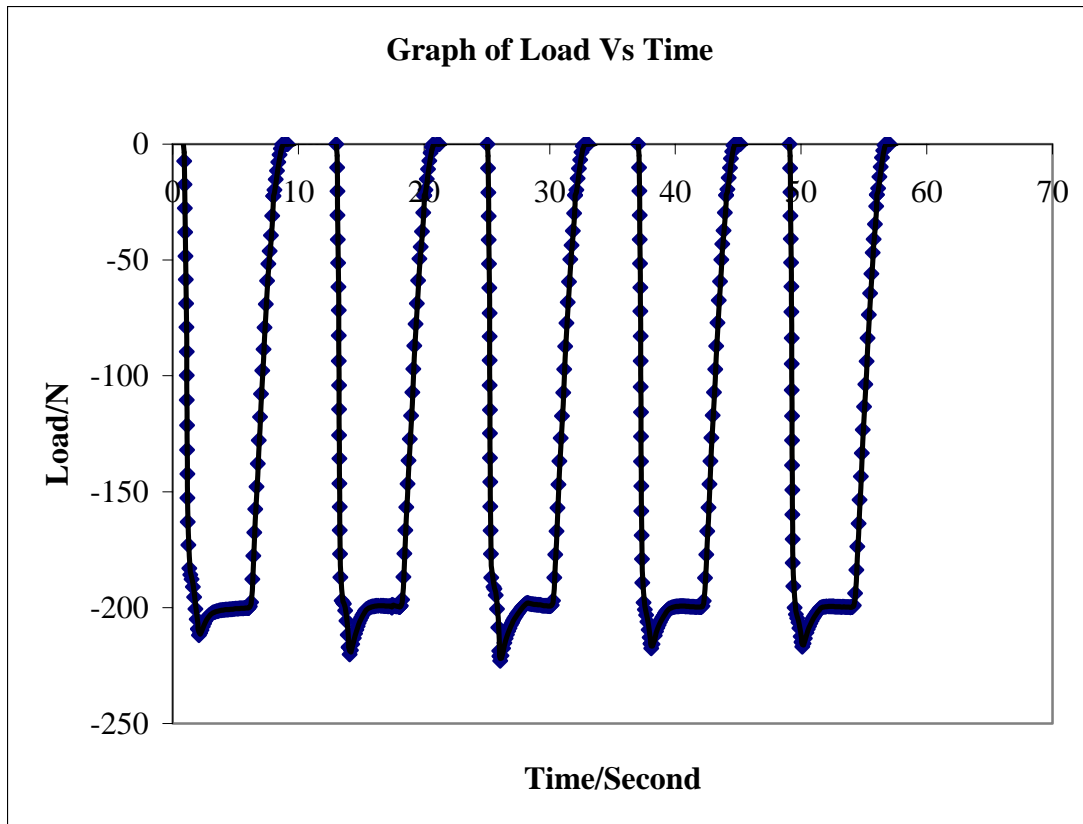


Fig4.3.6: A load of 200N was applied for a time span of 2 seconds. The 200N force was applied for another 3 seconds and the force was gradually reduced to zero force within another 2 seconds. This was an actual Bruxism event simulation. [65, 66].

The sensor was calibrated by loading the sensor and observing the voltage output of the sensor. The results are presented in the following paragraph.

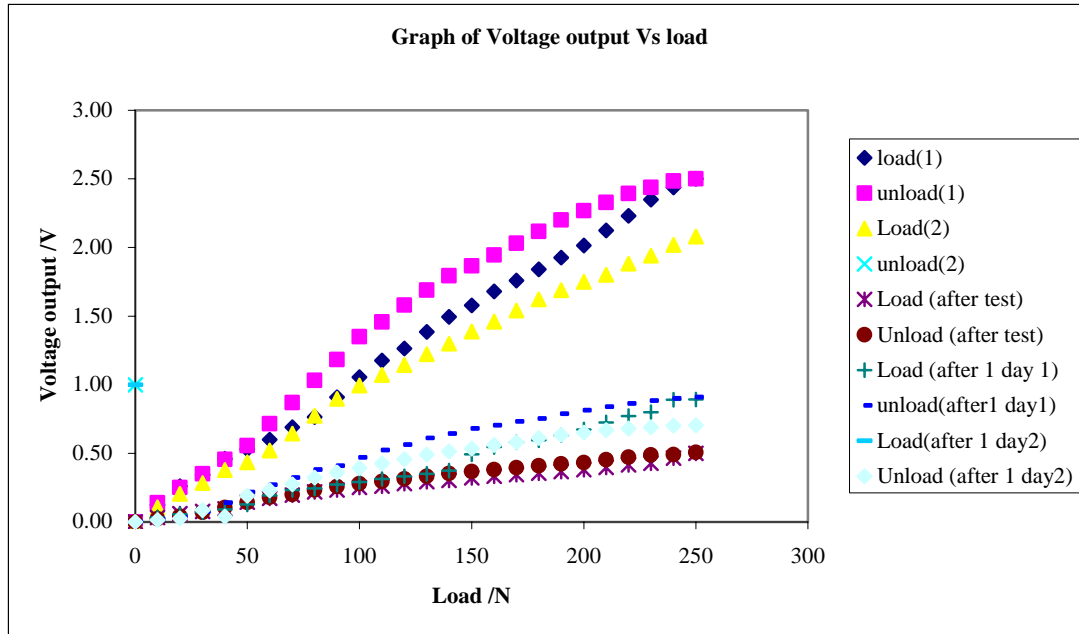


Fig4.3.7: Loading Unloading Graph for the Flexi-force Sensor

Although the specifications from the manufacturer had stated that this sensor would give good repeatable readings, experiments conducted proved otherwise. This deterioration of voltage output over time could be attributed to the plastic nature of the polyester and the other constituent materials that were used in the sensor. Similar trends were observed by Nikonovas et.al [55] and Carpaneto et.al [56].

4.4 Photo-Resist Sensor

The Photo-Resist Sensor was subjected to different loading patterns to determine the output and to check its consistency under the different loading rates and patterns. Instron 5848 Microtester Instron Blue-hill software was programmed to simulate the loading profile. Figure 4.4.1 gives the calibration curve

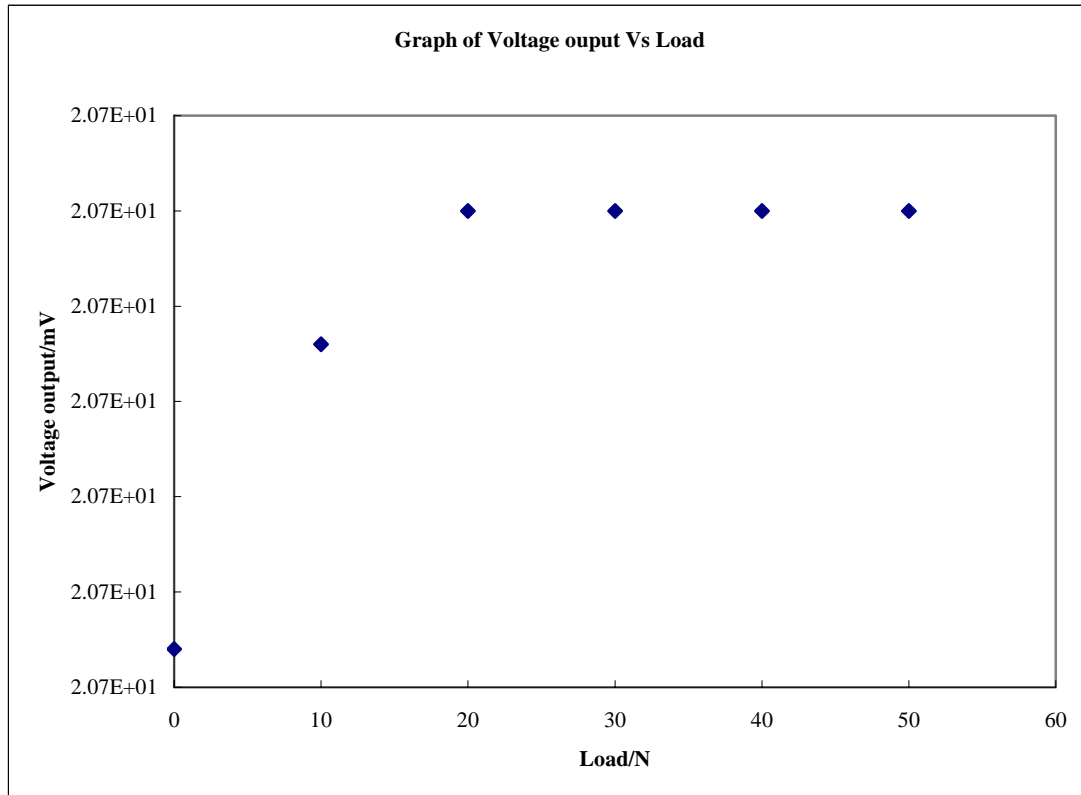


Fig 4.4.1: Calibration curve for the photo-resist sensor

From the graph, although only forces up to 50 N were measured, the sensor was not very sensitive and thus this sensor would not be very suitable for our application. Although this sensor was fabricated (mainly due to its low cost) its low sensitivity makes it unsuitable for this application.

4.5 Strain Gage Sensor (with diaphragms)

The strain gage sensor was subjected to different loading patterns to determine the output and to check its consistency under the different loading rates and patterns. Two different diaphragms (Stainless Steel/ aluminum) were used and the results were compared. Instron 5848 Microtester Instron Blue-hill software was programmed to simulate the loading profile. The results are given in the following Figures

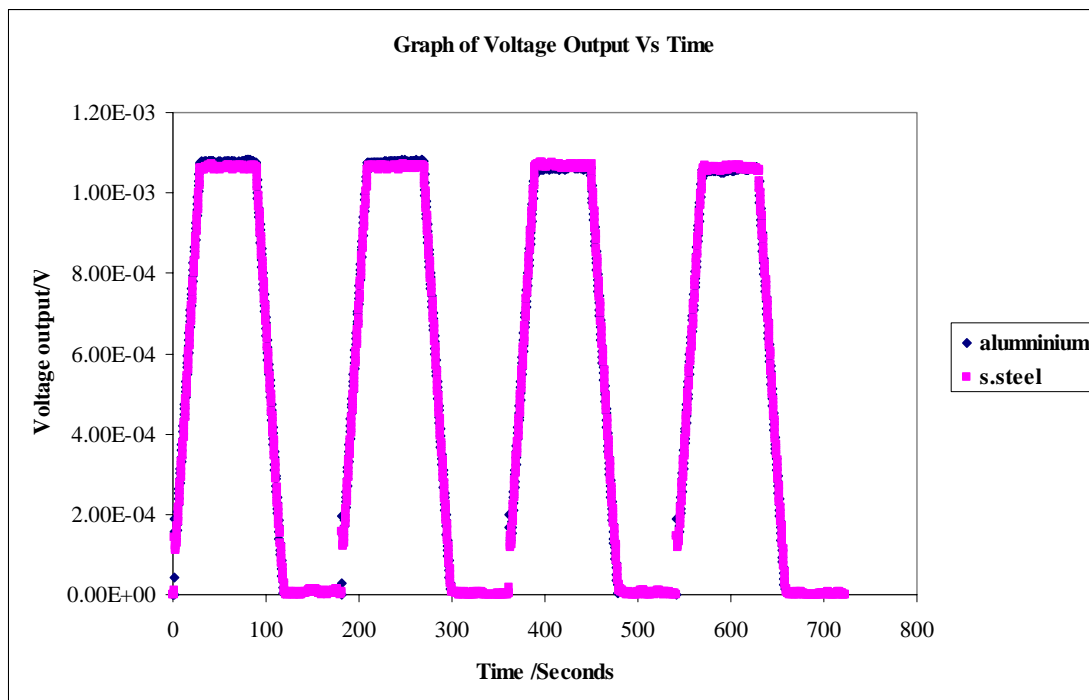
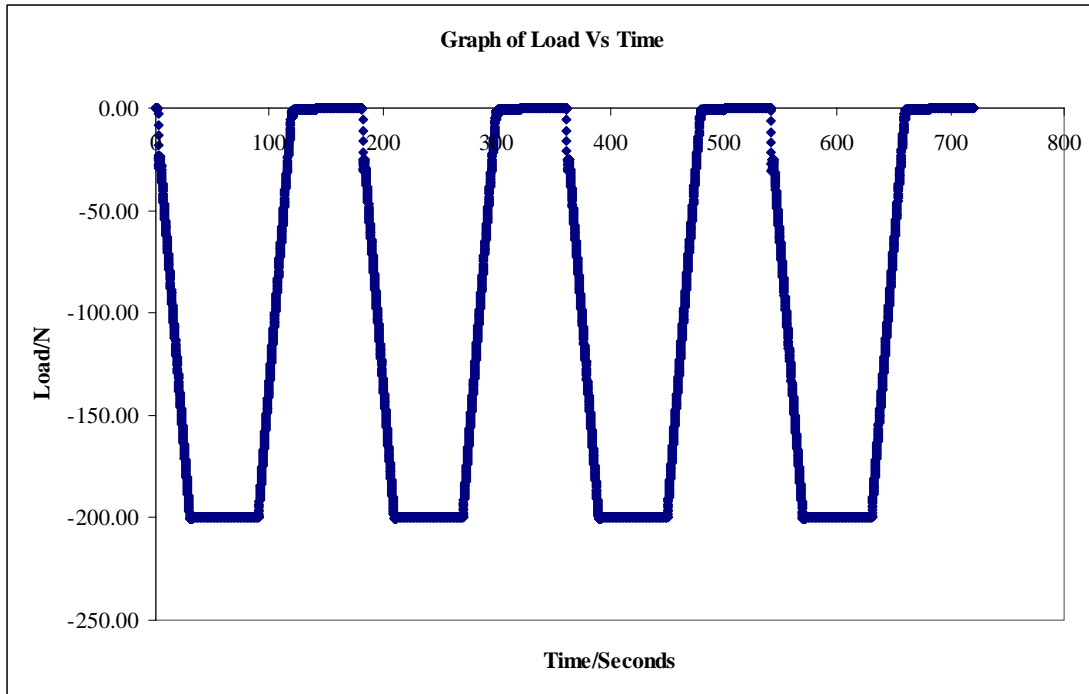


Fig4.5.1: A load of 200N was applied for a time span of 30 seconds. The 200N force was applied for another 60 seconds and the force was gradually reduced to zero force within another 30 seconds.

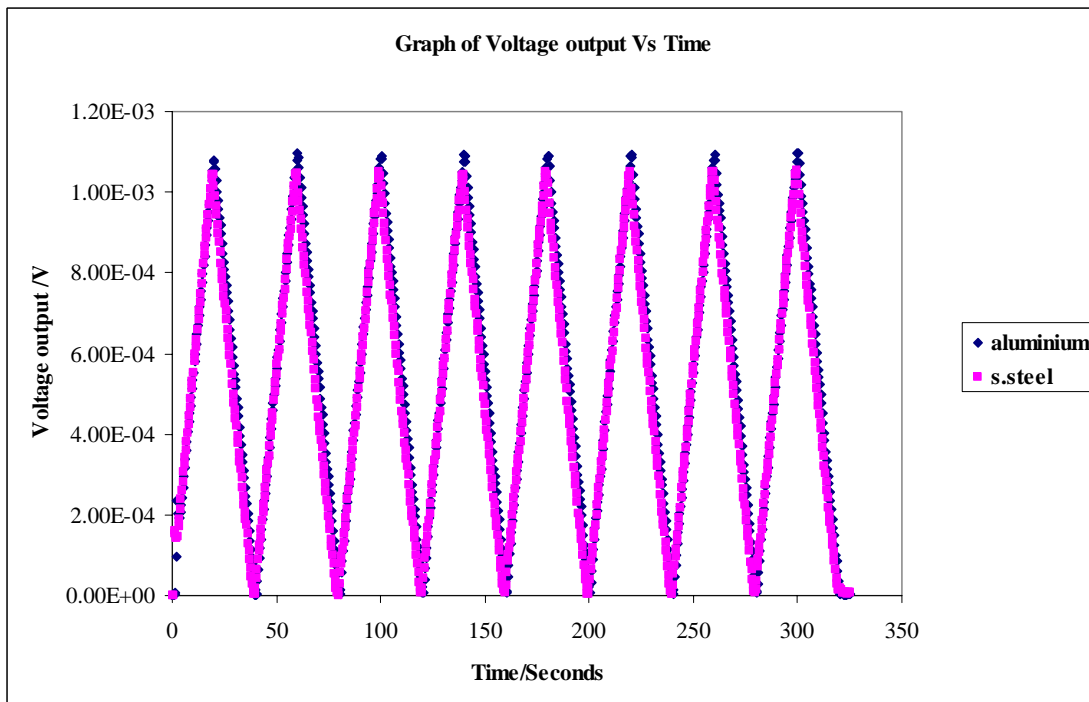
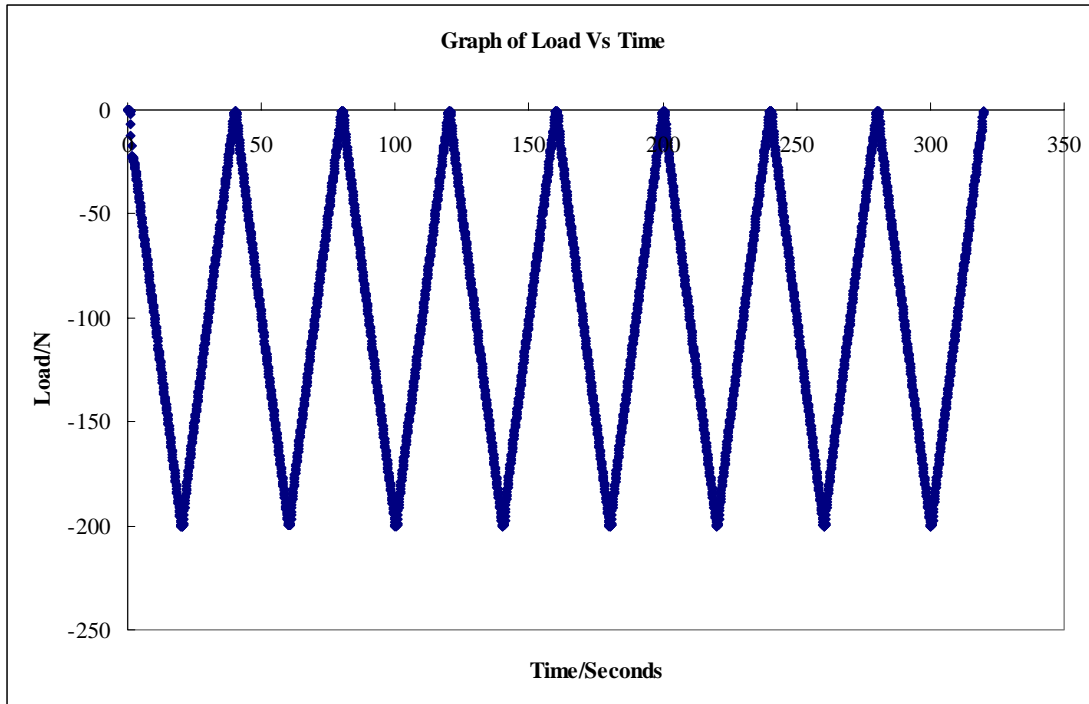


Fig4.5.2: A load of 200N was applied continuously for a time span of 20 seconds and that load was gradually removed to zero force within a time span of another 20 seconds

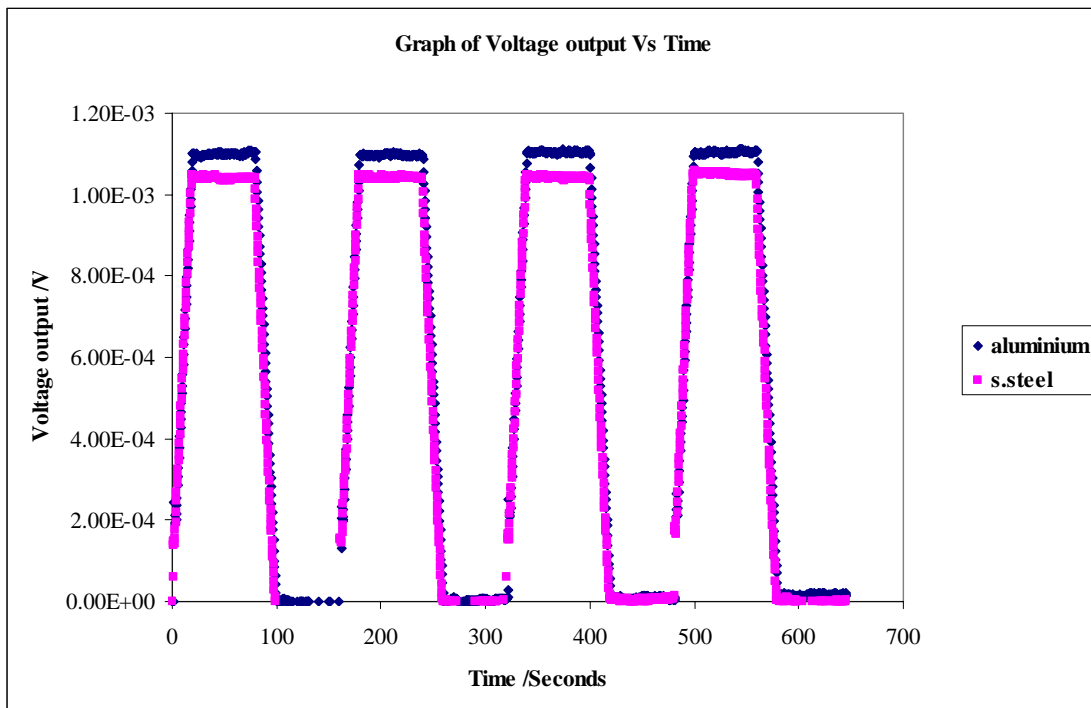
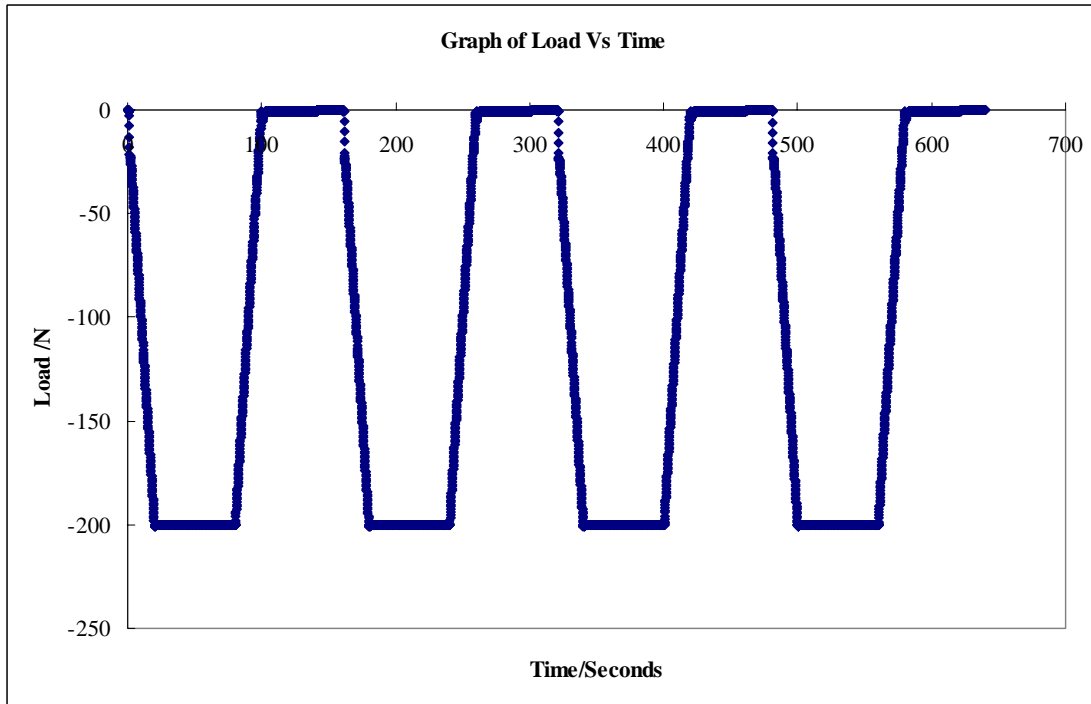


Fig4.5.3: A load of 200N was applied for a time span of 20 seconds. The 200N force was applied for another 60 seconds and the force was gradually reduced to zero force within another 20 seconds.

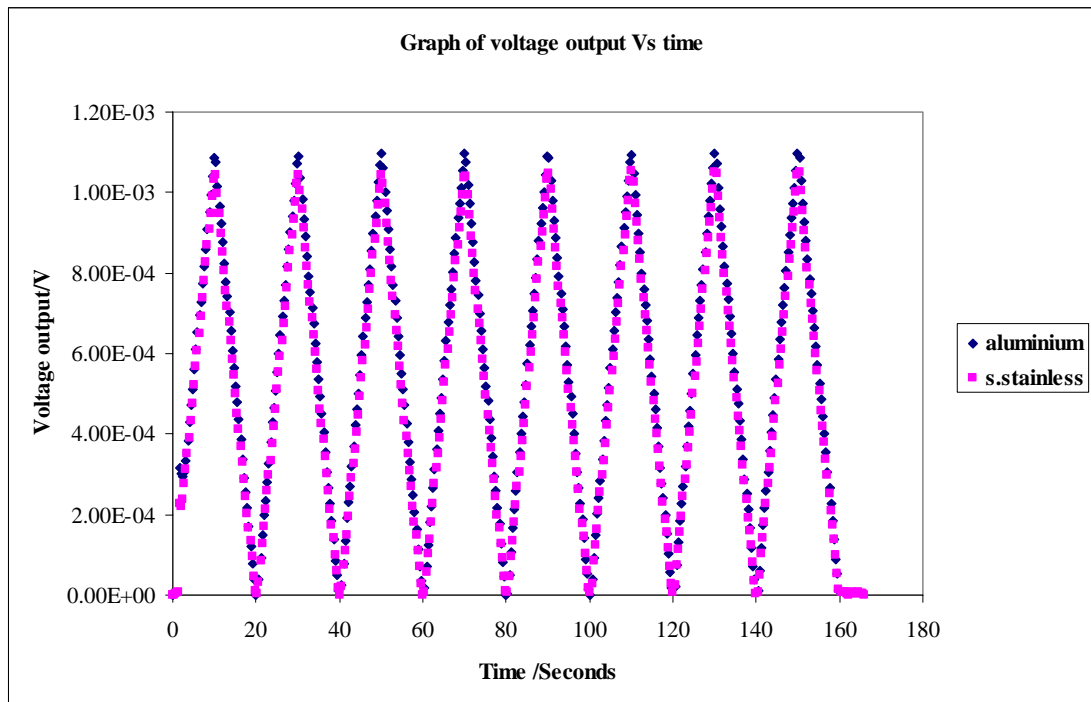
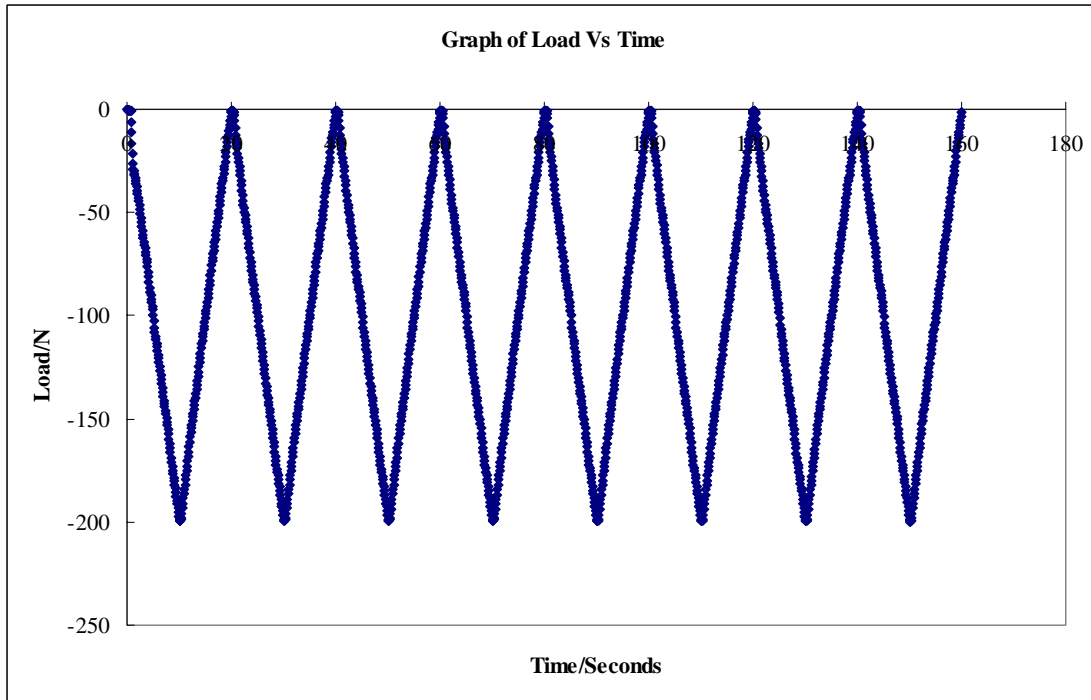


Fig4.5.4: A load of 200N was applied continuously for a time span of 10 seconds and that load was gradually removed to zero force within a time span of another 10 seconds

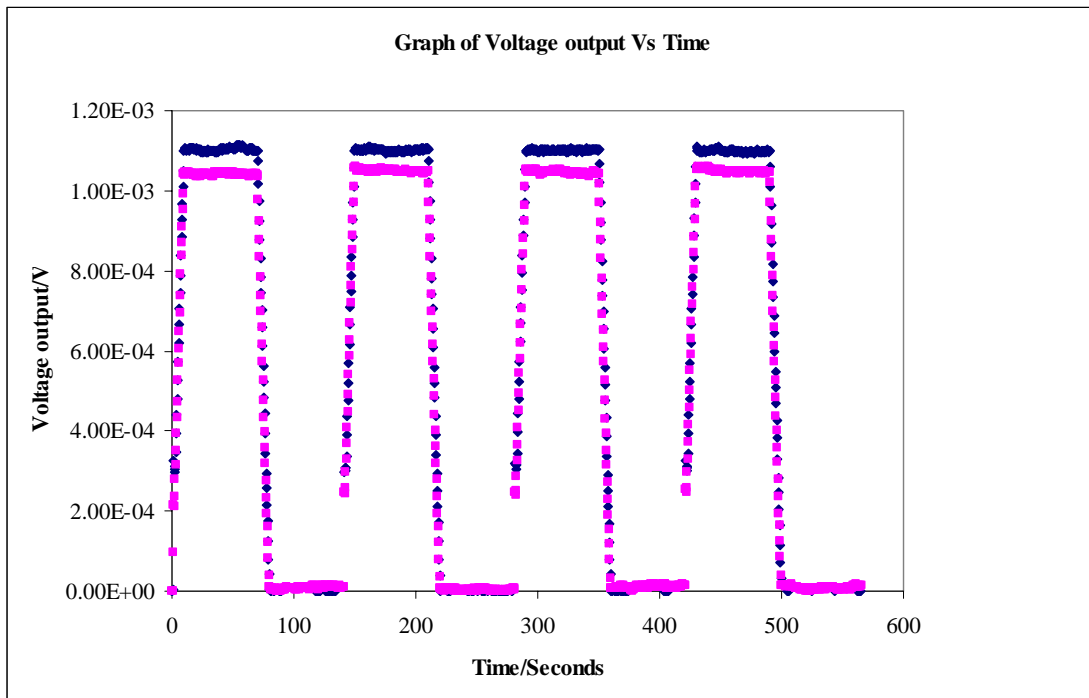
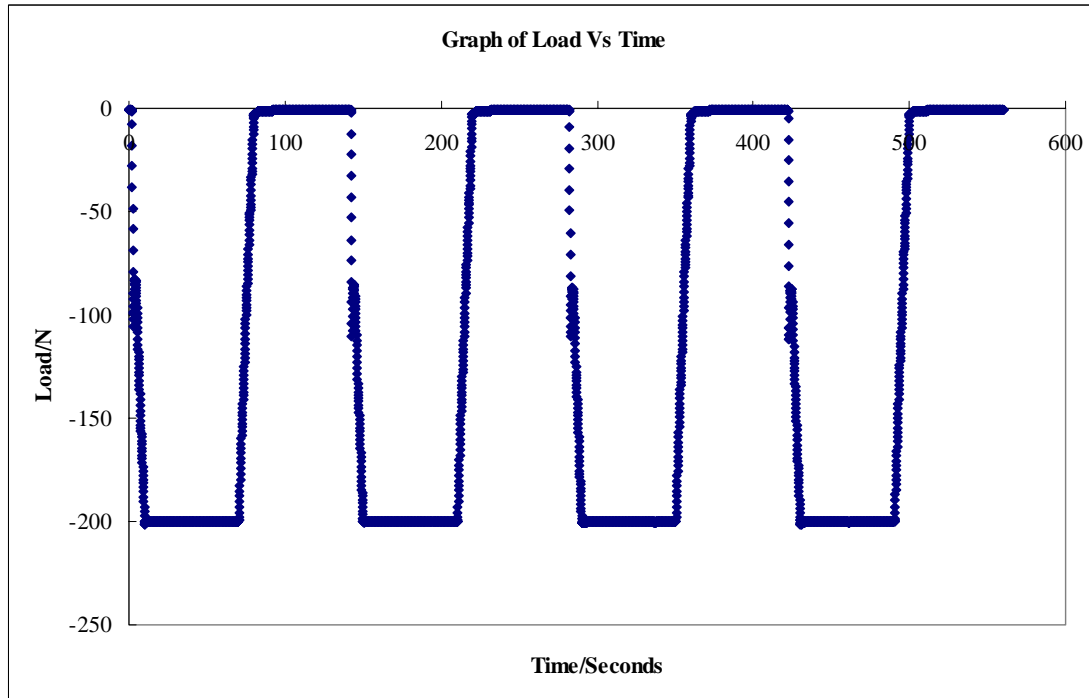


Fig4.5.5: A load of 200N was applied for a time span of 10 seconds. The 200N force was applied for another 60 seconds and the force was gradually reduced to zero force within another 10 seconds.

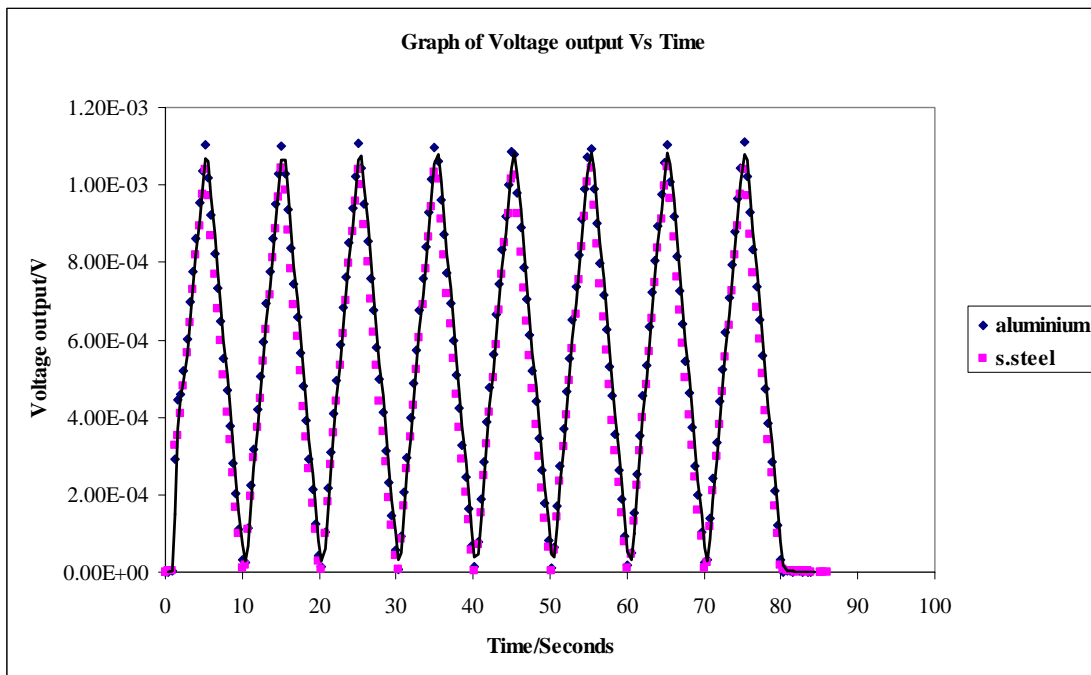
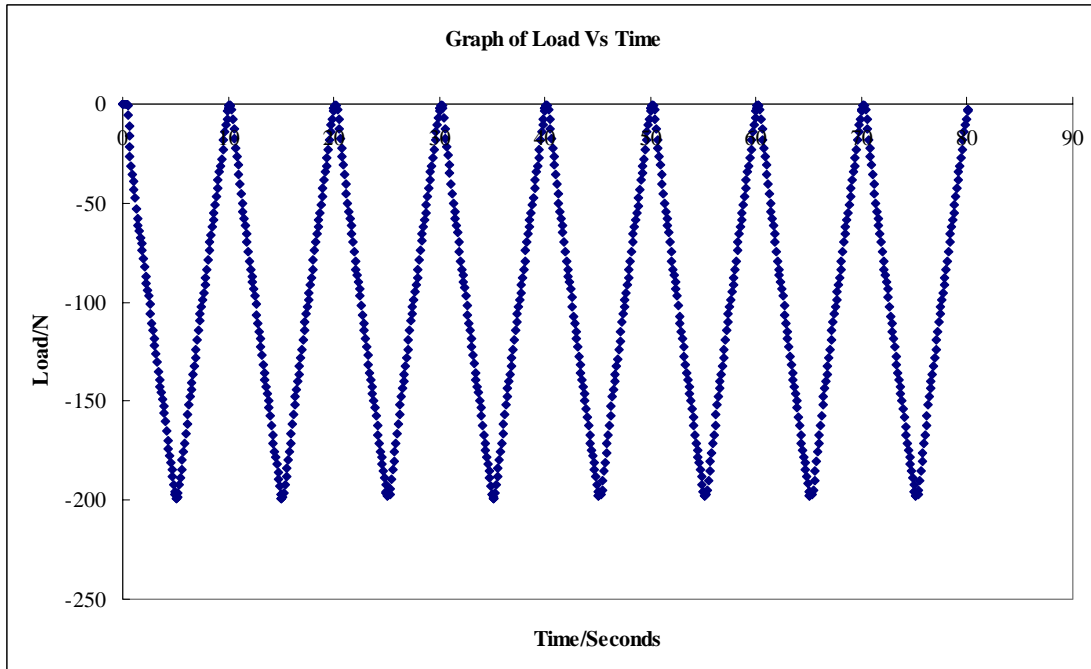


Fig4.5.6: A load of 200N was applied continuously for a time span of 5 seconds and that load was gradually removed to zero force within a time span of another 5 seconds.

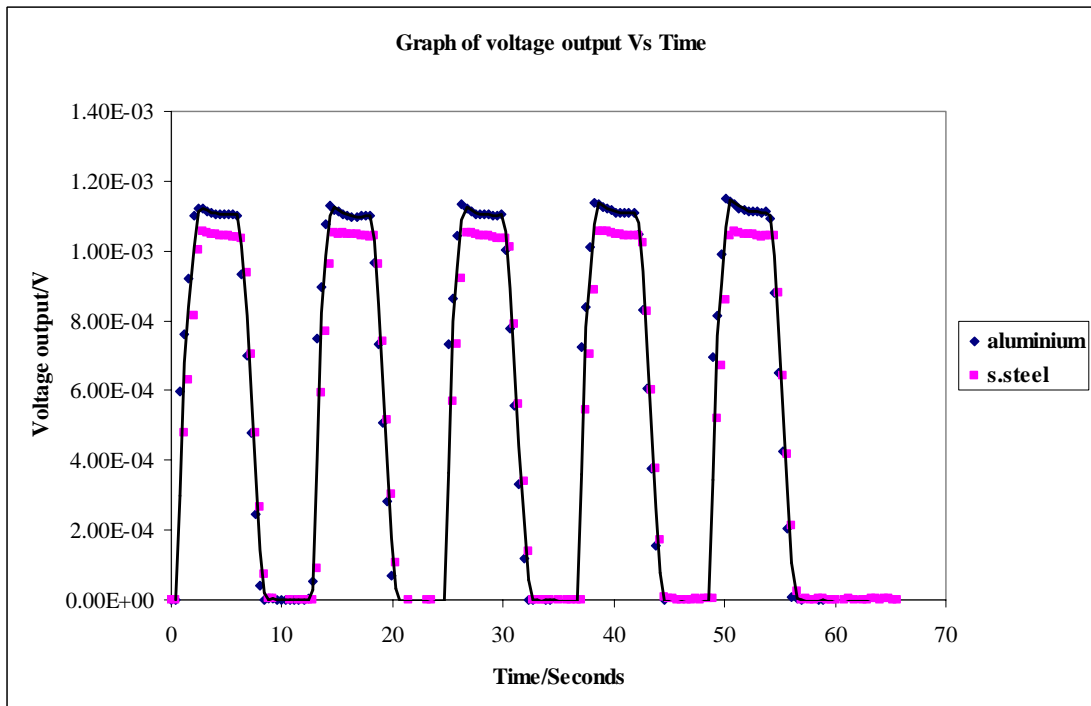
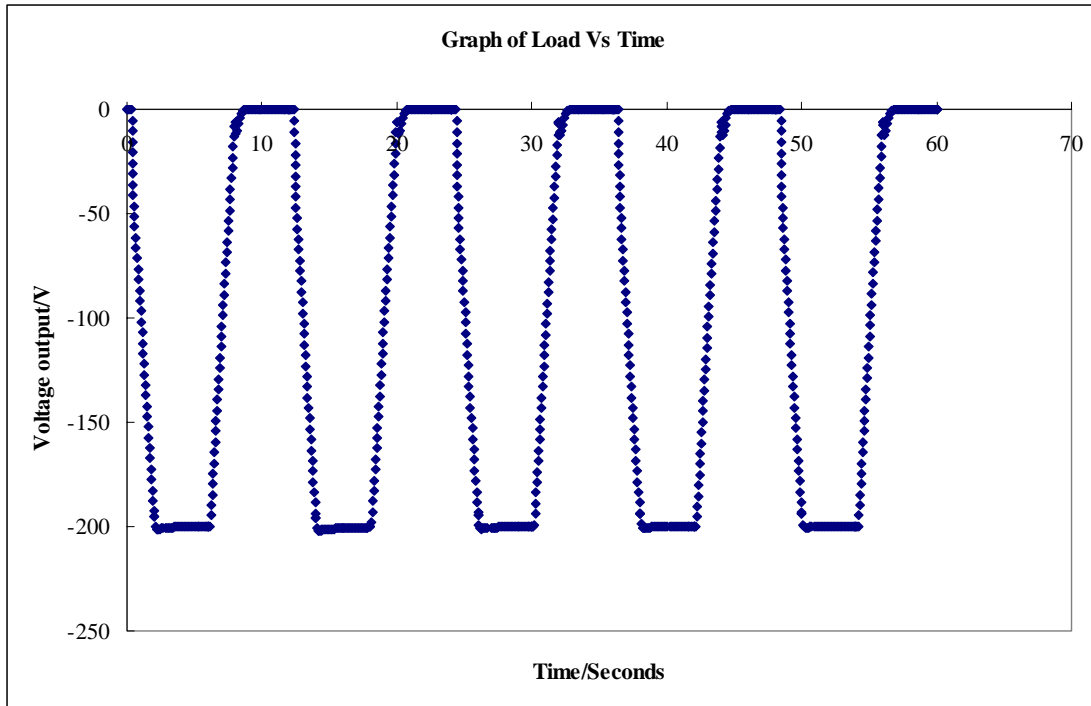


Fig4.5.7: A load of 200N was applied for a time span of 2 seconds. The 200N force was applied for another 3 seconds and the force was gradually reduced to zero force within another 2 seconds. This was an actual Bruxism event simulation. [65, 66].

From the experiments that were carried out, it seems that the aluminum diaphragm gives a greater voltage output as compared to stainless steel. This is not surprising as aluminum has smaller young's modules (approximately 70Gpa) and is less stiff than stainless steel (approximately 195Gpa) which results in a greater deflection that would result in a greater output.

Although the experiments that were carried out gave favorable results, the diaphragms were still deemed too big as sensors in the application for detection of bruxism forces. Further experiments were carried out by just embedding the strain gages directly in orthodontic resin. This would reduce the size of the sensor. In order to reduce the size of the sensor, the strain gages were directly embedded onto the orthodontic resin and the voltage output from the sensor system was tested. They were placed in two different directions (in the z and x-direction) to determine the direction that results in a higher voltage output with respect to the load. The directions are depicted below together with the cross-sectional view of the splint in Figure 4.5.8.

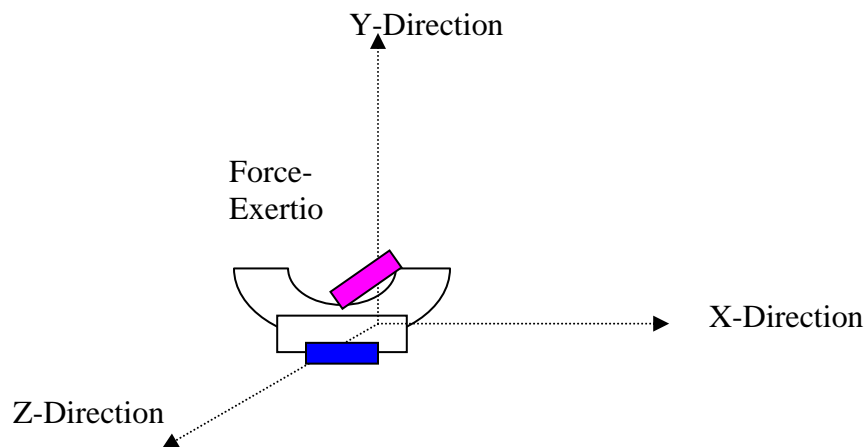


Fig4.5.8: The direction of measurement of the Voltage output.

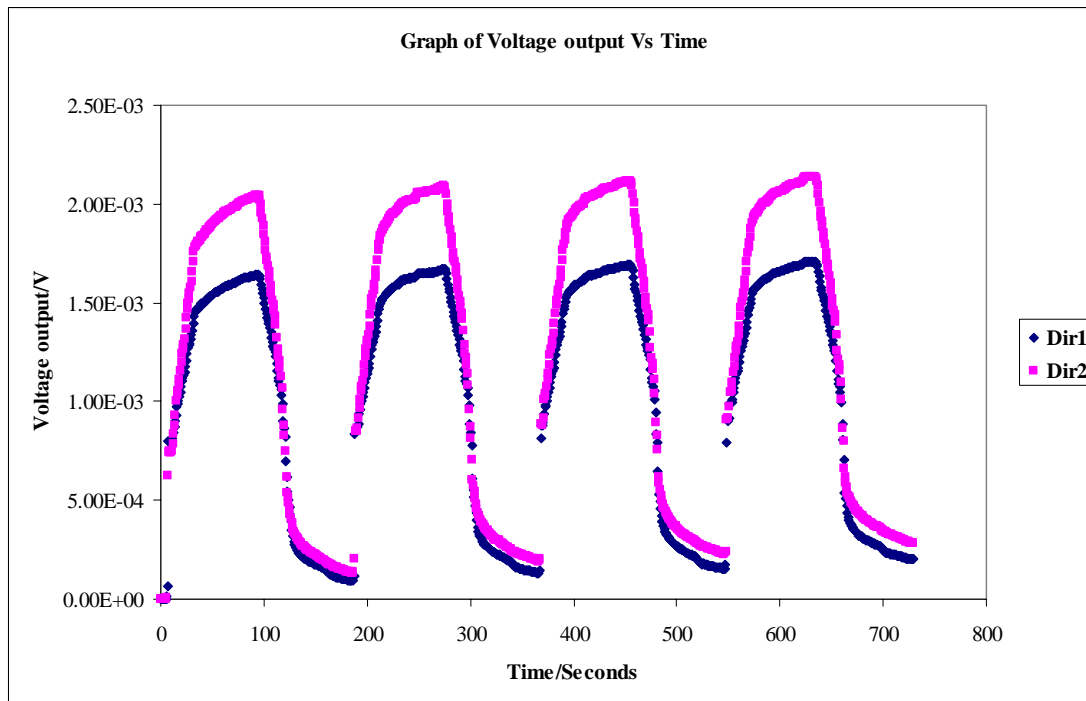
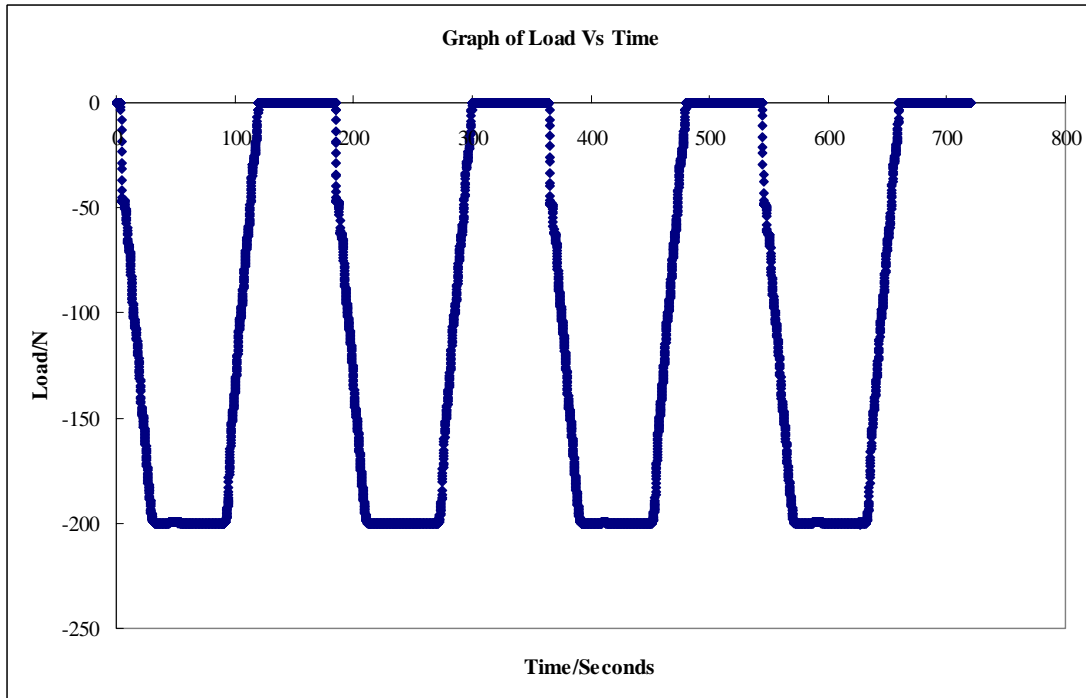


Fig4.5.9: A load of 200N was applied for a time span of 30 seconds. The 200N force was applied for another 60 seconds and the force was gradually reduced to zero force within another 30 seconds.

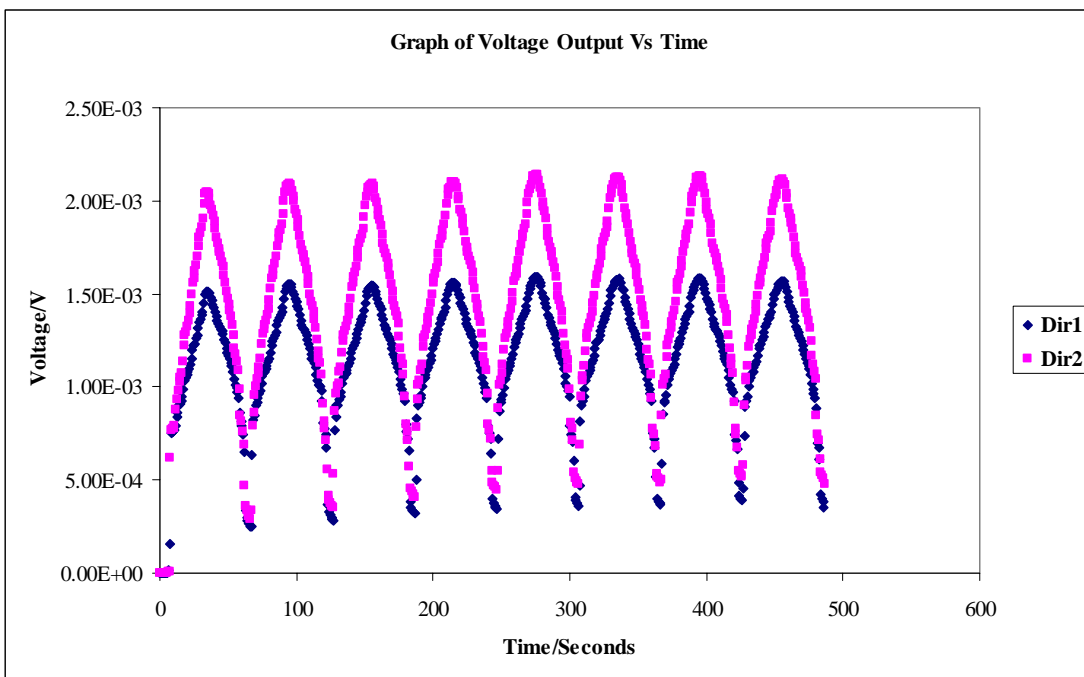
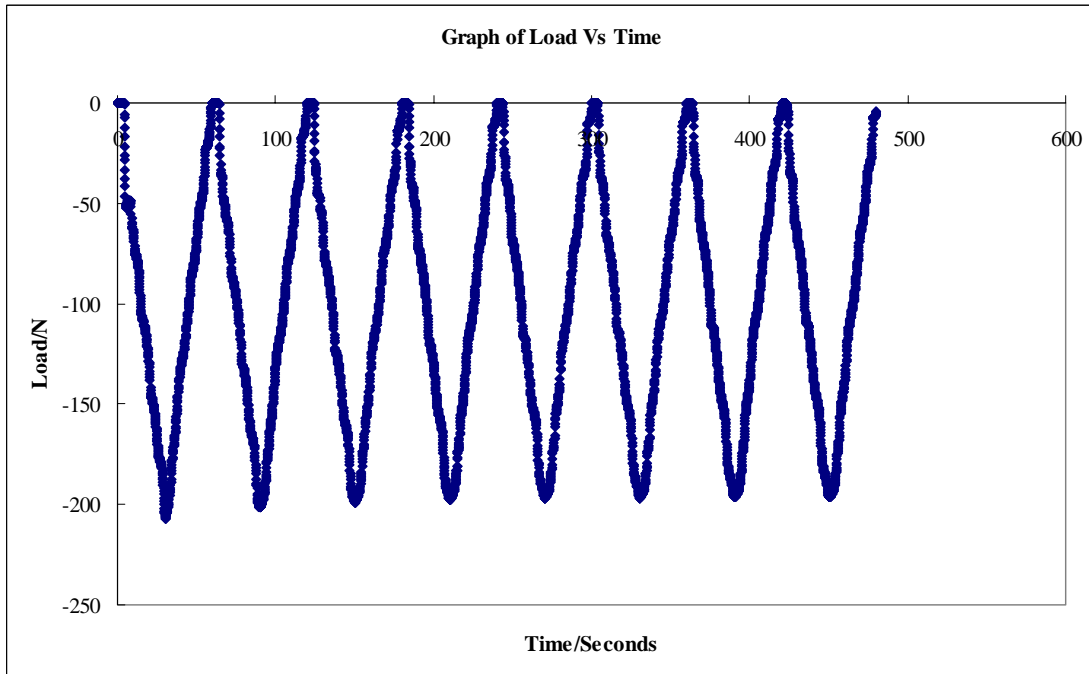


Fig4.5.10: A load of 200N was applied continuously for a time span of 30 seconds and that load was gradually removed to zero force within a time span of another 30 seconds.

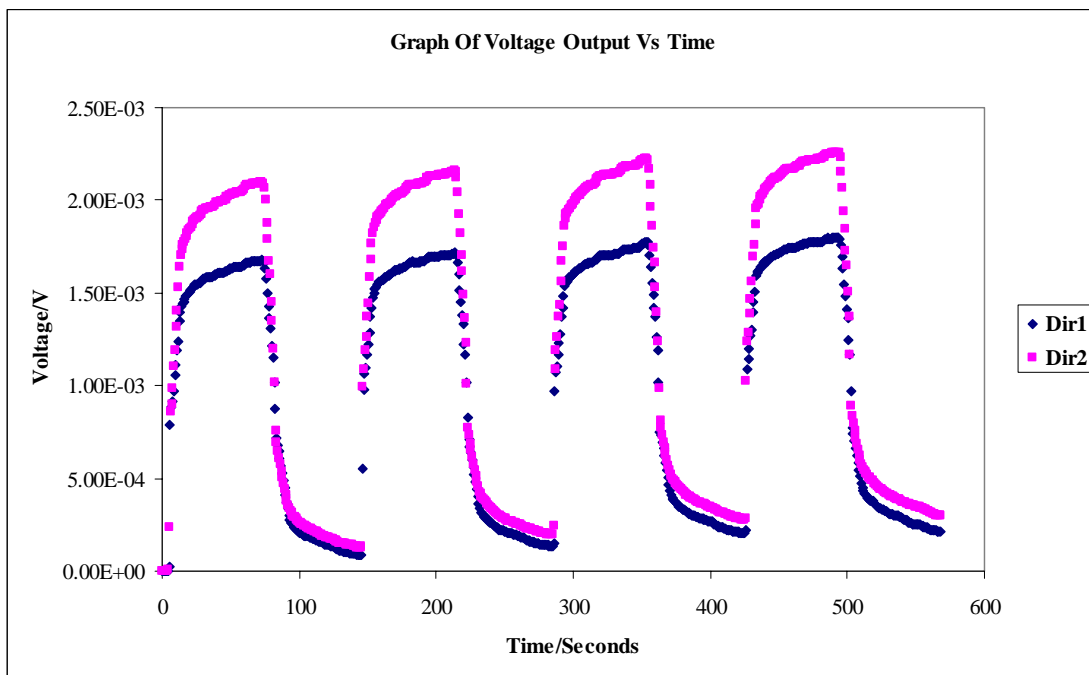
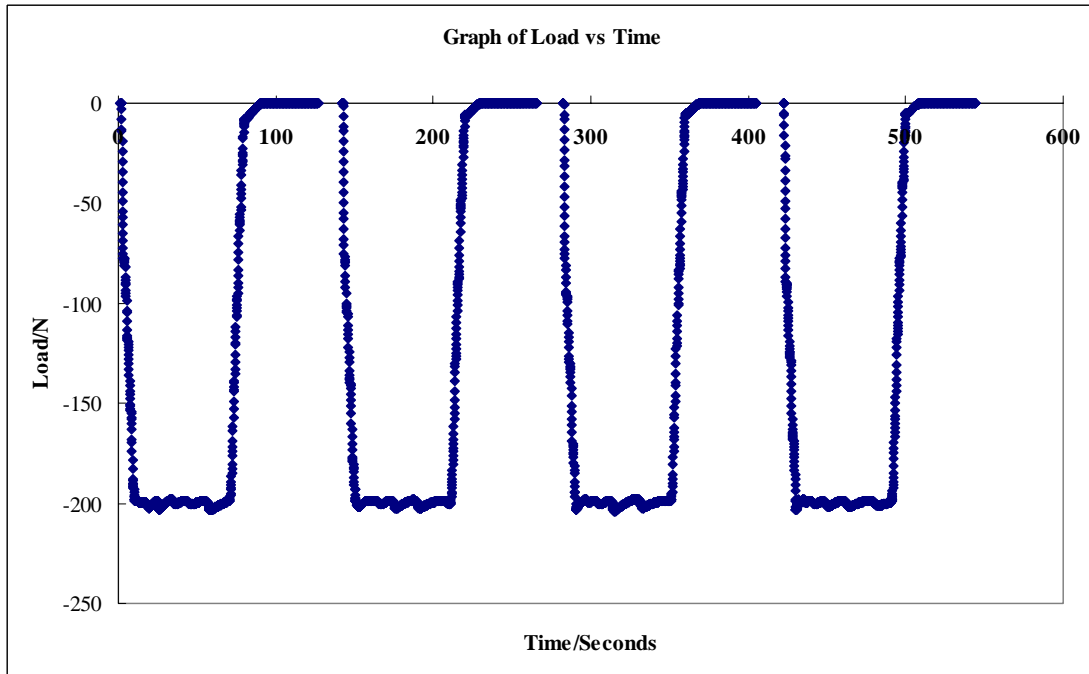


Fig4.5.11: A load of 200N was applied for a time span of 10 seconds. The 200N force was applied for another 60 seconds and the force was gradually reduced to zero force within another 10 seconds.

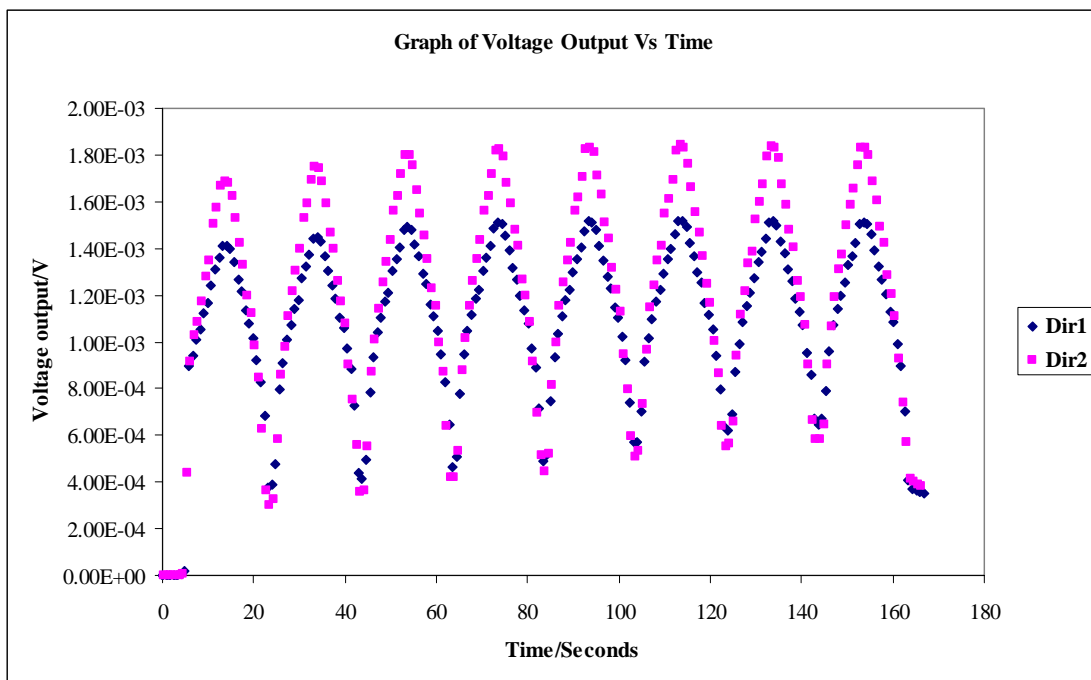
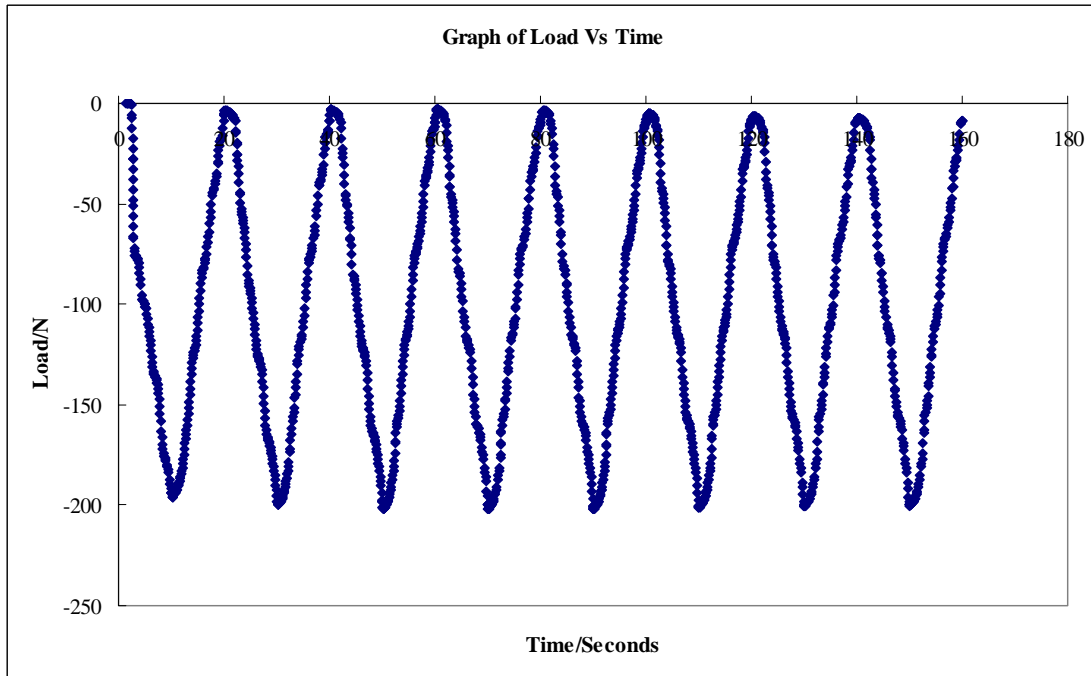


Fig4.5.12: A load of 200N was applied continuously for a time span of 10 seconds and that load was gradually removed to zero force within a time span of another 10 seconds.

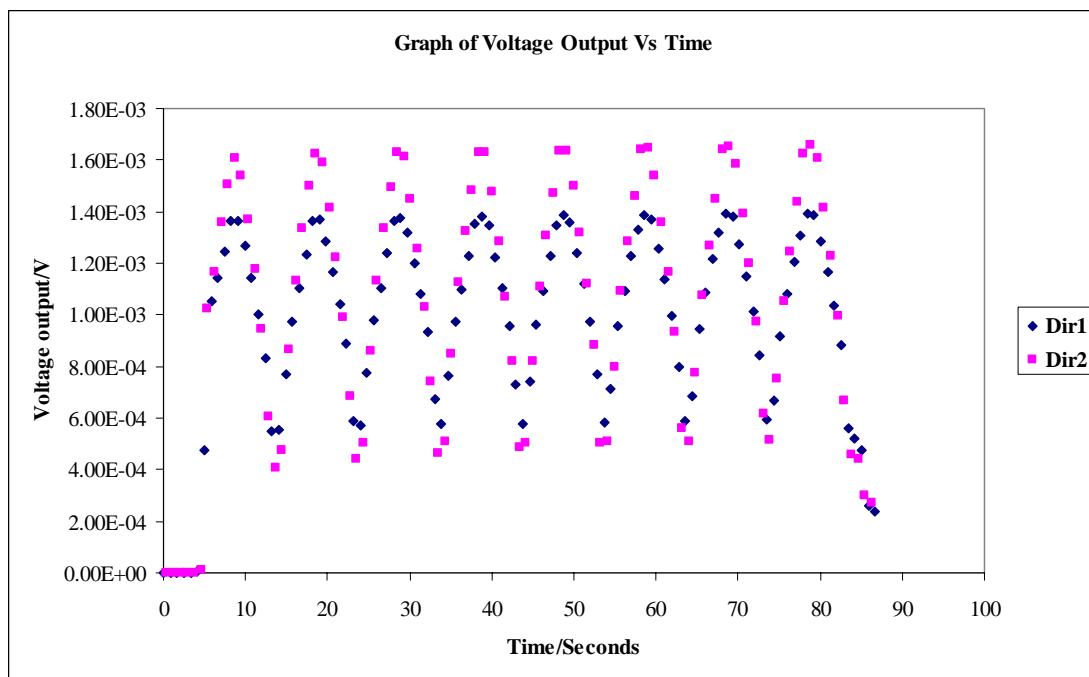
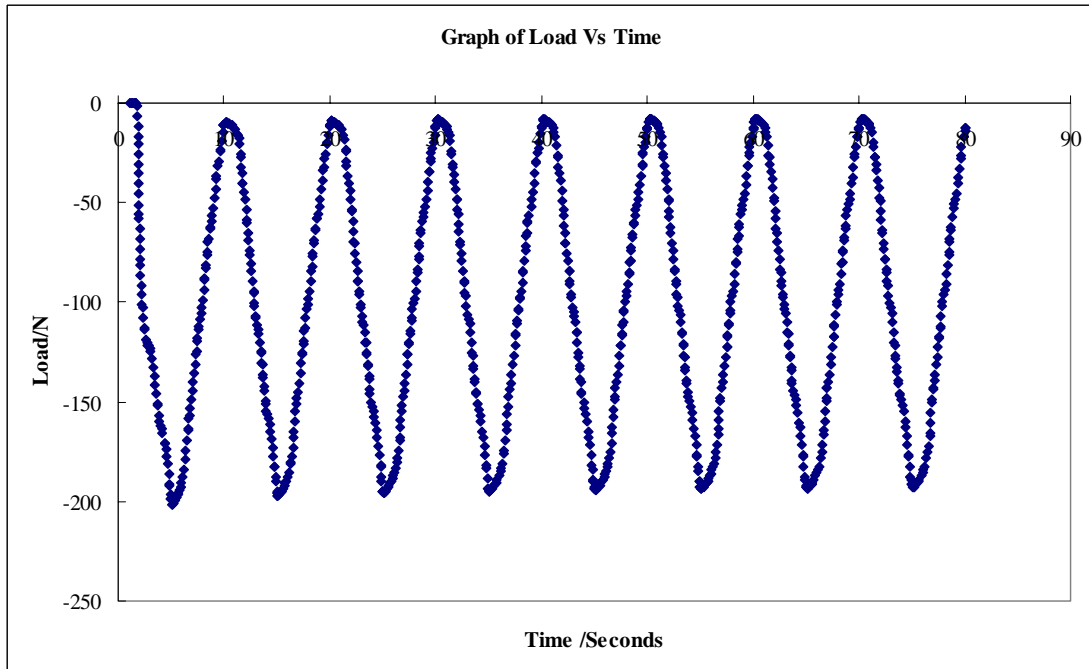


Fig4.5.13: A load of 200N was applied continuously for a time span of 5 seconds and that load was gradually removed to zero force within a time span of another 5 seconds.

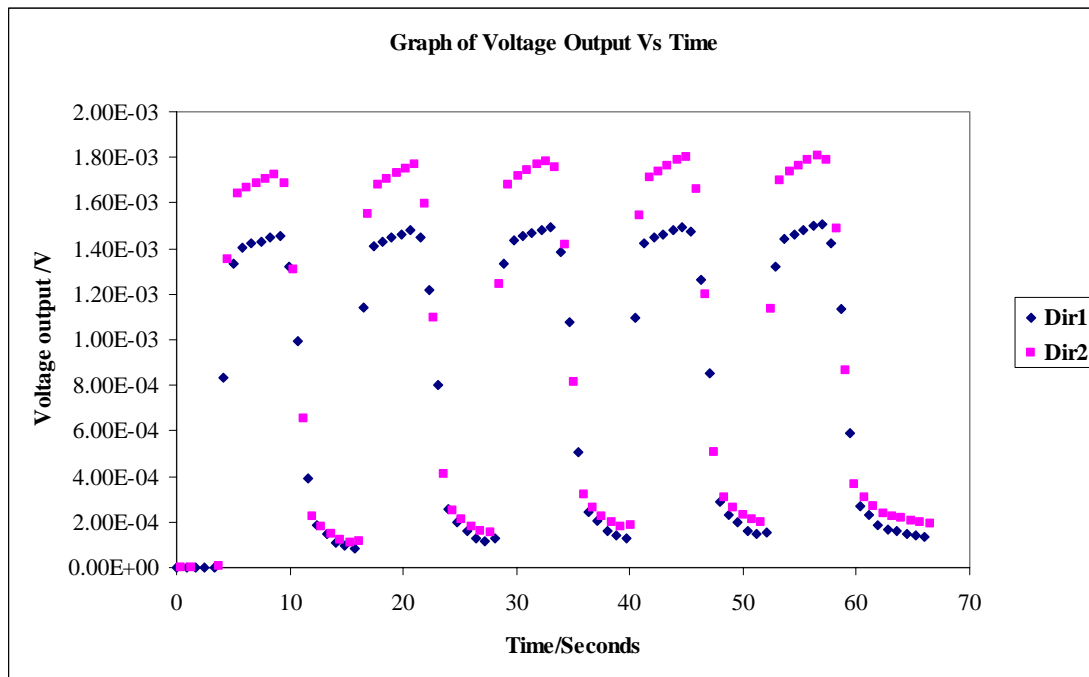
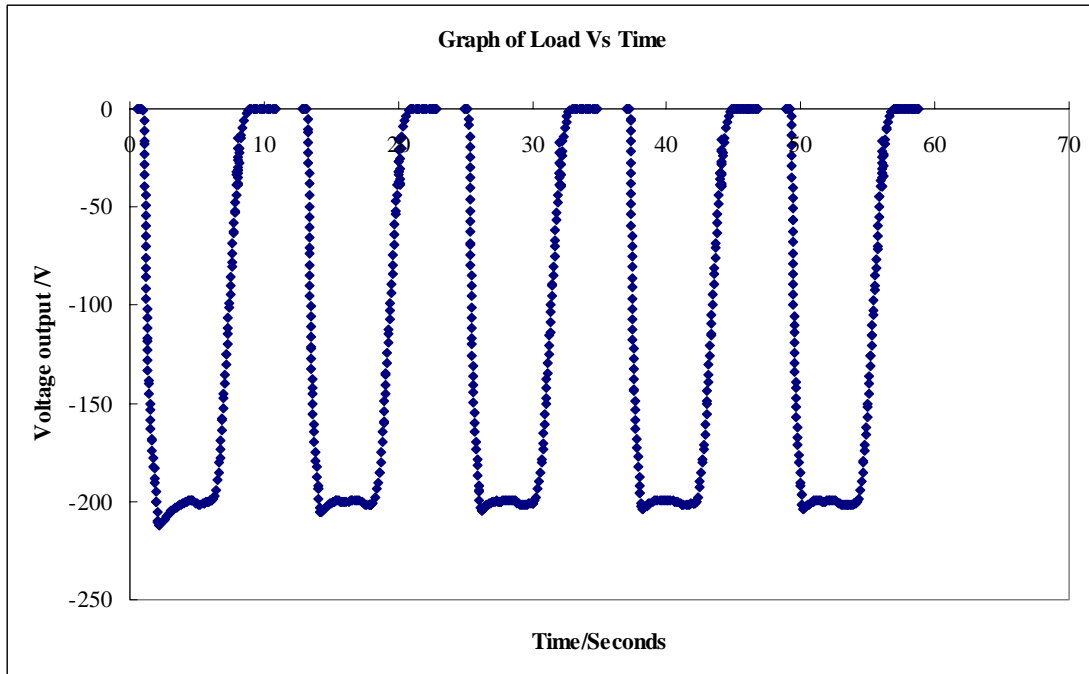


Fig4.5.14: A load of 200N was applied for a time span of 2 seconds. The 200N force was applied for another 3 seconds and the force was gradually reduced to zero force within another 2 seconds. This was an actual Bruxism event simulation. [65, 66].

From the experiments (Fig 4-5-9-4-5-14), it could be clearly seen that the voltage output in one direction is bigger than the other. This phenomenon is attributed to the fact that extension of the strain gage due to the force exertion in the Z-direction is much greater as compared to the X-direction. This could be further reinforced by the following equations.

$$\epsilon_z = +\frac{\sigma_z}{E} - \frac{\nu\sigma_x}{E} - \frac{\nu\sigma_y}{E}$$

$$\epsilon_x = +\frac{\sigma_x}{E} - \frac{\nu\sigma_z}{E} - \frac{\nu\sigma_y}{E}$$

The stress experienced in the z-direction is much greater as compared to the stress experienced in the x-direction. Thus it would be better to place the sensor in the z-direction as it gives a much higher voltage output. Although the right direction for placing the sensor was found, the voltage output in that direction is still small, thus when this sensor is interfaced with other circuitry, (example a microprocessor); there would be interference of noise which might lead to inaccurate results. In order to overcome this problem, a piezoresistive strain gage (that has a gauge factor about 75 times more than an ordinary foil strain gage) would be tested.

4.6 Piezoresistive Strain Gage Sensor

The piezoresistive strain gage sensor was subjected to different loading patterns to determine the output and to check its consistency under the different loading rates and patterns. Instron 5848 Microtester Instron Blue-hill software was programmed to simulate the loading profile. The results are given in the following Figures

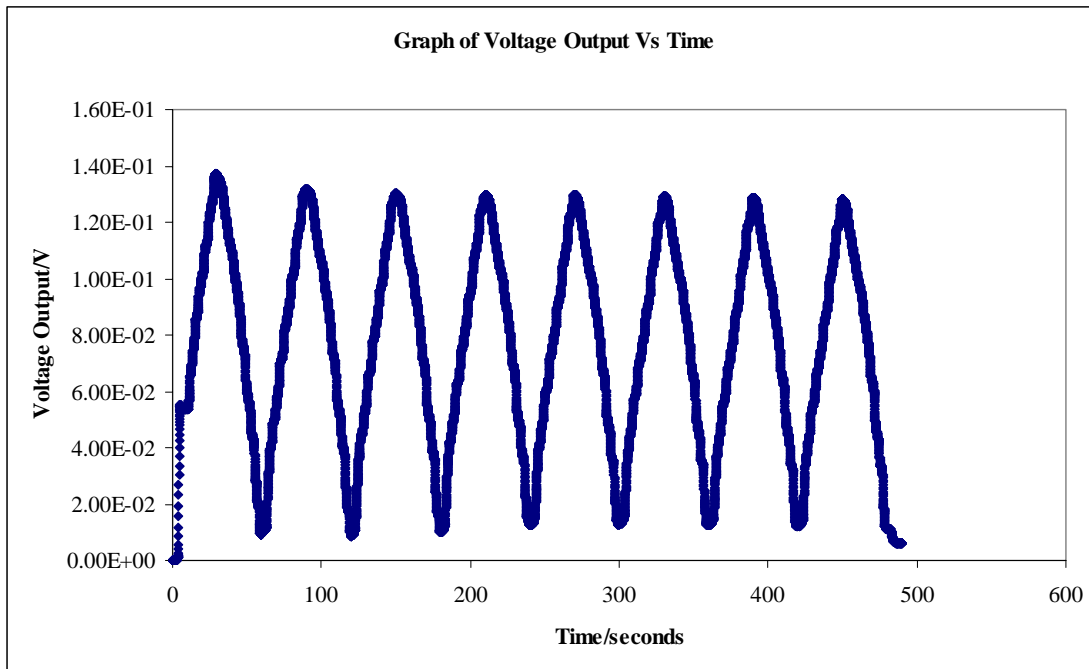
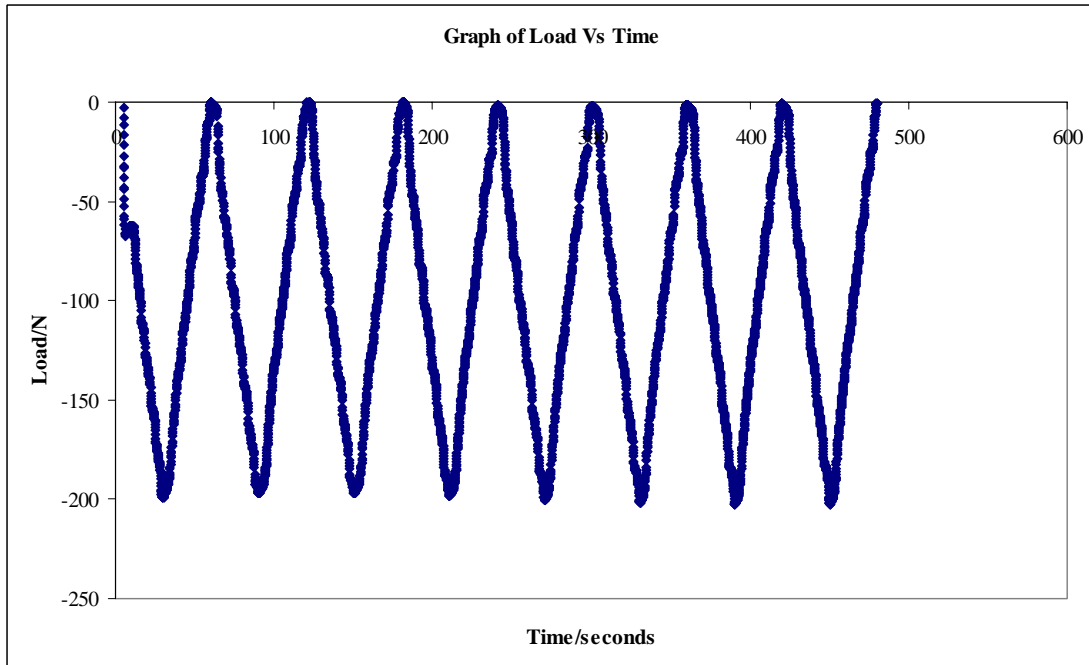


Fig4.6.1: A load of 200N was applied continuously for a time span of 30 seconds and that load was gradually removed to zero force within a time span of another 30 seconds.

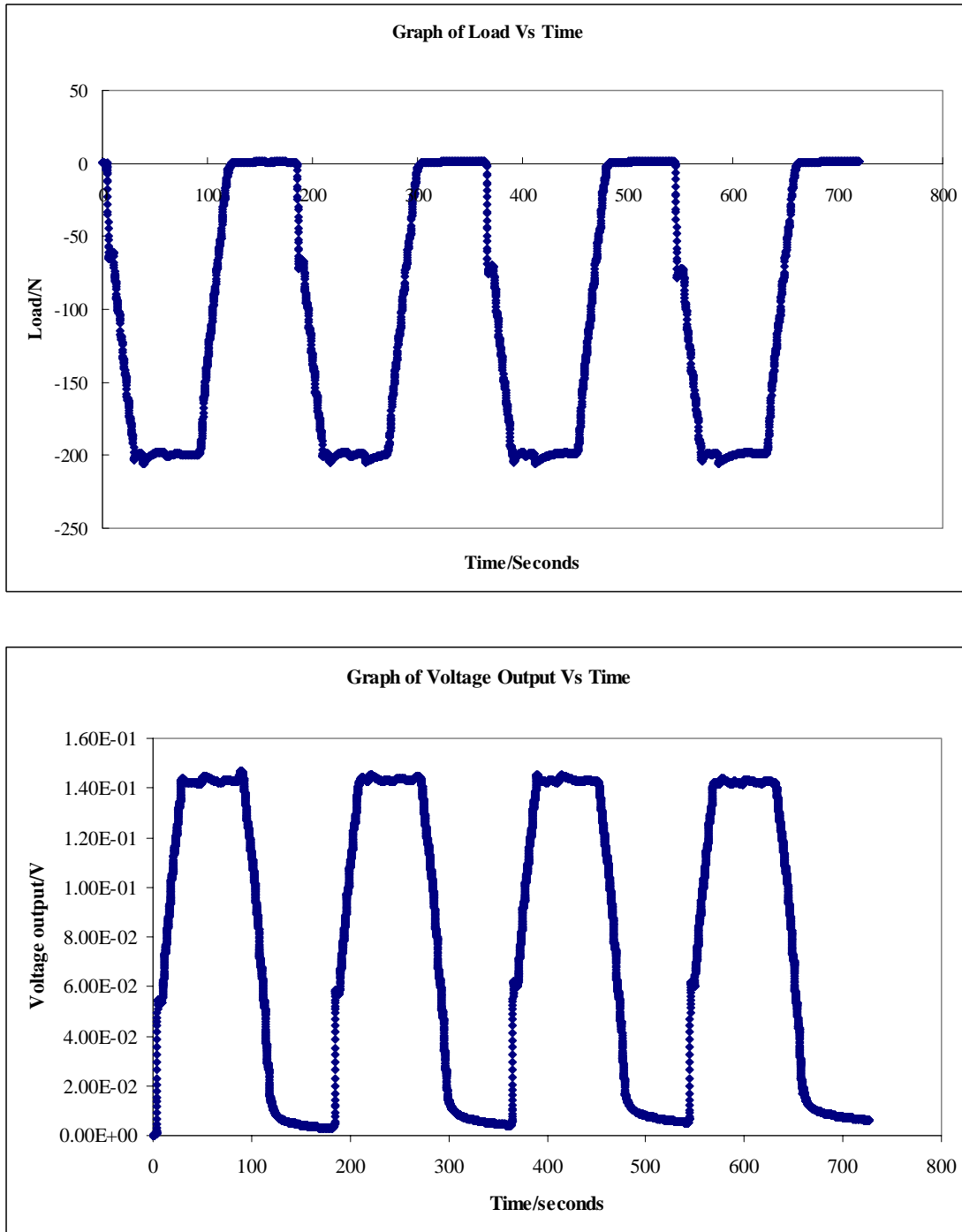


Fig4.6.2: A load of 200N was applied for a time span of 30 seconds. The 200N force was applied for another 60 seconds and the force was gradually reduced to zero force within another 30 seconds.

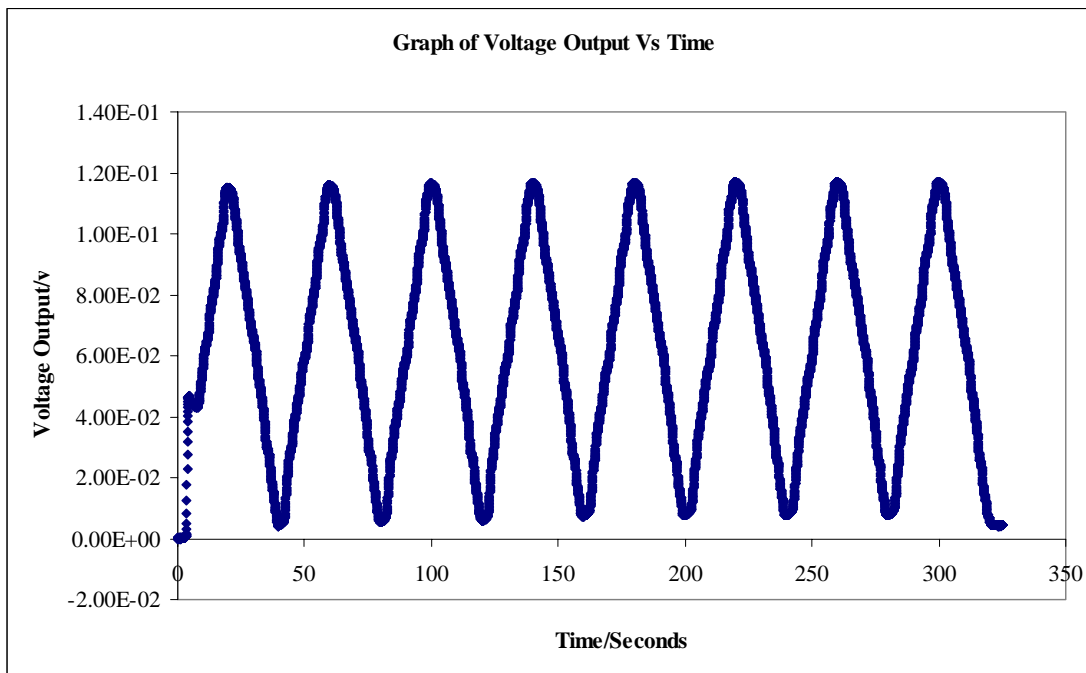
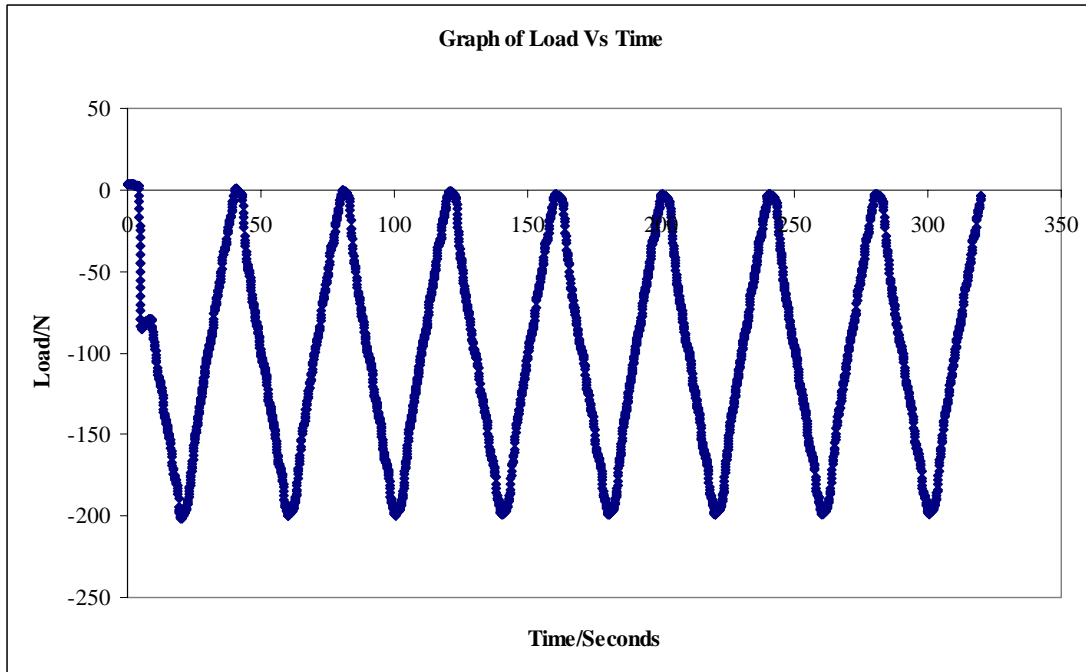


Fig4.6.3: A load of 200N was applied continuously for a time span of 20 seconds and that load was gradually removed to zero force within a time span of another 20 seconds.

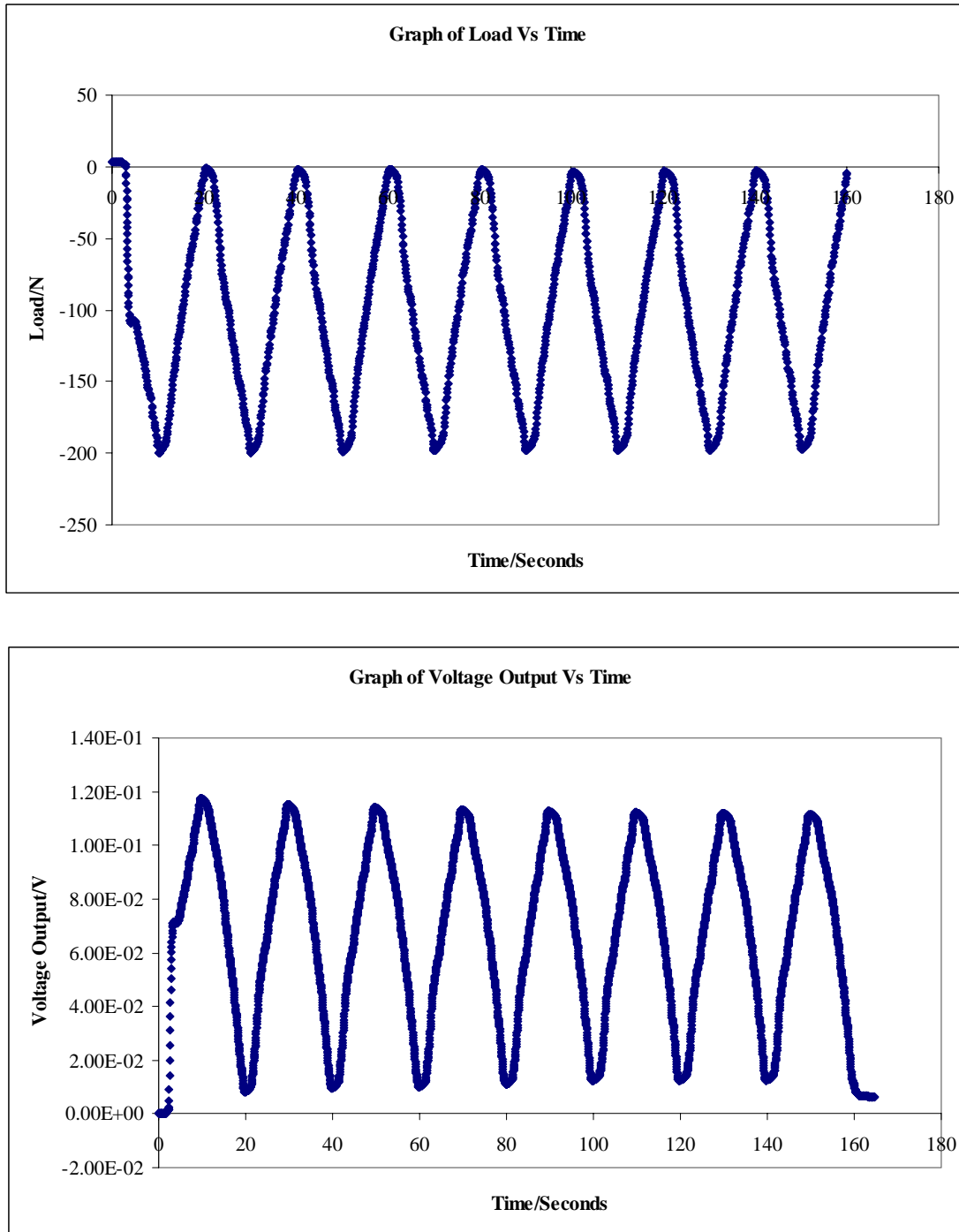


Fig4.6.4: A load of 200N was applied continuously for a time span of 10 seconds and that load was gradually removed to zero force within a time span of another 10 seconds.

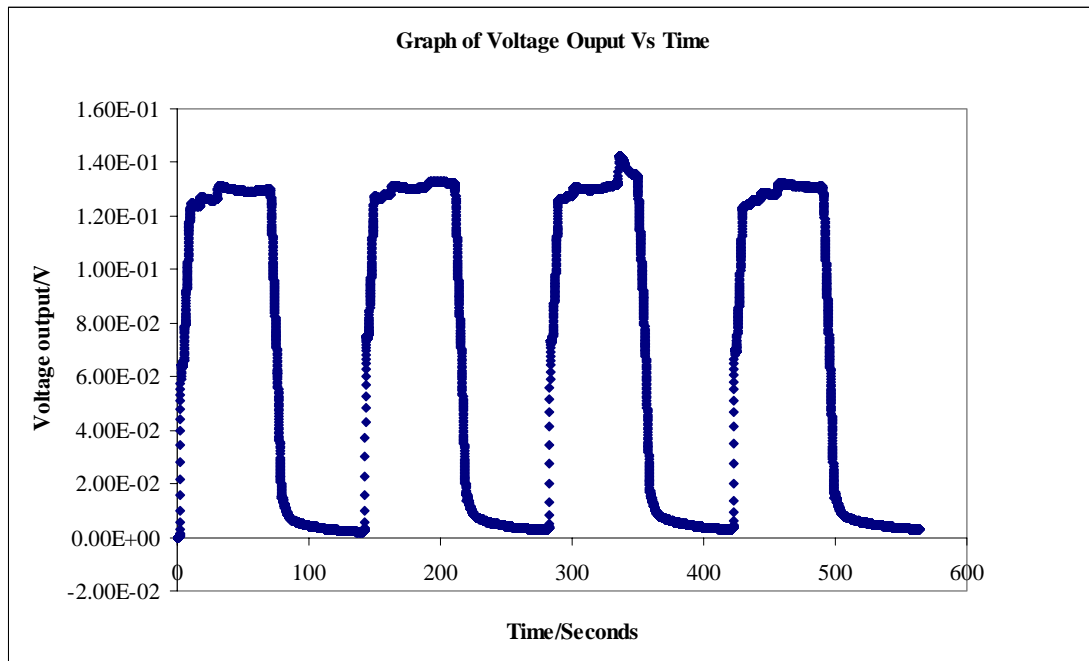
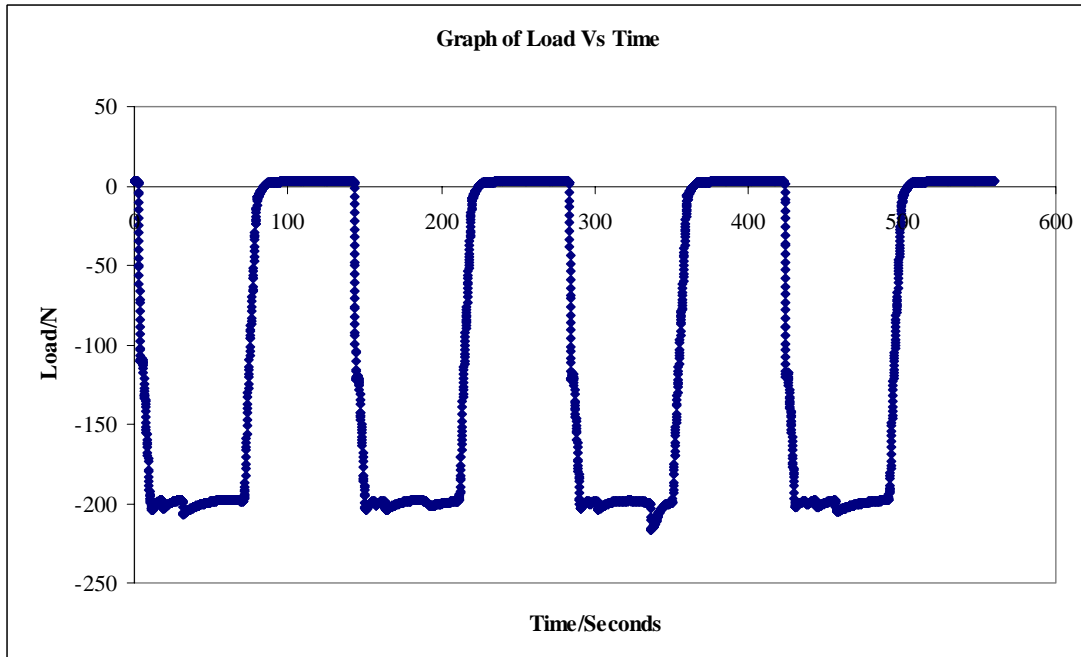


Fig4.6.5: A load of 200N was applied for a time span of 10 seconds. The 200N force was applied for another 60 seconds and the force was gradually reduced to zero force within another 10 seconds.

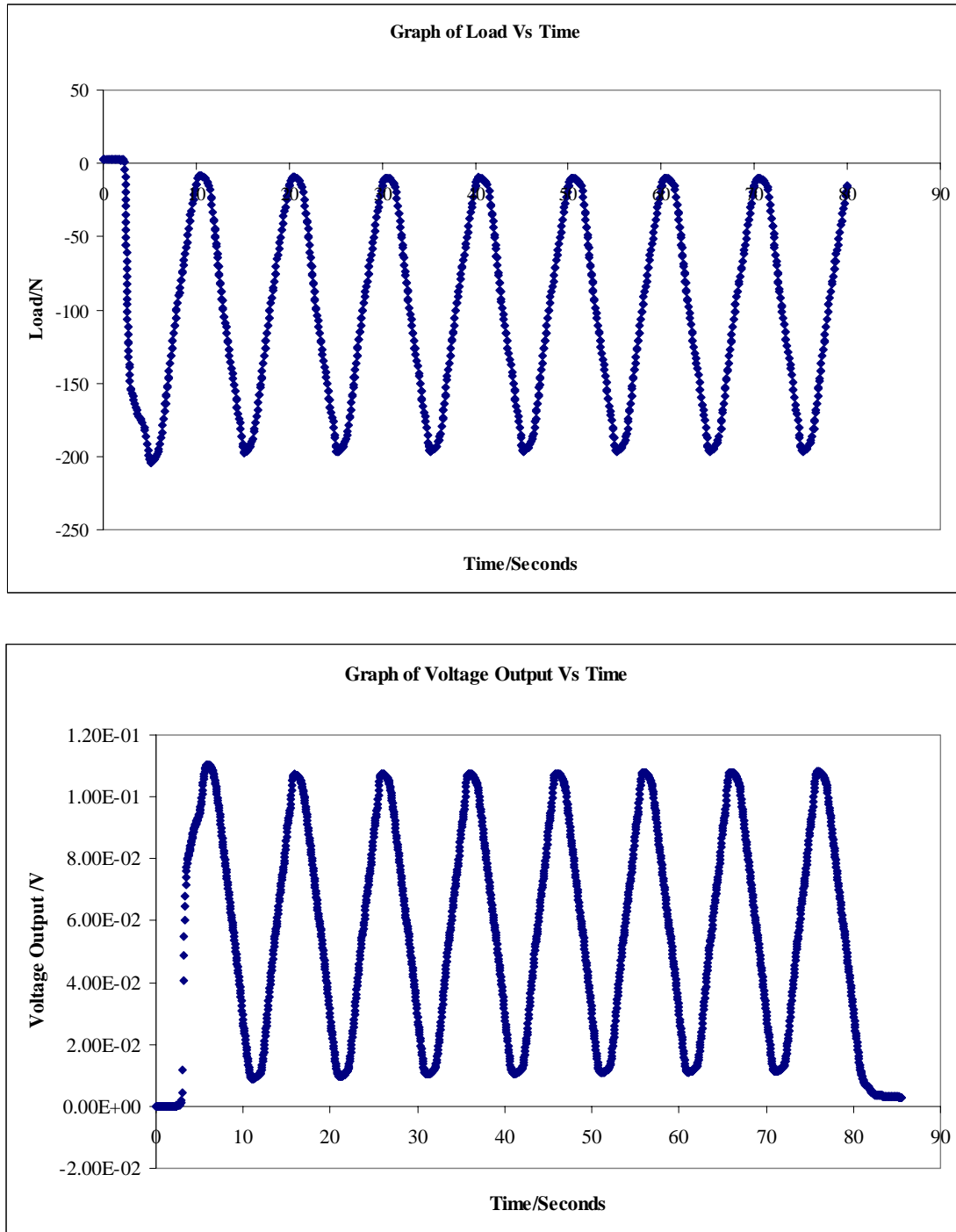


Fig4.6.6: A load of 200N was applied continuously for a time span of 5 seconds and that load was gradually removed to zero force within a time span of another 5 seconds.

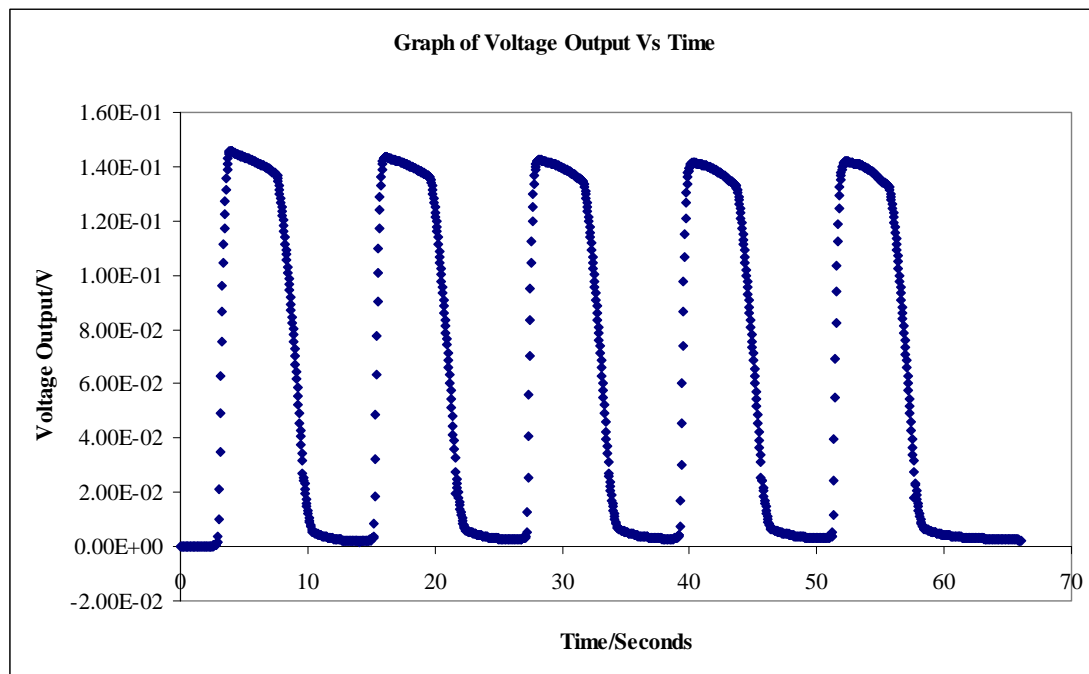
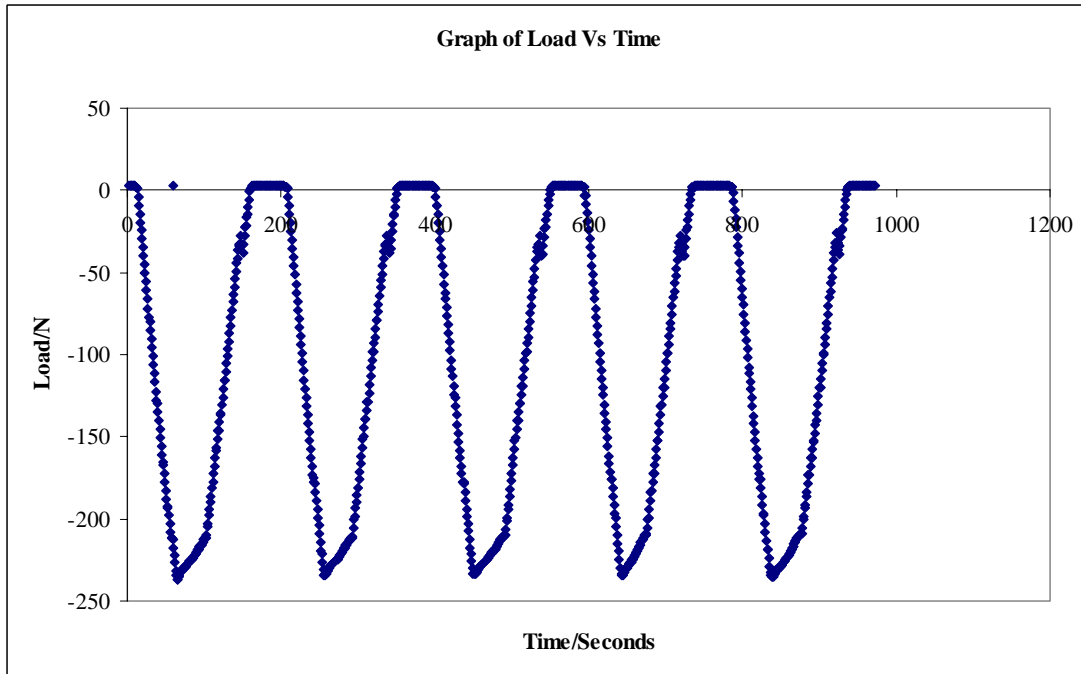


Fig4.6.7: A load of 200N was applied for a time span of 2 seconds. The 200N force was applied for another 3 seconds and the force was gradually reduced to zero force within another 2 seconds. This was an actual bruxism event simulation. [65, 66].

The following graph shows the calibration curve of Voltage output Vs Force.

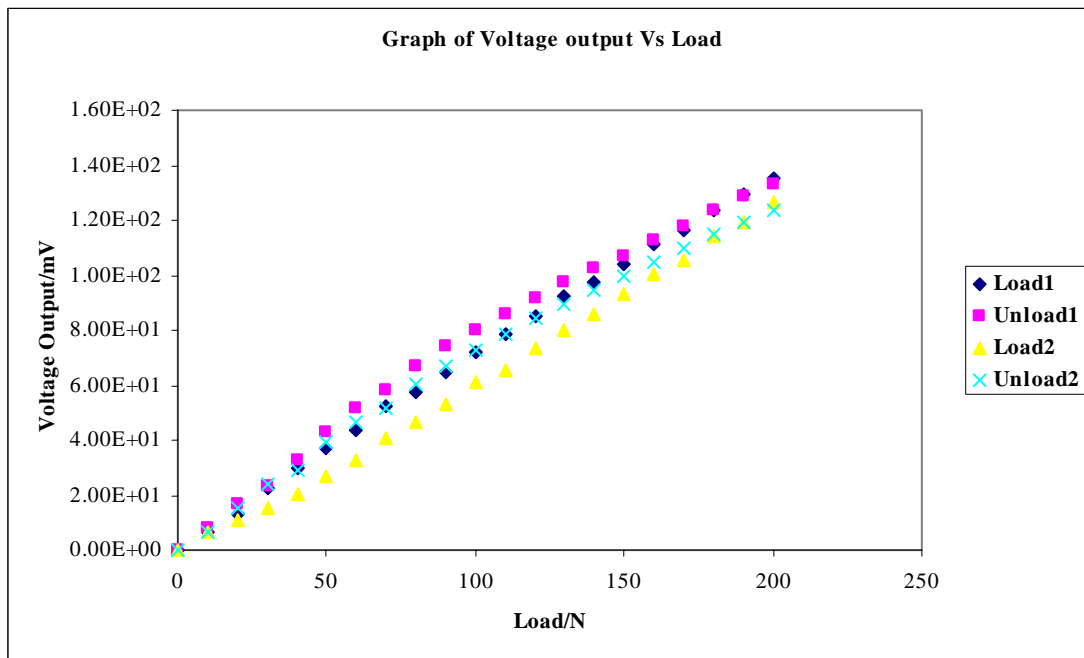


Fig4.6.8: Loading and Unloading graph of the piezoresistive Sensor.

From the experimental results, it is quite clear that this sensor actually gives consistent readings. There is less than $\pm 10\%$ error in the repeatability experiments and thus it would be a suitable sensor for the use as bruxism force detector. Due to its high gage factor (the reason to its high gage factor as compared to a constantan strain gage is given in chapter 2 of this thesis), it gives a high voltage output, thus noise would not play a significant role in the voltage output that is obtained. This sensor would be the most suitable sensor to be used as a bruxism detection sensor.

CHAPTER 5: Wired Force Sensor Interfaced to SD Card

5.1 S8051 Signal Processing Chip

The sensor for Bruxism force detection has been successfully fabricated and this sensor has to be interfaced to a suitable microcontroller in order to process the data (i.e. to display and store the data) from the sensor. The S8051 microcontroller designed by Chew [67] and Sheng [68] was chosen as this microcontroller was a mixed-signal I.C. chip that contains a signal conditioning unit (this would help to eliminate the unwanted signals, i.e. noise by means of inbuilt filter system), 12-bit analogue to digital converter, (which would be ideal to convert the analogue signals to digital signals) and a microprocessor to process the signals. The following diagram gives a pictorial view of the S8051 chip.

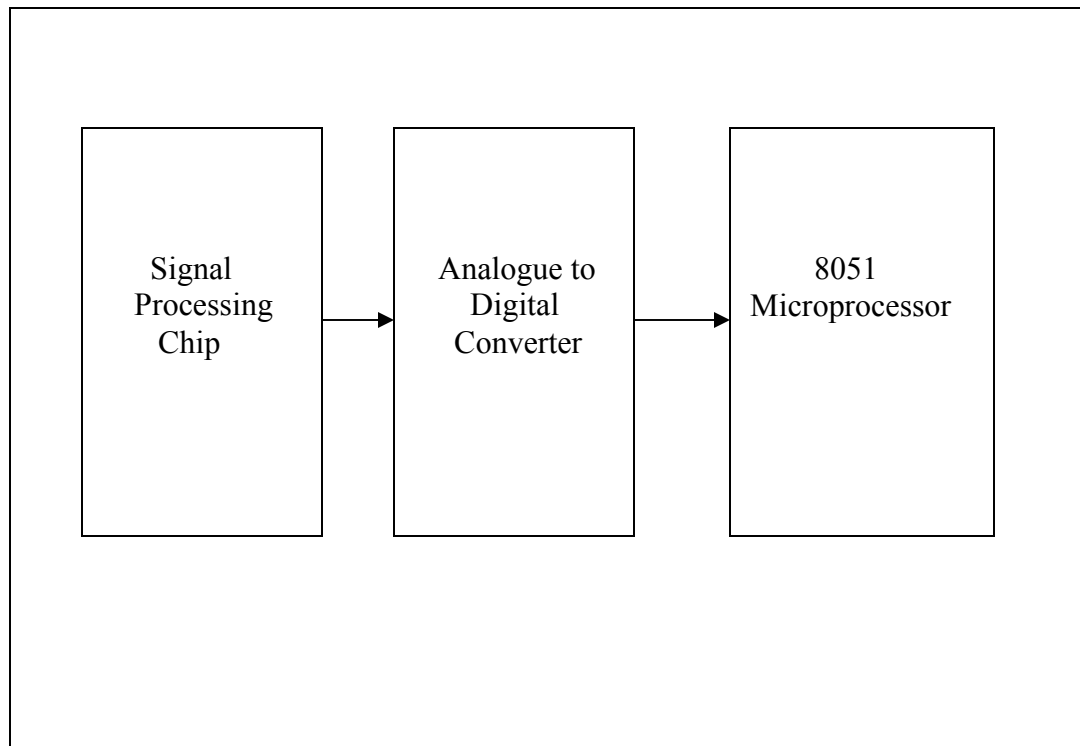
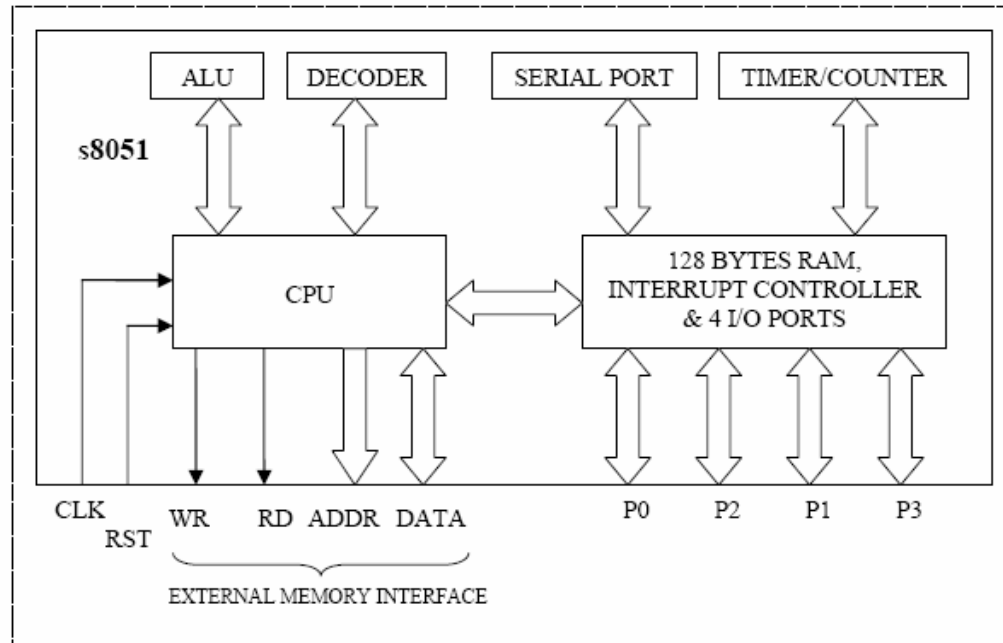


Fig5.1.1:S8051 Chip

An overview of the S8051 (digital part) used in this project is given below in figure 5.1.2.



8-bit CPU
Extensive Boolean processing (Single-bit logic) capabilities
64K bytes Program Memory address space
64K bytes Data Memory address space
128 bytes of on-chip Data RAM
32 bidirectional and individually addressable I/O lines
Two 16-bit timers/counters
Full duplex UART
6-source/5-vector interrupt structure with two priority levels
8 Oscillator periods per machine cycle

Fig5.1.2: The Functions of the S8051 chip

One of the distinct factors of this S8051 microcontroller as compared with the standard Intel 8051 microcontrollers is that most of the instructions are executed in one machine cycle containing 8 clock cycles as compared to the standard Intel 8051 where instructions are executed in one machine cycle of 12 clock cycles.

It was stated that this microcontroller would be roughly 1.8 times faster than a standard Intel 8051 given the same operating frequency [67, 69]. This microcontroller has an additional feature of interfacing to a SD (Secure Digital) card to store large amount of information. The Use of SD card allows the easy transfer of files to and from PC with a SD card reader. The S8051 design also includes the ability to load its program from the SD card. The following paragraphs would describe more on the SD Card Boot Loader.

5.1.1: SD Card Boot Loader [67]

Since the S8051 has an additional feature of being able to load its program from the SD card into an external SRAM (Static Random Access Memory) chip, it would eliminate the need for an external ROM (Read only Memory) to the S8051 and it would also allow the 8051 firmware to be updated easily. In order to use this feature, the S8051 would start executing from an internal ROM that stores a fixed pre-designed program (loader.c) that would load binary data from a file in the SD card (program. bin) into an external SRAM chip and resets the internal registers and continue execution from the external SRAM. The S8051 (with SD Card Loader) Block Diagram is shown below.

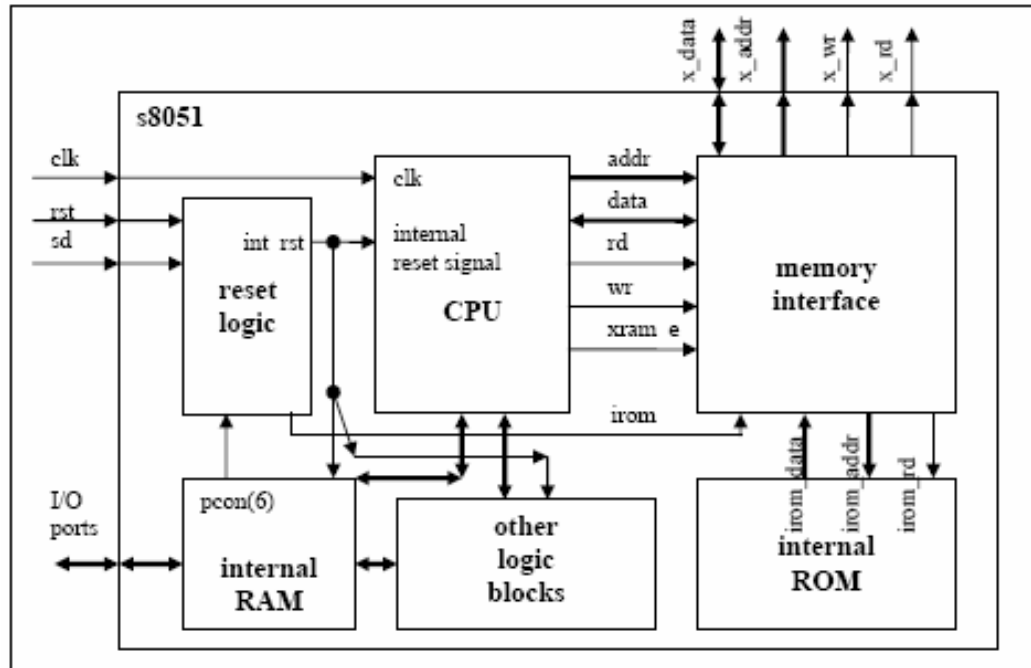


Fig5.1.3: Block Diagram of the 8051 chip

The following paragraphs would give an overview of the SD Card and how it is being interfaced to a microcontroller.

5.1.2: SD Card

The SD Card can provide up to 1024 millions bytes (1GB) of memory using flash memory chips that were specifically designed for use in the mass storage application.

The high capacity, small form factor and its low voltage operation (3.3V) makes it very suitable for our application. The SD card provides an option of interfacing with external devices by means of two Communication Protocols, the SPI (Serial Peripheral Interface) bus interface and the SD Bus interface. In this project, the SPI bus interface is chosen, due to its ease of implementation and it also requires less number of pins. SPI is described further in detail.

5.1.3: Serial Peripheral Interface

SPI which stands for Serial Peripheral Interface is a synchronous protocol that allows a master device to initiate communication with slave devices such as memory, displays, ADCs and other similar products. The following paragraphs would describe the basic SPI operation [70].

SPI is often referred to as a three-wire interface and there are two modes, namely the master and slave mode. Almost all implementations of SPI require two DATA lines, a CLOCK line, a CHIP SELECT and a common ground. The DATA lines are referred to as MOSI (Master out Slave in) and MISO (Master in Slave out). The Master device (in our case the microcontroller) provides the clock signal and determines the state of the chip select line (i.e. it activates the slave that it wants to communicate with). The slave device (in our case the SD card) receives the clock and chip select from the MASTER. The key operation in SPI involves the transfer of a byte of data between the Master and the currently selected slave; simultaneously, a byte of data will be transmitted back from the Slave to the Master. It is important to note that when Data is transmitted; the incoming data must be read before it is transmitted again. If the incoming data is not read, the data will be lost and the SPI module might be disabled. Data has to be exchanged between devices. There is no one way communication. The Data exchanges are controlled by the CLOCK line, or more commonly known as SCK (Serial Clock Line). The following figure 5.1.4 illustrates the shift registers at the heart of the SPI protocol and figure 5.1.5 illustrates cascading several SPI devices

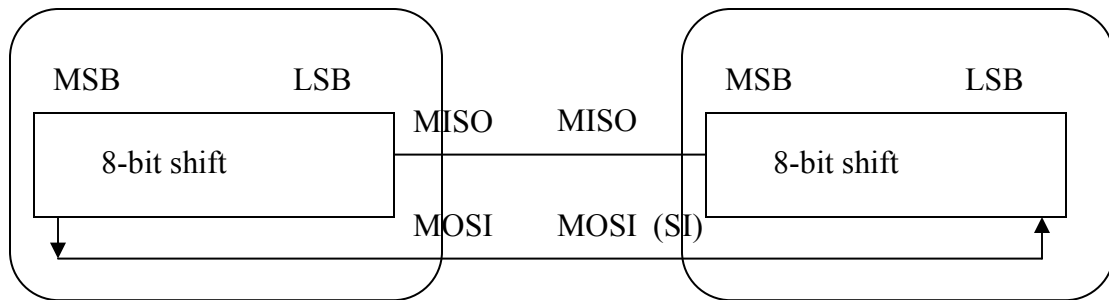


Figure 5.1.4: Single Slave and Master

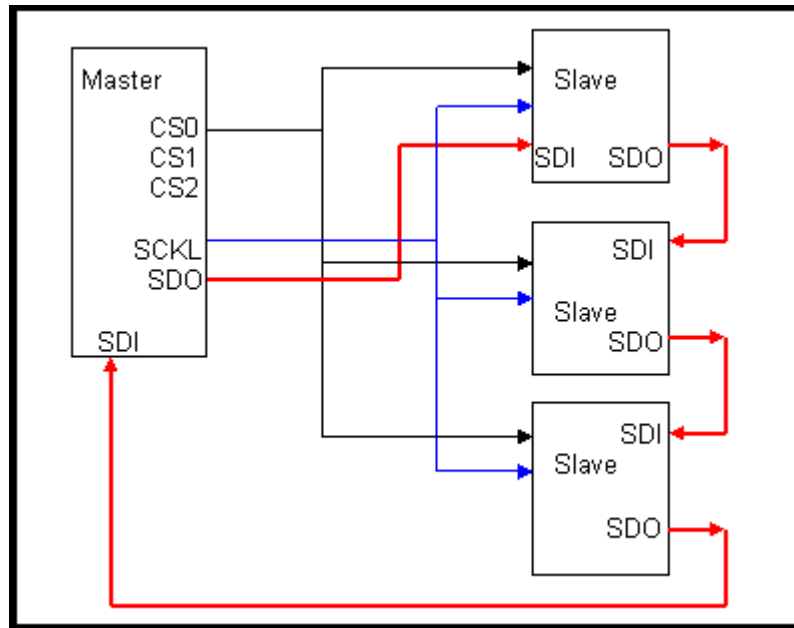


Fig5.1.5: Cascading several SPI Devices

5.1.4: Data Exchange Protocol

Slave select (more commonly known as SS) signal line is the line that controls the use of a particular slave. This line indicates to a slave that the master wishes to start an SPI data exchange between that slave device and itself. This signal is mostly active low. It has an additional function of resetting the SPI slave so that it is ready to receive the next byte. In SPI typical data exchange occurs during either the rising or falling edge of SCK. The following diagram gives an example of a typical SPI communication [71, 72].

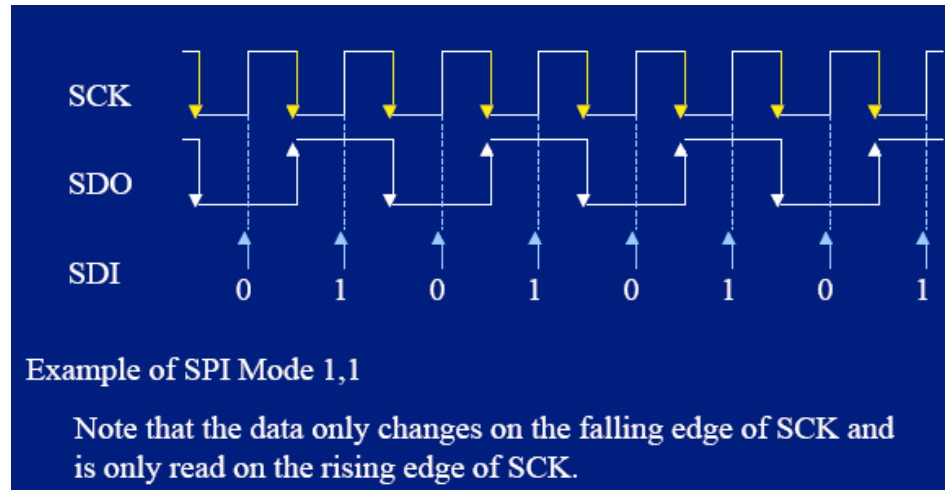


Fig5.1.6: Typical SPI Communication

The following paragraphs would give an in-depth knowledge of the SPI communication Protocol.

5.2: SPI BUS PROTOCOL [72]

The SPI channel for an SD card is byte-oriented, which means that every command or data block is built of 8-bit bytes and are byte aligned (multiples of 8 clocks). The SPI messages are built in the following manner. It is clearly depicted in table 5.2.1

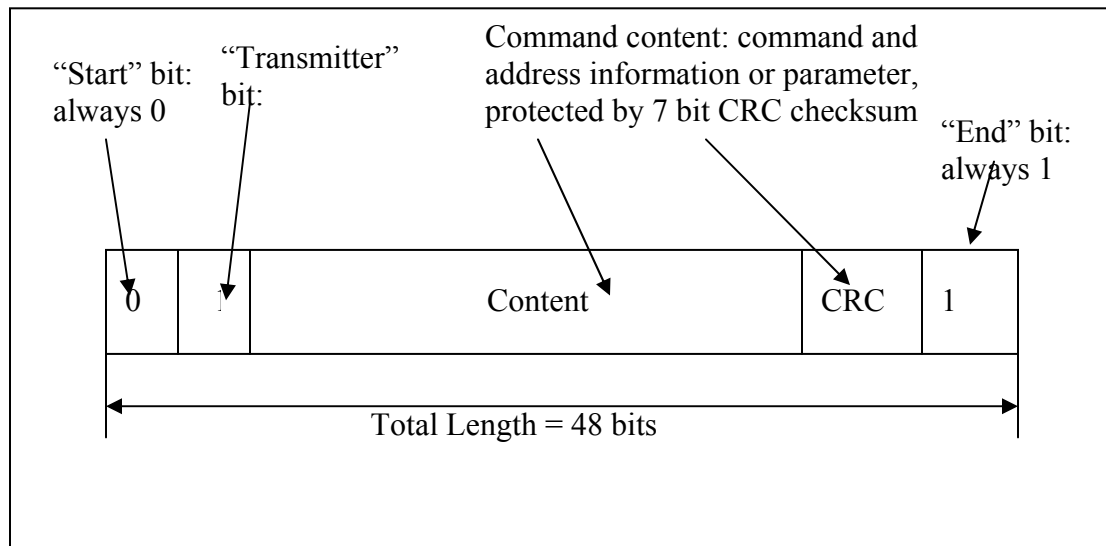
Command
Response
Data-block tokens

Table 5.2.1: SPI Messages

The host first initiates a communication by selecting the respective slave (i.e. by making SS=0);

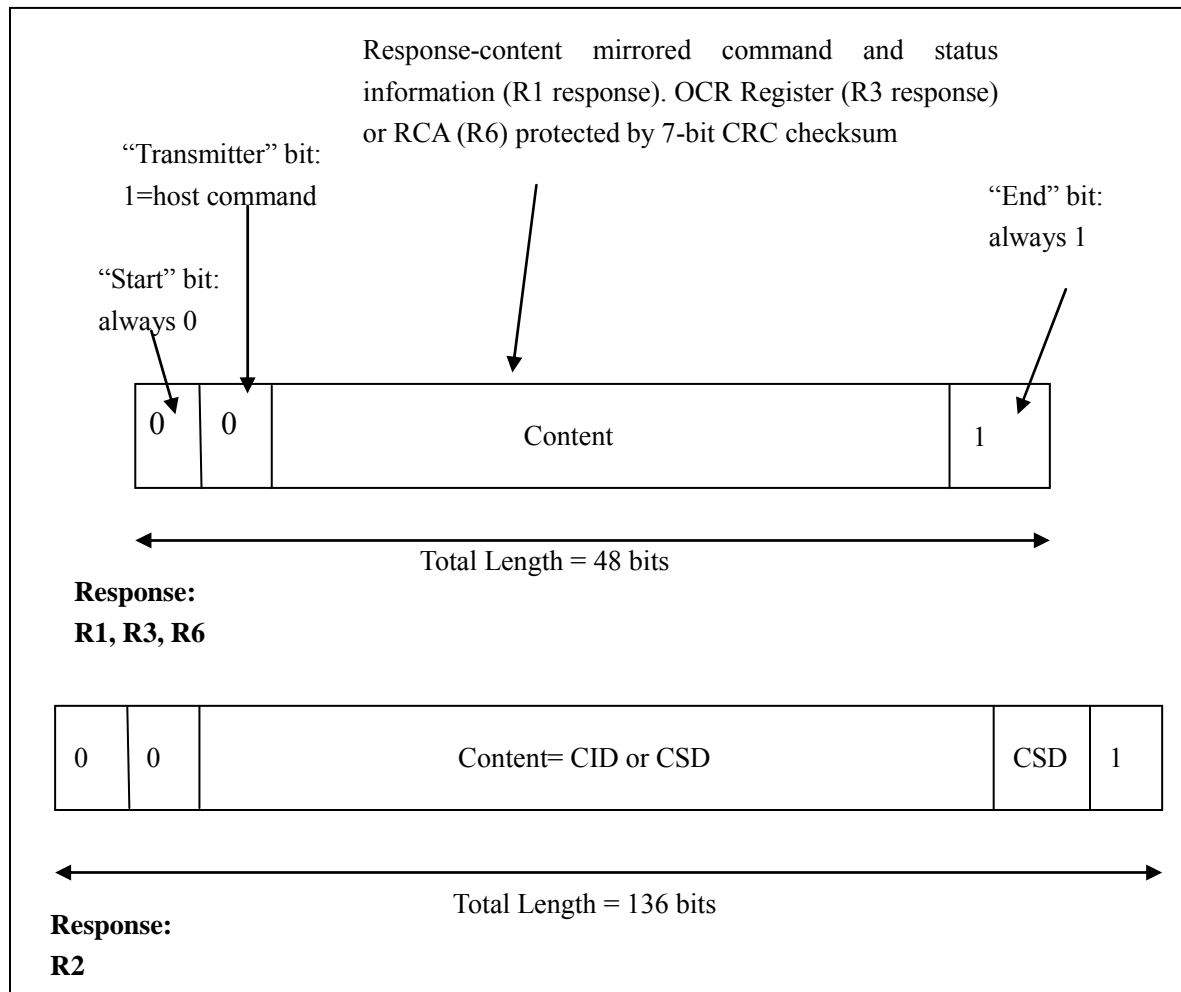
It then sends a command (the command description are presented later in this chapter).

The coding scheme of the command Token is illustrated below.

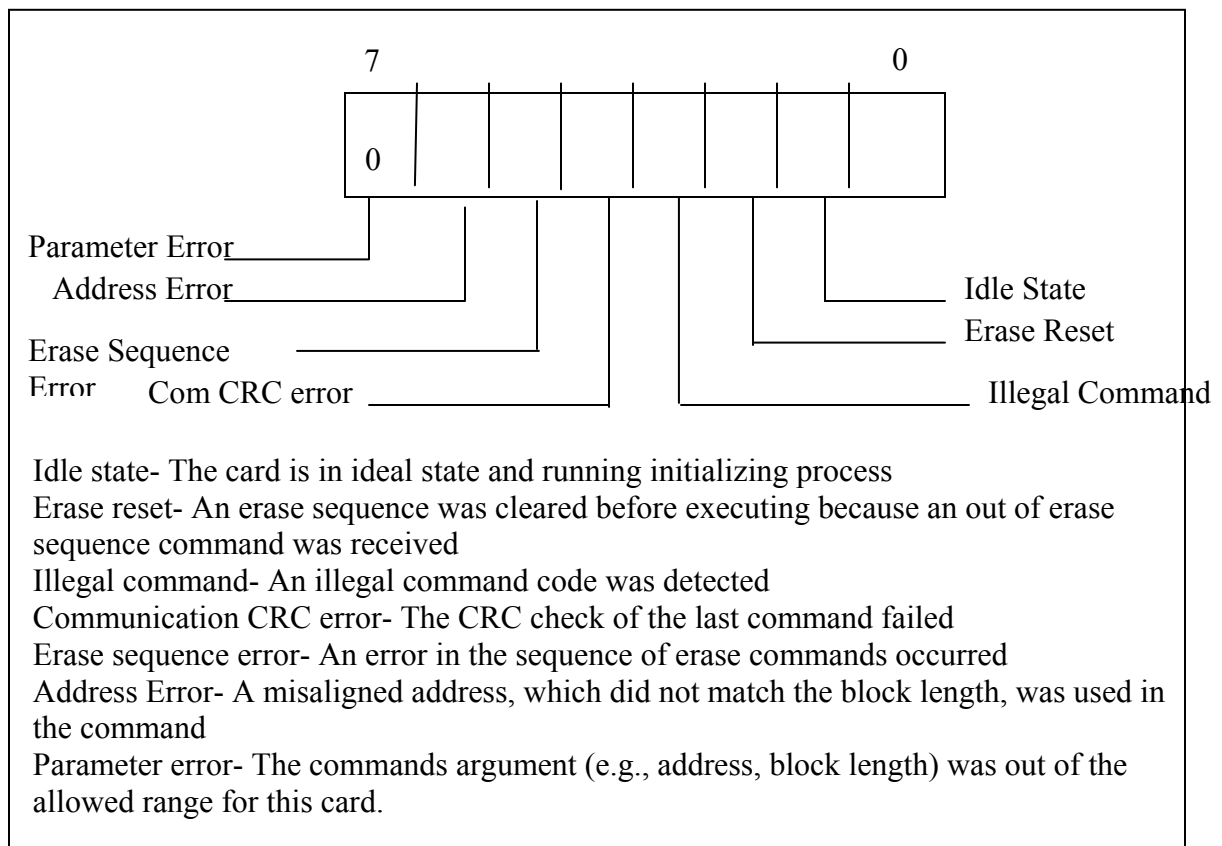


Each command token is preceded by a start bit (0) and it ends by an end bit 1. The total length is 48 bits. CRC bits are there to prevent any transmission errors; (in SPI mode, the SD card offers a non protected mode and thus CRC bits are treated as “don’t care” state). It is also important to take note that in the CMD line, the transmission starts with the MSB bit first and ends with LSB bit.

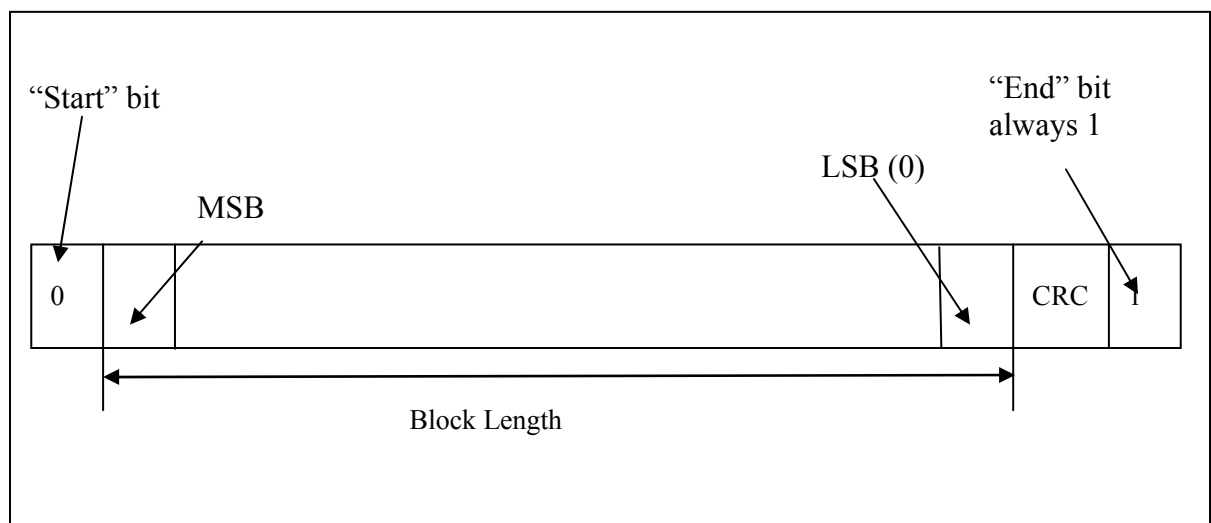
After the command token, the selected slave would then respond to the command by sending an 8 or 16 bits response structure. If there is any problem with the data-retrieval, the slave would respond with an error response. The coding of the Response token is illustrated below. (The type of response expected from each command would be discussed in the command description chapter later)



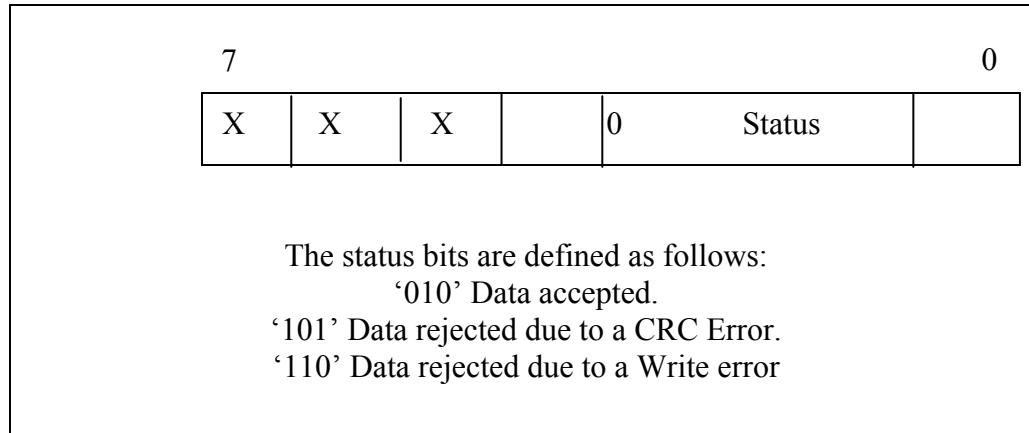
The structure of the R1 response would be elaborated in the following diagram. As this project does not deal with R2, R3, and R6 responses, it would not be discussed. Further details could be obtained from [70].



Once this process has finished the data is then sent. It is important to take note that a set block length (of data) sent or received has to be 512 bytes and any length of less than 512 bytes will lead to an error. The following diagram illustrates the coding schemes of a Data Packet Format.

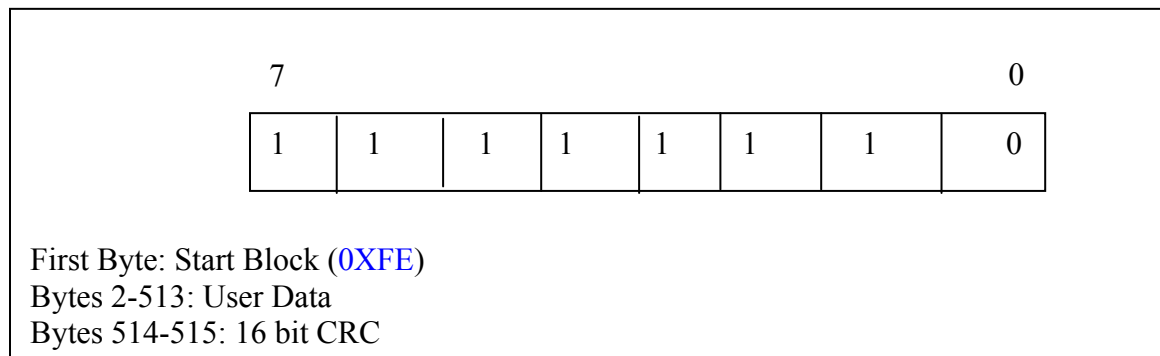


Every data block written to the card is acknowledged by a data response token, the format (1 byte long) is illustrated below.

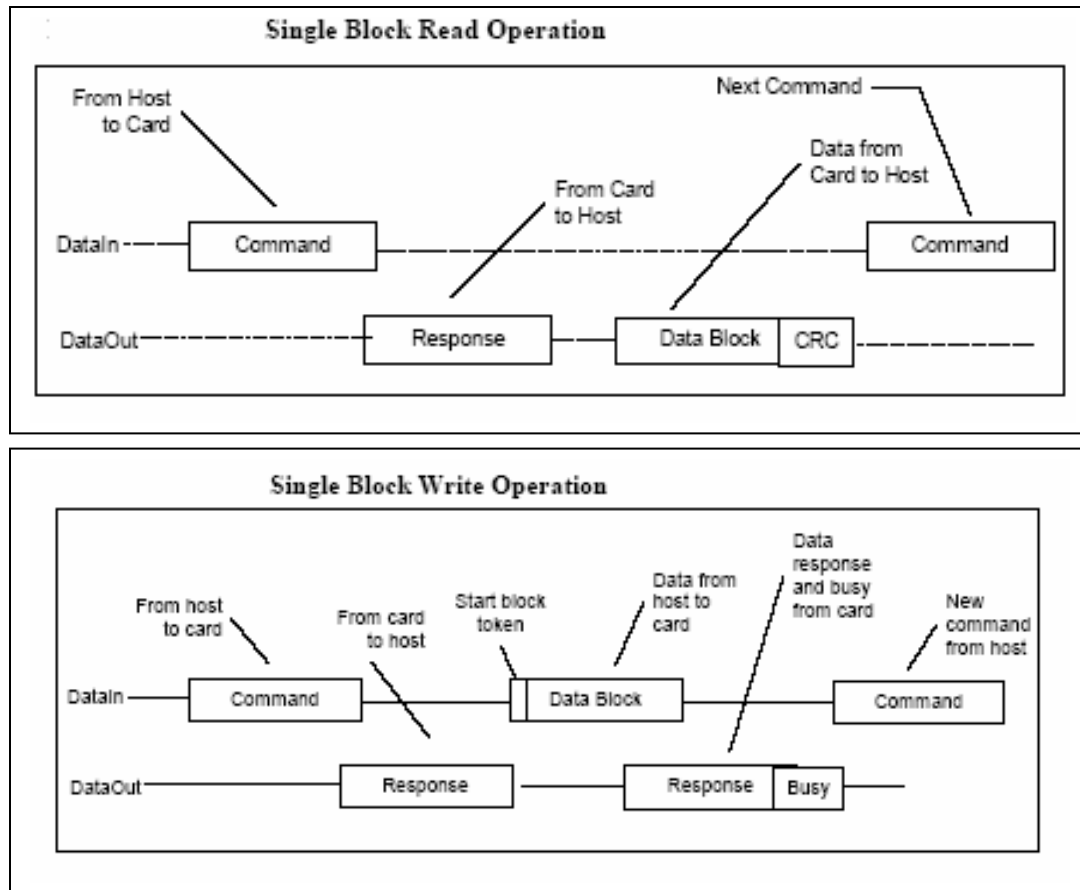


It is also important to note that the read and write commands have data transfers associated with them; data is transmitted or received via data tokens. All data types are transmitted MSB.

Data tokens are 4 to 515 bytes long and the format is of as follows for a single Read, single Write and multiple Read block.



The Single Read block operation and Single Write block operation are illustrated below:



The Command description that was described earlier is explained further in the following diagram.

SPI Bus Command Description

CMD Index	SPI Mode	Argument	Resp	Abbreviation	Description
CMD0	Yes	None	R1	GO_IDLE_STATE	Resets the SD Card.
CMD1	Yes	None	R1	SEND_OP_COND	Activates the card's initialization process.
CMD2	No	---	---	---	---
CMD3	No	---	---	---	---
CMD4	No	---	---	---	---
CMD5	Reserved for I/O mode (refer to SDIO Card Specification).				
CMD6	Yes	[31:0] Mode 0 0: Check function 1: Switch function [30:24] Reserved (all 0) [23:20] Reserved for function group 6 (all 0 or 0xF) [19:16] Reserved for function group 5 (all 0 or 0xF) [15:12] Reserved for function group 4 (all 0 or 0xF) [11:8] Reserved for function group 3 (all 0 or 0xF) [7:4] Function group 2 for command system [3:0] Function group 1 for access mode.	R1	SWITCH_FUNC	Checks switchable function (mode 0) and switches card function (mode 1).
CMD7	No	---	---	---	---
CMD8	Reserved.				
CMD9	Yes	None	R1	SEND_CSD	Asks the selected card to send its card-specific data (CSD).
CMD10	Yes	None	R1	SEND_CID	Asks the selected card to send its card identification (CID).
CMD11	No	---	---	---	---
CMD12	Yes	None	R1b	STOP_TRANSMIS	Forces the card to

CMD Index	SPI Mode	Argument	Resp	Abbreviation	Description
				SION	stop transmission during a multiple block read operation.
CMD13	Yes	None	R2	SEND_STATUS	Asks the selected card to send its Status Register.
CMD14	Reserved.				
CMD15	No	---	---	---	---
CMD16	Yes	[31:0] block length	R1	SET_BLOCKLEN	Selects a block length (in bytes) for all following block commands (read & write). ¹
CMD17	Yes	[31:0] data address	R1	READ_SINGLE_BLOCK	Reads a block of the size selected by the SET_BLOCKLEN command. ²
CMD18	Yes	[31:0] data address	R1	READ_MULTIPLE_BLOCK	Continuously transfers data blocks from card to host until interrupted by a STOP_TRANSMISSION command.
CMD19	Reserved.				
CMD20	No	---	---	---	---
CMD21 ... CMD23	Reserved.				
CMD24	Yes	[31:0] data address	R1	WRITE_BLOCK	Writes a block of the size selected by the SET_BLOCKLEN command. ³
CMD25	Yes	[31:0] data address	R1	WRITE_MULTIPLE_BLOCK	Continuously writes blocks of data until a stop transmission token is sent (instead of 'start block').
CMD26	No	---	---	---	---
CMD27	Yes	None	R1	PROGRAM_CSD	Programming of the programmable bits of the CSD.
CMD28	Yes	[31:0] data address	R1b	SET_WRITE_PROT	If the card has write protection features, this command sets the write protection bit of the addressed group. The properties of write protection are coded in the card specific data

CMD Index	SPI Mode	Argument	Resp	Abbreviation	Description
					(WP_GRP_SIZE).
CMD29	Yes	[31:0] data address	R1b	CLR_WRITE_PROT	If the card has write protection features, this command clears the write protection bit of the addressed group.
CMD30	Yes	[31:0] write protect data address	R1	SEND_WRITE_PROT	If the card has write protection features, this command asks the card to send the status of the write protection bits.
CMD31	Reserved				
CMD32	Yes	[31:0] data address	R1	ERASE_WR_BLK_START_ADDR	Sets the address of the first write block to be erased.
CMD33	Yes	[31:0] data address	R1	ERASE_WR_BLK_END_ADDR	Sets the address of the last write block in a continuous range to be erased.
CMD34 ... CMD37	Reserved for each command system set by switch function command (CMD6). Detailed definition can be referenced in each command system specification.				
CMD38	Yes	[31:0] stuff bits	R1b	ERASE	Erases all previously selected write blocks.
CMD39	No	---	---	---	---
CMD40	No	---	---	---	---
CMD41	Reserved				
CMD42	Yes	[31:0] stuff bits	R1	LOCK_UNLOCK	Used to set/re-set the password or lock/unlock the card. A transferred data block includes all the command details. The size of the data block is defined with SET_BLOCK_LEN command.
CMD43- CMD49 CMD51	Reserved.				
CMD50	Reserved for each command system set by switch function command (CMD6). Detailed definition can be referenced in each command system specification.				
CMD52 ... CMD54	Reserved for I/O mode (refer to SDIO Card Specification).				
CMD55	Yes	[31:0] stuff bits	R1	APP_CMD	Notifies the card that the next command is an application-specific command rather than a standard command.

CMD Index	SPI Mode	Argument	Resp	Abbreviation	Description
CMD56	Yes	[31:0] stuff bits, [0]: RD/WR ⁴	R1	GEN_CMD	Used either to transfer a Data Block to the card or to get a Data Block from the card for general purpose/application specific commands. The size of the Data Block is defined with SET_BLOCK_LEN command.
CMD57	Reserved for each command system set by switch function command (CMD6). Detailed definition can be referenced in each command system specification.				
CMD58	Yes	None	R3	READ_OCR	Reads the OCR Register of a card.
CMD59	Yes	[31:1] stuff bits, [0:0] CRC option	R1	CRC_ON_OFF	Turns the CRC option on or off. A '1' in the CRC option bit will turn the option on, a '0' will turn it off.
CMD60-CMD63	Reserved for manufacturer.				

The SD card was formatted in FAT16 (File allocation table) file system so that the files created under MS Windows could be read from the S8051 [67]. A brief overview of a FAT 16 system is described below.

5.3: FAT16

A disk is a device that is actually used to store all the files. One of the common methods of storing the files is by means of a file allocation table. FAT is a patented file system that was developed by Microsoft for MS-DOS and it is the primary file-system for consumer versions of Microsoft Windows up to and including Windows Millennium edition. It is one of the ways many commercial consumer devices such as digital cameras, PDAs and MP3 players organize their files. FATs' relative easy usage and low overhead makes it very attractive to be implemented in many commercial products [73].

There are several versions of the FAT file system. The initial version was FAT12. It was mainly used as a filesystem for floppy disks. It had a lot of limitations for example: It had no support for hierarchical directories, the cluster addresses were confined to only 12-bits long (that made the coding a bit difficult and tricky) and also the disk size was stored as a 16-bit count of sectors, which limited the size to 32 MB. In order to overcome the limitation in the file system size, FAT 16 was introduced. Cluster addresses were increased to 16-bit, allowing for a greater number of clusters (up to $2^{16}=65536$) and consequently much greater filesystem sizes. FAT 16 was able to support a maximum partition size of 2 GB. (The FAT filesystem was limited to 65,536 clusters. The size of the cluster has to be a power of 2 and has to be less than 65,536 bytes. Thus the maximum number of clusters by the maximum cluster size would be $32768 (2^{15})$. Thus $2^{15} * 2^{16} \approx 2\text{GB}$. Further developments were undertaken in the FAT system (for example FAT 32,

VFAT were developed to overcome the storage limitations). These developments would not be discussed further as in this project only FAT16 was implemented [69]. FAT16 was chosen because it could be implemented with devices up to 2 GB in size and it is also relatively easy to implement. FAT12 is not able to support drives that are found in the current technologies and FAT32 is more difficult to implement as compared to FAT16.

5.3.1: Overview of FAT16 File System:

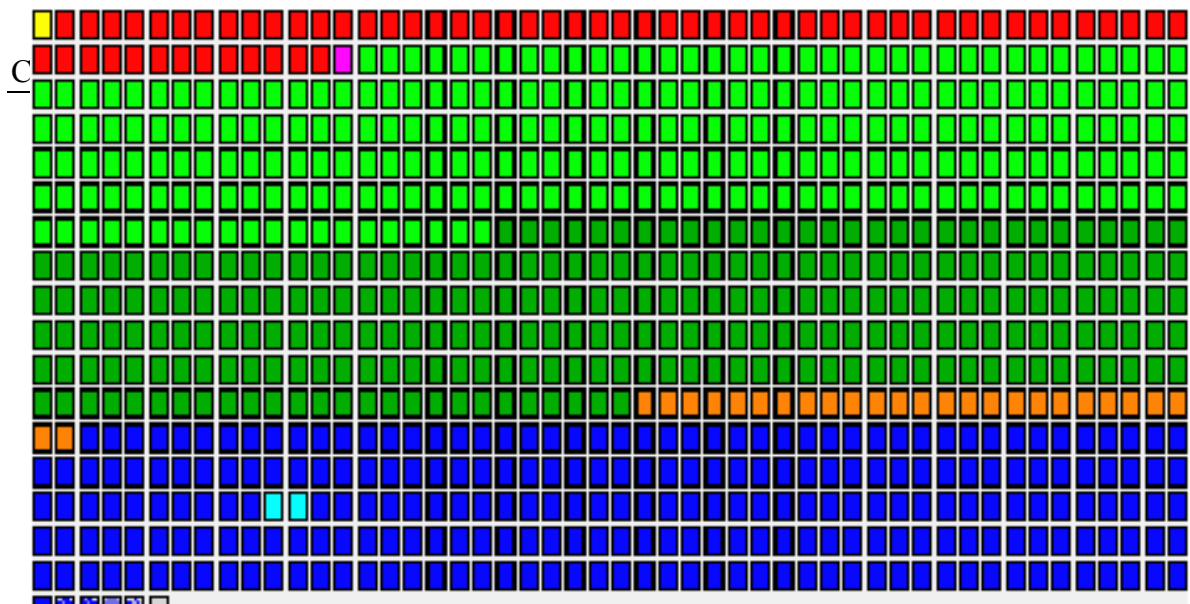
The following table 5.3.1 gives a relative layout of a FAT16 file system with only one partition as it appears in the memory:

Memory Device
Master Boot Record
FAT16 Boot Record
FAT Tables
Directory Table
Data

Table 5.3.1: Layout of a FAT16 file system

From the table above it could be clearly seen that the location of every single entry is dependent on the information of the previous entry. Only the relative location of information can be ascertained without getting information of the device. It should also be noted that each FAT has its own protocol pertaining to what information each sector has and where exactly these sectors are located.

The Figure 5.3.2 gives a scale diagram of the start of the disk with a FAT16 partition [75, 76].



Where:

- Master Boot Record
- Sectors 1-62
- Fat16 Boot Record
- Fat 1
- Fat 2
- Root Directory
- Sub Directory
- Data

I block represents 512 bytes

Fig5.3.2:FAT16 Partition

5.3.2: Master Boot Record:

The Master Boot Record or commonly known as MBR is always located in the first memory sector; sector 0. This is the first set of code the computer will read and its main function is to boot an operation system from it. The MBR is 512 bytes long (usually one sector in most memory devices) and it contains the partition table. Each entry in the MBR occupies 16 bytes. Table 5.3.3 shows the breakdown of the MBR and its hexadecimal offsets of each component.

Table 5.3.3: Breakdown of the MBR and its Hexadecimal offsets

Offset	Description	Size
000h	Executable Code (Boots Computer)	446 Bytes
1BEh	1 st Partition Entry	16 Bytes
1CEh	2 nd Partition Entry	16 Bytes
1DEh	3 rd Partition Entry	16 Bytes
1EEh	4 th Partition Entry	16 Bytes
1FEh	*Executable Marker (55h Aah)	2 Bytes

* It should be noted that sector[510]=0x55 and sector[511]=0xAA, if and only if the contents of the sector as a byte array.

The Table 5.3.4 shows an example of one partion entry:

1 partition entry is as shown below:

0	1	2	3	4	5	6	7	8	9	A	B	C	D	E	F	
														80	01	
01	00	06	EF	3F	2F	3F	00	00	00	C1	12	0B	00			

And it is read as:

80	01	01	00	06	EF	3F	2F	3F	00	00	00	00	C1	12	0B	00
----	----	----	----	----	----	----	----	----	----	----	----	----	----	----	----	----

Table 5.3.4: One Partition Entry

When developing a non-bootable memory interface, the only entries that matter are the partition tables. In most cases, only one partition is used for good memory management and thus the most imporant entry is the 1st partition at 1BEh. Table 5.5.5 gives the information in the entry of a single partition.

Table 5.3.5: Information to one single partition

Offset	Description	Size
00h (0x1BEh)	Current State of the Partition	1 Byte
01h(0x1BF)	Beginning of the Partition-Head	1 Bytes
02h(0x1C0,0x1C1)	Beginning of the Partition-Cylinder/Sector	2 Bytes
04h(0x1C2)	Type of Partitions	1 Byte
05h(0x1C3)	End of Partition-Head	1 Byte
06h(0x1C4,0x1C5)	End of the Partition-Cylinder/Sector	2 Bytes
08h(0x1C6,0x1C7,0x1C8,0x1C9)	No of Sectors between MBR and Partition (starting sector relative to the start of the Disk)	4 Bytes
0Ch(0x1CA,0x1CB,0x1CC,0x1CD)	No of Sectors in the Partition	4 Bytes

The only information that is relevant from the MBR for this project is the starting sector relative to the start of the disk. As Non-Disk drives do not have cylinders and heads, the information pertaining to cylinders and heads are not relevant for a SD card.

5.3.3: FAT16 Boot Record

The FAT16 boot record is the information that is actually located at the beginning of every partition. For the case of Windows XP, it is located at sector 0. In cards that are formatted with an MBR, the MBR would specify the beginning of the partitions and the FAT16 boot record would be the very first sector of that partition (512 bytes). The FAT16 boot record contains the basic information about the overall structure of the FAT file systems, for example: the sector size, cluster size and etc. This boot record is very important to be able to read the storage system. Without this, the operating system would not be able to know what type/size it is dealing with. The Table 5.3.6 shows the contents of the FAT16 Boot record with the appropriate offsets.

Table 5.3.6: FAT16 Boot record with the appropriate offsets

Offset	Description	Size
00h	Jump Code and NOP(no operation)	1 Byte
03h	OEM Name	8 Bytes
0Bh	Bytes per Sector	2 Bytes
0Dh	Sectors per Cluster	1 Byte
0Eh	Reserved Sectors	2 Bytes
10h	Number of Copies of FAT	1 Byte
11h	Maximum Root Directories Entry	2 Bytes
13h	Number of Sectors in a partition smaller than 32Mb	2 Bytes
15h	Media descriptor	1 Bytes
16h	Sectors per FAT	2 Bytes
18h	Sectors per Track	2 Bytes
1Ah	Number of Heads	2 Bytes
1Ch	Number of Hidden Sectors in Partition	4 Bytes
20h	Number of Sectors in Partition	4 Bytes
24h	Logical Drive number of the Partition	2 Bytes
26h	Extended Signature (29h)	1 Byte
27h	Serial Number of Partition	
2Bh	Volume name of Partition	11 Bytes
36h	FAT Name(FAT16)	8 Bytes
3eh	Executable Codes	448 Bytes
1FE	Executable Marker (55h Aah)	2 Bytes

The information found in the FAT Boot Record is very important in the handling of the rest of the information. Any device that implements FAT16 just needs to remove this information from the FAT16 Boot Record before finding the location of the Directory table. The following paragraph would give a detail explanation of some the terms that have been used in the coding for this project. Most of the terms are self explanatory. The rest of the information could be found in reference [76].

Bytes per Sector, refers to the number of bytes in each physical sector. In this project, there are 512 Bytes per Sector.

Sectors per Cluster refer to the number of sectors in each cluster and it varies depending on the partition. The following table gives the range for FAT16 (It is assumed that the sector size is 512 Bytes). It should also be noted that the cluster size should not exceed 32768 bytes and the reason was given in the earlier paragraphs.

Size ranges (MB)	Fat Type	No of Sectors	Cluster Size(Bytes)
16-127	16	4	2048
128-255	16	8	4096
256-511	16	16	8192
512-1023	16	32	16384
1024-2047	16	64	32768

Number of FAT copies- There are usually 2 copies of these tables. The use of two copies is to prevent data loss if one or part of one FAT copy is corrupted

5.3.4: FAT Tables

When a file is stored in a storage device, the file is broken up into cluster size pieces and it is then written to the data area. At this point, it is worthwhile to elaborate a bit on clusters. Cluster is actually a group of sectors. (for example sectors 21,22,23,24 could be collectively be called cluster 3). It is important to take note that cluster is only used in the data area. The file system is stored in sectors, only the files (and directories) are stored in the areas that are referred to as clusters. Clusters aids in the storage space. For example if there are no clusters, the maximum size that FAT16 could support is $2^{16} \times 512$ bytes (1 sector is 512 bytes) $\approx 33\text{MB}$. Now assuming that there are 32 sectors per cluster, it can now support: $2^{16} \times 64(\text{sectors/cluster}) \times 512\text{bytes} \approx 2\text{GB}$. It is also a good

practice to have small cluster size. The following statement highlights the former statement. When a file is stored, it is broken up into cluster sized pieces. Each cluster can only be used to hold part of one file and the rest of the space is wasted, so a larger cluster size equates to a potential larger waste per file. For example: a one byte file that is stored on a storage system that has a cluster of 4KB will mean a loss of 3.999KB.

The FAT table is the single most important element in data management systems. It contains the location of all the parts of every file and also has information on how they are connected. For every cluster on the storage system, there is an entry in the File Allocation Table. At this entry in the FAT, a single word value either points to the next cluster or it contains an End of file (EOF). The Figure 5.3.7 clearly illustrates the entries on a FAT.

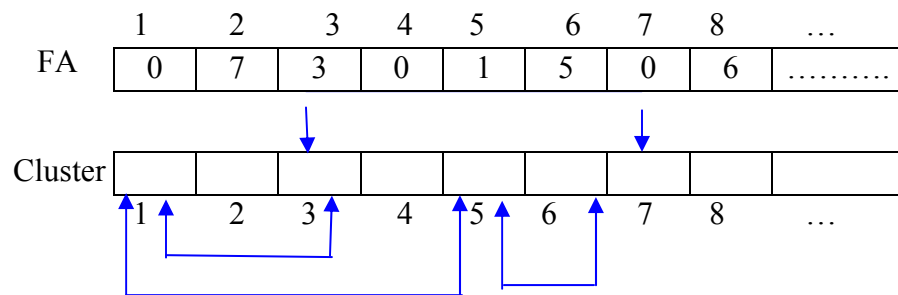


Figure 5.3.7: Entries of FAT

The following table 5.3.8 gives the valid FAT16 values:

Table 5.3.8: Valid FAT16 values

Value	Description
0000h	Free Cluster
0001h-0002h	Not allowed
0003h-FFEFh	Number of the next cluster
FFF7h	One or more bad sectors in cluster
FFF8h-FFFFh	End-of-file

5.3.5: Directory Table

The Directory table contains all the file entries in the order they are entered. Each entry is 32 bytes long, and the directory table can contain 512 entries. The structure of the data file entries is of as follows:

Offset	Description	Size
00h	Name of the File	8 Bytes
08h	Extension of the File	3 Bytes
0Bh	Attribute	1 Byte
16h	Time	2 Bytes
18h	Date	2 Bytes
1Ah	Start Cluster	2 Bytes
1Ch	File Size	4 Bytes

As the description clearly states the file entries, no further explanation would be given about the entries. It is worthwhile to take note that window application does not require the attribute, the time, or the date of the file to read or use it. The remaining entries should be filled when a directory is being created or written. Once the file being written to is determined, a search through files names would find its match. From than, the start cluster could be found, and then the FAT tables need to be accessed to determine what cluster is to be read or written to.

5.3.6: Data Area

The data area of a storage system is where the contents of the files (and directories) are stored. Figure 5.3.9 clearly illustrates a data entry diagram [2].

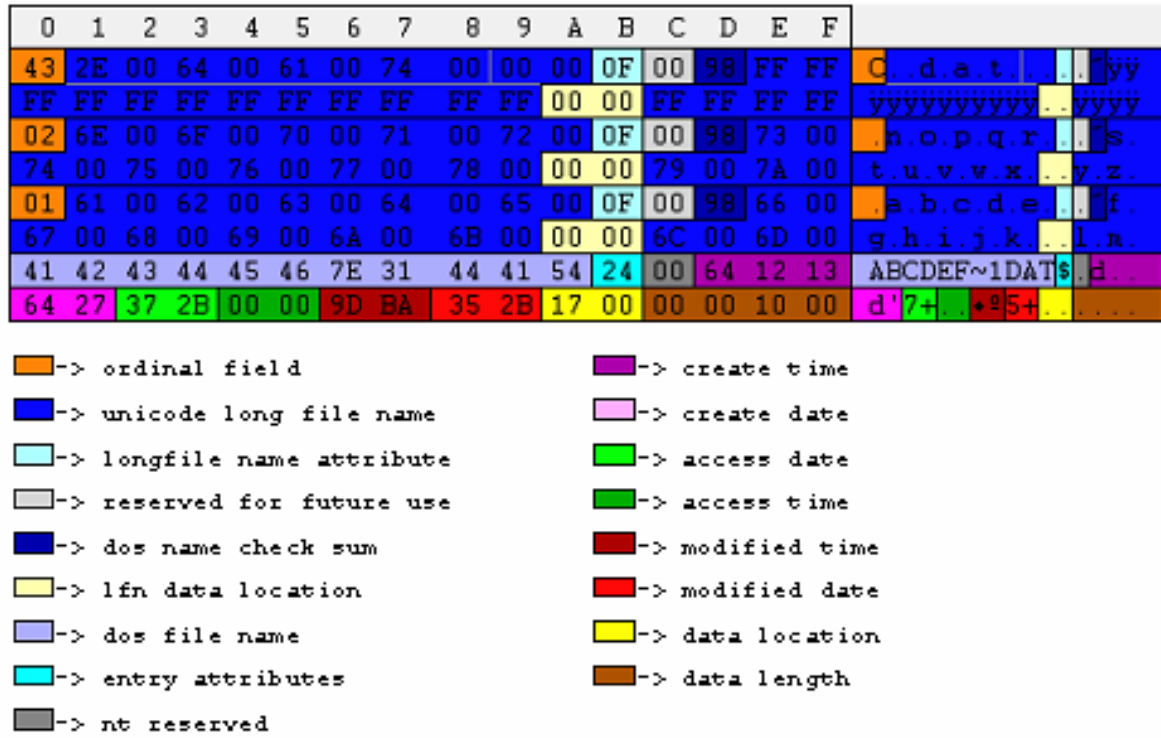


Fig5.3.9: Data Entry Diagram

The following paragraphs would discuss on the calculation alogorithms that were used in the code to access the file [76]:

Entity to calculate	Calculation algorithms
FATRegion start =	ReservedRegion + ReservedSectors
Root Directory Start Region =	FATRegion + (NumberofFATs * SectorsPerFAT)
DataRegion =	Root Directory Start Region + ((RootEntriesCount * 32)/ BytesPerSector)
FATRegion_Size =	NumberofFATs * SectorsPerFAT
RootDirectoryRegion_Size =	(RootEntriesCount * 32)/ BytesPerSector
DataRegion_Size =	(TotalNumberOfSectors - (ReservedRegion_Size + FATRegion_Size + RootDirectoryRegion_Size)) / SectorsPerCluster
First Sector of cluster N =	DataRegion + ((N-2) * SectorsPerCluster)

5.4: Analoue Portion of the Chip:

The Analogue part of the chip would be discussed briefly. It consists of an Instrumentation amplifier (IA), a low pass filter (LPF) and an analogue-to-digital converter (ADC).

A 6th order switched capacitor Butterworth low pass filter with a cut-off frequency of 125Hz was implemented to eliminate any unwanted high frequency interferences.

The bio-electric signal that was acquired was converted into digital domain by means of a 12-bit successive approximation analogue-to-digital converter. For more details of the analogue part of the S8051 chip, readers are directed to [68].

Figure 5.4.1 depicts a simple diagram of the analoue part of the s8051 chip.

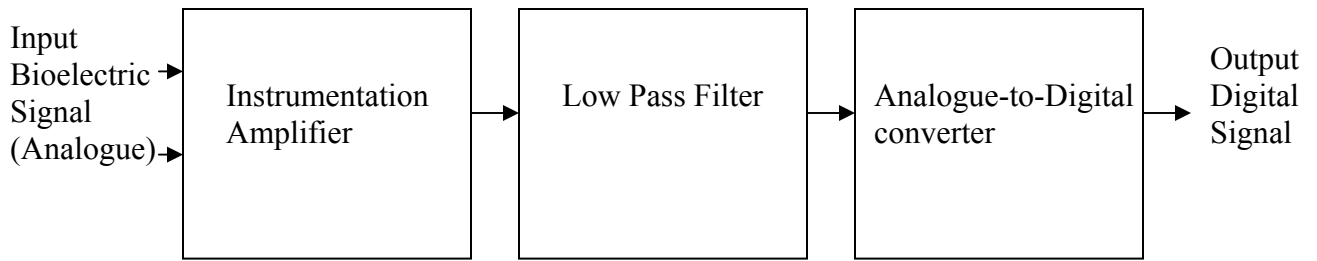


Figure 5.4.1: Analogue portion of the s8051

5.5: Circuit Design

A Circuit was designed to interface the sensor to the SD card. Some of the more important features of the circuit design would be discussed in this chapter.

SRAM (AS7C3256) and flash memory (M29W010B) are needed because, reading and writing in a SD card can only be done in 512 byte blocks and the S8051 does not have such high memory content, as such data has to be temporarily stored in either of the chips until 512 bytes of data have been collected before they are sent to the SD card for storage [71]. A NAND gate chip (74F10) was used so that all the lower order data would be stored in the flash memory (M29W010B) and the SRAM (AS7C3256) is only activated when Address line 15 (high order address) is activated. This S8051 has an additional feature of being able to load its program directly from the SD card. RS 232 was added to the design for a communication link between the microcontroller and a personal computer. 555 timers were used to drive the Strobe (20 kHz), Filter Clock (10 kHz) and ADC Clock (20 kHz). The following figure gives the PCB design. The Development tools that were used for the design were ExpressPCB [79], free CAD software that is available on the internet (for the schematic diagram) and Protel PCB software for the PCB layout.

5.6: PCB Fabrication and Component Assembly

The PCB is a double layer with through-hole plated vias. For good PCB layout, good grounding is necessary and thus the copper filled ground has to be as large as possible. The ground pad of the chip has to be mounted properly on the PCB in order to provide a path for good thermal dissipation and proper grounding. The performance of the system could be affected by noise produced by the supply side and thus decoupling is a very important part of PCB layout. To minimize these effects, all the power supply pins are properly decoupled and this could be done by using decoupling capacitors. To ensure signal integrity, the tracks should not be designed very narrowly. Thus, the track width for signal lines were designed to 10mils and power lines were designed to a width of 25 mils. Vias of diameter 0.4mm were used for good connection to ground.

Due to the many vias that were present in the PCB, it was sent out for fabrication. A total of 10 PCB were fabricated. The PCB was fabricated on FR-4 substrate. The mounting and soldering of most of the components were done on a rework station as these components were to be surface mounted. The Metcal AR5000 rework station that is shown in Figures 5.6.1 and 5.6.2 was used.



Fig5.6.1: Metcal AR500 rework station

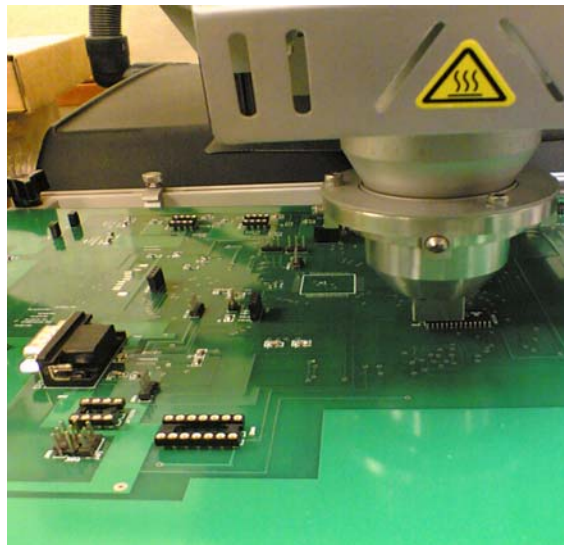


Fig5.6.2: Surface mounting of components using the Metcal AR500

The Metcal AR500 rework station is versatile equipment that is very suitable for low volume surface mount assembly of PCB. Its pick and place capability together with its in-built camera system is capable of mounting QFN and ball grid array (BGA) chips very precisely. After the placement of components, the machine performs hot air-reflow to solder the components onto the PCB. The reflow profile and the temperature was monitored and controlled precisely with the use of the Metcal AR500 support software. Further details of this equipment may be found in [80]. The other components namely the capacitors, resistors and the 555 timers are hand soldered using a soldering machine. The whole interface circuitry is shown in Figure 5.6.3.

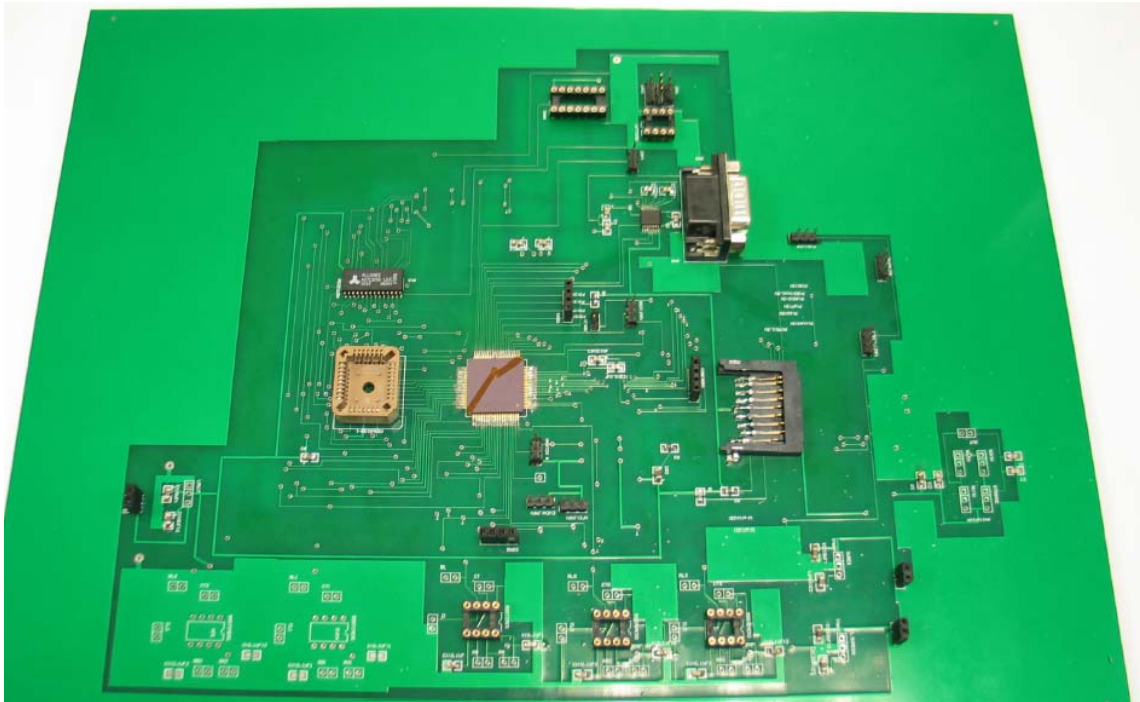


Fig5.6.3: the interface circuitry

5.7: Testing

Testing was carried out on the interface circuitry to determine whether each of the digital and analogue parts of the microcontroller that was developed was functioning properly. This bruxism force sensor module provides a way to record data or monitor the patient. It is very suitable for the patient to record the data at his own comfort without the need for the patient to make trips to the doctor. However, it does not provide real-time monitoring as the data is recorded in SD and thus it could only be read when the device is detached from the patient. A wireless module would be suitable for a real time monitoring. The following chapter describes the development of a wireless module.

CHAPTER 6: Wireless Sensor

6.1 Introduction to Zigbee

A low-power wireless transceiver based on the IEEE 802.15.4/ZigbeeTM standard was used to interface the sensor to the personal computer. The hardware of the transceiver was built using chipsets that were readily available commercially [82]. The pressure sensor would be mounted on the printed circuit board for integration with the transceiver module to form a wireless sensor node. Zigbee devices were selected for this application compared to some other devices such as GPRS/GSM or 802.11b/Wi-Fi or 802.15.1/Bluetooth because of its superior functionalities. As compared to the other wireless technologies, Zigbee devices are known to consume much lesser power. More detailed explanation of Zigbee devices, its protocol and solutions could be found in [81, 82]. Zigbee devices are very commonly used in wide range of applications that include:

1. Asset tracking
2. Home automation and control
3. Industrial Control
4. Energy Management

5. Medical Sensing and Monitoring

6.2: Zigbee Solution

The Zigbee node that was used for this project comprised a microcontroller (MCS08GT60), a radio frequency (RF) transceiver that is able to operate in the 2.4GHz unlicensed ISM band and some external analogue circuitry components.

6.2.1: Microcontroller

The Microcontroller that was used for this sensor is MCS08GT60 [83]. Some of the main features of the chip are:

1. 60KB Flash Memory- This is more than sufficient for Zigbee Development since the memory space that is required for a typical Zigbee full functional device is about 32KB. This Flash memory is on-chip in-circuit programmable.
2. 48 Pins quad flat no lead (QFN) package- The chip is available in QFN package with a size of 7mm by 7mm that would be able to achieve a small node size.
3. Serial Peripheral Interface (SPI) unit- The SPI port is utilized for interface with the transceiver unit
4. 8 Channel, 8 bit analogue-to-digital converter (ADC).
5. 39 general-purpose input/ (GPIO) pins- This could be used for interface with the RS232 chip and other peripherals.

6.2.2: Transceiver Unit:

The transceiver unit is interfaced with the Microcontroller and the antenna. The main function of the transceiver is to modulate/demodulate and transmit/receive data wirelessly between different nodes by means of RF. The transceiver chip that has been used in this project is MC13192 [84]. The main features of the transceiver are as follows:

1. 802.15.4 1 PHY and MAC layer- This chip has the 802.15.4 PHY modem and MAC layer that can support star and mesh networking. The Zigbee-compliant devices could be implemented by means of the addition of a Zigbee protocol stack.

2. 250kbps offset-Quadrature Phase Shift Keying (OQPSK)- This modulation and demodulation is compatible with IEEE 802.15.4 standards. The transmit/receive frequency is 2.4 GHz
3. Low power consumption: 20-30 mA in operation mode
4. Transmit power 0dBm and receive sensitivity of -92dBm at 1% packet error rate (PER)
5. Small form factor (32 pin QFN package)

The other components are discussed in depth elsewhere [79].

6.2.3: Antenna

The antenna has been used to transmit the data wirelessly from one node to another. The MC13192 transceiver chip that has been used in this setup has differential RF inputs and outputs that are very suitable for a balanced antenna structure printed on a circuit board. Antennas were printed on the circuit board instead of using a chip antenna due to the fact that latter requires more space and it would also result in a higher cost. A combination of chip capacitors, resistors and inductors together with micro strip lines printed on PCB provide impedance matching between the transmit/receive pins of the MC13192 and the antenna.

6.3: Full Wireless module

Figures 6.3.1, 6.3.2 and 6.3.3 give a pictorial view of the wireless module [79]

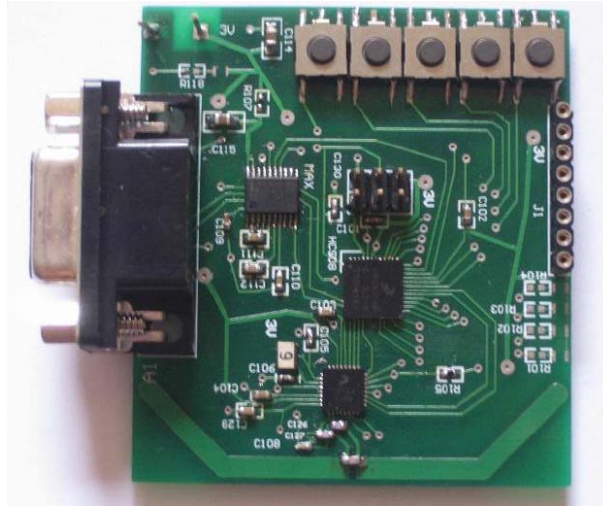


Fig 6.3.1: Transceiver Module

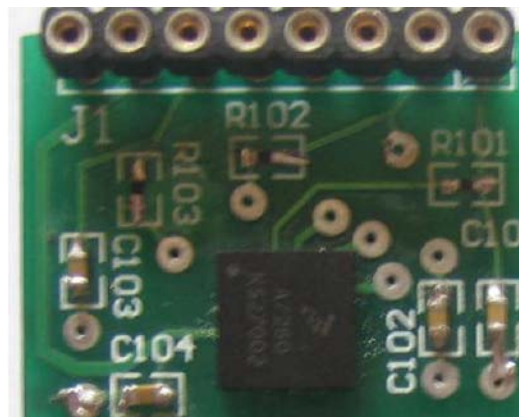


Fig 6.3.2: Sensor Module

6.4: Implementation

6.4.1: Development tools

The software development for the transceiver module includes programming the flash memory of the MCU with the protocol stack and application codes. The Codewarrior integrated development suite was used for the software development. All the necessary functions such as coding, compiling, debugging and flash programming that is required for software development were combined into this single software development suite.

6.4.1.1: Codewarrior development suite

The Codewarrior from Metrowerks is a complete integrated development suite that could be used for hardware bring-up through programming applications [85]. The Codewarrior contains the following set of tools:

- Integrated development environment.

The coding, compiling, debugging and flash programming could be done using this integrated development environment in a single software package. This integrated development environment simplifies the software development and it also ensures compatibility between the different functions.

- Editor, compiler, linker and assembler

The Codewarrior has the capability to support C, C++ or assembly language. This particular project was done using C-programming. Figure 6.4.1 shows the editor which is

a program used for writing the source code that is then compiled, linked and assembled into a project file.

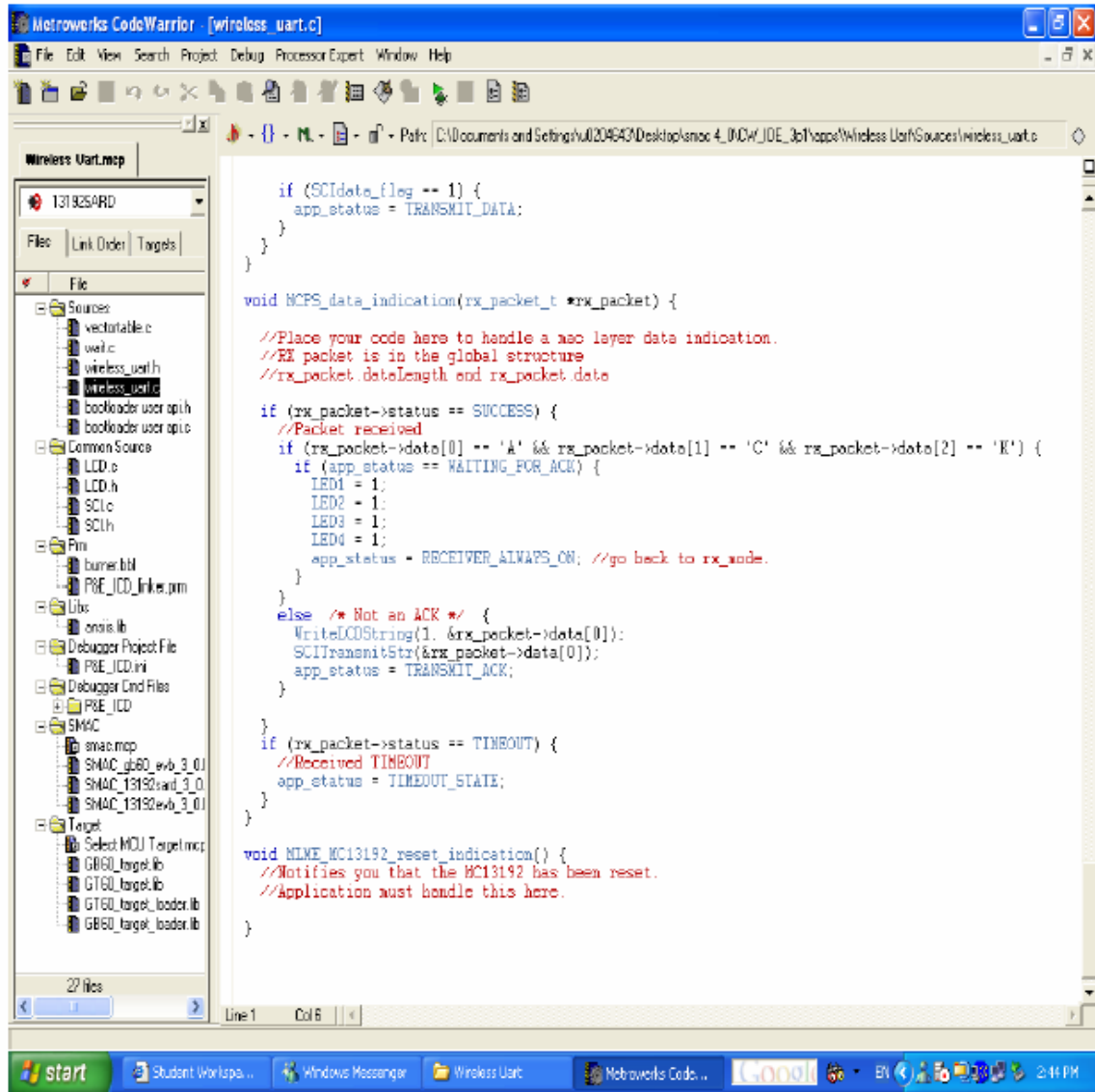


Figure 6.4.1: Editor and Compiler

Figure 6.4.2 shows the simulator and debugger. Once the application codes have been built, the simulator and debugger will run and check for any syntax or logic errors.

Once the application code has been built successfully, it has to be flashed onto the memory of the Microcontroller. The BDM multi-link cable as shown in Figure 6.4.3 has been used in this project to provide the interface for in-circuit emulation, debugging and programming between the personal computer and the Microcontroller. This provides an avenue for the application codes to be programmed onto the memory content of the Microcontroller.



Figure 6.4.2: BDM multi-link cable

6.5: Application

The Piezoresistive bruxism force detector sensor that has been developed would be interfaced to the wireless transceiver to provide a wireless transmission of the voltage signals from the sensor to a personal computer. The sensor would be attached to one wireless transceiver board and it would act as the Sensor node. The other transceiver board would act as master node and it would be attached to the RS232 port of the PC. The sensor node will measure any force on the bruxism force detector and would transmit the data and display it on a personal computer. A graphic user interface or more commonly known as GUI would be available on the personal computer to display the data. As the sensor output was in terms of millivolts, and in order to increase the sensitivity of the sensor (to fully utilize the sensor output to be between 0-3V), amplification (10 times) was done on the signal output from the sensor before the signal was processed for wireless transmission. The amplification was done by means of an amplification chip (LM358N) and suitable resistor values.

Upon the start or upon reset, the application initializes its necessary parts and sets the channel. It would then check for any button press. If a button is pressed, the board is set to transmit mode and it would then be the wireless node. If there is no press of button, by default, it would act as a master node and it would be set in a receiver mode. When the sensor node receives a voltage output from the bruxism force detector, the analogue data would be sampled by the 8-bit in-built Analogue to Digital converter to convert the analogue voltage signals to digital voltage signals. The transceiver unit would transmit the data in a digital format. The master node would receive these packets and send the data to the personal computer by means of the RS232 serial port. The graphical user

interface will display the data on the screen. This voltage output displayed from the personal computer would be double checked with the voltage output from the sensor before transmission by means of an Agilent Data-logger (34901A, 20 channels multiplexer; data acquisition unit). The following figure 6.4.1 shows the full setup for the testing procedure

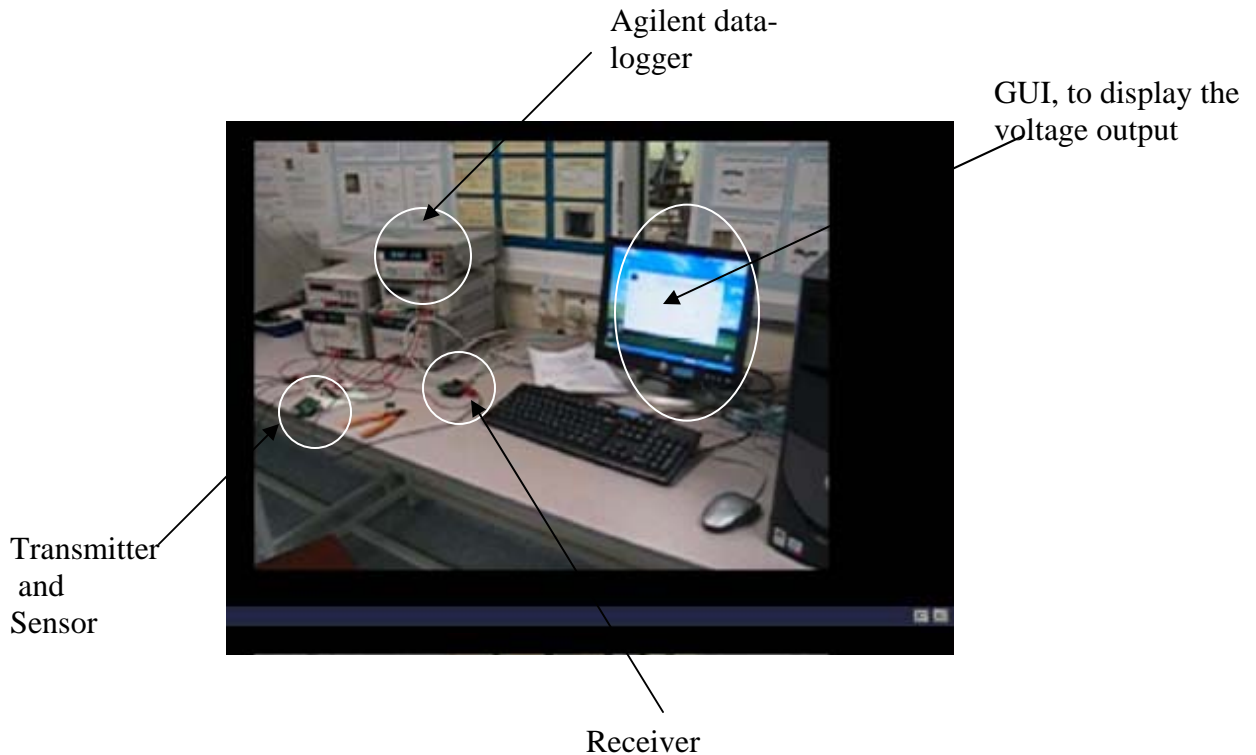


Figure 6.5.1: Full setup for the test procedure

6.6: Results and Discussion

A working prototype of the wireless pressure sensor has been successfully built and tested. In wireless UART, a peer-to-peer wireless transfer of data between the transceiver modules were carried out. The voltage output displayed on the Agilent Data-logger corresponded with the voltage output displayed on the personal computer but there was a slight discrepancy due to the resolution of the microcontroller in the Zigbee module. The

microcontroller that was used in the Zigbee module had a resolution of 8 bits and thus it could only display values up to one decimal place. As thus the values that were transmitted from the sensor were truncated. This is exemplified in the following table.

Table: 6.6: Voltage Output table

Voltage output from Agilent Data-Logger/V	Voltage output from Transmitter/V
0.235	0.2
0.255	0.2
0.295	0.2
1.35	1.3
1.65	1.6
1.95	1.9

The sensor was than calibrated by applying a known force by means of the Instron 5848 Micro-tester and observing the voltage output from the Zigbee transmitter that was displayed on the personal computer. Figure 6.6.1 gives a clear depiction of the experimental setup.

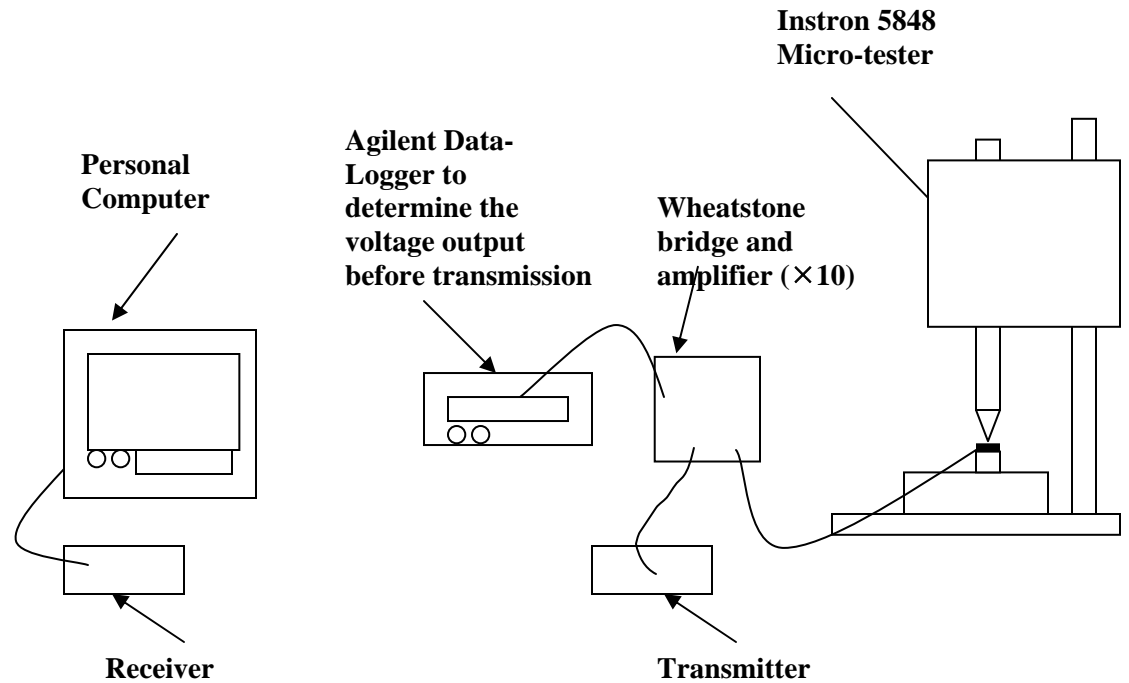


Fig 6.6.1: Experimental setup for calibration of the sensor

Figures 6.6.2-6.6.6 depict the actual setup.

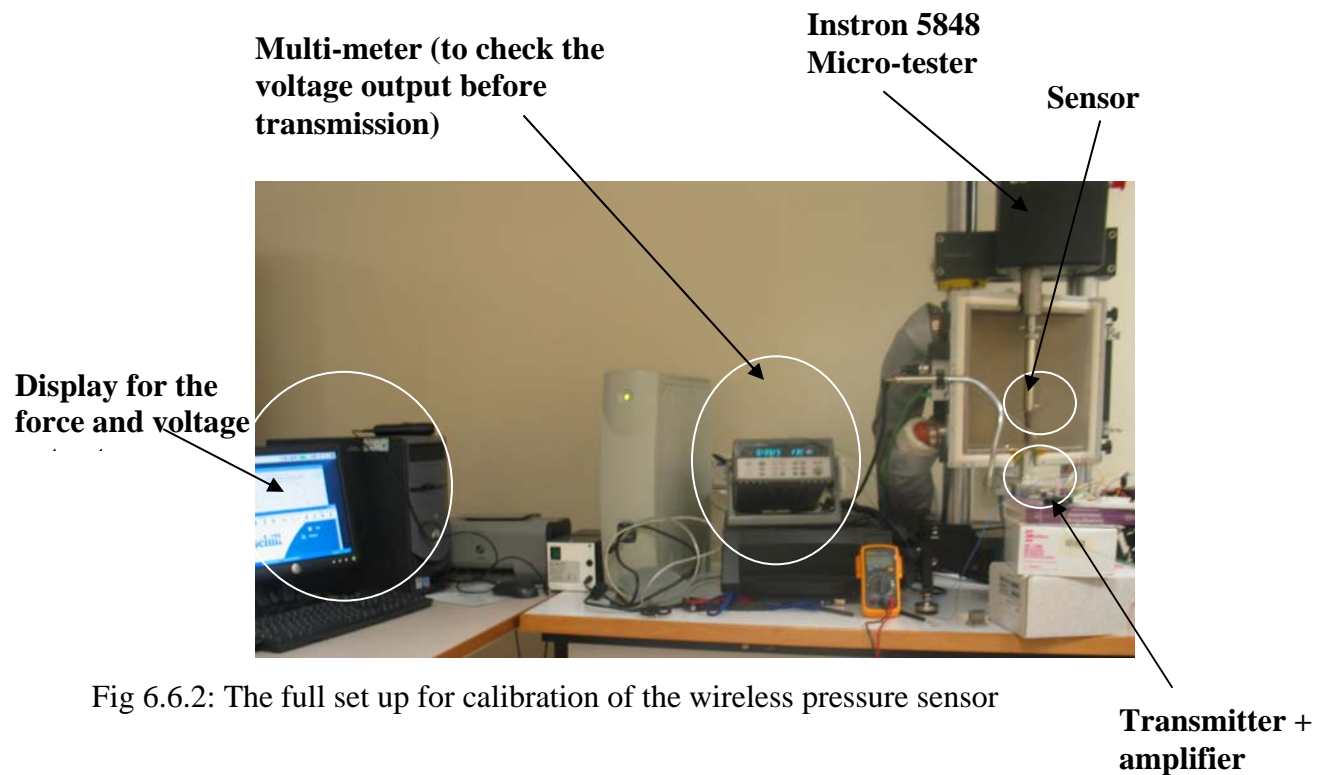


Fig 6.6.2: The full set up for calibration of the wireless pressure sensor

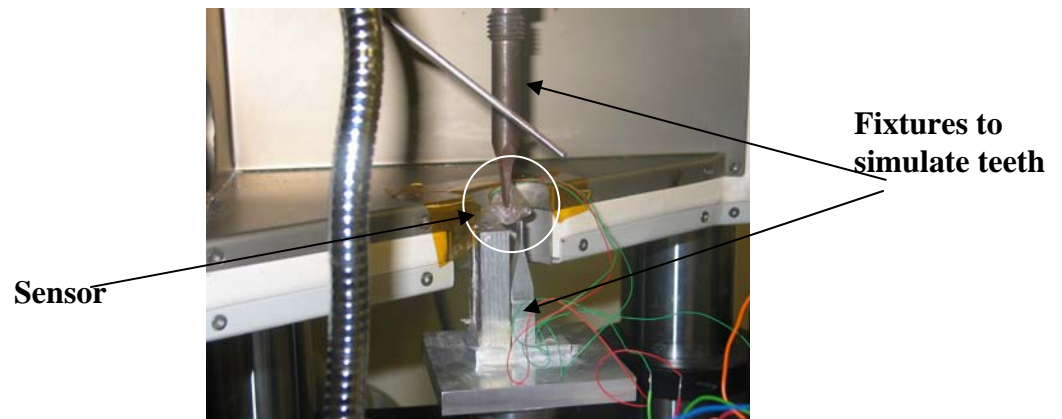


Fig 6.6.3: Sensor and fixture to simulate teeth.

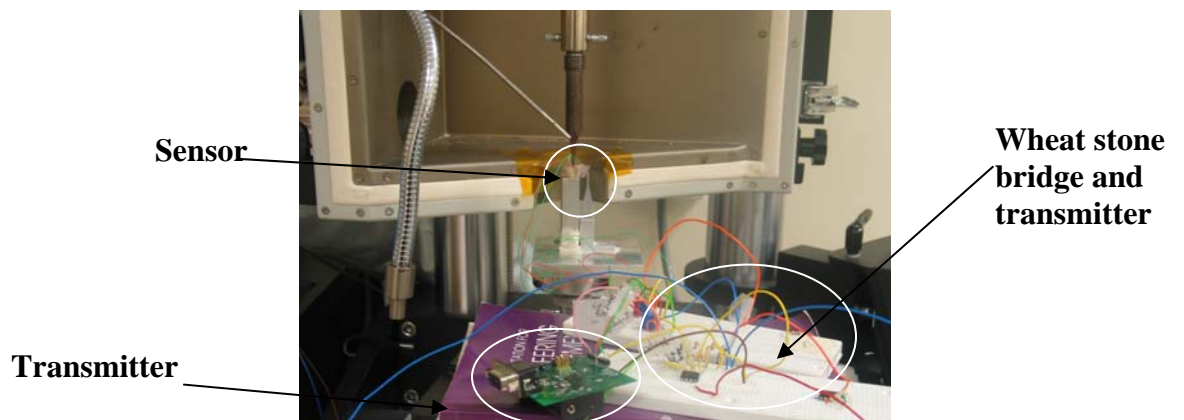


Fig 6.6.4: The sensor, transmitter, wheat stone bridge and amplifier

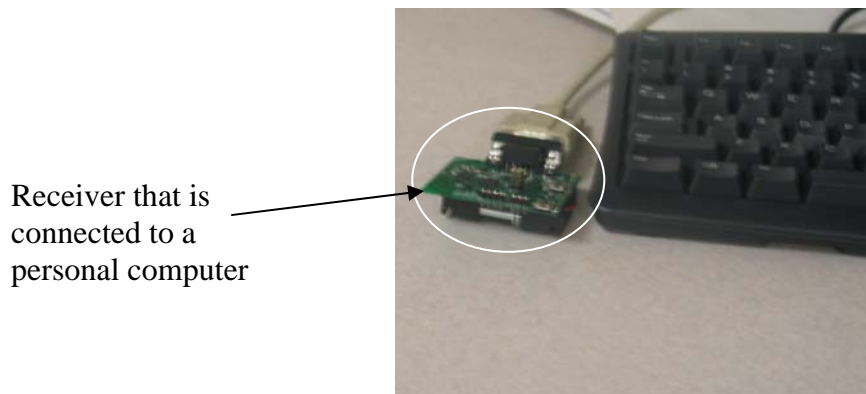


Fig 6.6.5: Receiver

Zigbee module that displays voltage output

Instron 5848 Micro-tester software that displays the force

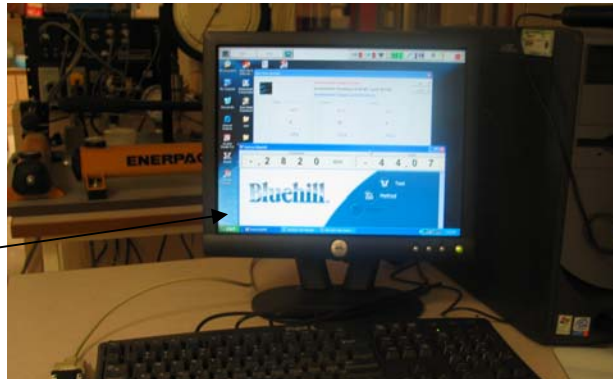


Fig 6.6.6: Voltage output and force display

The results that were obtained from the calibration test is displayed below in figure 6.5

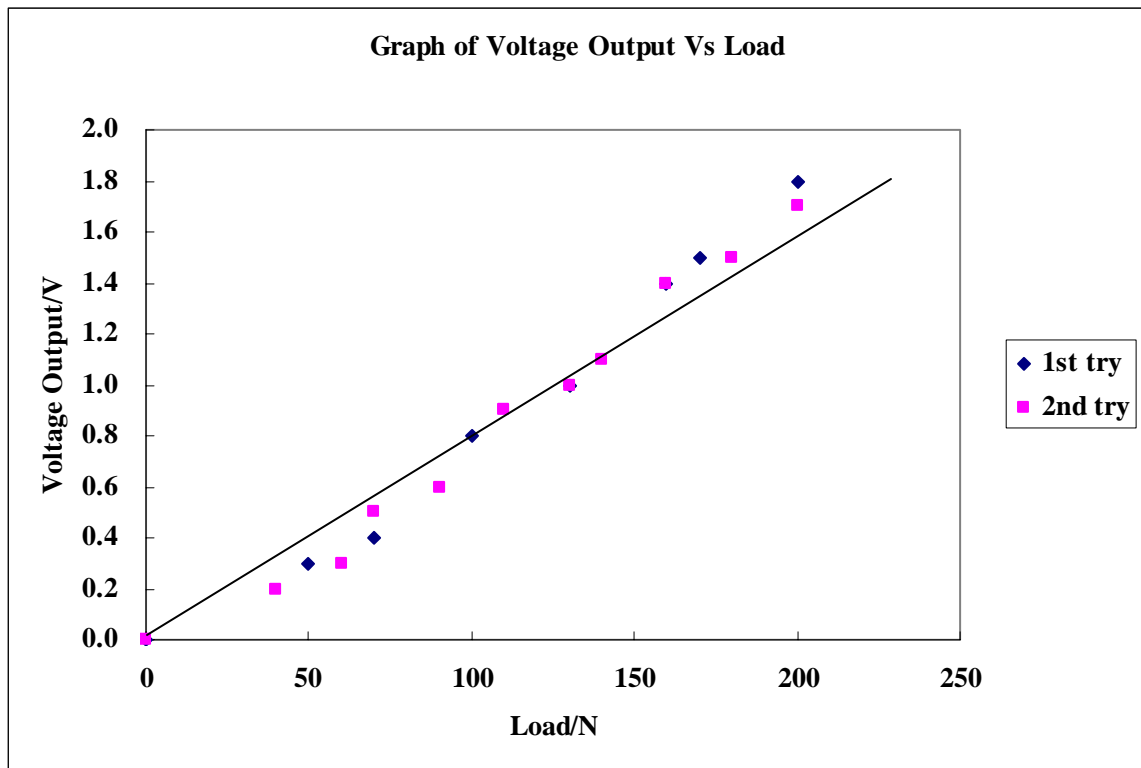


Fig 6.6.7: Calibration curve.

It can be seen from the calibration curve that the voltage output does not exactly vary linearly with the load. This could be attributed to the resolution of the Zigbee module. As the microcontroller in the Zigbee module has a resolution of 8 bits, it is only able to

display values up to one decimal place and thus the accuracy in the calibration has to be compromised. A higher bit (16 bit or 32 bit) microcontroller would give a more accurate reading. Once the calibration had been done, a line of best fit was drawn and the relationship between the voltage output and load was determined. The following equation describes the relationship between the voltage output and the applied load

$$L = 117.6 \times V$$

where L is the load and V is the voltage output. A simulated bruxism event was then conducted to validate the use of the sensor module as a bruxism force detector. The following section would describe the test that was conducted.

6.7: Validation of Sensor Module as Bruxism Force Detector

A simulated bruxism event test as shown in Figure 6.7.2 was conducted. The patient was asked to bite the sensor and simulate a bruxism event. The experimental setup for this test is depicted in Figure 6.7.1. As currently the Zigbee module does not have the feature to store data, the voltage output from the sensor was recorded using the Agilent Data-Logger and the readings on the transmitted voltage signals were observed visually. Figures 6.7.3 and 6.7.4 show the outcome of the test that was conducted.

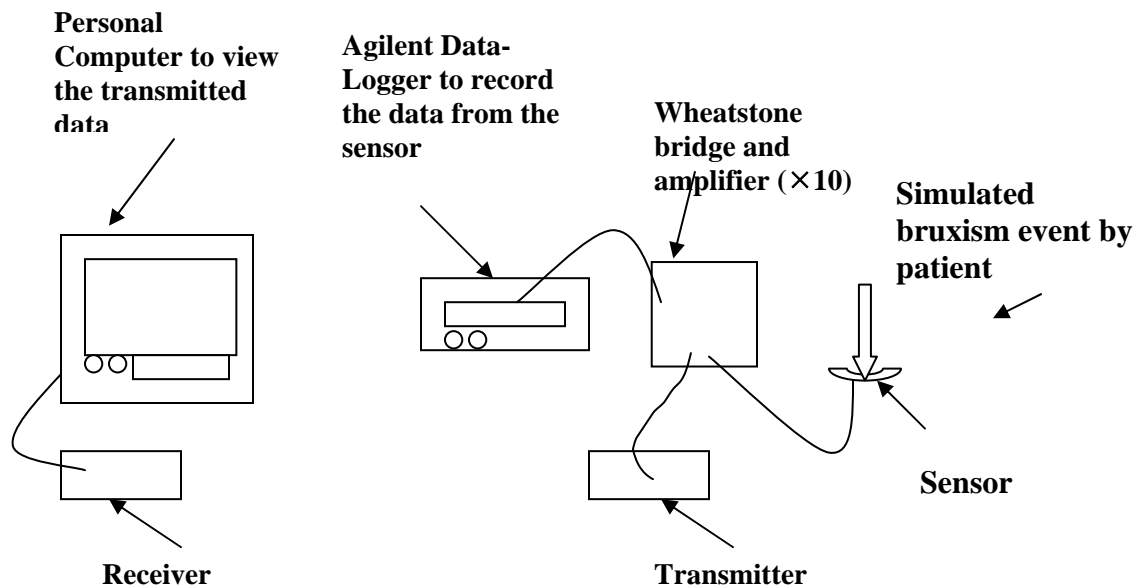


Fig 6.7.1: Experimental setup for simulating an actual bruxism event



Fig 6.7.2: Simulated bruxism event

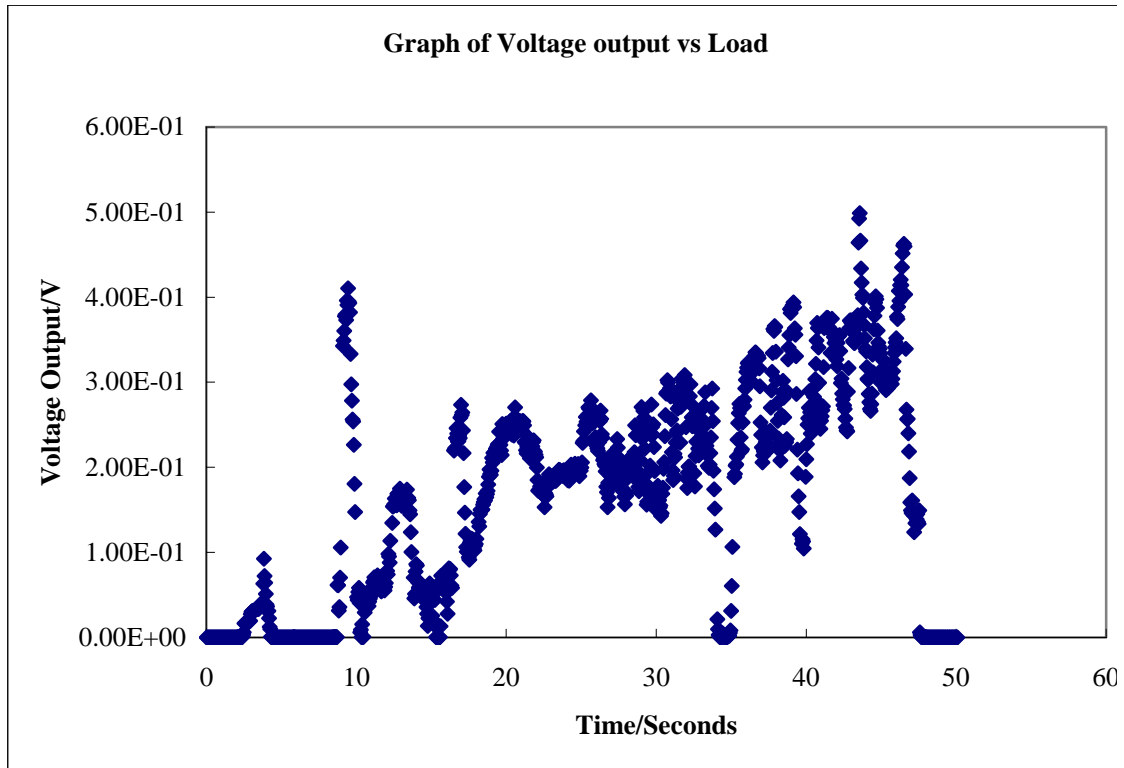


Fig 6.7.3: Voltage output Vs Time graph

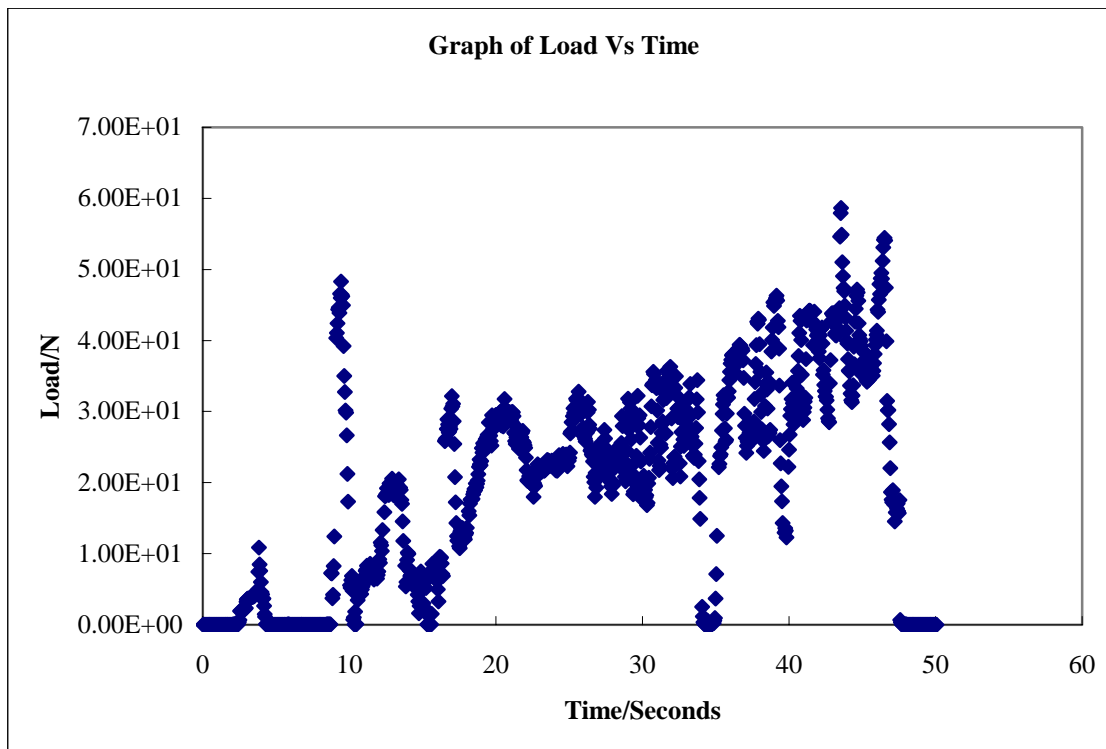


Fig 6.7.4: Load Vs Time graph

The Load in Figure 6.7.4 was determined from the voltage output from figure 6.7 and by substituting the voltage values into the voltage output-load relationship that was determined in the earlier section. The Load distribution graph in Fig 6.8 was compared with a previously published paper that described bruxism forces [86]. Figures 6.7.5 and 6.7.6 show the comparison. The maximum force recorded for the simulated event (from figure 6.7.5) is about 50N and it is lying in the lower region of the reference graph in figure 6.7.6 (the region is circled in the reference graph). By comparing the forces, it could be deduced that this patient is suffering from very mild bruxism as the forces recorded were much smaller than the forces experienced by heavy bruxism patients [86].

The wireless sensor module has been successfully calibrated and tested. The following paragraphs would describe the final prototype of the sensor that would be fabricated.

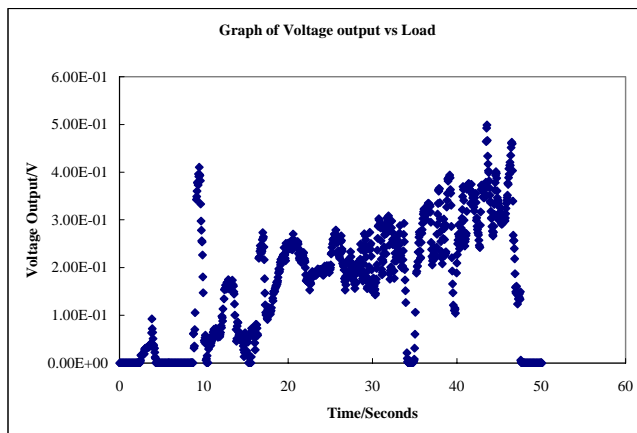


Fig 6.7.5: Actual simulated bruxism event

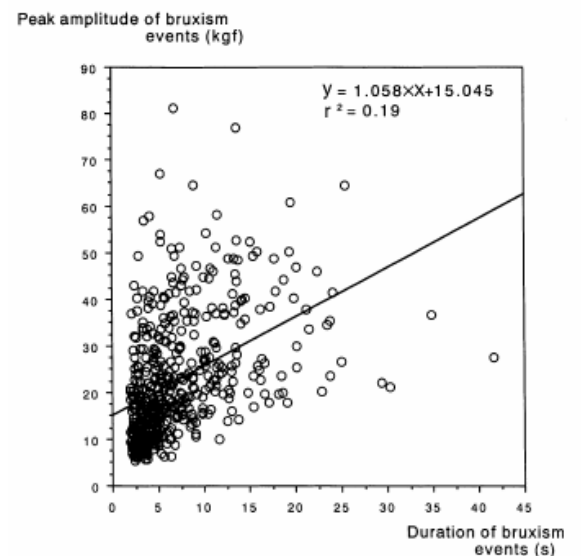


Fig 6.7.6: Reference graph [86]

6.8: Final Prototype

The node size of the first prototype is about $57\text{mm} \times 52\text{mm} \times 0.8\text{mm}$ and the sensor is currently not in the same PCB board as the transceiver module. The PCB design for a second prototype with a reduced board size and integrated bruxism force detector would be sent for fabrication soon. The Figure 6.8.1 and Figure 6.8.2 shows the final prototype that would be fabricated

Mouth guard which is attached to the interface circuitry by means of a stainless steel. The stainless steel is bonded to the stainless steel by means of orthodontic resin

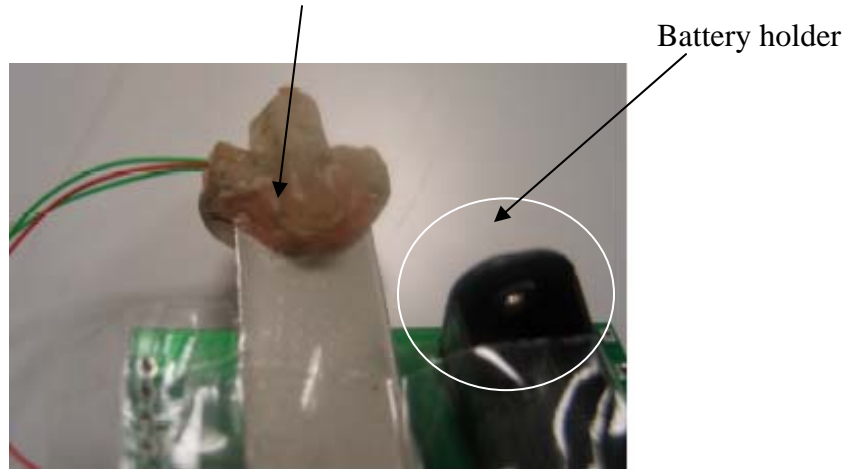


Figure 6.8.1: Backview of the final prototype

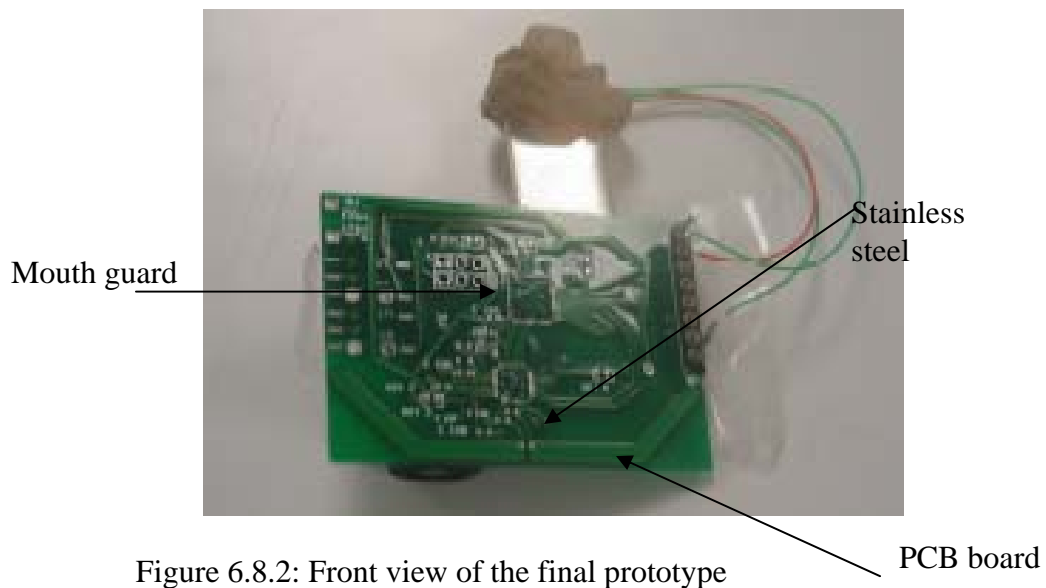


Figure 6.8.2: Front view of the final prototype

CHAPTER 7: SUMMARY and CONCLUSION

Force sensors for bruxism force detection have been widely studied but no suitable device has been developed up to date. In this thesis, different type of sensors have been fabricated and tested for use as a force sensor in bruxism force detection. A wireless module was also developed to interface the sensor to a personal computer, so that physiological readings could be monitored remotely and it also provides a comfortable environment for the patient.

In this project, different type of sensors were fabricated and tested. The sensors included piezoelectric sensors, piezoresistive sensors (Honeywell FSL05N2C), Thin Film Flexi-force Sensor, constantan strain gage sensor and piezoresistive strain gage sensor. The sensors were subjected to different load cycle patterns at different rates to a maximum force of up to 200 N. The sensors were tested for their repeatability, linearity, hysteresis and drift. . The following observations were made for each individual sensor:

- Piezoelectric sensors could only be used to measure dynamic forces and it is not a suitable sensor to measure static forces. As bruxism events include both dynamic and static actions, this sensor was not suitable for this application
- Piezoresistive sensor (Honeywell FSL05N2C) measured both the static and dynamic forces accurately. Even though it is a suitable sensor to measure forces, the fabricated sensor was more than 5mm thick and thus was not suitable for use in this application as it would cause discomfort for the patient.
- Thin Film flexi-force sensor did not provide repeatable readings during loading and unloading. The deterioration of the voltage output could be attributed to the plastic

nature of the polyester and the other constituent materials that were used in the sensor.

- Constantan strain gage sensors were tested. Its small size and low cost makes it an ideal sensor. Constantan strain gages gave accurate readings, but their small voltage signal output (due to their small gage factor) makes it unsuitable for this application. If the signal output is very small, these signals would be corrupted during transmission of the signals from the transmitter to receiver from external noise.
- Piezoresistive strain gages sensor was tested. The small size of the sensor, its high voltage output (due to its high gage factor) and its consistent readings during calibration makes it a suitable sensor for this application.

An interface circuitry was designed and fabricated to store the physiological data from the sensor to a Secure Digital (SD) card. This Bruxism force sensor module provides a way to record data at his own comfort but it is not possible to provide real time monitoring as the data is recorded in a SD card and thus the readings could only be read when the device is detached from the patient.

A wireless integrated sensor module was developed and successfully tested. The wireless force sensor was calibrated by means of an Instron 5848 Micro-tester and the transmitted signals were verified with an Agilent Data-logger that was used to measure the signal lines prior to transmission. An actual simulated bruxism event was successfully

conducted to validate the use of the sensor module as a bruxism force detector. A working prototype of a bruxism force detector has been successfully built and tested.

6.2.1: Recommendations for Further Work

- A program could be developed to store the transmitted data in the PC. Currently the Zigbee module does not have a feature to store the transmitted data. It can only display the values on a personal computer
- The Zigbee module could be further utilized to store other physiological data other than bruxism force as it has a three input channel.
- The resolution of the microcontroller that is used in the Zigbee module is only 8 bits and thus the accuracy of the transmitted data has to be compromised as the display data are truncated. Further work could be done to incorporate a 16 bit or 32 bit microcontroller to improve the resolution.
- The node size could be further reduced using a system on chip (SOC) solution.
- The interface circuitry for the SD card could be further studied and miniaturized.

REFERENCES:

1. NTI-TSS, <http://www.nti-tss.com/>
2. The glossary of prothodontic terms. The Academy of Prothodontics. Journal of Prosthet Dent 1994; 71: 41-112
3. Takeuchi H., Ikeda T, and Clark G.T., “ A piezoelectric film based intrasplint detection method for bruxism.”, Journal of Prosthet Dent., 2001, Aug 86(2): 195-202
4. Pegamalian A., Rudy T.E., Zaki H.S., and Greco C.M; “ The association between wear facets, bruxism and severity of facial pain in patients with temporomandibular disorders, The Journal of Prosthetic dentistry, Volume 90 , No2, pp 194-200
5. Richard A. N, Principles of Bioinstrumentation; John Wiley & Sons 1988
6. Allocca J.A., Stuart A., Transducers theory & applications., Reston Publishing Company, 1984
7. Ahlgren J., Owall B., “ Muscular activity and chewing force: A polygraphic study of human mandibular movements”., Archievs of Oral Biology, 1970, Vol 15, pp : 271-180
8. Carlsson S.G., Gale E.N., “ Biofeedback treatment for muscle pain associated with thw temporomandibular joint”, Journal of Behavior Therapy and Experimental Psychiatry, Volume 7, pp: 383-385, 1976
9. Feehan, M. and Marsh N., “ The reduction of bruxism using contingent EMG audible biofeedback : A case study”, Journal of Behavior Therapy and Experimental Psychiatry, Volume 20, pp: 179-183, 1989
10. Iwasa M., Sugimori M., Kurachi Y. and Nagumo M., “ Changes in bite force and occlusal contacts in patients treated for mandibular prognathism by orthognathic surgery”, Journal of Oral Maxillofac Surgery, Volume 56, pp:850-855,1998
11. Miyawaki S., Tanimoto Y., Araki Y., Katayamam A., Imai M. and Mamamoto T.T., “ Relationships among nocturnal jaw muscle activities, decreased esophageal pH, and sleep positions”, American Journal of Orthodontics and Dentofacial Orthopedics, Volume 126, No 5, pp:615-619, 2004
12. Casas J.M., Beemsterboer P., and Clark G.T., “ A comparison of stress-reduction behavioral counseling and contingent nocturnal EMG feedback for the treatment of bruxism”, Behaviour Research and Therapy, Volume 20, pp:9-15,1982

13. Nishigawa K., Kondo K., Takeuchi H., and Clark G.T., “ Contingent electrical lip stimulation for sleep bruxism: A pilot study, The Journal of Prosthetic Dentistry, volum 89, Number4, pp: 412-417, 2003
14. Godaux E., and Desmedt J.E., “ Exteroceptive suppression and motor control of the masseter and temporalis muscles in normal man” , Brain Research, Volume 85, pp: 447-458, 1975
15. Piezoelectric tutorials from Morgan Ceramics
<http://www.morganelectroceramics.com/piezoguide1.html>
16. <http://www.piezo.com/>
17. Sakaguchi R.L, Wenande B.S., Delong R., Anderson G.C. and Douglas W.H., “ A piezoelectric film transducer for dental occlusal analysis”, Clinical Materials, Volume 10, pp:145-151,1992
18. Piezo film sensors technical manual by Measurement specialties,
<http://www.msiusa.com/download/pdf/english/piezo/PART1-INT.pdf>
19. Rottner K. and Richter E-J., “ Effects of occlusal Morphology on the Accuracy of Bite Force Measurements Using Thin Film Transducers”, The International Journal of Prosthodontics, Volume 17, pp:518-523,2004
20. Takeuchi H., Ikeda T and Clark G.T., “A piezoelectric film-based intrasplint detection method for bruxism”, The Journal of Prosthetic Dentistry, Volume 86, pp:195-202,2001
21. Watanabe T., Ichikawa K. and Clark G.T “ Bruxism Levels and Daily Behaviours: 3 Weeks of Measurement and Correlation”, Journal of Orofacial Pain, Volume 17, pp:65-73,2003
22. Baba K., Clark G.T., Watanabe T., and Ohyama T., “ Bruxism Force Detection by Piezoelectric Film-Based Recording Device in Sleeping Human”, Journal of Orofacial Pain ,Volume 17,pp:58-64, 2003
23. National instruments
<http://Zone.ni.com/devzone/conceptd.nsf/webmain/8A433A0DBCF0D5148625685500758ACA>
24. National Physical laboratory, NPL,
<http://www.npl.co.uk/force/faqs/transtypes.html#foil>
25. Callister W.D. Jr., “Materials Science and Engineering an Introduction”, John Wiley & Sons,Inc, 2000

26. Loffler F., Siewert C., and Ascher C., “ Manganin thin film sensor for force sensing”, Surface coatings & Technology, Volume 174-175, pp:1287-1292, 2003
27. Ugural A.C., “Mechanics of materials”, McGRAW-Hill International edition, 1991
28. Dechow P.C., and Carlson D.S, “ A Method of Bite Force Measurements in Primates”, Journal of Biomechanics, Volume 16, pp:797-802,1983
29. Lundgren D. and Laurell L., “ Occlusal forces in prosthetically restored dentitions: a methodological study”, Journal of Oral Rehabilitation, Volume 11, pp:29-37.
30. Sinn D.P. Assis E.A. and Throckmorton G.S., “ Mandibular Excursions and Maximum Bite Forces in Patients with Temporomandibular Joint Disorders”, Journal of Oral Maxillofacial Surgery, Volume 54, pp: 671-679,1996
31. Bergmann G., Graichen F., Siraky J., Jendrzynski H. and Rohlmann A., “MultiChannel Strain Gauge Telemetry for Orthopedic Implants”, Journal of BioMechanics. Volume 20, pp:169-176.,1988.
32. Pures R., “Capacitive sensors: When and how to use them”, Sensors and Actuators A, Volume 37-38, pp:93-105, 1993
33. Clark S. and Wise K., “Pressure sensitivity in anisotropically etched thin diaphragm pressure sensor”, IEEE trans Electronic Devices, Volume 26,pp:1887-1896,1979
34. Tekscan,Inc (Boston M.A), <http://www.tekscan.com/dental.html>
35. Harvey W.L., Osborne J.W., and Hatch R.A., “ A preliminary test of the replicability of a computerized occlusal analysis system”, Journal of Prosthetic Dentistry. Volume 67(5), pp:697-700
36. Dobo-Nagy C, Fejerdy P., Angyal J., Harasztosi L., Daroczi L., Beke D., and Wesselink P.R., “Measurements of periapical pressure created by occlusal loading”, International Endodontic Journal, Volume 36, pp:700-704, 2003
37. Hsu M, Palla S., and Gallo L.M., Sensitivity and reliability of the T-scan system for occlusal analysis. Journal of Craniomandible Disorder. Volume 6 , pp: 17-23, 1992
38. Saracoglu A., Ozpinar B., “ In Vivo and in Vitro Evaluation of Occlusal Indicator Sensitivity”, Journal of Prosthetic Dentistry, Volume 88(5), pp: 522-526, 2002
39. Nielsen S.T., Soerensen D.D., Libergren P., Yoganathan A.P., and Nygaars H., “Miniature C-shaped Transducers for Chordae Tendineae Force Measurements”, Annals of Biomedical Engineering, Volume 32(8), pp: 1050-1057, 2004

40. Tun T.N., Toh S.L., Akkipeddi R, and Rahman M., “ Contact Pressure measurements using silicon-based $\text{Al}_x\text{Ga}_{1-x}\text{As}$ Semiconductor Pressure Sensors”, *Sensors and Actuators A*, Volume 118, pp: 190-201, 2005
41. Yamamoto A., Nawachi N., Tsutsumoto T., and Terayama A., “Pressure sensor using p-type polycrystalline diamond piezoresistors”, Volume (14), pp: 657-660, 2005
42. Druzhinin A., Lavitska E., and Maryamova I., “ Medical pressure sensors on the basis of silicon microcrystals and SOI layers”, *Sensors and Actuators B*, Volume 58, pp: 415-419, 1999
43. Chang C.C, Lieu C.T, and Hsieh M.K., “ Study of the fabrication of a silicon pressure sensor”, *International Journal of electronics*, Volume 82, pp:295-302, 1997
44. Ravary B., Pourcelot P., Bortolussi C., Konieczka S., and Denoix N.C., “ Strain and force transducers used in human and veterinary tendon and ligament biomechanical studies”, *Clinical Biomechanics*, Volume 19, pp:433-447,2004
45. Blechschmidt-Trapp R.A., Hohlflod O, Muller R and Werthschutzky R., “Piezoresistive sensors for medical applications exemplified by a probe for measure pressure in the rectum”, *Biomed Tech(Ber)*, Volume 47, pp:43-47, 2002
46. Ferrarin M., Andreoni G and Pedotti A, “Comparative biomechanical evaluation of different wheel chair seat cushions, *Journal of Rehabilitation Research and Development*, Volume 37(3), pp:315-324,2000
47. Wang L.and Beebe D.J., “ Characterization of a silicon-based shear-force sensor on human subjects”, *IEEE Transactions on Bio-medical Engineering*, Volume49(11), pp:1340-1347, 2002
48. Beebe D.J., Hsieh A.S., Denton D.D., and Radwin R.G., “ A silicon force sensor for robotics and medicine”, *Sensors and Actuators A*, Volume 50, pp: 55-65, 1995
49. Baba K, Tsukiyama Y. and Clark T.G., “ Reliability, validity and utility of various occlusal measurement methods and Techniques”, *The Journal of Prosthetic Dentistry*, Volume 83, pp:83-89,2000
50. Harris M.L., Morberg P., Bruce W.J.M and Walsh W.R., “ An improved method for measuring tibiofemoral contact areas in total Knee arthroplasty: a comparison of K-Scan sensor and Fuji-film”, *Journal of Biomechanics*, Volume 32, pp:951-958,1999
51. Platt D., Wilson A.M., Timbs A., Wright I.M., and Goodship A.E., “ Novel force transducer for the measurement of tendon force in vivo”, *Journal of Biomechanics*, Volume 27,pp:1489-1493,1994

-
52. Papakostas T.V., Lima J. and Lowe M., “ A Large area force sensor for smart skin Applications”,
<http://www.media.mit.edu/resenv/classes/MAS965/readings/PapakostasSmartSkin.pdf>
 53. Jensen T.R., Radwin G.R, and Webster J.G., “ A Conductive polymer sensor for measuring external finger force”, Journal of Biomechanics, pp:851-858, 1991
 54. Hedman T.P., “A new transducer for facet force measurement in the lumbar spine: Benchmark and in vitro test results”, Journal of Biomechanics, Volume25(1), pp: 69-80,1992
 55. Nikonovas A., Harrison A.J.L, Hoult S. and Sammut D, “ The application of force sensing resistor sensors for measuring forces developed by the human hand”, Journal of Engineering in Medicine, Volume 218, pp: 121-126
 56. Carpaneto J., Micera S., Zaccone F., Vecchi F., and Dario P., “ A sensorized thumb for force closed-loop control of hand neuroprostheses”, Volume 11(4), pp: 346-352, 2003
 57. Fernanades C.P., Glantz P.J., Svensson S., and Bergmark A., “A novel sensor for bite force determinations”, Dental materials, Volume19, pp:118-126,2003
 58. Malmstadt H.V., Enke C.G and Crouch S.R., “ Electronics and instrumentation for engineers”, The Bengamin/Cummings Publishing Company Inc, 1981
 59. Maalej N and Webster J.G., “ A miniature electrooptical force transducer”, IEEE Transactions on Biomedical Engineering, Volume35(2), pp:93-98,1988
 60. Sombatsompop N, Intawong N-S and Intawong N-T, “ Design and construction of Photo-Conductive light pressure sensor for highly viscous fluids”, Sensors and Actuators A, Volume 102, pp:76-82,2002
 61. Sun Y; Potasek D.P.; Bell D.J. and Nelson B.J; “ Drosophila flight force measurements using a MEMS micro force sensor; Proceedings of the 26th Annual International Conference of the IEEE EMBS, pp:2014-2017,2004
 62. PIEZOTECH S.A. - 7 rue du General Cassagnou - 68300 Saint-Louis – France
<http://www.piezotech.fr/>
 63. Malmstadt H.V., Enke C.G. and Crouch S.R, “ Electronics and Instrumentation for Scientists”,The Benjamin/cummings Publishing Company,Inc, 1981
 64. Honeywell Sensing and Measurement;
<http://catalog.sensing.honeywell.com/printfriendly.asp?FAM=force&PN=FSL05N2C>

65. Clarke N.G. and Townsend G.C., “Distributation of nocturnal bruxing patterns in man”, Journal of Oral Rehabilitation, Volume 11, pp:529-534, 1984
66. Clarke N.G., Townsend G.C. and Carey S.E., “Bruxing pattern in man during sleep”, Journal of Oral Rehabilitation, Volume 11, pp:123-127, 1984
67. Chew W.S., 8051, Masters Thesis, 2004
68. Hong J.S., IC Implementation of Bioelectric Acquisition System, Masters Thesis, 2004
69. MCS[®]51 Microcontroller Family User’s Manuel; INTEL
70. Pont M.J., Patterns for Time-Triggered Embedded Systems., ACM Press, 2001
71. Microchip website: www.microchip.com
72. Sandisk SD card, Product Manual Version 2.2, Document number. 80-13-00169, Nov 2004.
73. Microchip website: www.microchip.com
74. Pont.M.J., Embedded Systems., ACM Press, 2001
75. Wikipedia the free encyclopedia,
http://en.wikipedia.org/wiki/File_Allocation_Table
76. <http://www.beginningtoseethelight.org/fat16/>, Clark
77. <http://home.freeuk.net/foxy2k/disk/disk3.htm>, Jonathan Fox
78. Microsoft Hardware White Paper, FAT: General Overview Of On-Disk Format, Microsoft, 1999
79. <http://www.expresspcb.com/>, ExpressPCB
80. http://www.okinternational.com/product_advanced/apr5000, Metcal
81. Yang O.W, “ Development of 802.15.4/Zigbee[™] Transceiver Module”, FYP Thesis, 2006
82. Freescale Semiconductor, Sensor Applications Reference Design User Guide, Rev 1.5, 2005-2007
83. Freescale Semiconductor, Freescale MCS08GT60 Datasheet Rev.2.3, 2004

84. Freescale Semiconductor, Freescale MC13192 Datasheet Rev.2.9,2005
85. Freescale Semiconductor, Application Note AN2616, Getting Started With HCS08 and Codewarrior Using C, Rev 1.0, 2005
86. Nishigawa E., Bando E., and Nakano.M, “Quantitative study of bite force during sleep associated bruxism”, Journal of Oral Rehabilitation, Volume 28, pp:481-491, 2001

APPENDIX

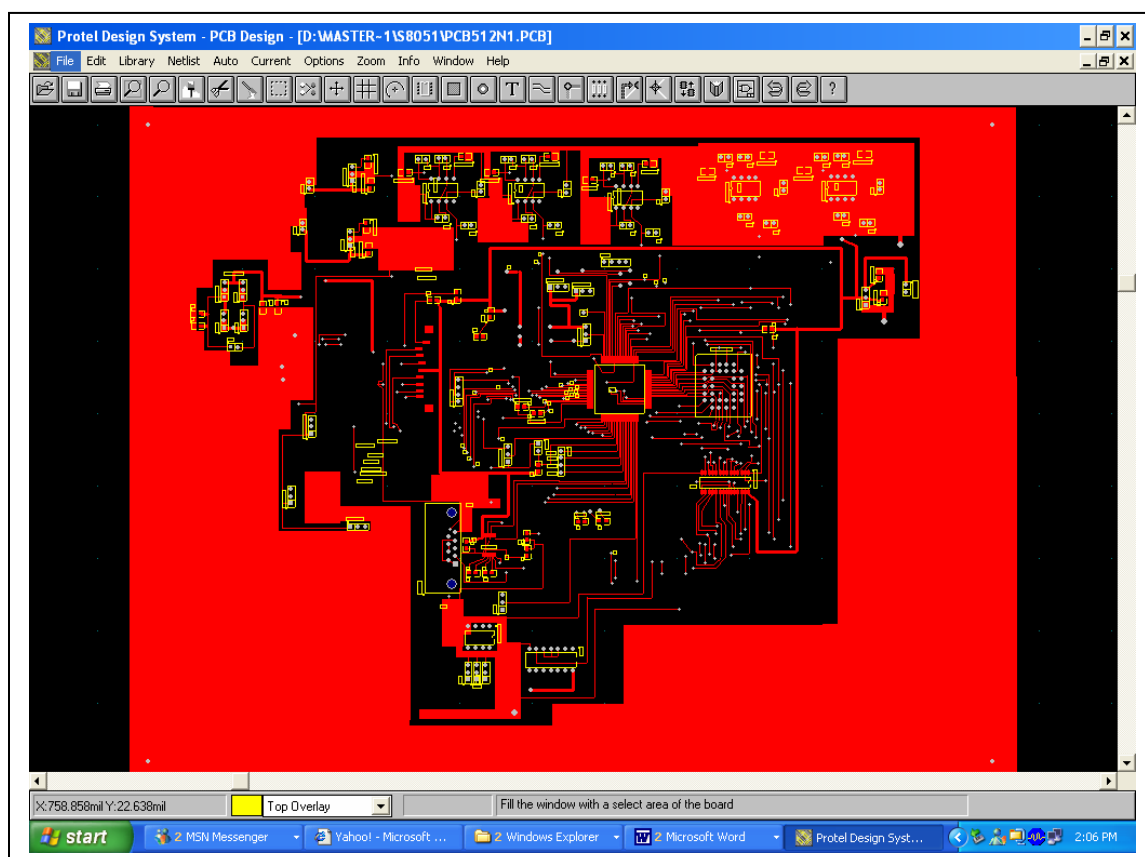


Fig A.1: Top Layer for the PCB design for interfacing the sensor to a SD card

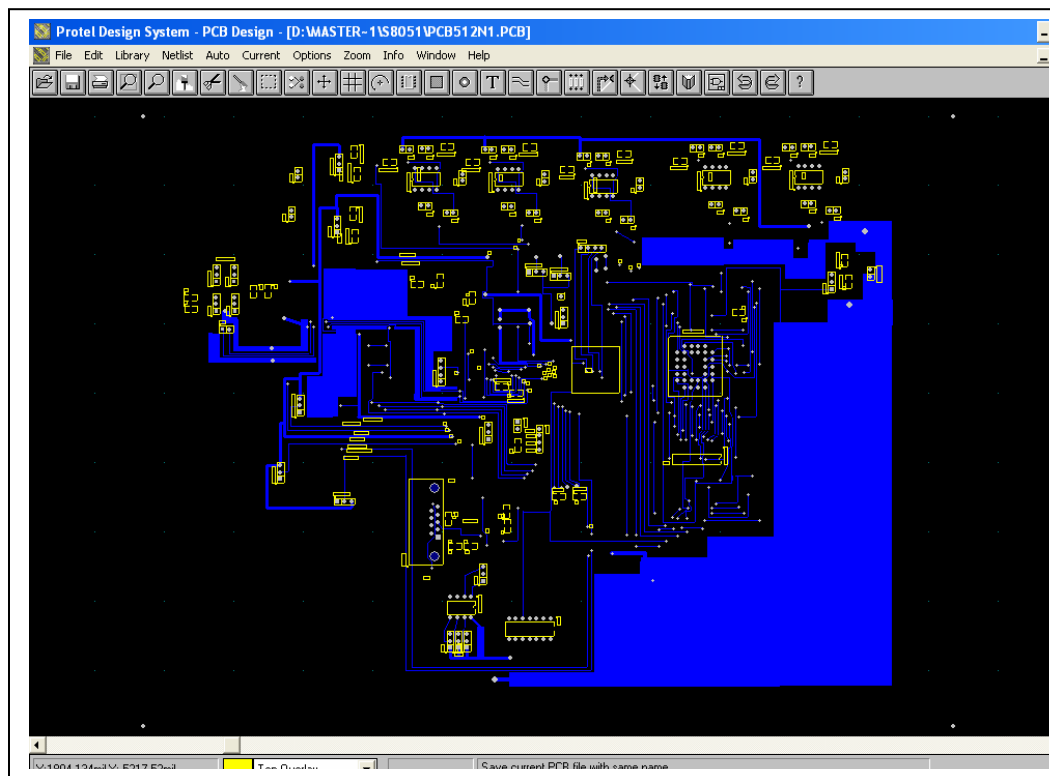


Fig A.2: Bottom- Layer for the PCB design for interfacing the sensor to a SD card

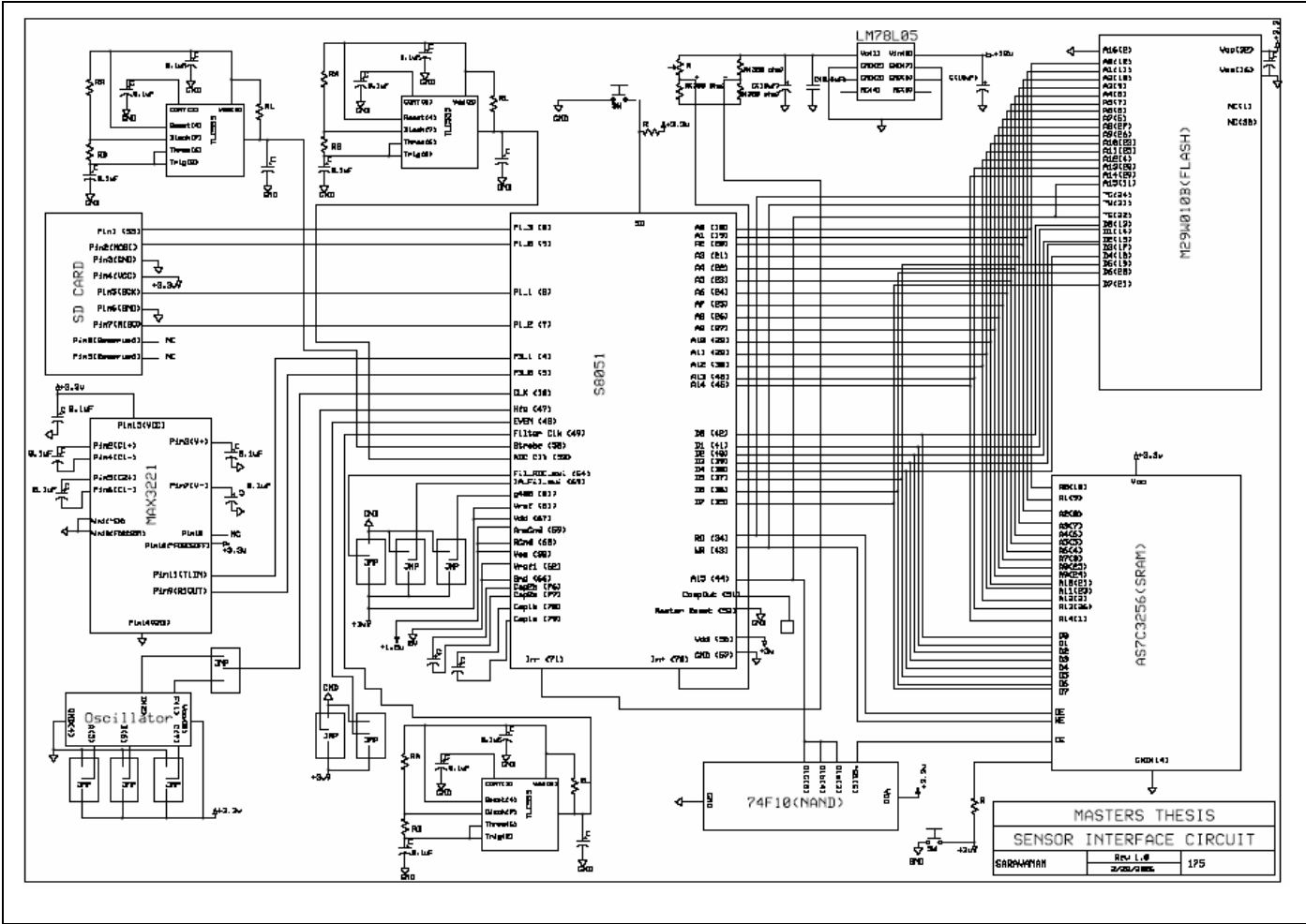


Fig A.3: Schematic circuit diagram for interfacing the sensor to the SD card